

HELI VALTNA-LUKNER

Superluminally propagating
localized optical pulses



TARTU UNIVERSITY
PRESS

The study was carried out at the Institute of Physics, University of Tartu.

The dissertation was admitted on June 18, 2010 in partial fulfilment of the requirements for the degree of Doctor of Philosophy in Physics (Applied Physics), and allowed for defence by the Council of the Institute of Physics, University of Tartu.

Supervisor: Prof. Acad. Peeter Saari
Institute of Physics, University of Tartu, Estonia

Opponents: Prof. Ari T. Friberg
Aalto University, Helsinki, Finland
University of Eastern Finland, Joensuu, Finland
Royal Institute of Technology, Stockholm, Sweden

Dr. Rüdiger Grunwald
Max-Born-Institute for Nonlinear Optics and Short-Pulse
Spectroscopy, Berlin, Germany

Defence: August 27, 2010, at the University of Tartu, Tartu, Estonia

ISSN 1406–0647
ISBN 978–9949–19–420–9 (trükis)
ISBN 978–9949–19–421–6 (PDF)

Autoriõigus: Heli Valtna-Lukner, 2010

Tartu Ülikooli Kirjastus
www.tyk.ee
Tellimus nr. 382

TABLE OF CONTENTS

LIST OF PUBLICATIONS INCLUDED IN THE THESIS	7
1. INTRODUCTION	10
2. LOCALIZED WAVES	15
2.1. Mathematical description of the localized waves	15
2.2. Geneology and optical generation principles	18
2.2.1. Generic superluminal family	20
2.2.2. Subfamily of superluminal pulses with a propagation- invariant wavefunction	22
2.2.3. Subluminal family	23
2.2.4. Luminal family	24
2.2.5. Negative group velocities	24
2.2.6. Asymptotic behavior of the wavefunctions	25
2.3. Accelerating and decelerating Bessel-type waves	26
3. INTERFEROMETRIC TECHNIQUES FOR SPATIOTEMPORAL MEASUREMENTS OF ELECTRIC FIELD	29
3.1. Spatial interferometry	30
3.1.1. The method	30
3.1.2. Impulse and frequency response of optical system	36
3.2. Spectral interferometry	38
3.3. Spatial-spectral interferometry and SEA TADPOLE	40
3.3.1. Spatial-spectral interferometry method	41
3.3.2. SEA TADPOLE	44
3.4. Discussion and Conclusions	45
4. EXPERIMENTS	48
4.1. Experiments on superluminal localized waves with hyperbolic support of the spectrum	49
4.1.1. Propagation of the Bessel pulse in dispersive media [30, 31]	50
4.1.2. Linear X pulse by means of nonlinear interaction	51
4.2. Experiments on Bessel-X pulses	51
4.2.1. Spatiotemporal measurement of the correlation function of the Bessel-X pulse [29]	52
4.2.2. Measurement of the superluminal group velocity in a gas chamber [32]	52
4.2.3. Autocorrelation measurements of few-cycle Bessel-X pulses [34, 63, 91]	53
4.2.4. Low-resolution spatiotemporal measurements of Bessel-X pulse with Shack-Hartmann detector [37]	53
4.2.5. High-resolution spatiotemporal measurements of Bessel-X pulse with SEA TADPOLE [VI]	54
4.2.6. Discussion	55
4.3. Proof-of-the-principle experiment on focus wave mode [33]	56

4.4. Experiments on accelerating and decelerating Bessel-type waves ...	57
4.4.1. Generation of accelerating and decelerating Bessel pulses by axicon and lens	57
4.4.2. Formation of decelerating Bessel pulse in diffraction	58
4.5. Conclusion	60
SUMMARY	61
SUMMARY IN ESTONIAN	62
ACKNOWLEDGEMENTS	64
REFERENCES	65
PUBLICATIONS	71

LIST OF PUBLICATIONS INCLUDED IN THE THESIS

- I P. Saari, M. Menert and H. Valtna, “Photon localization barrier can be overcome”, *Opt. Commun.* **246**, 445–450 (2005).
- II H. Valtna, K. Reivelt and P. Saari, “Modifications of the focused X wave as suitable models of strongly localized waves for realization in the optical domain”, *J. Opt. A: Pure Appl. Opt.* **8**, 118–121, (2006).
- III P. Saari, K. Reivelt, H. Valtna, “Ultralocalized superluminal light pulses”, *Laser Phys.* **17**, 297–301, (2007).
- IV H. Valtna, K. Reivelt, P. Saari, “Methods for generating wideband localized waves of superluminal group velocity”, *Opt. Comm.* **278**, 1–7 (2007).
- V A. Averchi, D. Faccio, E. Rubino, H. Valtna Lukner, A. Panagiotopoulos, P. A. Loukakos, S. Tzortzakis, A. Couairon, and P. Di Trapani, “Linear X-wave generation by means of Cross Phase Modulation in Kerr media” *Opt. Lett.* **33**, 3028–3030 (2008).
- VI P. Bowlan, H. Valtna-Lukner, M. Löhmus, P. Piksarv, P. Saari, and R. Trebino, “Measurement of the spatio-temporal field of ultrashort Bessel-X pulses”, *Opt. Lett.* **34**, 2276–2278 (2009).
- VII H. Valtna-Lukner, P. Bowlan, M. Löhmus, P. Piksarv, R. Trebino, and P. Saari “Direct spatiotemporal measurements of accelerating ultrashort Bessel-type light bullets” *Opt. Express* **17**, 14948–14955 (2009).
- VIII P. Saari, P. Bowlan, H. Valtna-Lukner, M. Löhmus, P. Piksarv, R. Trebino “Directly recording diffraction phenomena in time domain” *Laser Physics*, **20**, 948–953 (2010).
- IX M. Löhmus, P. Bowlan, R. Trebino, H. Valtna-Lukner, P. Piksarv, P. Saari “Directly recording diffraction phenomena in the time domain” *Lihtuanian Journal of Physics* **50**, 69–74 (2010).
- X P. Saari, P. Bowlan, H. Lukner, M. Löhmus, P. Piksarv, R. Trebino “Time-and-space-domain study of diffracting and “non-diffracting” light pulses” *Lihtuanian Journal of Physics* **50**, 121–127 (2010).
- XI P. Saari, P. Bowlan, H. Valtna-Lukner, M. Löhmus, P. Piksarv, and R. Trebino “Basic diffraction phenomena revisited in time domain” *Opt. Express* **18**, 11083–11088 (2010).
- XII K. Reivelt, H. Valtna, and P. Saari “Optical generation of superluminal localized wave solutions of homogeneous wave equation”, *Northern Optics Conference Proceedings, IEEE*, 13–16 (2006).
- XIII P. Bowlan, H. Valtna-Lukner, M. Löhmus, P. Piksarv, P. Saari, R. Trebino “Measurement of the spatiotemporal electric field of ultrashort superluminal Bessel-X pulses” *Optics and Photonics News*, **20**, 42 (2009).

Note: Publications prior marriage in year 2008 are published with maiden name Heli Valtna, later publications under name Heli Valtna-Lukner (except for one in Optics Letters where the name is Heli Valtna Lukner).

AUTHOR'S CONTRIBUTION

Here the author contribution to the original publications is indicated. The Roman numerals correspond to those in the list of publications.

- I Performing numerical calculations on localization of the wave fields.
- II Investigating the properties of the focused X wave and its modifications, writing the manuscript and preparing the figures under supervision of the coauthors.
- III Investigating the subject of generating superluminally propagating localized waves by means of diffraction grating and suggesting the specific optical element – cylindrical diffraction grating; providing figures 1, 4 and 5.
- IV Performing calculations on elaborated optical scheme, writing the manuscript and preparing the figures.
- V Participating in both experiments in Como, January 2008 and in Heraklion, April 2008.
- VI Preparing the experiment and consulting during the experiments, which were carried out in Atlanta. Preparing and supervising the numeric simulations.
- VII Suggesting the experiment idea, preparing and consulting during experiments, analyzing data, writing manuscript and preparing figures.
- VIII Preparing the experiments and consulting during the measurements.
- IX Preparing the experiments and consulting during the measurements.
- X Preparing the experiments and consulting during the measurements.
- XI Preparing the experiments and consulting during the measurements.
- XII Investigating the subject of generating superluminally propagating localized waves by means of diffraction grating and suggesting the specific optical element – cylindrical diffraction grating; providing figures 1, 4 and 5.
- XIII Preparing the experiment and consulting during the experiments, which were carried out in Atlanta. Preparing numeric simulations.

OTHER PUBLICATIONS OF DISSERTANT

- a. A. Dubietis, G. Tamošauskas, P. Polesana, G. Valiulis, H. Valtna, D. Faccio, P. Di Trapani, A. Piskarskas, “Highly efficient four-wave parametric amplification in transparent bulk Kerr medium” *Opt. Express* **15**, 11126–11132 (2007).
- b. H. Valtna, A. Dubietis, G. Tamošauskas, P. Polesana, J. Galinis, D. Majus, G. Valiulis, D. Faccio, P. Di Trapani, A. Piskarskas “Efficient four-wave parametric amplification and spatial soliton generation in transparent isotropic medium with Kerr nonlinearity”, *Lithuanian Journal of Physics* **47**, 403–410 (2007).
- c. H. Valtna, G. Tamosauskas, A. Dubietis, and A. Piskarskas, “High energy broadband four-wave optical parametric amplification in bulk fused silica”, *Opt. Lett.* **33**, 971–973 (2008).
- d. A. Dubietis, H. Valtna, G. Tamošauskas, J. Darginavičius and A. Piskarskas “Efficient ultrafast four-wave optical parametric amplification in condensed bulk media”, Springer Series in Chemical Physics, *Ultrafast Phenomena XVI Proceedings of the 16th International Conference, Palazzo dei Congressi Stresa, Italy, June 9–13, 2008*, eds. P. Corkum, S. De Silvestri, K. A. Nelson, E. Riedle, R. W. Schoenlein, **92**, 792–794 (2009).

I. INTRODUCTION

Light is an electromagnetic wave, whose propagation is governed by Maxwell's equations, or equivalently, by the wave equation. It follows from the equations that generally a wave in free space is subject to a lateral spread due to diffraction and a temporal spread in linear media due to dispersion. The smaller the initial spatial dimensions or temporal duration of the wave packet, the larger the spread will be.

In the first half of the 20th century several solutions to Maxwell equations and wave equation were found which describe a “nondiffracting” beam [1] – a monochromatic wave field with a bright peak surrounded by concentric rings in the transverse plane, described with Bessel function – or “distortion-free progressing waves” (pulses) in free-space [2, 3]. Very theoretical and abstract nature of the problem yielded a long silence on this subject.

This topic was not revisited until 1983 when it attracted the interest of James Neill Brittingham who claimed that he discovered a family of three-dimensional, nondispersive, source-free, classical electromagnetic pulses – focus wave modes (FWM) [4] – which propagate luminally along a straight line in free space. Brittingham's claim that FWM contain finite energy was soon shown to be faulty [5] because any finite energy solution of the wave equation will irreversibly lead to dispersion and the spreading of the energy [6, 7]. FWM with infinite energy could propagate infinitely far without any change but it would also require an infinitely large aperture. Using a real, finite aperture would limit both the field energy and propagation depth that the field's intensity profile could propagate without any apparent distortion or change. However, the depth of field of the distortion free propagation would still considerably exceed that of a Gaussian pulse with a comparable waist size.

The subject of localized waves – wave fields with inherent broad spectrum and localized “bulletlike” intensity maximum, which is tightly confined to area with dimensions in order of few wavelengths, propagate with a constant group velocity, without any spread or distortion up to infinite distances in theoretical limit – became a research field of its own rights [8]. In the following years a number of localized waves and their finite energy counterparts were derived (see [9] and references therein).

Aside general angular spectrum synthesis representation attempts to find more closed-form solutions, to generalize and unveil the underlying connections between different solutions and to find a structure inherent to the localized waves brought to attention the following techniques and schemes:

- i) Complex source points moving at a constant velocity parallel to the real axis of propagation [10];
- ii) “Sink-and-source charge” distributions moving superluminally along the propagation axis [11, 12, 13];
- iii) “Bi-directional plane wave decomposition” [14];

- iv) Transforming a diffracting solution of the isotropic-homogeneous (or free-space) scalar wave equation in $(n+1)$ -dimensional space into a non-diffracting solution in an n -dimensional space [15];
- v) Considering the angular spectrum of plane waves and analyzing new solutions as temporal derivatives of the fundamental X-wave [16, 17] yielding an unified description scheme [18];
- vi) (Lorentz) boost representation [9];
- vii) Composing localized waves as a superposition of inclined plane wave pulses integrated over the polar angle [13].

It is interesting to mention that the localized waves kinematically resemble hypothetical particles tachyons [19, 20, 21].

However, describing localized waves as superposition of plane waves in momentum space has contributed most to opening their physical nature and led to comprehensive classification scheme where any localized wave can be derived via a Lorentz transformation, as a relativistically aberrated and Doppler shifted version of a simple “seed” wave [22, 23, 24].

In the spectral representation the ‘building block’ of a three-dimensional localized wave is a Bessel beam [25] whose 3-dimensional field’s transversal cross-section is described by a Bessel function. In the axially symmetric case it becomes a 0th order Bessel function of the 1st kind. The latter can be generated as monochromatic superposition of plane waves, whose k -vectors, originating from the cone apex, lie uniformly on the surface of the cone. This is the simplest “diffraction free beam”, which can easily be generated experimentally using a conical lens called axicon, or by placing an annular aperture at the focal plane of a spherical lens [26] (for overview, see [27]).

A localized wave is obtained when synchronized Bessel beams with different frequencies and of appropriate cone angle are superposed. The specific functional dependence between cone angle and the frequency of the constituents of the wavefield arises from the dispersion relation and the requirement that the group velocity is constant. As we will see in the following chapter, those two obvious conditions constitute the genealogy where the waves are classified according to their group velocities to luminal, subluminal and superluminal families [22–24].

First experimental proof of a localized wave dates back to year 1992, when an acoustic supersonic localized wave, called an X-wave, was generated with an ultrasonic Bessel annular array transducer [28]. Existence of an electromagnetic or even optical localized wave remained questionable because of the ‘causality’ issues: quite often the spectrum of the wave field extend down to zero-frequencies and some fields are composed of forward and backward propagating plane wave constituents. The superluminal group velocity of some pulses, the X-wave for example, was thought to be unphysical as well. In the optical region additional obstacles rise while trying to generate a specific quasi-singular spatial distribution of plane wave constituents by factorizing spatial and temporal dependencies, as is the case with microwave antennas. Instead, the most straightforward approach for generating the suitable spatial distribution of the

plane wave constituents would require the use of a hypothetical circular slit with a frequency-dependent radius, an achromatic lens and an ultrabroadband light source of ultrashort pulses. Not to mention the recording device with approximately micrometer spatial and femtosecond temporal resolution to measure this complicated spatiotemporal profile of the field with necessary resolution.

For the first time the X-like spatiotemporal profile of the optical Bessel-X pulse was successfully measured in 1997 in an interferometric experiment, using an arc lamp as the ultrabroadband light source [29]. In the same year, and chronologically preceding the abovementioned experiment, the temporal behavior and nondispersive propagation of optical superluminal localized wave in linear media with normal dispersion was demonstrated in field autocorrelation experiment [30, 31]. With those experiments the existence of optical localized waves was explicitly proven.

In the following years more experiments in the optical domain were carried out. The superluminal group velocity of an ultrashort optical Bessel beam pulse was measured over its entire depth of field by recording consequent snapshots of the ionization front induced by the pulse; a group velocity of $1.111c$ was reported [32]. The spatial distribution of the electric field of the luminal focus wave mode, generated with a concave axicon and a diffraction grating, in order to obtain proper angular distribution of the plane wave constituents, was measured interferometrically [33]. Complete first and second order spatiotemporal autocorrelations of a sub- 10 -fs localized, Bessel-X, wave packet have also been measured [34]. (Experiments have been conducted also in microwave [35] and terahertz frequencies [36]).

Recently high-resolution spatiotemporal measurements of the Bessel-X pulse were reported using an interferometric technique called SEA TADPOLE [VI, XIII]. Similar, but lower resolution measurements were made using Shack-Hartman sensor in combination with the FROG technique to characterize the input pulse [37].

The superluminal group velocity of localized waves is in some sense just a “side effect”, while the most important feature of these fields is their spatial and temporal confinement and ‘diffraction free’ nature. Yet this intriguing property of superluminality has drawn lot of attention and started debates, even after being experimentally demonstrated several times [31–36, VI, X]. It has been questioned whether a superluminal group velocity *in free space* is in accordance with relativistic causality. The confusion arises from the fact that speed of light is highest possible propagation velocity for *signal*, but this limit is erroneously ascribed also to the *group velocity*, which need not be a physically profound quantity. In localized waves, which propagate rigidly with superluminal group velocity, the Poynting vector, which indicates the direction of energy flow, lies along the propagation axis. However, the energy flux, as required by causality, is not superluminal. Misconceptions about superluminality and causality have been addressed in [8, 13, 38, X].

It has been theoretically studied and experimentally demonstrated that Bessel pulses can accelerate or decelerate [39, VII] due to spherical aberration in

lenses, appropriately shaped nonlinear profiles of conical lens (axicon) or specific optical systems. Their bullet-like, central, intense apex and accompanying Bessel rings become smaller or larger as the pulse propagates, but the central spot of these pulses still remains localized and intense. Moreover, a decelerating Bessel pulse is also formed when an ultrashort pulse is diffracted off a centrosymmetric obstacle or aperture [40, 41, VIII, IX, XI]. If a plane wave pulse is diffracted off an opaque disc, the decelerating Bessel pulse appears as the well known Poisson-Arago spot.

In nonlinear optics it has been shown that the diffractive and dispersive spreading of an intense, focused ultrashort Gaussian wave packet can be balanced in transparent materials by a third order nonlinear processes and result in the *spontaneous* formation of a ‘nonlinear X wave’ [42]. This is very different from the linear case because the pulse shaping is done by the nonlinear process. The outcome depends on both the pulse parameters and the nonlinear properties of the media. The propagation of intense femtosecond pulses in nonlinear media must be analyzed with sophisticated numerical algorithms taking into account the space-time couplings in all coordinates (see [43], and references therein).

In the nonlinear optics community, the wave fields possessing nondiffractive properties in dispersive or nonlinear media are called conical waves. The subclass of conical waves which also propagate without temporal spread in a dispersive media are called X waves. It appears that the strong driving pulse which has spontaneously formed to a nonlinear X wave in media with third order nonlinearities will induce the temporal change in the refractive index. If a weak, linearly propagating probe pulse, which can be also centered to another wavelength, is delay-matched with the strong driving pulse, the refractive index change caused by the former will affect that linear probe pulse and shape it into a linear X wave, possessing the nondispersive and nondiffractive propagation properties [V].

Localized waves are not only intriguing for mathematical physics, physical and quantum optics [I] but have a number of prospective applications as well.

Bessel beams and pulses are used in optical trapping and particle micro-manipulation [44]; in fluorescence microscopy [45]; in biophotonics [46] for fs-optical transfection and “as an optical syringe” enabling multi-photon excitation processes in a needle like line of light [47]. In atomic optics Bessel beams can constitute a non-diffracting optical atom guide or applied as atom traps used for example to obtain Bose-Einstein condensates. For overview, see [48, 49].

Invariant propagation of the intense core of the Bessel pulse is used to drive and guide filaments in bulk media and gases [50]. These can be applied to write the waveguides into bulk media or to extend the longitudinal range of plasma channels created in the atmosphere. The latter are used, for example, for remote spectroscopy and lightning control [51].

Also, several linear optical imaging or image transfer setups were proposed in [8, 22, 52, 53, 54].

Various second and third order nonlinear processes were studied under Bessel pulse illumination and the conical nature of the localized waves has been utilized for non-collinear phase matching.

In this thesis we study superluminally propagating localized waves and accelerating and decelerating Bessel-type waves. These are somewhat distorted modifications of the Bessel-X pulse, which form in the apexes of expanding-collapsing toroidal waves. We remain in the scope of wave optics, where light is described with the scalar wavefunction, which obeys the wave equation and can be attributed to either linearly polarized electric or magnetic field component of the electromagnetic field.

The thesis is organized as follows:

In Chapter II we give an outline of the mathematical formalism, derive the localized wave solutions, introduce the genealogy, and study the principles of optical generation of localized fields. We briefly discuss the accelerating and decelerating Bessel-type waves.

We use the general term *light bullets* for propagation invariant localized waves and accelerating or decelerating Bessel-type waves throughout the thesis.

Chapter III is dedicated to spatiotemporal characterization techniques of the electric field with complicated spatial distribution and spatiotemporal coupling. We focus on comparing and studying interferometric techniques, which in combination with the FROG or SPIDER methods, allow for the full spatiotemporal measurement of the unknown electric field. We extend the treatment of the interferometric techniques to the case of stationary and ergodic input fields. By doing so we demonstrate that optical white-noise-like input signal can be used to characterize the unknown field formed by the optical system and to retrieve the frequency and hence also the impulse response of the optical system.

In Chapter IV we present an overview of optical experiments on both propagation invariant and accelerating light bullets. Applicability and outcomes of different interferometric and non-interferometric measurement techniques are discussed.

2. LOCALIZED WAVES

The localized waves are ultrawideband wave packets with both spatially and temporally tightly confined instantaneous intensity distribution propagating without any spread or distortion in free space or in linear media. In this chapter we make a brief introduction to the localized wave theory and give guidelines to derive a wavefunction of a localized wave through applying the constant group velocity condition to the general solution of the scalar wave equation. The genealogy of the localized waves and the physical principles for generating the waves are shown to arise also from combining the constant group velocity condition and the dispersion relation in the momentum space.

The properties of the accelerating and decelerating Bessel-type waves are discussed in the end of the chapter.

2.1. Mathematical description of the localized waves

Let us start from the scalar wave equation:

$$\Delta\Psi - \frac{1}{c^2} \frac{\partial\Psi}{\partial t^2} = 0.$$

The general solution to the scalar wave equation can be written as a superposition of the monochromatic plane waves:

$$\Psi(\mathbf{r}, t) = \int_{-\infty}^{\infty} d\omega \int \int_{-\infty}^{\infty} A(\mathbf{k}, \omega) \exp(i\mathbf{k}\mathbf{r} - i\omega t) d\mathbf{k}, \quad (1)$$

where $\mathbf{k} = \mathbf{e}_x k_x + \mathbf{e}_y k_y + \mathbf{e}_z k_z$ is the wave vector with projections k_x, k_y, k_z to orthogonal base vectors $\mathbf{e}_x, \mathbf{e}_y, \mathbf{e}_z$; $\mathbf{r} = \mathbf{e}_x x + \mathbf{e}_y y + \mathbf{e}_z z$ is the position vector in the coordinate space (x, y, z) ; t is time; ω is the frequency and $A(\mathbf{k}, \omega)$ the spectral distribution.

For the wavefield with axial symmetry, propagating along z -axis, it is convenient to write the general solution in the cylindrical coordinates:

$$\Psi(\rho, z, t) = \int_{-\infty}^{\infty} dk_z \int_0^{\infty} dk \Phi(k, k_z) J_0(\rho \sqrt{k^2 - k_z^2}) \exp(ik_z z - ikct), \quad (2)$$

where ρ is the radial coordinate and $\Phi(k, k_z)$ describes the spectral distribution. Here and hereafter the normalizing constants have been omitted.

The dispersion relation $\frac{\omega^2}{c^2} = k^2 = k_x^2 + k_y^2 + k_z^2$ reduces the number of free spectral variables in k -space. The axial symmetry allows one to eliminate one

more free variable as the integration over polar angle yields $J_0(\rho\sqrt{k^2 - k_z^2})$ – a zeroth order Bessel function of the first kind, and $k^2 = k_z^2 + k_\rho^2$. Hence, the 4-dimensional multiple integral in Eq. (1) reduces to double integral in Eq. (2).

The term $J_0(\rho\sqrt{k^2 - k_z^2})\exp(ik_z z - ikct)$ in Eq. (2) describes a monochromatic Bessel beam [25]. The localized waves, as any axially symmetric wave field, comprise of the Bessel beams. Let us study under which circumstances the axially symmetric wave field is a localized wave.

Let us assume that the group velocity $v_g = \frac{d\omega}{dk_z}$ is constant. From there it follows that the k_z and k must be bound linearly $c \frac{dk}{dk_z} = const$,

$$k = \frac{a}{c}k_z + b, \quad (3)$$

where c is the speed of light and, for the time being, a and b are arbitrary constants with dimensions of speed and wave number, respectively. In the (k, k_z) plane the condition (3) describes a line, with slope a/c and intercept b . In the (k, k_z, k_ρ) space the line becomes a plane. In the same space one can depict the domain of wave numbers as a cone $k^2 = k_z^2 + k_\rho^2$. (See Figure 1.)

Let us take a quick excursion to the (k, k_z, k_ρ) space. One point in the (k, k_z, k_ρ) space defines a monochromatic Bessel beam with wave number k and longitudinal component k_z and hence the cone angle $\theta = k_z/k$. The transversal component of the wave field is not free parameter, but is defined by the dispersion relation.

The intersection of a plane, Eq. (3), with the cone is a line. The power spectrum of a wave packet traveling at constant group velocity must be non-zero only along the line. The points of the support where the power spectrum of the wave packet is not zero, define the spatial distribution of plane waves in k -space. Hence, for propagation invariance of the intensity profile of the wave packet the support of its spectrum in the momentum space has to be a line coinciding with a conical section. (See Figure 1.)

The spectral distribution $\Phi(k, k_z)$ of the Bessel beam constituents of a localized wave can be written as a product of two functions: $\sigma(k)$, which is smooth and slowly varying function of the wave number and $\vartheta(k, k_z)$, which is rapidly changing, ideally a singular, function of k and k_z and determines the shape of the support

$$\Phi(k, k_z) = \sigma(k)\vartheta(k, k_z) = \sigma(k)\delta(k - \frac{a}{c}k_z - b). \quad (4)$$

In combination of Eq. (2) and Eq. (4) we obtain a general solution for axi-symmetric wave fields with constant group velocity:

$$\Psi(\rho, z, t) = \left| \frac{c}{a} \right| \exp\left(i \frac{bc}{a} z\right) \times \int_{\frac{bc}{c-a}}^{\infty} dk \sigma(k) J_0 \left[\rho \sqrt{k^2 - \left(\frac{c}{a}k - \frac{bc}{a}\right)^2} \right] \exp\left[ik \left(\frac{c}{a}z - ct\right) \right]. \quad (5)$$

One can see that the wavefunction defined by Eq. (5) depends on variables z and t through the combination $\frac{c}{a}z - ct$, which corresponds to the propagation variable $z - v_g t$, where v_g is the group velocity. Hence the modulus squared of the field expressed by Eq. (5) propagates invariantly with group velocity $v_g = a$. Let us define $\beta = v_g / c$, which is also the slope of the line in Eq. (3). The constant b is the intercept of the line, Eq. (3), with the k -axis. Here it is sufficient to note that the smallest wave number of the support of the spectrum is defined as $k_{\min} = \frac{b}{1 \pm v_g / c}$. The term $\exp\left(i \frac{bc}{a} z\right)$ constitutes a phase shift, invariant of the spectral variable k .

Several closed-form expressions are obtained from the general expression of the propagation-invariant fields, Eq. (5), by inserting specific power spectrum and restrictions to the group velocity v_g and the constant b . For example, assuming $b = 0$ and choosing exponentially decaying spectrum yields the well-known *X-wave* [28] or, with the same spectrum, $\beta = 1$ and $b \neq 0$, the *focused wave mode* [9]. However, the existence of the closed-form expressions is rather occasional. For number of experimentally feasible waves the field intensity distribution is to be calculated using numerical integration.

It has been shown that the singular support of the spectrum in the spectral distribution (4) yields infinite energy [6, 7, 22]. As a result, number of finite energy modifications were derived (see, for example, [8, 9, II] and references therein). The finite energy content is obtained by defining nonsingular support of the spectrum concentrated in the vicinity of the ideal singular support of the spectrum. Experimentally more obvious solution would be truncating the fields's amplitude. But, mathematically the truncating would require calculating diffraction integrals, which most often can be taken only numerically while, making the spectrum nonsingular allows one to choose suitable function, which would decay rapidly in the vicinity of the support line and for which the closed-form expression of the field can be found with the help of integration tables. Due to the finite energy content the "modified" localized waves their intensity will slowly decrease over the propagation, yet, often the dimensions of the intense peak at chosen height (for example half maximum or $1/e$) remains unchanged and the field depth of invariant propagation exceeds considerably that of the common focused fields.

Despite the existence of several closed form solutions, in most cases the finite energy modification does not provide a better approximation to the localized wave field measured in experiment than the idealistic infinite energy solution. Instead, calculating the “modified” field profiles sets higher demands to the computing engine. In experiment, generally there exists a volume behind the optical system, where the diffraction effects caused by the aperture are negligible and field can be very well approximated to the ‘ideal’ one, with a singular support of the spectrum. Under these circumstances it is most practical to simulate the field by calculating the field intensity distribution of the ‘ideal’ field and to insert the spectrum of a specific light source to the general solution for axisymmetric wave fields, Eq. (5).

The finite energy modifications can be seen as sums of ideal, infinite energy localized waves. If the function describing spectral distribution is not tightly localized around singular support line, but is wider, the wave field constitutes a sum of localized waves with (appreciably) different group velocities. Instead of invariant propagation, space-time focusing is established. The subject is treated in more detail in chapter II of [8] and references therein.

If the Bessel beam constituents of the wave field, Eq. (5), are synchronized, i. e. their initial phases are correlated, an ultrashort propagation-invariant wave field is formed in coordinate space. Such a field can be generated by means of a femtosecond pulse and optical system shaping suitable support of the spectrum. Often some of the prerequisite conditions is not met. The propagation-invariant fields with variable spectral coherence properties are considered in [22, 55, 56].

2.2. Geneology and optical generation principles

In previous section we derived general expression for axially symmetric propagation-invariant fields called localized waves, Eq. (5). Let us now classify the localized waves into four families based on the shape of the support of the spectrum in momentum space – hyperbola, line, parabola or ellipse [24]. The shape of the support of the spectrum is directly related to the group velocity of the wave field, but does not depend on the exact shape of the power spectrum or carrier frequency of the wave field. The principles of experimental generation of the wave field arise from the shape of the projection of the support line on (k_z, k_ρ) -plane. This is the angular distribution of the plane wave, or the Bessel beam, constituents.

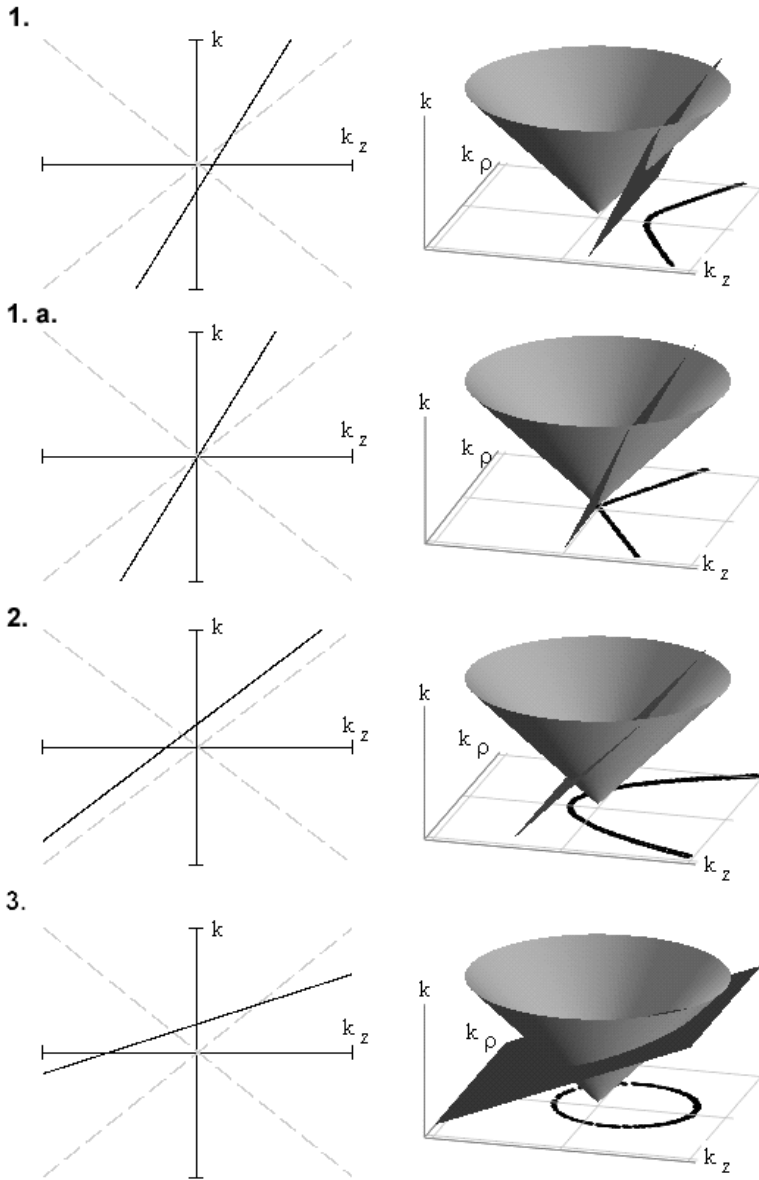


Figure 1. The classification of the localized waves into 4 families based on the group velocity and shape of the support of the spectrum. 1. – generic superluminal family with hyperbolic support of the spectrum; 1. a. – Subfamily of superluminal pulses with a propagation-invariant wavefunction with straight-line support of the spectrum; 2. – luminal family with parabolic support of the spectrum; 3. – subluminal family with elliptical support of the spectrum.

The names of specific localized wave solutions refer to certain closed form expressions with certain power spectrum and shape of the support of the spectrum. Those cannot be considered as a basis of wave field classification. Rather, the closed-form solutions serve as a well-known and thoroughly studied model fields for a specific family.

In previous section we showed that the group velocity of a wave field is constant if the wavenumber and its longitudinal projection are combined linearly Eq. (3). The slope of the line is group velocity v_g in the units of c , and the intercept b was related to the smallest wave number. Intersection of the dispersion cone and the plane defined by Eq. (3) constitutes the support of the spectrum in the (k, k_z, k_ρ) space. Let us consider following special cases.

2.2.1. Generic superluminal family

The group velocity is *superluminal*, hence the slope of the line (3) is $\beta > 1$. Intercept b can take arbitrary values, except being equal to zero, $b \neq 0$. The support of the spectrum in the (k, k_z, k_ρ) space and also its projection to the (k_z, k_ρ) -plane is *hyperbola*. See **1.** on **Figure 1**. The smallest wave number $k_{min} \geq c \times b / (v_g + c)$, if $b > 0$ and $k_{min} \geq c b / (v_g - c)$ if $b < 0$. The values of the group velocity range from c to infinity, $c < v_g < \infty$.

The representatives of this family are the cylindrical wave of infinite group velocity [57] and focused X wave (FXW) [9]. Both have exponentially decaying, towards higher frequencies, spectrum shifted to optical region. The cylindrical wave can be considered as a “seed” wave to other superluminally propagating localized waves, which can be obtained via Lorentz transforming the cylindrical wave [24].

The wavefunction of the FXW is obtained by inserting spectral function

$$\Phi_{FXW}(k, k_z) = \exp[-\gamma(\beta k - k_z)\Delta] \delta(k - k_z\beta - k_{z0} / \gamma)$$

into Eq. (2) and with the help of Laplace transform table, for example [58], the closed form expression for FXW is obtained:

$$\Psi_{FXW}(\rho, z, t) = \frac{\exp\left(-|k_{z0}| \sqrt{\rho^2 + [\Delta - i\gamma(z - v_g t)]^2}\right)}{\sqrt{\rho^2 + [\Delta - i\gamma(z - v_g t)]^2}}, \quad (6)$$

$$\times \exp\left[i\gamma k_{z0} \left(\frac{v_g}{c} z - ct\right)\right]$$

where Δ is a positive constant characterizing the length of the pulse and lowest wavenumber k_{min} is related to k_{z0} as

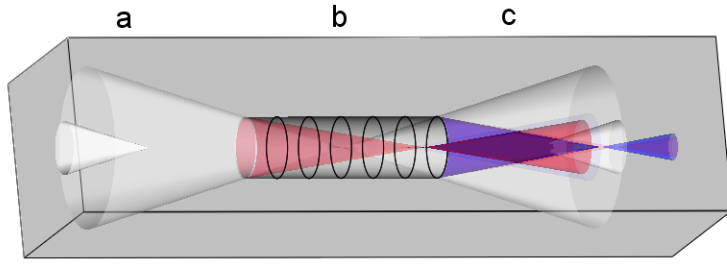


Figure 2. 3D scheme of the superluminal localized wave generator. Ultra wideband convergent conical light pulse (in region a) enters a cylindrical diffraction grating (b). The localized wavefield is formed within the dark rhombic region c. Brighter cones coming out from the generator depict propagation of the 0th diffraction order and – in accordance with the range of the source spectrum – the “red” and “blue” boundary surfaces of the 1st diffraction order. [III]

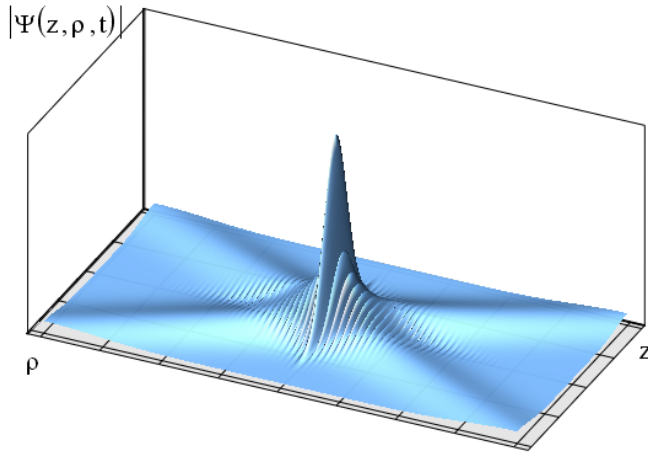


Figure 3. The modulus of the SpLW. Dependence on z (increasing from the left to right) and a lateral coordinate ρ while $ct = 0$ is depicted. Plots are normalized and numerical values of the parameters are: the pulse velocity $v_g = 1.048c$; the Gaussian spectrum with $FWHM = 47 \text{ nm}$ is centered on 800 nm . The plotting range for the lateral coordinate ρ is $144 \mu\text{m}$ while for the axial coordinate z it is $72 \mu\text{m}$. The gray shading in both plots is a result of ‘lighting’ used to better reveal the relief of the surface. The modulation pattern in the region of the central maximum appears due to the relatively narrow spectrum.

$$k_{\min} \geq -k_{z0} \frac{\sqrt{\beta+1}}{\sqrt{\beta-1}}.$$

In the limiting case $v_g \rightarrow \infty$, the FXW described with Eq. (6) becomes the cylindrical wave; if $k_{z0} = 0$, the X-wave and if $v_g \rightarrow c$, $k_{z0} > 0$ the focus wave mode.

It has been demonstrated that the hyperbolic support of the spectrum can be generated exactly by means of a diffraction grating, whereas the group velocity is related to the angle of incidence towards grating normal $\theta_i = \text{asin}(\beta^1)$. In order to obtain axially symmetric field with almost equal to c , the cylindrical diffraction grating with circular grooves engraved to the inner surface of a reflective cylinder must be illuminated with a Bessel-X pulse. (See Figure 2) Illuminating a transmissive cylindrical diffraction grating normally, with cylindrical impulse converging towards the optical axis, will result in formation of the cylindrical wave of infinitely large group velocity. [III, IV, XII]

The modulus of an experimentally feasible superluminally propagating localized wave (SpLW) is depicted on

Figure 3. The exponentially decaying spectrum of FXW has been replaced with a Gaussian one and the numerical values of the parameters have been chosen suitably for an optical realization.

2.2.2. Subfamily of superluminal pulses with a propagation-invariant wavefunction

If the plane (3) in (k, k_z, k_ρ) -space has slope $\beta > 1$ on (k, k_z) plane, but it crosses the origin, i. e. the intercept $b = 0$, the group velocity is *superluminal*, but the support of the spectrum in the (k, k_z, k_ρ) space and also its projection to the (k_z, k_ρ) -plane degenerates from hyperbola to a *straight line*. This means that all the plane-wave constituents of the localized wave propagate under the same fixed angle θ , called cone angle, relative to the z-axis. See **1. a.** on Figure 1. The smallest wave number of the support of the spectrum is 0.

The group and phase velocities of the localized waves of this family are equal and thus the field amplitude as well as the intensity distribution propagate invariantly.

Well known X-wave [59] and Bessel-X wave [53] belong to this family. The spectrum of the X-wave is white, whereas that of the Bessel-X pulse is Gaussian, having central wavelength in the optical region.

The wavefunction of the X-wave can be derived taking $k_{z0} = 0$ in Eq. (6):

$$\Psi_X(\rho, z, t) = \frac{1}{\sqrt{\rho^2 + [\Delta - i\gamma(z - v_g t)]^2}} \quad (7)$$

It is shown in [53] that the wave function of the Bessel-X pulse can be derived by inserting a Gaussian-like spectral function

$$\Phi_{BX}(k, k_z) = \frac{d_0}{\sqrt{2\pi}} \sqrt{\frac{k}{k_0}} \exp\left[d_0^2 (k - k_0)^2 / 2\right],$$

where d_0 is the pulse's reciprocal bandwidth and k_0 the carrier wavenumber, into Eq. (2). With a minor approximation, a resultant closed-form equation yields

$$\begin{aligned} \Psi_{BX}(\rho, z, t) = & \sqrt{1 + i \frac{d}{k_0 d_0^2}} \exp\left[-\frac{1}{2d_0^2} (\rho^2 \sin^2 \theta + d^2)\right] \\ & \times J_0\left[\left(1 + i \frac{d}{k_0 d_0^2}\right) \rho k_0 \sin \theta\right] \exp(ik_0 d) \end{aligned} \quad (8)$$

where $d = zc / v_g - ct$.

The support of the spectrum of the Bessel-X pulses can be generated by means of annular slit and achromatic lens or conical lens called axicon, neglecting the dispersion of the axicon material. The Bessel-X pulses are most widely studied localized waves and are generated in several experiments [29, 31, 32, 34, 37, VI, XIII]. The field amplitude of an optically realizable Bessel-X pulse resembles that of the FXW depicted on Figure 3.

2.2.3. Subluminal family

If the slope of the line (3) is smaller than 1, $\beta < 1$, the group velocity $v_g < c$ is subluminal and intercept $b < 0$. The support of the spectrum in the (k, k_z, k_ρ) space and also its projection to the (k_z, k_ρ) -plane is ellipse. See 3. on Figure 1. The wave numbers vary in the range $k_{min} \geq c b / (v_g + c)$ and $k_{max} \leq c b / (v_g - c)$; the group velocity varies in the range from zero to c , $0 < v_g < c$.

A Mackinnon pulse [60] is a representative of this family of localized waves. In principle, it is possible to generate the support of the spectrum in the finite bandwidth by combining dispersive, refractive and diffractive optical elements.

A Lorentz transformation “seed” to a localized wave in this family is monochromatic spherical standing wave, with $v_g = 0$. The larger the speed of the reference frame of the seed wave in respect to the laboratory frame, the larger the group velocity and the bandwidth of the wave in the laboratory frame. [24]

2.2.4. Luminal family

If the slope of the line in Eq. (3) is equal to 1, $\beta = 1$, the group velocity $v_g = c$ is luminal and intercept $b > 0$. The support of the spectrum in the (k, k_z, k_ρ) space and also its projection to the (k_z, k_ρ) -plane is parabola. (See 2. on Figure 1.) The smallest wave number is $k_{min} \geq -b/2$.

A seed to the localized waves in the luminal family is a monochromatic collimated beam propagating in an ultrarelativistic frame towards negative direction of the z axis. In the laboratory frame it turns out to be a wideband localized wave propagating almost luminally in the positive direction of the z axis. [24]

Well known and extensively studied *focused wave mode* (FWM) belongs to this family of the localized waves. Inserting the spectrum

$$\Phi_{FWM}(k, k_z) = \exp[-\Delta(k + k_z - b/2)] \delta(k - k_z - b/2) \times \Theta(k^2 - (k_z - b/2)^2)$$

into the Eq. (2) and integrating, yields the wavefunction of the FWM:

$$\Psi_{FWM}(\rho, z, t) = \frac{\exp\{-\rho^2 b/2[2\Delta - i(z - ct)]\}}{2\Delta - i(z - ct)} \times \exp[-ib(z + ct)/2] \quad (9)$$

The field amplitude of optically realizable FWM resembles that of the FXW depicted on Figure 3.

The support of the spectrum of the focused wave mode can be generated in a finite spectral range by combining axicons, diffraction gratings and glassy samples or wedges with suitable dispersion curve. The field amplitude of a wideband luminal localized wave has been measured in interferometric experiment [33].

2.2.5. Negative group velocities

A specific shape of the support of the spectrum corresponds to a fixed value of the group velocity, regardless in which region of the support of the spectrum lays the power spectrum. The hyperbolic, parabolic and elliptic support lines can extend to both negative and positive k_z values.

From here it follows that even if the power spectrum lies in the region of the negative k_z values, i. e., the Bessel beam constituents propagate towards negative direction of the propagation axis z , the resulting wave field propagates at

specified group velocity, which may be sub-, super- or simply luminal, towards the positive direction of the propagation axis.

As an alternative, one can choose the group velocity negative, which means the slope $\beta < 0$, and choose the angular distribution of the Bessel beam constituents on the support line to the region where the k_z is positive. See also [61].

2.2.6. Asymptotic behavior of the wavefunctions

Let us study the asymptotic behavior of the closed form localized wave solutions introduced above. In the first column of the Table 1 there are shown the radial asymptotic behavior at instant $t = 0$, position $z = 0$ and $\rho \rightarrow \infty$ of the modulus of a wavefunctions of FXW, X-wave, Bessel-X pulse¹ and FWM. In the second column is shown the longitudinal asymptotic behavior, $t = 0$, $\rho = 0$ and $z \rightarrow \infty$, of the same wavefunctions.

Table 1. Asymptotic behavior of the closed-form localized wave solutions.

$\Psi(\rho \rightarrow \infty, z = 0, t = 0)$	$\Psi(\rho = 0, z \rightarrow \infty, t = 0)$
$ \Psi_{FXW}(\dots) \infty \sim \frac{\exp(- k_{z0} \rho)}{\rho}$	$ \Psi_{FXW}(\dots) \infty \sim \frac{1}{z}$
$ \Psi_X(\dots) \infty \sim \frac{1}{\rho}$	$ \Psi_X(\dots) \infty \sim \frac{1}{z}$
$ \Psi_{BX}(\dots) \infty \sim \frac{\exp(-const\rho^2)}{\rho}$	$ \Psi_{BX}(\dots) \infty \sim \sqrt{z} \exp(-const \times z^2)$
$ \Psi_{FWM}(\dots) \infty \sim \exp(-b\Delta\rho^2)$	$ \Psi_{FWM}(\dots) \infty \sim \frac{1}{z}$

One can see that the FXW, Bessel-X pulse and FWM exhibit high localization in transversal plane, where the decay is faster than exponential dependence of the coordinate, $\exp(-\rho)$. In the longitudinal dimension the decay of all the wave fields, except Bessel-X pulse equals that of the Bessel function being reciprocal to the longitudinal coordinate. Different from the other localized wavefields considered, the Bessel-X pulse is comprised of plane wave pulses, where all the plane-wave constituents travel under the same angle towards optical axis. The decay in both longitudinal and transversal cross-sections is exponential.

¹ An approximation was made to obtain the closed-form wavefunction of the Bessel-X pulse. However, this should not affect the asymptotic behavior studied in this chapter.

However, the decay along the X-branches of the Bessel-X pulse is weak, being reciprocal to the inverse coordinate.

Hence, the localized waves can exhibit high localization in two spatial coordinates (the radial ones) out of three. This is important and can be utilized, for example, in image transfer and detection with ultrafast temporal shutter.

2.3. Accelerating and decelerating Bessel-type waves

Accelerating and decelerating Bessel-like pulses are also shown to arise from diffraction off the annular obstacles or apertures [40], spherical aberration in lenses, and appropriately shaped nonlinear profiles of axicons [62]. Basically, if a surface of an axicon deviates from the cone, yet remains axially symmetric towards optical axis – for example the Gaussian-shaped microaxicon profiles [34, 63], or simply spherical tip of an axicon, will result in accelerating or decelerating Bessel-type pulses. The accelerating and decelerating pulses were measured in experiments [41, VII–XI].

A method to generate Bessel-X pulses relies on the fact that its Fourier transform is a ring. Hence, illuminating an annular aperture with ultrashort pulse and placing it to the focal plane of an achromatic lens will form the localized wave called Bessel-X pulse. In this arrangement the lens will transform spherical wave fronts emerging from the annular slit to double conical surface.

Let us discard the lens and analyze the propagation of the ultrashort pulse behind an annular slit. For intuitive description we can use the Huygens-Fresnel principle. Each point of the slit can be considered as a source of spherically expanding waves whose temporal profile is governed by that of the primary wave. This will yield an expanding, semi-toroidal wave-field immediately behind the slit.

As the pulse propagates further, the tube radius of the half torus becomes larger than the annular-slit radius R , and at times $t > R/c$ the wave-field evolves like a spindle torus, i.e., different parts of the torus start to overlap. Of course, the wave-field is treatable as a mathematical surface only for infinitesimally short delta-like pulses in time. Real ultrashort pulses are at least several cycles long, and so yield an interference pattern in the overlap region (see insets of Figure 4). The radial dependence of the field in the interference region is approximately a zeroth-order Bessel function of the first kind.

As the wavefield evolves in time, the intersection region propagates along the z -axis and the angle between the normal of the torus surface and the z -axis (θ) decreases. For ultrashort pulses, this intersection region is small, and the angle θ is approximately the same for all points within it at a given instant. Therefore the field in the intersection region is approximately equivalent to the center of a Bessel beam or the apex of a Bessel-X pulse (see also [40]). The smaller the angle θ – also called the *axicon angle* – the larger the spacing between the Bessel rings and the smaller the superluminal velocity of the pulse. Hence, an annular ring transforms an ultrashort pulse into a decelerating Bessel

wavepacket propagating along the z -axis. Of course, outside of the intersection region, where there is no interference to generate phase fronts that are perpendicular to the z -axis or a Bessel profile, the phase and pulse fronts expand with a constant velocity c and propagate in their normal directions.

It is also possible to generate such fields by axicon in combination with a lens. If the lens is concave, the field behind it evolves similarly to what was described above, and a decelerating pulse is generated. On the other hand, a convex lens (see Figure 4) results in an increasing angle θ as the pulse propagates and hence an accelerating pulse. In both cases their bullet-like, central, intense apex and accompanying Bessel rings become smaller or larger as the pulse propagates, depending on whether the torus shrinks towards a ring or expands towards a sphere. But the central spot of these pulses is still localized and intense over a propagation distance considerably longer than that of a Gaussian beam with a comparable waist size.

Let us present here the mathematical description of the accelerating pulses for the case of ultrashort pulses for which is sufficient to considering only the intersection region close to the optical axis. Here the field is approximately conical, or it is a cylindrically symmetrical superposition of plane waves propagating at a fixed angle θ to the z axis. In this case, the field can be described using the known expression for the field of a Bessel-X pulse

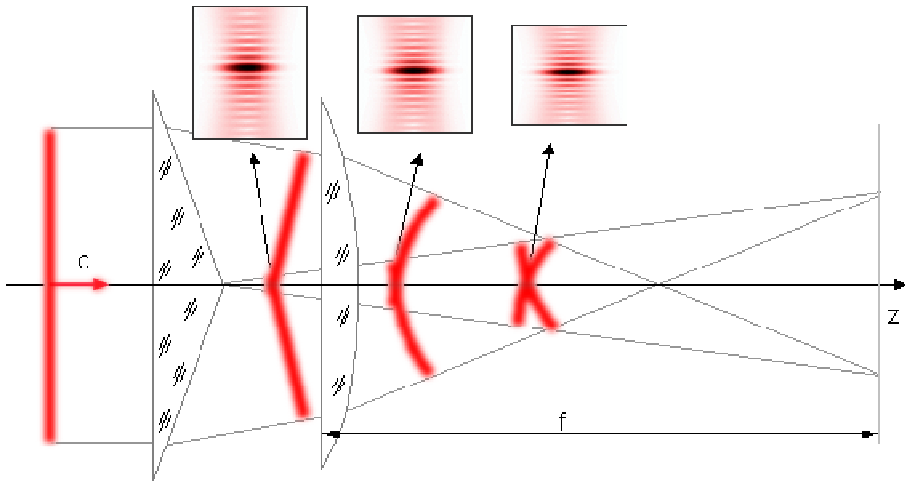


Figure 4. Schematic of the formation of accelerating pulses from a plane-wave pulse moving to the right with velocity c . The red strips depict the pulses' intensity profiles in space at four different times. The conical surface of the axicon transforms the plane-wave pulse into a Bessel-X pulse, and the convex lens then yields the accelerating pulse. The inset plots show the expected intensity vs. x and t for three different positions z . [VII]

$$\Psi(\rho, z, t) = \int_0^{\infty} d\omega G(\omega - \omega_0) J_0 \left[\frac{\omega}{c} \rho \sin \theta(z) \right] \exp \left\{ i \frac{\omega}{c} [z \cos \theta(z) - ct] \right\}$$

where ρ , z , and t are the spatial (cylindrical) and temporal coordinates, and $G(\omega - \omega_0)$ is the (Gaussian-like) spectrum of the pulse having a central frequency ω_0 . However, unlike the case of the Bessel-X pulse, here the axicon angle depends on the propagation distance z from the lens with the focal length f as $\theta(z) = \arctan[|f - z|^{-1} \tan \theta_a]$, where θ_a is the axicon angle without the lens. Because the group velocity of the wave-packet along the z direction is given by $v_g = c/\cos(\theta)$, the group velocity of the Bessel pulses will be superluminal and accelerate if f is positive and decelerate if f is negative. The approximations made in this approach are valid as long as the pulse duration τ is much shorter than its characteristic time of flight given by f/c .

3. INTERFEROMETRIC TECHNIQUES FOR SPATIOTEMPORAL MEASUREMENTS OF ELECTRIC FIELD

In this chapter we give an overview of the methods and techniques used to measure the spatiotemporal dependence of electric field of the light bullets – ultrashort optical pulses with a localized, bullet-like intense core and a residual double-conical spatial intensity profile.

To reconstruct the electric field of an optical pulse in space and time one needs to measure both the field's amplitude and phase over the space domain of interest. It is sufficient to determine the field's amplitude and the phase in either the spectral or time domain because the amplitude and the phase in the other can be unambiguously reconstructed using the Fourier transformation. Although spatiotemporal couplings should not be ignored, let us, for the time being, acquaint ourselves with the issues of temporal and spatial measurements separately.

First we will discuss, the temporal measurements. In the optical region the electric field oscillates about 10^{15} times per second, thus measuring the field with an oscilloscope would require sub-femtosecond resolution, which cannot be reached. To date the best temporal resolution, achieved in streak cameras is ~ 100 fs, but they record the intensity versus time and thus lose the phase information. Another option is to measure the unknown pulse using a cross-correlation technique with shorter pulse, but this is often not possible because there is no shorter reference pulse available in the femtosecond regime. And again, this would record only the temporal amplitude profile of the field. As a result, a method to fully characterize ultrashort optical pulses needs to encode the phase, which is lost in time-averaging intensity detection, in a measurable intensity from which it can be unambiguously reconstructed.

Until recently, the second order autocorrelation measurement was most widespread method to characterize the temporal behavior of an ultrashort pulse. It allows one to find the root-mean-square duration of the pulse but the field's (spectral) phase – the only thing that separates, for example, δ -like pulse from white noise – cannot be determined. But today there are two self-referencing methods that measure both the field amplitude and phase of an unknown pulse. These are: spectrally resolved autocorrelation, called Frequency Resolved Optical Gating (FROG) [64, 65, 66] and spectral shearing interferometry, called SPectral Interferometry for Direct E-field Reconstruction (SPIDER) [67, 68]. (See also [69] for an overview.) In addition, new methods, for example, multiphoton intrapulse interference phase scan (MIIPS) [70] have recently been introduced. Similar to the autocorrelation, self-referencing methods are based on instantaneous nonlinear processes and require relatively high pulse energies.

Now, having in hand a temporal pulse characterization method, in a straightforward manner one could simply sample the spatial domain of interest with, say using a FROG or SPIDER device to yield the spatiotemporal behavior of

the pulse. Unfortunately there are technical difficulties with spatial resolution, lack of intensity, setup stability *etc.* Instead, a number of spatiotemporal pulse characterization techniques combined with FROG and SPIDER are emerging: two-dimensional sharing interferometry [71], wave-front sensing with Shack–Hartmann detector [72] and complete retrieval of the optical amplitude and the phase using (k_{\perp}, ω) spectrum (CROAK) [73, 74], for example. In this thesis we focus on *linear interferometry* between a suitably chosen and pre-characterized reference wave field and the ‘unknown’ wave field.

In the following sections of this chapter we introduce the principles of spatial² interferometry, spectral interferometry and a spatial-spectral interferometric technique, called SEA TADPOLE. All the methods yield the phase of the unknown wave field in respect to the reference one. We show that the methods can be applied for finding the optical setup’s response function or measuring the spatial distribution of the input field.

We study the performance of the interferometric measurement techniques under illumination with spatially coherent but spectrally non-correlated fields. This means that the field amplitude is random function of time yet the phase fronts are uniform in transverse direction. Hence, the results and properties discussed in this chapter are valid not only for coherent laser light, which is an important special case, but also applicable to the output of white light laser or spatially filtered (broad-spectrum) arc lamp. In the end of this chapter we discuss the ranges of application of different methods.

3.1. Spatial interferometry

Spatial interferometry, or simply interferometry, yields the interference pattern between a reference and unknown wave field in coordinate space, which allows one to resolve the phase difference between the two fields.

3.1.1. The method

Let us assume that the input field is spatially coherent and has a broadband spectrum, but is spectrally non-correlated meaning that the spectral phases of the frequency components are not correlated. To this end we add a stochastic phase term $\phi(\omega)$ in the mathematical expression for field. We assume that the field remains statistically stationary and ergodic, which means that statistical ensemble averages can be substituted with averaging over time. Let us note that

² To draw a distinction between use of the term interferometry as a general method, ‘interferometry’ observed in coordinate space and ‘spectral interferometry’ measured with spectrometer in the frequency space, we use the term ‘spatial interferometry’ for the second case. In this thesis we also make distinction between spatial interferometry and its variant called spatial-spectral interferometry.

a train of ultrashort pulses with fixed intervals between the peaks, delivered, for example, by an ideal femtosecond laser, can be also treated as a stationary signal, if the initial phase of the pulse train varies from realization to realization. In the following, the phrase ‘propagation of the field’ is used to indicate the ‘propagation of field’s intensity distribution’.

Let us explicitly examine the setup based on the Mach-Zehnder interferometer [75], where the incident field is divided into two by beam splitter. A linear optical system generates the “unknown field” in the object arm while second part of the input field serves as a reference: it travels on the reference arm and its wavefront is unchanged, only its delay in respect to unknown field can be adjusted. We assume that the auxiliary optical elements – beam splitters and mirrors – do not cause any additional and unwanted distortions to the fields. The interference pattern of the spatially superposed and delay-matched fields can be measured with a time-averaging 2D matrix intensity-recording device at a fixed position on propagation axis (see Figure 5). This setup also assures that in case the field intensities are low enough, the propagation through the optical system in the object arm remains linear and all the spectral components of the unknown wave field are also present in reference field. With these conditions met, the resolved spatial phase will not be distorted.

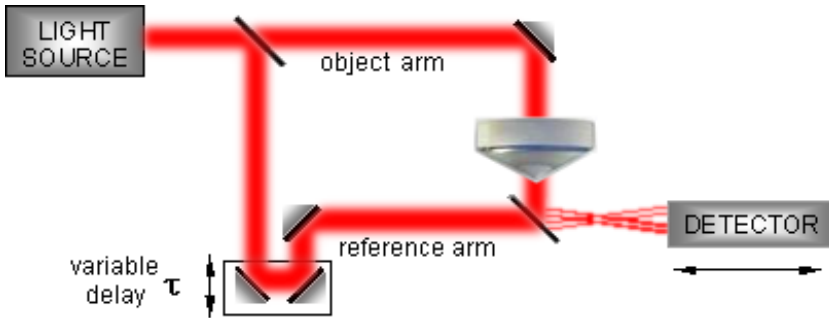


Figure 5. Spatial interferometry setup based on a Mach-Zehnder interferometer. The unknown field in the object arm is formed by means of the conical lens called axicon. In the reference arm there is a variable delay line. It is assumed that the auxiliary optical elements do not cause any additional distortions to the phase front. In the interferometer’s output, the fields are overlapped both spatially and temporally. The resulting interference pattern $I(x,y)$ at a fixed z and t is recorded with a time-averaging 2D matrix intensity detector.

We denote the complex unknown field as $E_{unk} = E_{unk}(x, y, z, t)$ and the complex reference field as $E_{ref} = E_{ref}(x, y, z, t + \tau)$, where t stands for time, τ for adjustable delay and x, y, z for space coordinates, which in a more compact notation are referred to as the vector $\mathbf{r} = \mathbf{e}_x x + \mathbf{e}_y y + \mathbf{e}_z z$ with orthogonal unit vectors $\mathbf{e}_x, \mathbf{e}_y$ and \mathbf{e}_z . The z -axis is directed along the optical axis which is also the propagation direction of the fields. With the time-averaging 2D matrix detector one can record the intensity $I=I(x,y)$ at a fixed position z and a fixed delay τ .

$$\begin{aligned} I &= \left\langle \left(E_{ref} + E_{unk} \right)^* \left(E_{ref} + E_{unk} \right) \right\rangle_t \\ &= \left\langle |E_{ref}|^2 \right\rangle_t + \left\langle |E_{unk}|^2 \right\rangle_t + 2 \operatorname{Re} \left(\left\langle E_{ref}^* E_{unk} \right\rangle_t \right) \end{aligned}$$

where $\langle F \rangle_t = \lim_{T \rightarrow \infty} \frac{1}{2T} \int_{-T}^T F(t) dt$ denotes time the average of the argument function F and the ergodicity of fields E_{unk} and E_{ref} allows us to replace ensemble averages with time averages. The first two components $\left\langle |E_{ref}|^2 \right\rangle_t$ and $\left\langle |E_{unk}|^2 \right\rangle_t$ are the time averaged intensities of the reference and unknown wave fields which can be easily recorded separately by blocking the other arm of the interferometer. The argument of the third component, the interference term,

$$\begin{aligned} \left\langle E_{ref}^* E_{unk} \right\rangle_t &= \left\langle E_{ref}(x, y, z, t + \tau)^* E_{unk}(x, y, z, t) \right\rangle_t, \\ &= \Gamma(x, y, z, \tau) \end{aligned}$$

is the mutual coherence function of the two fields [76, 77]. Full 4-dimensional image is obtained while scanning both the z and τ parameter values and properly augmenting analyzed intensity $I(x,y)$ traces.

Conveniently, with a suitably chosen input and thus also a reference wave field, there is a simple and elegant method for measuring the additional phase generated by the optical system in object arm. As in the holography, the field on the reference arm is comprised of plane waves [22, 29, 33]. All plane-wave components propagate parallel to the optical axis and their phase fronts are flat. Following the example in chapter 4 from [77], let us represent $E_{ref}(\mathbf{r}, t)$ as a Fourier' integral with respect to the time variable:

$$E_{ref}(x, y, z, t + \tau) = \int_{-\infty}^{\infty} s(\omega) e^{i\omega(t+\tau) - i\frac{\omega}{c}z + i\phi(\omega)} d\omega, \quad (10)$$

where the spectral density is defined by averaging the modulus square of the function $s(\omega)$ over different realizations of the field $\left\langle s(\omega)^* s(\omega) \right\rangle_t = S(\omega)$, and the function $\phi(\omega)$ denotes the (stochastic) spectral phase originating directly

from the light source and it is the same for both the reference and the unknown fields. The function $s(\omega)$ is stochastic, as it varies from one realization to another. The spectral density $S(\omega)$, defined as the average over different realizations of the function $s(\omega)$, is deterministic.

The unknown field comprises plane waves with an arbitrary angular distribution introduced to the field by the optical system in the object arm. The electric field is given by:

$$E_{unk}(x, y, z, t) = \int_{-\infty}^{\infty} s(\omega') F(\mathbf{r}, \omega') e^{i\omega' t + i\varphi(\mathbf{r}, \omega') + i\phi(\omega')} d\omega', \quad (11)$$

where $F(\mathbf{r}, \omega')$ is a real function expressing the spatial distribution and $\varphi(\mathbf{r}, \omega')$ an additional phase introduced by the optical system. The transmittance of the optical system is taken into account by the function $F(\mathbf{r}, \omega')$.

To explain the definition of the unknown field let us write it as a wave field that is a general solution $g(\mathbf{r}, t)$ to the scalar wave equation, so it is a sum of plane waves:

$$g(\mathbf{r}, t) = \iiint_{-\infty}^{\infty} A(\mathbf{k}, \omega) \exp[i(\mathbf{k}\mathbf{r} - \omega t)] d\omega d\mathbf{k},$$

where the real function $A(\mathbf{k}, \omega)$ denotes the spectrum. Let us separate the temporal frequency spectrum $\sigma(\omega)$ and the part describing the angular distribution $\Xi(\mathbf{k}, \omega)$:

$$A(\mathbf{k}, \omega) = \sigma(\omega) \Xi[k_x(\omega), k_y(\omega), k_z(\omega)].$$

Now, we can denote the field as $F(\mathbf{r}, \omega) = \left| \iiint \Xi(\mathbf{k}, \omega) \exp[i(\mathbf{k}\mathbf{r})] d\mathbf{k} \right|$ and $\varphi(\mathbf{r}, \omega) = \arg \left(\iiint \Xi(\mathbf{k}, \omega) \exp[i(\mathbf{k}\mathbf{r})] d\mathbf{k} \right)$.

As an illustrative example, we assume cylindrical symmetry and propagation-invariant waves, where the angular distribution of the plane wave constituents is $\theta_F(\omega)$. For this case we can write the field as follows:

$$g(\mathbf{r}, t) = \int_0^{\infty} s(\omega) J_0 \left[\sqrt{x^2 + y^2} \omega \sin \theta_F(\omega) \right] \exp \left[i\omega t - i \frac{\omega}{c} z \cos \theta_F(\omega) \right] d\omega. \quad (12)$$

From the given equation $F(\mathbf{r}, \omega) = J_0 \left[\sqrt{x^2 + y^2} \omega \sin \theta_F(\omega) \right]$ and

$$\varphi(\mathbf{r}, \omega) = -\frac{\omega}{c} z \cos \theta_F(\omega).$$

Let us now return to the construction of the spatial interferometry trace. As mentioned above, we can separately record the components

$$I_{ref}(\mathbf{r}) = \left\langle \left| E_{ref}(\mathbf{r}, t) \right|^2 \right\rangle_t = \int_{-\infty}^{\infty} S(\omega) d\omega,$$

and

$$I_{unk}(\mathbf{r}) = \left\langle |E_{unk}(\mathbf{r}, t)|^2 \right\rangle_t = \left| \int_{-\infty}^{\infty} s_{unk}(\omega) F(\mathbf{r}, \omega) d\omega \right|^2$$

by blocking the other arm of the interferometer, and later subtracting the intensity patterns from the interferometer trace.

Before we start analyzing the interference term of the trace, it is important to stress that $F(\mathbf{r}, \omega)$, describing spatial dependence of spectral amplitudes of the frequency components, and $\varphi(\mathbf{r}, \omega)$, describing the phase introduced by the optical system, are deterministic functions and remain invariant with respect to the different realizations of the ensemble. The stochastic nature of the field is expressed in $s(\omega)$ and phase $\phi(\omega)$. In case the field is ergodic and stationary, as we assumed earlier, the ensemble average can be substituted with time average and we can write for the cross-spectral density

$$\left\langle s(\omega)^* s(\omega') \right\rangle_e = \left\langle s(\omega)^* s(\omega') \right\rangle_t = S(\omega) \delta(\omega - \omega'). \quad (13)$$

The interference term reads:

$$\begin{aligned} 2 \operatorname{Re} \left\langle E_{ref}^* E_{unk} \right\rangle_t &= 2 \operatorname{Re} \left\langle \int_{-\infty}^{\infty} s(\omega) e^{-i\omega(t+\tau) + i\frac{\omega}{c}z - i\phi(\omega)} d\omega \times \right. \\ &\quad \left. \int_{-\infty}^{\infty} s(\omega') F(\mathbf{r}, \omega') e^{i\omega't + i\varphi(\mathbf{r}, \omega') + i\phi(\omega')} d\omega' \right\rangle_t \\ &= 2 \operatorname{Re} \int_{-\infty}^{\infty} S(\omega) F(\mathbf{r}, \omega) e^{i\frac{\omega}{c}z + i\varphi(\mathbf{r}, \omega) - i\omega\tau} d\omega, \quad (14) \\ &\equiv V(\mathbf{r}, \tau) \end{aligned}$$

which is basically *mutatis mutandis* the electric field of the unknown wave field:

- Temporal dependence is replaced by that of the time delay τ , meaning that one can “freeze” the unknown field by interfering it with plane wave field;
- The phase introduced by the optical system in the object arm $\varphi(\mathbf{r}, \omega)$ is

replaced by $\frac{\omega}{c}z + \varphi(\mathbf{r}, \omega)$, which rescales the z-axis by factor

$1 + \frac{z \cdot \omega}{c \cdot \varphi(z, \omega)}$. For example, in experiment [29] the micrometer-range z

dependence of the field was scaled into a centimeter range.

- The frequency integration is carried out over the cross-spectral density instead of square root of the unknown field spectral density.

In a spatial interferometry measurement, the transversal spatial resolution is determined by the pixel size of the detector, longitudinal spatial resolution by

detector positioning step and the phase scaling factor $\frac{\omega}{c}z + \varphi(\mathbf{r}, \omega)$, and the

temporal resolution depends on the delay step.

To illustrate the scaling property, let us benefit from the general expression for the cylindrically symmetric superposition of plane waves (12), from which one can see that for the case of localized waves the phase depends only on z -coordinate

$$\varphi(\mathbf{r}, \omega) = -\frac{\omega}{c} z \cos \theta_F(\omega) \quad \text{and rescaling factor is given by}$$

$$\frac{\omega}{c} (1 - \cos \theta_F(\omega)).$$

In case the reference and the unknown fields are identical or only time-shifted, the ‘spatial’ interference do not occur. Thus a wave field cannot be used to measure itself with interferometric technique.

It is possible to adapt data analysis routine, which is very similar to that for spectral interferometry and is introduced in detail in the following section. The analysis involves extracting the interference term from the recorded intensity trace, Fourier’ transforming it to the spatial frequency space, shifting it to zero frequencies and inverse transforming the filtered trace to coordinate space. This allows one to extract the spatial phase at fixed instant $t = \tau$ of the unknown field.

The unknown field can be reconstructed if the interference pattern can be completely resolved with the detector. This restricts the angular distribution of the plane wave constituents of the unknown field. Based on the Nyquist sampling criterion, the smallest spatial period Λ in the interference pattern ought to be at least twice as large as pixel linear dimension l . $k_{pmax} = 2\pi/2l$ is the largest transversal wave vector component which can be satisfactorily measured. Accordingly the plane wave constituent of the unknown field can deviate from the optical axis by the angle $\theta = k_{pmax}/k$, where $k = \omega/c = 2\pi/\lambda$ is the wave vector. For an optical experiment we can make a realistic estimation for the deviation angle θ . If the wavelength is $\lambda = 600nm$, and detector pixel side is $l = 5nm$ wide, the wave pattern can be resolved when the plane wave components are not dispersed from optical axis by more than $0.06rad$ or 3.4° .

Let us point out that spatial interferometry cannot be used for recording the fields when the k -vectors from different plane wave constituents are strongly dispersed. Namely, the z -axis scaling depends on the angular distribution

$\varphi(\mathbf{r}, \omega)$ as $\frac{\omega}{c} z - \varphi(\mathbf{r}, \omega)$. As a result the scaling is not uniform for the different plane wave constituents and the recorded field amplitude does not follow exactly the input field.

These two restrictions are independent. For example, in an ultrashort localized wave, called a Bessel-X-pulse, all the plane wave constituents travel under the same angle towards optical axis and in this case the method works flawlessly if the angle θ , called axicon angle, is less than $\theta < k_{pmax}/k$. But the spectral interferometry measurement of the focused Gaussian pulse, where k -vectors of the plane-wave constituents are dispersed in the range $0 \text{ deg} < \theta < k_{pmax}/k$, would yield a spatial field amplitude distribution different from that of the Gaussian field due to the z -axis rescaling.

3.1.2. Impulse and frequency response of optical system

The spatially resolved impulse and frequency response of an optical system can be measured with spatial interferometry if the signal remains stationary, ergodic and spatially coherent. The response functions can be measured in the spectral range of the input field or, if the spectrum³ of the input signal can be approximated to white noise, in the whole transmittance region of the optical system on the object arm.

The field $E_{unk}(t)$ at a position $P(x, y, z)$ is the time-convolution of the initial signal $E_{in}(t)$ and the impulse response $h(t)$ of the optical system at the same given space position $P(x, y, z)$ on the object arm $E_{unk}(t) = E_{in}(t) \otimes h(t)$. Based on the Fourier transform convolution theorem, in the spectral representation the convolution operation is replaced by a product and the field reads $\tilde{E}_{unk}(\omega) = \tilde{E}_{in}(\omega)H(\omega)$, where $H(\omega)$ is the frequency response of the optical system. Based on Eq. (10) and, (11) we can write the initial and the unknown fields in frequency domain:

$$\tilde{E}_{in}(\omega) = s(\omega)e^{i\phi(\omega)},$$

and

$$\tilde{E}_{unk}(\omega) = s(\omega)F(\omega)e^{i\phi(\omega)+i\phi(\omega)}.$$

$\tilde{E}_{unk}(\omega)$ in respect to the initial field $\tilde{E}_{in}(\omega)$ reads:

$$\tilde{E}_{unk}(\omega) = \tilde{E}_{in}(\omega)F(\omega)e^{i\phi(\omega)}, \quad (15)$$

from which follow the frequency response

$$H(\omega) = F(\omega)e^{i\phi(\omega)}, \quad (16)$$

and impulse response

$$h(t) = \int_{-\infty}^{\infty} H(\omega)e^{i\omega t} d\omega. \quad (17)$$

Different from the initial and the unknown field, the response functions characterize the optical system and neither of them depend on the stochastic phase $\phi(\omega)$ or the field amplitude $s(\omega)$ of an ensemble realization.

Bearing in mind, that the reference pulse is nothing but a delay-shifted initial pulse $E_{ref}(t - \tau) = E_{in}(t)e^{-i\omega\tau}$, let us once more calculate the correlation function at a position $P(x, y, z)$, where the unknown field is expressed through the impulse response $\tilde{E}_{unk}(\omega) = s(\omega)H(\omega)e^{i\phi(\omega)}$:

³ Here the term ‘spectrum’ is used as a synonym of spectral density of the power spectrum. The field spectrum or field amplitude is sometimes referred also as square root of spectral density.

$$\begin{aligned} \langle E_{ref}^* E_{unk} \rangle_t &= \left\langle \int_{-\infty}^{\infty} s(\omega) e^{-i\omega(t-\tau) - i\phi(\omega)} d\omega \int_{-\infty}^{\infty} s(\omega') H(\omega') e^{i\omega't + i\phi(\omega')} d\omega' \right\rangle_t \\ &= \int_{-\infty}^{\infty} S(\omega) H(\omega) e^{i\omega\tau} d\omega = V(\tau) \end{aligned} \quad (18)$$

One can see that the correlation function depends on deterministic functions – the spectral density $S(\omega)$, defined by (13), the frequency response of the optical system $H(\omega)$, Eq. (16), and the delay τ . In case the spectrum of the input field can be approximated as white spectrum in the transmittance region of the optical system, the spatially resolved impulse response $h(\tau)$, Eq. (17), of the optical system can be retrieved directly from the correlation function $V(\tau)$, Eq. (18), by scanning the delay in spatial interference measurement.

In the case where the width of the initial field spectral density function is finite, the later appears as an additional coefficient in the integration over the frequencies and can be eliminated, if the trace is Fourier' transformed with respect to the time/delay τ , to frequency space:

$$\tilde{V}(\omega) = \int_{-\infty}^{\infty} V(\tau) e^{-i\omega\tau} d\tau = S(\omega) H(\omega).$$

From there the frequency response can be extracted by dividing out the spectral density of the initial field $S(\omega)$:

$$H(\omega) = \frac{\tilde{V}(\omega)}{S(\omega)}.$$

Inverse Fourier transforming the frequency response to the time domain, Eq. (17), yields the impulse response of the optical system in the spectral region, where the initial field spectrum is defined and non-zero.

We have shown that in order to retrieve the impulse or frequency response of the optical system at a space position P , the field intensities at different delay values can be recorded with a one pixel time-averaging detector. A matrix detector adds transversal spatial dimensions and scanning the detector position along z -axis allows to retrieve the full 3-dimensional impulse and frequency response. This allows one to characterize the optical system on the object arm.

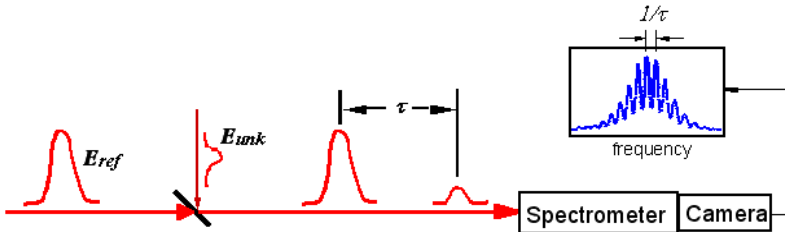


Figure 6. The principle of spectral interferometry. The reference field and the unknown field are delayed with respect to each other and superposed collinearly. The fields enter the spectrometer where the time delay is manifested in spectral fringes. (From reference [78].)

Combining Eq. (15) and (16) it is obvious, that knowing the frequency response of the optical system, allows one to calculate also spatiotemporal field distribution as if the optical system was illuminated with a transform-limited pulse, which has the spectrum of the initial field. Moreover, this method does not have the restriction to the angular distribution of the plane wave constituents arising from the z -axis rescaling, as it was the case while deducing the field distribution directly from the interference term of the spatial interferometry measurement.

3.2. Spectral interferometry

Spectral interferometry is a linear frequency-domain interferometric technique. A time delay is introduced between collinearly propagating unknown and reference wave fields. This yields interference in the *frequency* domain and allows one to extract spectral phase of the unknown pulse in respect to that of the reference pulse [79]. To compare: in the case of *spatial* interferometry two wave fields were overlapped in *space* and their (spatial) interference was recorded. In this paragraph we generalize the treatment of the method for the case of frequency non-correlated reference and unknown fields originating from the same initial field.

Again, let us assume that the ergodic and stationary input field has broadband spectrum, for which the phases of different frequency components are non-correlated and this is, again, manifested in stochastic phase term $\phi(\omega)$. In analogy with spatial interferometry, the spatially coherent input field⁴ is divided into two parts and one part of the initial field constitutes the reference with adjustable delay and the other is shaped linearly to the unknown field by optical system on the object arm. (See Figure 5.) At the output of the interferometer the fields are overlapped and enter the spectrometer. See Figure 6.

The reference field reads $\tilde{E}_{ref}(\omega) = \tilde{E}_0(\omega)e^{i\phi(\omega)+i\omega\tau}$, where $\tilde{E}_0(\omega)$ is field complex amplitude. The optical system on the object arm adds the phase $\varphi'(\omega)$ and their transmission function is manifested in $F(\omega)$. The unknown field reads

$$\begin{aligned}\tilde{E}_{unk}(\omega) &= \tilde{E}_0(\omega)F(\omega)e^{i\phi(\omega)+i\varphi'(\omega)} \\ &= \tilde{E}_{ref}(\omega)F(\omega)e^{i\varphi'(\omega)-i\omega\tau}.\end{aligned}\tag{19}$$

From there it follows that the frequency response $H(\omega)$ of the optical system on the object arm is:

$$H_{SI}(\omega) = F(\omega)e^{i\varphi'(\omega)}\tag{20}$$

Again, we assume that the spectrum of the reference pulse contains all the spectral components of the unknown pulse.

⁴ In fact, the spatial coherence is required for formation the unknown field on the object arm. While recording only frequency-, not spatial-coordinate dependent phase distortions the method will work equally well with identical spatial modes on object and reference arm.

Spectrometer detector will record at its input time-averaged signal, which due to the ergodicity is equivalent to average over different realizations of ensemble:

$$S_{SI}(\omega) = \left\langle [\tilde{E}_{ref}(\omega) + \tilde{E}_{unk}(\omega)]^* [\tilde{E}_{ref}(\omega) + \tilde{E}_{unk}(\omega)] \right\rangle_e \quad (21)$$

$$= S(\omega) + S(\omega)F(\omega)^2 + 2 \operatorname{Re} \left[S(\omega)F(\omega)e^{i\varphi(\omega) - i\omega\tau} \right]$$

where spectral density is $S(\omega) = \left\langle \tilde{E}_{ref}^*(\omega)\tilde{E}_{ref}(\omega) \right\rangle_e$. One can see that the phase of the interference term depends on delay and the phase shift introduced by the optical system on object arm, but not the stochastic phase originating from the initial field. As a result, the spatially resolved *frequency response of the optical system* (20) and the *phase difference between the unknown and reference fields* can be retrieved. The phase difference corresponds to unknown field phase in case the phase of the initial field is flat i. e. the initial field is transform-limited pulse.

The spectral interferometry trace can be analyzed by Fourier transforming the output signal to pseudo-time space (because the intensity, not the field, is transformed). The term, which is shifted towards pseudo-time axis positive values by τ , contains the phase difference between unknown and reference pulse. This term should be filtered out and shifted to pseudo-time origin, which removes the phase shift caused by delay τ . Inverse-transforming the term to frequency space will yield the desired phase. See Figure 7.

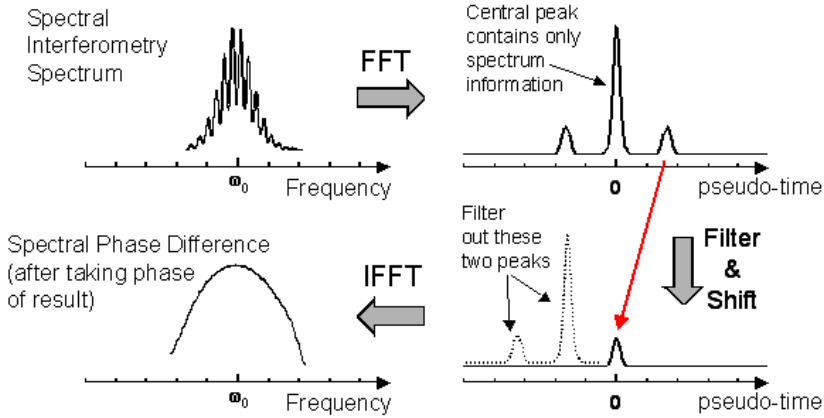


Figure 7. Illustrative schematic of spectral interferometry trace analysis routine. From reference [78]

Method called dual-quadrature spectral interferometry allows one to extract the phase difference with simpler data analysis, yet the experimental setup is more complex as both patterns corresponding to sine and cosine of the interference term must be recorded [66, 80].

In case the spectrum of the input field can be approximated to white spectrum, i. e. is constant, in the transmittance region of the optical system on the object arm of the interferometer, the interference term in the spectral interferometry trace (21) is the frequency response of the optical system (20) in that spectral region multiplied by the phase shift caused by the delay τ . If the spectrum of the input field is of finite extent and narrower than the transmittance region of the optical system and/or not constant, it is to be divided out from the interference term of (21) to obtain the frequency response of the optical system in the frequency range where the spectrum is non-zero.

To characterize temporally the unknown field, one must know the spectral phase and amplitude of the reference field. In case of optical pulses, FROG or SPIDER technique can be used. The method combining FROG and spectral interferometry is called TADPOLE – Temporal Analysis by Dispersing a Pair Of Light E-fields [66, 81].

Spectrometer records a $S_{SI}(\omega)$ trace at a fixed space position $P=(x,y,z)$. To obtain a 4-dimensional trace $S_{SI}(\mathbf{r}, \omega)$, one should scan the space coordinates in all three dimensions. In experimental setup perfect collinearity between the reference and unknown fields has to be achieved in order to avoid introducing additional phase between the fields and thus the setup needs to be mechanically very stable. So far, this has become an obstacle while measuring the spatial distribution of the frequency response of the optical system from where the spatial distribution of the unknown field would follow.

The spectral resolution required for spectral interferometry is reciprocal of the maximum temporal extent of the compound wave field duration: delay between the coherent fronts of the fields plus coherence times of both field. This means that one can resolve the phase difference with the price of loosing resolution compared to simply measuring the unknown wave field spectrum. This may limit the spectral width of the fields that can be measured [66].

3.3. Spatial-spectral interferometry and SEA TADPOLE

Spatial-spectral interferometry is a linear electric field characterization technique in which the interfering reference and unknown fields are directed to an imaging spectrometer where the trace is resolved spectrally. The method, which bears an inherent resemblance to spectral holography [82], was originally used to determine group delay of optical elements, namely dielectric mirrors [83, 84], but was soon applied also for characterizing femtosecond pulses [85] and became a practical supplement to both SPIDER (SEA SPIDER) [86] and FFOG-based TADPOLE (SEA TADPOLE) [87] ultrashort pulse characterization methods.

Often the SEA SPIDER and SEA TADPOLE are referred as spectral interferometry methods. We do not oppose this terminology but still prefer to use the

term spatial-spectral interferometry, originating from [85], in this thesis. Our motivation is to draw distinction between the spectral interferometry and its variant extended to two dimensions.

3.3.1. Spatial-spectral interferometry method

Although several different setups have been proposed [83, 85–87] the working principle is the same. Let us consider a setup, where the interferometer part is similar to both spatial and spectral interferometry schemes. We generalize the treatment of the method for the broadband, frequency non-correlated, spatially coherent and stationary fields. The input field is split into two: a reference field with adjustable delay and unknown field, which is generated by propagating the input field through the linear optical system on the object arm (see Figure 5). Fields entering the spectrometer are crossed under small angle 2θ yielding spatial interference fringes on a matrix detector. The fringes appear towards the axis ξ , perpendicular to the frequency ω axis. As a result, the interference pattern is spectrally resolved along the frequency axis. Resulting 2D image carries phase and amplitude information about electric field of the unknown field. The temporal delay between two fields is set to 0 avoiding occurrence of spectral fringes. Figure 8 illustrates the setup for SEA TADPOLE configuration.

Electric fields of the reference and the unknown fields read:

$$\tilde{E}_{ref}(\mathbf{r}, \omega) = \tilde{E}_0(\mathbf{r}, \omega) e^{i\phi(\omega) + i\omega\tau + i\frac{\omega}{c}\xi \sin(\theta)}$$

and

$$\begin{aligned} \tilde{E}_{unk}(\mathbf{r}, \omega) &= \tilde{E}_0(\mathbf{r}, \omega) F(\mathbf{r}, \omega) e^{i\phi(\omega) + i\varphi(\mathbf{r}, \omega) - i\frac{\omega}{c}\xi \sin(\theta)} \\ &= \tilde{E}_{ref}(\mathbf{r}, \omega) F(\mathbf{r}, \omega) e^{i\varphi(\mathbf{r}, \omega) - i2\frac{\omega}{c}\xi \sin(\theta)} e^{-i\omega\tau} \end{aligned}$$

where $\tilde{E}_0(\mathbf{r}, \omega)$ is field complex amplitude and $\phi(\omega)$ the (stochastic) phase. θ is the half of the crossing angle of the fields in the spectrometer. Consistently to the spatial and spectral interferometry description in the previous chapters, $F(\mathbf{r}, \omega)$ and $\varphi(\mathbf{r}, \omega)$ describe the deterministic changes introduced to the field by the optical system – the spatial distribution and the phase, respectively. We have also included the phase shift originating from delay, $e^{-i\omega\tau}$, for the sake of generality. As noted above, it is convenient to choose $\tau = 0$.

One can easily see that the impulse response of the optical system at fixed position $P=(x, y, z)$ is

$$H(P, \omega) = F(P, \omega) e^{i\varphi(P, \omega) - i2\frac{\omega}{c}\xi \sin(\theta)} \quad (22)$$

The spatial-spectral interferometry trace at space point P reads:

$$\begin{aligned}
 S_{SSI}(\omega) &= \left\langle [\tilde{E}_{ref}(P, \omega) + \tilde{E}_{unk}(P, \omega)]^* [\tilde{E}_{ref}(P, \omega) + \tilde{E}_{unk}(P, \omega)] \right\rangle_e \\
 &= S(P, \omega) + S(P, \omega)F(P, \omega)^2 \\
 &\quad + 2 \operatorname{Re} \left[S(P, \omega)F(P, \omega) e^{i\varphi(P, \omega) - i2\frac{\omega}{c}\xi \sin(\theta)} e^{-i\omega\tau} \right]
 \end{aligned} \tag{23}$$

where spectral density is $S(P, \omega) = \left\langle \tilde{E}_{ref}^*(P, \omega) \tilde{E}_{ref}(P, \omega) \right\rangle_e$. Different from the *spectral interferometry*, the trace is 2-dimensional (ξ, ω) , and contains additional phase term $e^{-i2\frac{\omega}{c}\xi \sin(\theta)}$, which is caused by the setup and remains constant over different realizations of the ensemble.

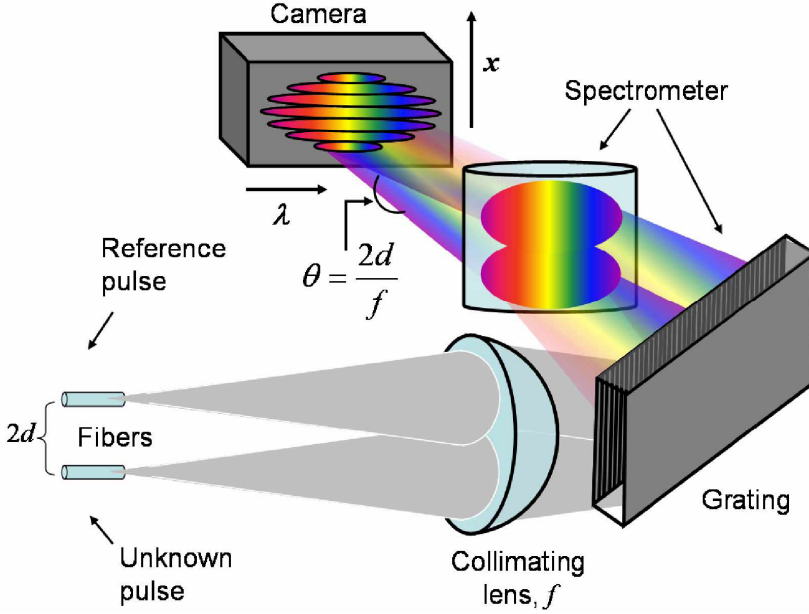


Figure 8. Experimental setup for spatial-spectral interferometry based on SEA TADPOLE technique: reference- and unknown pulses enter the imaging spectrometer from fibers. The fiber outputs are set at distance $2d$ from each other to yield spatial fringes in vertical ξ -axis. The interference pattern is spectrally resolved in horizontal direction yielding $S(x, \omega)$ distribution of the spectrum. [87]

The results (22) and (23) demonstrate, that regardless of the phase relations between initial fields frequency components, from the interference term of the spatial-spectral interferometric measurement trace it is possible to (i) resolve the phase difference between the unknown and reference fields, and (ii) the fre-

quency response of the optical system on object arm of the interferometer⁵. The result does not depend whether one used either white noise or train of δ -like pulses as the input field. The above shown principles apply also to SEA TADPOLE device – a realization of a spatial-spectral interferometry method described in following section.

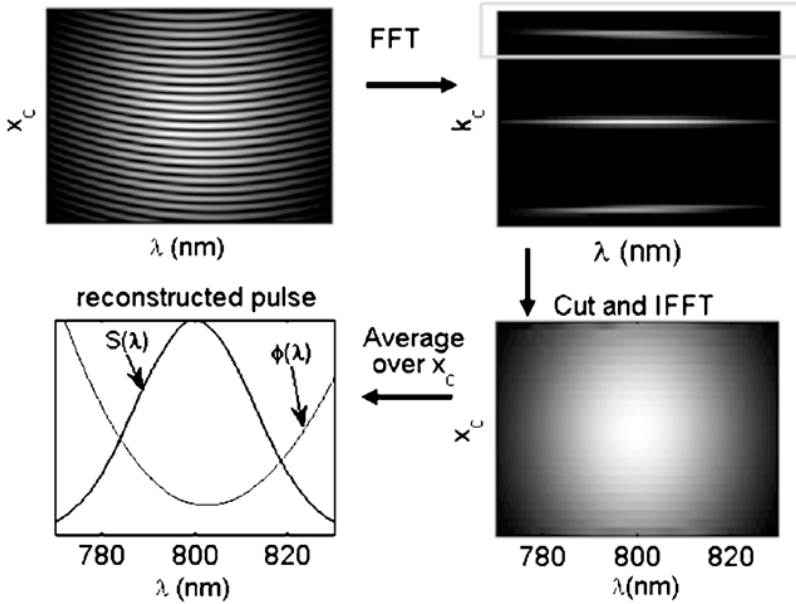


Figure 9. Illustrative algorithm for analyzing SEA TADPOLE and also spatial-spectral interferometry trace. [88]

Although the spatial-spectral interferometry trace can be intuitively interpreted, the analyzing routine is similar to that of the spectral interference method. One should subtract I_{ref} and I_{unk} from the intensity trace, Fourier' transform interference term trace to *spatial frequency* space, discard negative frequency terms, shift the positive *spatial frequency* spectrum to zero-frequencies and remove the phase shift initiating from the field crossing under angle 2θ . (Though, the later is often negligible and does not need subtraction.) The Fourier' inverse-transform of the result to coordinate space yields spectral density and phase of the spectral component (see Figure 9).

In analogy with *spectral* interferometry, in order to obtain the frequency response of the optical system on the object arm (22), the spectral density is to be divided out from the analyzed interference term (23). In case one divides the term with square root of spectral density, one obtains spectral amplitude and the

⁵ For example, in Ref. [88] the impulse response of the spectrometer of SEA TADPOLE device was measured with the help of an etalon.

phase of the field, which would have emerged from the optical system as if illuminated with transform-limited pulse having the same spectrum as the initial field did.

The impulse response and temporal evolution of the phase difference is obtained by Fourier' inverse-transforming the retrieved trace in respect to the frequency. The spatial dependence of them can be constructed by scanning the input field in all three space coordinates.

3.3.2. SEA TADPOLE

Spatiotemporal profiles of the light bullets have been successfully measured with SEA TADPOLE – Spatial Encoded Arrangement for Temporal Analysis by Dispersing a Pair of Light E-fields [VI–XI] – which is why we will briefly introduce this technique and its capabilities in following [88, 89, 90].

The SEA TADPOLE setup is shown on Figure 8. After propagating the fields through the interferometer both reference and unknown field are coupled into equal-length optical fibers. The spectral phase and amplitude of the unknown field in respect to that of the reference field can be reconstructed at space point with coordinates (x, y, z) . The spatial profile of the unknown field is obtained by scanning the space coordinates of the unknown field with the tip of the fiber (in this case the device is called scanning SEA TADPOLE).

Use of optical fibers for guiding the fields into spectrometer is a robust method for keeping crossing angle θ of the fields in spectrometer fixed and by this enhancing the device stability. In addition, the fiber mode size, which can be decreased down to the range of one micron, defines the spatial resolution of the measurement. As a result, electric fields with complex spatial intensity distribution have been successfully measured. Also, the SEA TASPOLE method is linear thus very weak fields can be measured or, consistently, intense fields can be recorded with high spatial resolution. The fields, in which plane wave constituents do not propagate towards optical axis at larger angles than the numerical aperture of the fiber, can be resolved without distortions.

SEA TADPOLE spectral resolution enhances that of the spectrometer in the case of smooth and slowly changing phase of the unknown pulse. As the SEA TADPOLE measures complex field E_{unk} rather than its amplitude squared $|E_{unk}|^2$, the spectra will be always better resolved in SEA TADPOLE than in the same device used as spectrometer by blocking the reference beam. While spectrometer is insensitive to phase information and measures convolution of its response function and unknown field amplitude squared, the SEA TADPOLE measures convolution of spectrometers response function and field complex amplitude. For example, in case of Guassian spectra the enhancement factor is $\sqrt{2}$, which can be understood that the width of the spectral field is $\sqrt{2}$ times wider than that of the intensity. Up to factor 7 times better resolution is obtained for measuring oscillatory field, double pulses for example, because $e^{i\omega\tau}$ is eigenfunction of convolution operator. [88]

In case the *unknown field's* phase features are smaller than the spectrometer's spectral resolution, SEA TADPOLE ends up with less accurate results than the same setup configured as spectrometer. The SEA TADPOLE device resolves the convolution between complex unknown field, rather than the field modulus square, and spectrometer's response function, which width is defined by the spectral resolution. Convolution acting on complex field can "mix up" the amplitude and phase information and yield distortions in retrieved spectrum of phase. [88]

3.4. Discussion and Conclusions

To conclude, the interferometry is a linear method, which allows one to record phase difference between two fields. Prerequisite conditions are stationarity and ergodicity of the fields. Thus the analysis and results obtained in this chapter are valid for describing the performance of the interferometric measurement techniques under illumination by different optical fields, ranging from train of ultra-short pulses to white-noise-like fields. All the frequency components of the unknown field should be present also in the spectrum of the reference field. As we aim to characterize the light bullets, the spectrum ought to be broadband. But we do not expect that the phases of the different frequency components to be correlated. This means that a femtosecond pulse is nothing but a special case and one could obtain the same results with, for example, white light laser or (spatially filtered) broad-spectrum arc lamp.

We have studied the configuration where the reference and unknown field originate from the same initial field and the unknown field with spatiotemporal couplings, bullet-like intense core and residual 3-dimensional double-conical spatial intensity profile is generated on object arm of the interferometer. In that case spatial coherence of the initial field is required also for spectral and spatial-spectral interferometry measurements. Otherwise, spatial coherence and transversal extent of the reference field, to match that of the unknown field, are essential only for the spatial interferometry measurement. In spectral or spatial-spectral interferometry experiments identical spatial modes are sufficient if the field's phase, which does not vary over space coordinates, is measured...

Under those conditions we have shown that:

Interference term in spatial interferometry, Eq. (14), measurement

- Describes the impulse response of the optical system on object arm (18), if the spectrum of the input field is in a good approximation white in the spectral region of interest (the transmission bandwidth of the optical system).
- Allows one to retrieve the *impulse and frequency response of the optical system* in the frequency range where the spectrum of the initial field is defined and not zero.
- Follows the *electric field distribution of the unknown field as if generated from transform-limited input pulse* (i. e. its phase is constant) by the optical

system on object arm at fixed z and $t=\tau$, where τ is delay, with minor rescaling, discussed in detail after Eq. (14).

If the field structure is scanned in all 4 space-time coordinates, where the time is substituted by the delay τ , the optical system and its capability to form optical field with complex spatiotemporal couplings can be characterized.

Interference term in spectral and spatial-spectral interferometry, Eq. (21) and (23) respectively

- Equals the frequency response $H(\omega)$ of the optical system on the object arm, Eq. (20) and (22), respectively, in case the spectrum of the input pulse can be approximated to the white spectrum in the in the range of transmission of the optical system.
- Allows one to retrieve the *frequency and impulse response of the optical system* in experiment with real light source having finite bandwidth, if the spectral density $S(\omega)$ is divided out.
- Allows one to retrieve phase difference between unknown and reference fields. If all four space-time (frequency) coordinates are scanned, one can estimate optical system capability to form the unknown field with a transform-limited pulse, which power spectrum is identical to the spectral density of the initial frequency non-correlated field.

From the results presented above, one can see, that as the spectrum of the frequency non-correlated sources is broader, they have an advantage over femtosecond lasers in the experiments, which aim to characterize the optical system consisting of various types of refracting and diffracting optical elements.

In addition, if the phase and amplitude of the initial field is known – say, the initial field is a femtosecond pulse, pre-characterized for example with FROG or SPIDER device – the unknown field can be fully spatiotemporally characterized.

The first experiments, in which the spatial behavior of superluminally propagating optical Bessel-X pulses and luminal Focus Wave Modes were measured, were based on spatial interferometry and carried out with spatially filtered Xe-arc lamp, which served as a optical white noise source [22, 29, 33]. Lately, the spatiotemporal characterization of the femtosecond Bessel-X pulse and accelerating-decelerating Bessel-type waves with spatial-spectral technique SEA TADPOLE [VI–XI, XIII] has been reported. The experiments are discussed and the results compared in the following chapter, Sections 4.2.5, 4.2.6, 4.4.1 and 4.4.2.

Here we abridge the analysis by saying that *spatial* interferometry is suitable for measuring the phase difference in either nearly monochromatic or very broadband fields with coherence time less than 10 femtosecond. The satisfactorily resolvable spectrum width of the *spectral* and *spatial-spectral* interferometry measurements is determined by the spectrometer parameters and thus the

methods are most suitable for the region in the middle – for fields with coherence time in order of tens up to few hundreds of femtoseconds.

Spatial, spectral and spatial-spectral interferometry are linear techniques and thanks to that they can measure very weak fields. For spectral interferometry it has been shown that train of pulses with pulse energy of $4.2 \times 10^{-21} J$ can be measured [81].

Interferometric techniques can be also used to ‘amplify’ the weak signals with the price of loosing contrast. In case the reference pulse is M times more intense than the unknown pulse, the fringe intensity is $4\sqrt{M}$ that of the unknown pulse [66].

4. EXPERIMENTS

Above we have introduced the theoretical background, principles of optical generation and classification of the localized waves and the light bullets in general. We have also gone through and elaborated on the interferometric measurement techniques for registering complicated spatial and temporal field amplitude profiles with white-noise-like input fields. In this chapter we give an overview of the experiments on localized waves conducted so far and compare the complementary measurements where applicable.

In optical generation of the localized wave the first task is to generate suitable angular distribution of the plane-wave constituents. This must lay on a quasi-singular support of the spectrum, which is either hyperbola, parabola, straight line or ellipse in momentum space (See chapter 2, Localized waves). For some families of the localized waves there are methods to form a suitable angular distribution in the whole transmittance range of the optical system, regardless the specific power spectrum of the light source. For other families the suitable angular distribution is achieved by carefully and precisely combining diffractive, refractive and dispersive optical elements. The angular distribution of the plane waves can be formed:

- Exactly in the whole range of the support of the spectrum for the representatives of the superluminal family of the localized waves by means of reflective diffraction grating;
- In good approximation in the whole range of the support of the spectrum for the superluminal localized waves with propagation-invariant-wave-function by means of axicon or combination of the annular slit and achromatic lens;
- In the spectral bandwidth of the light source by combining dispersive, diffractive and refractive optical elements for the luminal and subluminal localized waves.

For the case of the accelerating and decelerating Bessel-type waves, the group velocity and hence also the angular distribution of plane waves varies smoothly with the coordinate z . Yet, the support of the spectrum, on which the plane wave constituents lay on, must be that of a localized wave at any instant and correspondingly at any point on z -axis.

For a successful experiment one needs also suitable light source with broadband and spatially coherent radiation. In previous chapter we showed that in interferometric experiments the frequency non-correlated sources could be utilized as well.

Next crucial aspect is the choice of the wave field detection method because the electric field of an optical signal cannot be recorded directly. Hence, the various properties of the wave fields have been studied with different methods:

- Field's profile and correlation time (duration of the transform-limited pulse) by recording the field cross-correlation with the plane wave field in interferometric measurement [29, 31];

- Pulse's first and second order autocorrelation profiles in autocorrelation measurements [34];
- Pulse's velocity with snapshots of ionization front [32];
- Pulse's spatiotemporal profile, group velocity and duration with spatial-spectral interferometric techniques combined with FROG [VI–XI, XIII].
- Pulse's spatiotemporal profile, group velocity and duration by angular spectrum detection with Shack-Hartmann sensor [37].

The choice of the optical elements and the light source must take into account the resolution of the detection device. One must assure that the smallest feature of the generated wave field would be resolvable. The later condition can set rather strict limitations to the deviation angle of the plane wave constituent of the wave field in respect to the optical axis as the optical wavelengths remain below one micron, but the CCD pixel or single-mode fiber tip dimensions are in the range of few microns and above.

In the following we give an outline of the experiments on light bullets, considering all three above mentioned important aspects: generation of the support of the spectrum, choice of the light source, choice of the detection method and its realization. The experiment descriptions are organized based on the localized waves genealogy. In the frames of those subsets the experiment descriptions are in chronological order.

First we discuss the experiments on linear superluminally propagating localized waves with hyperbolic support of the spectrum. Those have been generated in dispersive media by means of linear optical system and by means of nonlinear interaction between intense pump pulse and weak seed pulse.

Secondly we study the special case – the Bessel-X pulses belonging to the 'subfamily of superluminal pulses with a propagation-invariant wavefunction'. Bessel-X pulse is most widely studied localized wave, which has been generated and measured in number of experiments. Different generation and measurement methods are compared and their application ranges discussed.

Thirdly we introduce the experiment on the focused wave mode with main emphasize on obtaining the suitable parabolic support of the spectrum.

Finally we discuss the experiments on accelerating and decelerating Bessel-type waves.

4.1. Experiments on superluminal localized waves with hyperbolic support of the spectrum

Let us start from considering the general case of the superluminally propagating localized waves where the support of the spectrum of the wave field is a hyperbola.

First, we discuss here the first experimental proof on localized waves, which demonstrated their nondispersive propagation in the linear media [30, 31].

Later, it was demonstrated that such a support can be generated exactly by means of a diffraction grating [III, IV, XII]. To obtain cylindrically symmetric field, the diffraction grating with low groove density ought to be engraved on the inner surface of reflective cylinder. Illuminating such a cylinder from one end with a light cone (Bessel-X pulse) would form a superluminally propagating localized wave exiting the other end of the cylinder with superluminal group velocity close to c . Normally incident plane wave pulse on transmissive cylindrical grating would generate a cylindrical wave of infinite group velocity (See also Paragraph 2.2.1). The sophisticated interplay between the parameters has been studied in [IV] and the experiment is in preparation.

Superluminally propagating localized waves with hyperbolic support of the spectrum have been generated in dispersive media by means of nonlinear interaction [V].

4.1.1. Propagation of the Bessel pulse in dispersive media [30, 31]

An axially symmetric ‘nondiffracting pulse’ was generated by means of a holographic element called lensacon – a circular diffraction grating with varying groove density – and a lens transforming the laser beam into a point source in the vicinity of the lensacon focus. The lensacon was optimized for 610 nm , had focal length of $f = 30\text{ cm}$ and cone angle $\theta = 0.01\text{ rad}$. Broadband frequency non-correlated pulse with 210 fs correlation time and centered to 615 nm was delivered by Rhodamine 6G dye laser pumped by Ar-ion laser.

The group-velocity-dispersion-caused spread of the pulse was compensated by careful choice of its angular spectrum, which resulted in a practically spread-free propagation through 7 cm glassy sample. The nondispersive propagation in the sample was demonstrated by recording the field cross-correlation between the fields at the sample input and output faces. The consequent delayed traces were recorded with CCD device and the field autocorrelation was obtained by calculating the pattern visibility.

In general, behind a circular diffraction grating with normal incidence, a *subluminally* propagating nondiffractive pulse is formed. In this experiment the proper positioning of the focusing lens in respect to the lensacon allowed to approximate the resulting angular dispersion to the linear dependence between longitudinal component of the \mathbf{k} -vector and the frequency ω . As a result, the field generated in the experiment was an approximation to a superluminally propagating localized wave with hyperbolic support of the spectrum. (Calling it a Bessel-X pulse, as is done in the reference [31], is not fully accurate in the context of this thesis.) The experiment was robust in the sense that the cross-correlation function width depended only on the phase difference gained in the glassy sample.

4.1.2. Linear X pulse by means of nonlinear interaction

In [V] it has been shown that intense driving pulse, which propagates without diffracting or dispersing, induces the temporal refractive index change in media with $\chi^{(3)}$ nonlinear susceptibility and can reshape a delay-matched weak probe pulse via cross phase modulation to nondiffractive and nondispersive pulse. Two experiments, with a filament and a pulsed Bessel beam as the strong driving pulse were performed. Experimental results from both measurements were verified with simulations, which solve numerically the nonlinear Schrödinger equation.

In the first experiment 1055 nm central wavelength and 1.2 ps duration intense pump pulse from Nd:glass laser was loosely focused on 2 cm thick fused silica sample. The pump pulse spontaneously formed a nondiffractive filament. Weak second harmonic probe pulse with 527 nm central wavelength was delay matched with the pump pulse and was subject to reshaping due to cross phase modulation induced by the pump pulse. There was no energy transfer between the spectrally well-separated pump and probe pulses. The angular distribution of the seed pulse was reshaped into hyperbola in the presence of the pump pulse. This was regarded as direct manifestation of the nondispersive propagation. The group velocity of the probe corresponded to that of the pump pulse and was superluminal. The nondiffractive nature of the reshaped probe pulse was observed directly by recording the propagation of $\sim 7.8\text{ }\mu\text{m}$ FWHM wide pulse peak over 5 mm in air.

In the second experiment a pulsed Bessel beam was used as a pump pulse instead of the filament. The pulsed Bessel beam was generated by means of 175° apex angle axicon from a 35 fs Ti:sapphire pulse positively chirped to 1 ps duration, centered at 800 nm . The probe pulse of same duration was centered to the second harmonic frequency of 400 nm . Cross-phase modulation induced reshaping of the angular distribution of the weak probe pulse to a hyperbola occurred while the pump and probe pulses were spatially and temporally overlapped in the fused silica sample. Hence the cross phase modulation can be exploited to generate spectrally isolated linear localized waves in dispersive media.

4.2. Experiments on Bessel-X pulses

Bessel-X pulse is a special case of the superluminally propagating localized waves. Its support of the spectrum in the momentum space has degenerated into a straight line crossing the origin. Hence all plane wave constituents propagate under the same angle θ towards optical axis. If the material dispersion can be neglected, the angular distribution of the field, generated by means of an axicon or the annular slit in the focal plane of an achromatic lens, approximates closely that of the Bessel-X pulses.

4.2.1. Spatiotemporal measurement of the correlation function of the Bessel-X pulse [29]

This is the original spatial interference experiment.

The angular distribution of the axially symmetric Bessel-X pulse was generated by placing an annular slit in the focus of an achromatic lens. This yielded in cone angle $\theta = 0.006 \text{ rad}$ (0.34°).

The setup was illuminated with white light noise from a superhigh pressure Xe-arc lamp, which covered whole visible region from blue up to near infrared, with ‘carrier’ wavelength of 600 nm . The correlation time of the field was $\sim 3 \text{ fs}$.

The Bessel-X field was cross-correlated with a plane wave pulse. To this end a pinhole was made in the center of the annular slit. The superluminally propagating Bessel-X pulse caught up with the preceding luminal plane wave pulse (its coherence front, to be exact). The group velocity difference served as “z-axis microscope”, which scaled the micrometer-range z dependence of the field into a centimeter range. The setup did not enable to change delay between the Bessel-X and the reference fields.

The field cross-correlation patterns were recorded with CCD camera, with pixel dimensions of $13.8 \mu\text{m} \times 16 \mu\text{m}$, in 70 positions along the z-axis. The measurement results were in good agreement with numerical calculations.

The cross-correlation between a complicated pulse and the plane wave pulse is studied in previous chapter, Section 3.1.1. It is shown that the plane-wave pulse “freezes” the Bessel-X field, allowing to record the correlation function with time averaging detector. The correlation time of the field had to be sub 10 fs to guarantee that the number of the interference fringes recorded is small enough to distinct the resulting pattern from trivial interference patterns and to resolve the X-branching of the field.

4.2.2. Measurement of the superluminal group velocity in a gas chamber [32]

The angular distribution of the plane wave constituents was generated by means of an axicon. The cone angle of the of the resulting pulse was rather large – 24.2° and the axicon material dispersion was taken into account. (Hence the term pulse Bessel beam is used for the generated pulse.)

Ultrashort femtosecond pulse of 70 fs duration, centered on 800 nm , was used to generate the pulse.

By recording shadowgrams of argon ionization front, which moves at the group velocity of the pulse and leaves plasma track, which persists even after the pulse has left, the group velocity of $(1.111 \pm 0.012) c$ was recorded. This was in good agreement with theoretical prediction and frequency domain interferometry measurement.

4.2.3. Autocorrelation measurements of few-cycle Bessel-X pulses [34, 63, 91]

Axially symmetric Bessel-X pulses and Bessel-like X-pulse arrays were generated by means of concave axicon mirror and SiO₂ microaxicon lenslet array. The cone angles were 0.1° and $\sim 0.27^\circ$ respectively. The microaxicon array was thoroughly studied in [63] was shown to have Gaussian profile. This only limits the field depth of the Bessel-X pulse propagation because only the region of the axicons where their profile can be approximated to cone can be utilized.

Ti:sapphire laser and hollow fiber self-phase-modulation setup followed by chirp compensation system generated a sub 10 fs duration initial pulse, centered around 790 nm . In one hand the ultrashort pulse was necessary to reduce the number of interference fringes in the recorded pattern and on the other hand to allow recording of the second order autocorrelation of the Bessel-X pulse.

First and second order autocorrelation functions of the Bessel-X (reflective axicon) and the Bessel-like X-pulse (microaxicons) pulse were measured. The patterns were recorded with CCD camera with imaging system. Thin, only $100\ \mu\text{m}$ thick, BBO crystal was used to obtain the second order autocorrelation images. Characteristic X-branching occurred on both autocorrelation maps and was in a good agreement with the theoretical predictions.

4.2.4. Low-resolution spatiotemporal measurements of Bessel-X pulse with Shack-Hartmann detector [37]

The angular distribution of the Bessel-X pulse was generated by means of a fused silica axicon, with apex angle 173.8° . The cone angle of resulting pulse is so small that the dispersion arising from the axicon material can be neglected.

The axicon was illuminated with $\sim 30\text{ fs}$ duration femtosecond pulses centered to 790 nm and having 28 nm bandwidth (FWHM) from Ti:sapphire oscillator.

A CCD camera was placed to the focal plane of the Shack-Hartmann detector, a lenslet array, to record the spatial phase derivative of the pulse, from which the field amplitude and the phase can be unambiguously retrieved. For spatiotemporal measurements a single FROG measurement must be taken in a space point where all frequency components are present. With several assumptions on the phase and propagation properties the spatiotemporal evolution and group velocity of the Bessel-X pulse were obtained.

The use of Shack-Hartmann detector in combination with autocorrelation was first proposed in [92]. The method introduced in reference [37] was served as simple and economic measurement technique and demonstrated on Bessel-X pulse. The spatial resolution of the Shackled-FROG (an acronym for above described measurement technique where Hartmann-Shack sensor is used in combination with FROG measurement to retrieve both field's amplitude and phase) is defined with the lenslet pitch and is in the order of tens of microns. Also, if the field has large bandwidth or strong spatial chirp, the frequency

dependent phase is to be resolved by using interference filters of directing the signal to imaging spectrometer after passing through the Shack-Hartmann sensor. One can claim also, that in case of the complicated pulses and single FROG measurement one will obtain temporal and spatial characterizations separately instead of the full spatiotemporal measurement.

4.2.5. High-resolution spatiotemporal measurements of Bessel-X pulse with SEA TADPOLE [VI]

The angular distribution of the Bessel-X pulse was generated by means of a fused silica axicon, with apex angle $\sim 176^\circ$ and the cone angle $\theta = 0.92^\circ$. The cone angle is so small that the dispersion arising from the axicon material can be neglected.

The axicon was illuminated with 30 fs duration ultrashort pulses centered to 800 nm and having 37 nm bandwidth (FWHM), originating from a Ti:sapphire oscillator.

The spatiotemporal profile $E(x, z, t)$ of the axially symmetric Bessel-X pulses was measured with spatial-spectral interferometric device called SEA TADPOLE (See section 3.3.2). The temporal resolution of 17 fs was decreased to 4.6 fs by zero filling. The spatial resolution of $\sim 5\text{ }\mu\text{m}$ was determined by the single-mode fiber tip size, but as the device measures complex field rather than the intensity, features with smaller dimensions can be resolved.

From the high resolution “snapshots of flight” images of the Bessel-X pulse both the fine structure around the intense core and inherent X-branching are revealed, see Figure 10. In addition to demonstrating the invariant propagation of the wave field over 8 cm distance on z -axis, the group velocity of the pulse along the z axis was determined to be $1.00012\text{ }c$ —within 0.001% error of the expected value of $1.00013\text{ }c$.

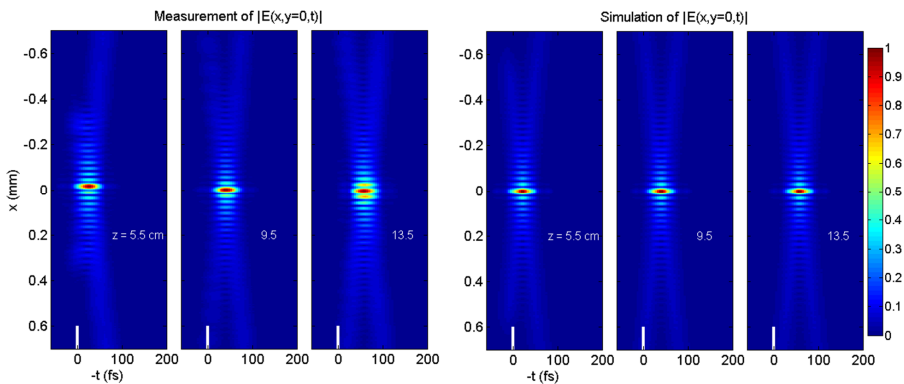


Figure 10. Left, the measured field amplitude of the Bessel-X pulse at three different distances z after the axicon; right, the corresponding simulations. Intensity is indicated by the scale. We normalized each field to have a maximum of 1. The white bar is to emphasize the location of $t=0$. [VI]

4.2.6. Discussion

From the experiment descriptions one can recognize the amount of time and effort dedicated for measuring the Bessel-X pulse by number of workgroups over the last long dozen years. In all the experiments the parameters of optical field generation and detection devices are optimized to maximum performance and often the complicated interplay between different parameters required high experience and ingenious idea to achieve reliable results in the experiment.

Out of all the experiments described above, the spatial and spatial-spectral interferometric experiments, [29] and [VI], are somewhat complementary and comparable. In spatial interferometry experiment [29] a broadband optical white-noise-like signal was used to obtain short correlation time and by cross-correlating the Bessel-X field with a plane wave field the impulse response of the optical system was measured. The later is *mutatis mutandis* of the field generated by transform-limited pulse with the spectrum of the white-noise-like input signal. In spatial-spectral interferometry experiment [VI] nearly transform limited 30 fs pulse was used and an unshaped portion of the input field served as a reference.

One difference between the experiments was that in *spatial-spectral interferometric* measurement at fixed z position a field dependence $E(\omega)$, or its Fourier pair, *temporal* behavior $E(t)$, was obtained. Scanning also lateral coordinates yielded $E(x, y, t)$. In *spatial interferometry* experiment with single measurement spatial distribution $E(x, y)$ was obtained. By scanning z -coordinate *spatial* dependence $E(x, y, z)$ was recorded. For propagation-invariant fields the propagation coordinate z and time t are combined via dependence $v_g z - t$, hence the $E(x, y, z)$ and $E(x, y, t)$ plots are equivalent and can be called “snapshots of flight”. For fields which do not propagate invariantly, the $E(x, y, z)$ and $E(x, y, t)$ representations are identical in a good agreement only if the plotting range of lateral coordinates x and y is small in respect to values of t and z . To obtain the electric field dependence $E(x, y, t)$ in spatial interferometric experiments for non propagation-invariant field the time t , manifested in delay τ , ought to be scanned with high resolution. And, respectively, to obtain the electric field dependence $E(x, y, z)$ in spatial-spectral interferometric experiments the coordinate z ought to be scanned with high resolution.

The spatial interferometric technique to measure the cross-correlation between complicated field and plane wave field works best with ultrabroadband, i. e. short correlation time fields, where the number of interference fringes is minimal, or with nearly monochromatic fields, where the phase difference can be found from relative fringe replacement and the number of the fringes does not matter. The spatial-spectral interferometry works best well with ultrashort pulses ranging from several picoseconds up to tens of femtoseconds. For shorter or longer pulses it can be challenging to achieve simultaneously necessary spectral bandwidth and resolution.

4.3. Proof-of-the-principle experiment on focus wave mode [33]

Focus wave mode (FWM) is “the original” localized wave introduced by Brittingham [4]. It propagates luminally in vacuum and linear media and the support of the spectrum in the momentum space is a parabola. Inherently the phase and group velocities of the pulse are not equal, thus the FWM can be considered as axially symmetric sum of tilted pulses of constant group velocity.

The FWM has been observed in only one experiment [33], which was preceded by investigation on generation of plane wave distribution, which could be approximate that of the parabolic support of the spectrum in the spectral band of the light source [93], and derivation of finite energy FWM obtained by applying finite aperture [94].

At first it was demonstrated that by combining the dispersion of a plano-concave axicon and diffraction grating and applying it to a light cone with apex angle θ_0 , allows one to approximate the parabolic support of the spectrum, in the range from 600 nm up to 1000 nm . Due to technical difficulties in manufacturing axially symmetric optical elements, in experiment the 2-dimensional FWM was generated instead of axially symmetric case.

Similar to spatial interferometric Bessel-X experiment [29], the wave field was generated from spatially filtered optical white noise of superhigh pressure Xe-arc lamp. This yielded a field with spectral band ranging from 600 nm up to 1000 nm with central wavelength of 800 nm and correlation time of $\sim 6\text{ fs}$.

The FWM was measured in interferometric cross-correlation technique, which is insensitive to the phase of the initial field and yields the phase difference introduced by the optical system. (See Chapter 3.)

Two measurements were conducted. In first of them the time delay τ with 0.43 fs step was scanned in three different z positions: $z=0\text{ cm}$, 25 cm and 50 cm . Electric field profiles $E(x, t)$ corresponding to the transform limited pulse with the spectral distribution of the initial field were retrieved. The measurement confirmed invariant propagation of the FWM over 50 cm and revealed characteristic X-branching and tilted phase surfaces.

In the second measurement the field was scanned over z axis with 3.1 mm step at fixed delay τ value. As the FWM propagates luminally, the envelope of the correlation pattern was position-invariant and the off-axis z -dependent pattern was a manifestation of the fact that the phase and the group velocities are not equal. The experimental results were in a good agreement with the theory.

4.4. Experiments on accelerating and decelerating Bessel-type waves

Accelerating or decelerating pulses arising from defects in axially symmetric optical elements or circular apertures (for example a beam clipping by the lens holder) are far more common in experimental situation than expected but they are usually considered as unwanted effect, subject to elimination in most experiments. In this research novel experimental methods have allowed us to observe the superluminally propagating pulses in time domain and classify them as counterparts of the localized waves. (See also Section 2.3)

4.4.1. Generation of accelerating and decelerating Bessel pulses by axicon and lens

In experiment [VII] accelerating and decelerating Bessel pulses were generated by combining positive and negative lens (with focal lengths of 153 mm and -152 mm , respectively) and a fused silica axicon (apex angle of 176° and hence cone angle $\theta=0.92^\circ$). The initial pulses originated from Ti:sapphire oscillator generating nearly transform limited pulses with 33 nm bandwidth, centered to 805 nm .

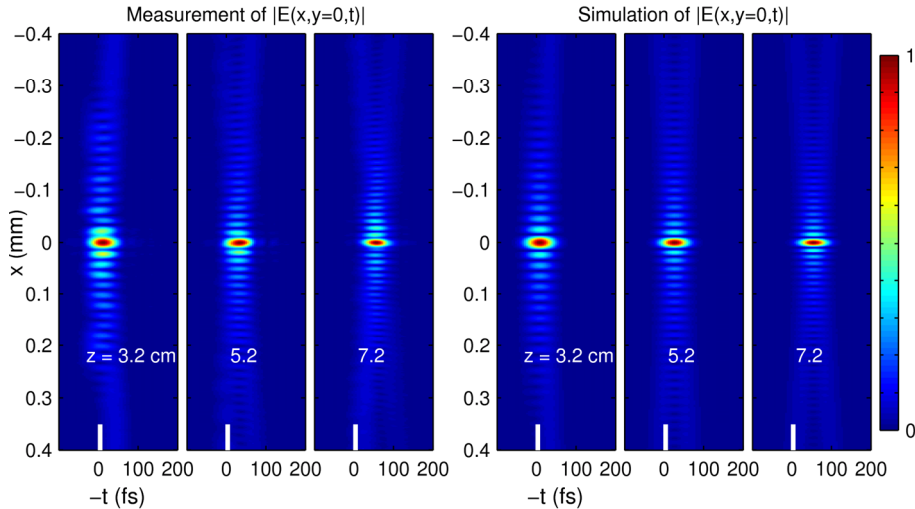


Figure 11. Comparison of the measured and calculated spatiotemporal profiles of the electric field amplitude of an *accelerating* Bessel pulse at three positions along the propagation axis (z). The color bar indicates the amplitude scale normalized separately for each plot. The white bar emphasizes $t = 0$, which is where the pulse would be located if it were propagating at c . [VII]

The accelerating and decelerating pulse evolution was recorded with $\sim 5 \mu\text{m}$ spatial and $\sim 5 \text{ fs}$ temporal resolution using SEA TADPOLE (see also experiment description in Section 4.2.5 and theoretical overview on spatial-spectral interferometric technique in Sections 3.3.1 and 3.3.2).

The axisymmetric field of accelerating Bessel pulses was scanned in one radial section on x axis, $y = 0$. The spatiotemporal field $E(x, t)$ was retrieved at different positions on z axis. From the data it was possible to determine and verify with theoretical calculations the following properties of the field:

- Spatiotemporal profiles of the field at different z values (see Figure 11);
- The temporal shift of the accelerating and decelerating pulse compared to the reference pulse traveling at speed of light c ;
- The pulse group velocity from the interference fringe spacing. The acceleration from $1.0002 c$ up to $1.0009 c$ over 4 cm of propagation and deceleration from $1.00007 c$ down to $1.00003 c$ over 12 cm of propagation were recorded;
- The compressing and stretching of the Bessel zone from 8 cm down to 5 cm in the case of accelerating pulse and up to 10 meters in the case of accelerating pulse;
- The decrease of the central maximum transversal dimensions of the accelerating pulse by the factor of 1.6 over 4 cm propagation and increase of the central maximum transversal dimensions of the decelerating pulse over 10 cm of propagation by the factor of 1.4 .

4.4.2. Formation of decelerating Bessel pulse in diffraction

In the case of ultrashort pulses, which are only few micrometers “thick”, the diffraction phenomena become spatiotemporal effect, which can be intuitively understood in the context of the boundary wave theory, first proposed by Young. According to his idea the diffraction pattern arises from the interference between a geometrical wave, “cut out” from the incident pulse by the aperture and propagating in accordance of the geometrical optics, and the boundary wave originating from the edge of the diffracting aperture.

Proper mathematical formulation to the boundary wave theory was developed by Maggy, Rubinowicz, Miyamoto and Wolf [95, 96, 97] and was shown to be equivalent to the Fresnel-Kirchhoff theory for the case of plane or spherical incident waves. In addition, the boundary wave approach presents the diffraction as a single contour integral along the diffracting boundary instead of a two-dimensional integration in the Fresnel-Kirchhoff theory.

It is shown theoretically [40] and experimentally [41, 98, 99, VIII–XI] that if the ultrashort plane wave or spherical pulse diffracts off the circular aperture, disk or slit, the on-axis radial distribution of boundary wave resembles that of the Bessel pulse and propagates superluminally in decelerating/ accelerating manner. The boundary wave pulse is known as the Arago-Poisson spot in monochromatic approach.

In Ref. [98] the formation of superluminal, decelerating phase front with continuous wave illumination was detected in both modified Young double slit experiment and in diffraction of a monochromatic field off a sphere. In the later a hole was drilled in the center of the sphere and the portion of the beam propagating through the hole served as a reference field, which intensity was modulated by the diffracted field. The intensity modulations were measured and the results were in good agreement with the theoretical predictions. Superluminal phase velocity behind an annular disk under continuous wave illumination has been observed also in [99].

A decelerating Bessel pulse was first observed in [41], where divergent spherical 20 fs duration ultrashort pulse was diffracted off a circular aperture. The on axis superluminal decelerating boundary wave pulse caught up the luminal geometrical pulse and caused modulations in the spectrum. Both axial intensity profile and the spectral modulations were measured and the existence of the decelerating pulse was confirmed.

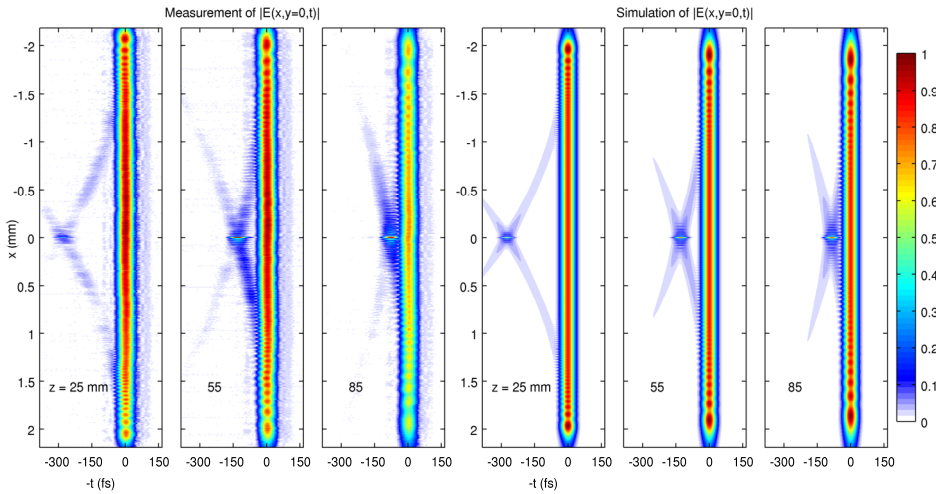


Figure 12. Formation and evolution of the diffracted field behind a circular hole 4 mm in diameter. The boundary waves interfere with each other and with the directly transmitted pulse, but the interference maximum on the axis (actually a temporally resolved spot of Arago) lags behind the direct pulse, and eventually catches up with it. [VIII]

Spatiotemporal measurements of electric field of 33 fs duration ultrashort pulse diffracting off an annular slit, disk and aperture were measured with high, $\sim 5\text{ }\mu\text{m}$ spatial and $\sim 5\text{ fs}$ temporal resolution using spatial-spectral interferometric technique SEA TADPOLE [VIII–XI]. Diffraction of an ultrashort pulse off a circular aperture is depicted on the left on Figure 12. The numeric calculations, based on boundary wave approach, show good agreement with the theory.

4.5. Conclusion

Existence of the localized waves and their peculiar properties like invariant propagation of the intensity distribution and superluminal group velocity have been explicitly demonstrated in numerous experiments. So far, the spatial-spectral interferometry combined with the FROG measurements has proven most comprehensive for registering full spatiotemporal profile of the wave fields with high spatial and spectral resolution. Although, demonstrating different properties of the wave fields might require different approach and measurement technique.

SUMMARY

This thesis belongs to the field of physical optics and gives an overview of the principles of theoretical derivation; optical synthesis and experimental measurement of optical wave fields called localized waves and accelerating and decelerating Bessel-type waves. These ultrashort localized waves have a broad spectrum, yet their energy is confined in an intense and spatiotemporally tightly localized peak and the intensity distribution propagates without any change or in strongly “subdiffractive” manner.

In the scope of this thesis:

- Superluminally propagating localized wave called Focused X Wave and its finite-energy modifications have been studied and their experimental implementation has been discussed;
- An optical setup for generating superluminally propagating localized waves with hyperbolic support of the spectrum has been proposed and thoroughly analyzed;
- The performance of spatial, spectral and spatial-spectral interferometry has been studied under illumination with spatially coherent white-noise-like signals. It was shown that all three methods allow for the retrieval of the impulse response of the optical system and for the characterization of the optical systems capability to generate complicated optical wave fields. In case the reference field is an ultrashort pulse whose spectral phase and amplitude are known, interferometric techniques allow for the full spatiotemporal measurement of the optical localized waves;
- Superluminally propagating localized waves have been generated in dispersive media by means of $\chi^{(3)}$ nonlinear process. The strong pump pulse reshaped the weak probe into a localized wave via cross phase modulation;
- The full spatiotemporal profile of the superluminally propagating localized wave called Bessel-X pulse have been experimentally measured with high spatial and temporal resolution using a device called SEA TADPOLE, which is based on a spatial-spectral interferometric technique. The group velocity of the pulse was determined with high precision;
- Superluminally propagating accelerating and decelerating Bessel pulses, a somewhat distorted modifications of Bessel-X pulses, were generated by propagating an input pulse through an optical system consisting of a lens and an axicon. The resulting spatiotemporal field was fully measured with the SEA TADPOLE;
- Formation of superluminally propagating and decelerating Bessel pulses in the diffraction process was explicitly demonstrated by propagating ultrashort pulses through circular apertures, disks and slits. The resulting fields were measured with high spatial and temporal resolution using SEA TADPOLE.

SUMMARY IN ESTONIAN

Superluminaalselt levivad lokaliseeritud valgusimpulsid

Käesolev doktoritöö tegeleb füüsilise optika valdkonda kuuluva lainelevi teemaatikaga. Töös uuritakse laiaribalisi optilisi lainevälju – lokaliseeritud laineid – millel moodustub terava energiamaksimum mõõtmega lainepikkuse suurusjärgus. Kui enamlevinud fokuseeritud laineväljad, näiteks Gaussi impulss, säilitavad levides sellist lokaliseeritust väga lühikeste vahemaade kestel, võivad lokaliseeritud lained levida teoreetilisel piiril lausa lõpmata pikki vahemaasid ilma kuju muutmata ning on seetõttu perspektiivikad paljude rakenduste jaoks.

Käesolevas töös on esitatud ülevaade lokaliseeritud lainete teoreetilisest tuletamisest (Peatükk 2), eksperimentaalse genereerimise ning mõõtmise printsiipidest (Peatükid 2 ja 3) ja nende printsiipide reaalistest rakendustest (Peatükk 4). Dissertandi originaalpanus (vt lk 8) on publitseeritud artiklites [I–XIII], millest esimesed 11 kuuluvad ETIS’ e kategooriasse 1.1, ja seisneb lühidalt järgnevas:

- Ülevalgusekiirusega (superluminaalselt) leviva lokaliseeritud laine, mida kutsutakse fokuseeritud X laineks, ning tema lõpliku koguenergiaga modifikatsioonide tuletamine, teoreetiline uurimine ning optilise genereerimise võimalikkuse näitamine [I, II].
- Superluminaalselt levivate lokaliseeritud laineväljade, mille spektri kandja on hüperboolikujuline, optilise genereerimise printsiibi väljatöötamine ja uurimine [III, IV, XII].
- Superluminaalselt leviva lokaliseeritud lainevälja genereerimine dispergeerivas keskkonnas läbi mittelinearse faaside ristmoduleerimise. Intensiivne “mittedifrageeruv” pumpav impulss indutseeris keskkonna murdumisnäitaja muutuse, mis omakorda tõi kaasa ajaliselt sünkroniseeritud prooviimpulsi muundumise leviinvariantseks laineväljaks [V].
- Ruumilise, spektraalse ja ruumilis-spektraalse interferomeetria kui elektrivälja registreerimise ning rekonstrueerimise meetodite uurimine ruumiliselt koherentsete, ent spektraalselt mittekorreleeritud laineväljade, so valge-müra signaali, korral. Õnnestus demonstreerida, et kõik nimetatud interferomeetrilised meetodid võimaldavad nimetatud tingimustel mõõta optilise süsteemi impulsskostet ning iseloomustada optilise süsteemi suutlikkust moodustada keeruka ruumilise struktuuriga optilist lainevälja ülilühikesest impulsist (Peatükk 30). Kasutades võrdlusimpulsina ülilühikesest femtosekundimpulssi, mille välja amplituud ja faas on teada, on võimalik läbi viia lokaliseeritud laineväljade kõrgeresolutsioonilisi ajalis-ruumilisi mõõtmisi ([VI–XI, XIII]).
- Lokaliseeritud lainevälja, mida kutsutakse Bessel-X impulsiks, mõõtmine kõrge ajalise ja ruumilise lahtusega, mis võimaldasid muuhulgas suure täpsusega määrata lainevälja superluminaalse rühmakiiruse. Mõõtmised viidi

läbi ruumilis-spektraalsel interferomeetrial põhineva SEA TADPOLE seadmega. [VI, XIII]

- Superluminaalselt, kiirenevalt ja aeglustuvalt levivate Besseli impulsside, mis on Bessel-X impulsi modifikatsioonid, optiline moodustamine läätsest ja aksikonist koosneva optilise süsteemi abil ning nimetatud laineväljade kõrge lahutusega ajalis-ruumiline mõõtmine ja iseäralike parameetrite määramine eksperimendis SEA TADPOLE'ga [VII].
- Ülilühikeste impulsside difrageerumisel ümmarguselt avalt, kettalt ja pilult moodustuva lainevälja mõõtmine kõrge ajalise ja ruumilise lahutusega. Nimetatud ajalis-ruumilised mõõtmised SEA TADPOLE'ga kinnitavad ja võimaldavad demonstreerida superluminaalselt, aeglustuvalt leviva Besseli impulsi, mida teatakse Arago-Poissoni täpina, moodustumist kirjeldatud difraktsiooni protsesside käigus. [VIII–XI]

ACKNOWLEDGEMENTS

I am most grateful to my supervisor, prof. acad. Peeter Saari, for guiding me to the intriguing subject of physical optics and sharing his endless knowledge during the PhD studies.

I thank also colleagues in Institute of Physics at University of Tartu, especially Kaido Reivelt, PhD, for sharing his expertise and understanding on the subject of localized waves; Rünno and Ants Lõhmus, PhD, for helping to solve number of technical issues starting from making the samples and ending with schemes for manufacturing non-existing optical elements; Agu Anijalg for his technical and administrative advice; Kõu Timpmann, PhD, for dedicating his time to help us with the Ti:sapphire laser.

I have gained great experimental experience during the year I spent in Vilnius University, Lithuania, studying nonlinear effects in Kerr media under supervision of prof. Audrius Dubietis and dr. Gintaras Tamošauskas (with Marie Curie Early Stage Training grant MEST-CF-2004-008048 (ATLAS)). I am also thankful for Italian colleagues prof. Paolo Di Trapani, prof. Daniele Faccio, Ottavia Jedrkiewicz, PhD, who organized two exiting experimental summer schools and who have done the honor of accepting me in their lab in Como, Italy for three weeks in January 2008, which led to joint publication [V].

Versatile collaboration with colleagues Pamela Bowlan, PhD, and prof. Rick Trebino in Atlanta, Georgia Institute of Technology has turned out to be very fruitful and led to extremely beautiful results. I thank Pamela also for editing parts of the thesis manuscript linguistically.

It has been pleasure to work together with the young colleagues Peeter Piksarv and Madis Lõhmus in Tartu and also with Paolo Polesana, Matteo Clerici, Alesandro Averchi and Eleonora Rubino in Vilnius, Italy and Greece.

Excellent friend and fellow student Kadri Isakar has been irreplaceable companion and moral support throughout the studies, especially in numerous existential discussions about becoming and being a physicist.

I thank my family for their support and I am especially grateful to my husband and our wonderful daughter for their cheerfulness, patience and for motivating me to work in the most efficient manner.

REFERENCES

- [1] H. Bateman, *Electrical and Optical Wave Motion*, (Cambridge University Press, Cambridge, 1915).
- [2] R. Courant and D. Hilbert, *Methoden der mathematischen Physik, Zweiter Band* (Springer, 1937, Berlin).
- [3] J. A. Stratton, *Electromagnetic Theory* (McGraw-Hill, New York, 1941).
- [4] J. N. Brittingham, "Focus waves modes in homogeneous Maxwell's equations: Transverse electric mode" *J. Appl. Phys.* **54** 1179, (1983).
- [5] T. T. Wu and R. W. P. King, "Comment on "Focus wave modes in homogeneous Maxwell's equations: Transverse electric mode" *J. Appl. Phys.* **56** 2587 (1984).
- [6] A. Sezginer, "A general formulation of focus wave modes" *J. Appl. Phys.* **57** 678 (1985).
- [7] T. T. Wu, and H. Lehmann, "Spreading of electromagnetic pulses" *Appl. Phys.* **58** 2064 (1985).
- [8] H. E. Hernandez-Figueroa, M. Zamboni-Rached, and E. Recami, eds., *Localized Waves: Theory and Applications* (J. Wiley, New York, 2008).
- [9] I. Besieris, M. Abdel-Rahman, A. Shaarawi, and A. Chatzipetros, "Two fundamental representations of localized pulse solutions to the scalar wave equation" *Prog. Electromagn. Res.* **19**, 1 1998.
- [10] Ziolkowski, R. W., "Exact solutions of the wave equation with complex source locations," *J. Math. Phys.* **26**, 861–863 (1985).
- [11] Palmer, M. R., and R. Donnelly, "Focused wave modes and the scalar wave equation," *J. Math. Phys.* **34**, 4007–4013 (1993).
- [12] P. Saari, "Superluminal localized waves of electromagnetic field in vacuo," in *Time's Arrows, Quantum Measurement and Superluminal Behavior, Scientific Monographs: Phys. Sci. Series*, D. Mugnai *et al*, eds. (CNR, Rome, Italy 2001), pp. 37 or arXiv:physics/0103054.
- [13] P. Saari, "Localized waves in femtosecond optics," in: *Ultrafast Photonics*, (Institute of Physics Publishing, Bristol and Philadelphia, 2004) pp. 317–340.
- [14] Besieris, I. M., A. M. Shaarawi, and R. W. Ziolkowski, "A bidirectional traveling plane wave representation of exact solutions of the scalar wave equation," *J. Math. Phys.* **30**, 1254–1269 (1989).
- [15] J. Lu, X.-L. Xu, and J. F. Greenleaf, "A New Approach to Obtain Limited Diffraction Beams" *IEEE Trans. Ultrason. Ferroelectr. Freq. Control* **42**, 850 (1995).
- [16] J. Fagerholm, A. T. Friberg, J. Huttunen, D. P. Morgan, and M. M. Salomaa "Angular-spectrum representation of nondiffracting X waves" *Phys. Rev. E* **54**, 4347 (1996).
- [17] A. T. Friberg, J. Fagerholm, and M. M. Salomaa, "Space-frequency analysis of nondiffracting pulses" *Opt. Commun.* **136**, 207 (1997).
- [18] J. Salo, J. Fagerholm, A. T. Friberg, and M. M. Salomaa, "Unified description of nondiffracting X and Y waves". *Phys. Rev. E* **62**, 4261–4275 (2000).
- [19] E. Recami "Superluminal Motions? A Bird's-Eye View of the Experimental Situation" *Foundations of Physics*, **31**, 1119–1135 (2001).
- [20] E. Recami, "On localized 'X-shaped' Superluminal solutions to Maxwell equations" *Physica A* 252 586–610 (1998).
- [21] A.O. Barut, G.D. Maccarrone, and E. Recami, "On the shape of tachyons" *Nuovo Cimento A* **71**, 509 (1982).

- [22] R. Donnelly and R. W. Ziolkowski, “Designing localized waves,” Proc. R. Soc. Lond., **A440**, 541–565, (1992).
- [23] K. Reivelt, P. Saari, [arXiv:physics/0309079v2](https://arxiv.org/abs/physics/0309079v2) (2003) (*PhD thesis of K. Reivelt*)
- [24] P. Saari, K. Reivelt “Generation and classification of localized waves by Lorentz transformations in Fourier space” Phys. Rev. E **69**, 036612 (2004).
- [25] J. Durnin, Exact solutions for nondiffracting beams. I. The scalar theory, J. Opt. Soc. Am. A **4**, 651–654 (1987).
- [26] J. Durnin, J.J. Miceli, and J.H. Eberly, Diffraction-free beams, Phys. Rev. Lett. **58**, 1499–1502 (1987).
- [27] D. MCGloin, and K. Dholakia “Bessel beams: diffraction in a new light” Contemporary Physics, **46**, 15 (2005).
- [28] J. Lu and J. F. Greenleaf “Experimental Verification of Nondiffracting X Waves”, IEEE Trans. Ultrason. Ferroelectr. Freq. Control **39**, 441 (1992).
- [29] P. Saari and K. Reivelt, “Evidence of X-Shaped Propagation-Invariant Localized Light Waves” Phys. Rev. Lett. **79**, 4135 (1997).
- [30] Sonajalg, H., and P. Saari, “Suppression of temporal spread of ultrashort pulses in dispersive media by Bessel beam generators,” Opt. Lett. **21**, 1162–1164 (1996).
- [31] Sõnajalg, H., M. Rästep, and P. Saari, “Demonstration of the Bessel-X pulse propagating with strong lateral and longitudinal localization in a dispersive medium,” Opt. Lett. **22**, 310–312 (1997).
- [32] I. Alexeev, K. Y. Kim, and H.M.Milchberg, “Measurement of the superluminal group velocity of an ultrashort Bessel beam pulse” Phys. Rev. Lett. **88**, 073901 (2002).
- [33] K. Reivelt and P. Saari, “Experimental demonstration of realizability of optical focus wave modes” Phys. Rev. E **66**, 056611 (2002).
- [34] R. Grunwald, V. Kebbel, U. Griebner, U. Neumann, A. Kummrow, M. Rini, E. T. J. Nibbering, M. Piche, G. Rousseau, and M. Fortin, “Generation and characterization of spatially and temporally localized few-cycle optical wave packets” Phys. Rev. A **67**, 063820 (2003).
- [35] D. Mugnai, A. Ranfagni, and R. Ruggeri, “Observation of Superluminal Behaviors in Wave Propagation” Phys. Rev. Lett. **84**, 4830 (2000).
- [36] Zhiping Jiang and Xi-Cheng Zhang, “2D measurement and spatio-temporal coupling of few-cycle THz pulses,” Opt. Express **5**, 243–248 (1999).
- [37] F. Bonaretti, D. Faccio, M. Clerici, J. Biegert, and P. Di Trapani, “Spatiotemporal amplitude and phase retrieval of Bessel-X pulses using a Hartmann-Shack sensor,” Opt. Express **17**(12), 9804–9809 (2009).
- [38] P. W. Milonni, “Controlling the speed of light pulses” J. Phys. B **35**, R31 (2002).
- [39] M. Clerici, D. Faccio, A. Lotti, E. Rubino, O. Jedrkiewicz, J. Biegert, and P. Di Trapani, “Finite-energy, accelerating Bessel pulses,” Opt. Express **16**, 19807–19811 (2008).
- [40] Z. L. Horváth, and Z. Bor, “Diffraction of short pulses with boundary diffraction wave theory,” Phys. Rev. E **63**, 026601–026611 (2001).
- [41] Z. L. Horvath, J. Klebniczki, G. Kurdi, A. P. Kovacs, “Experimental investigation of the boundary wave pulse” Optics Communications **239**, 243 (2004)
- [42] P. Di Trapani, G. Valiulis, A. Piskarskas, O. Jedrkiewicz, J. Trull, C. Conti, and S. Trillo, “Spontaneously generated X-shaped light bullets,” Phys. Rev. Lett. **91**, 93904 (2003).
- [43] D. Faccio, A. Couairon, and P. Di Trapani *Conical Waves, Filaments and Non-linear Filamentation Optics*. (Aracne, Rome, 2007).

- [44] V. Garces-Chavez, D. McGloin, H. Melville, W. Sibbett, and K. Dholakia, “Simultaneous micromanipulation in multiple planes using a self-reconstructing light beam” *Nature* **419**, 145–147 (2002).
- [45] P. Dufour, M. Piché, Y. De Koninck, and N. McCarthy, “Two-photon excitation fluorescence microscopy with a high depth of field using an axicon,” *Appl. Opt.* **45**, 9246–9252 (2006).
- [46] C. T. A. Brown, D. J. Stevenson, X. Tsampoula, C. McDougall, A. A. Lagatsky, W. Sibbett, F. J. Gunn-Moore, and K. Dholakia, “Enhanced operation of femtosecond lasers and applications in cell transfection,” *Journal of Biophotonics* **1**, 183–199 (2008).
- [47] X. Tsampoula, V. Garces-Chavez, M. Comrie, D. J. Stevenson, B. Agate, C. T. A. Brown, F. Gunn-Moore, and K. Dholakia, “Femtosecond cellular transfection using a nondiffracting light beam” *Appl. Phys. Lett.* **91**, 053902 (2007).
- [48] D. McGloin ja K. Dholakia, “Bessel beams: diffraction in a new light,” *Contemporary Physics* **46**, 15–28 (2005).
- [49] K. Dholakia ja W. Lee, “*Optical trapping takes shape: The use of structured light fields*,” (Academic Press, 2008), pp. 261–337.
- [50] P. Polesana, M. Franco, A. Couairon, D. Faccio, and P. Di Trapani, “Filamentation in Kerr media from pulsed Bessel beams,” *Phys. Rev. A* **77**, 043814 (2008).
- [51] P. Polynkin, M. Kolesik, A. Roberts, D. Faccio, P. Di Trapani, J.V. Moloney, “Generation of extended plasma channels in air using femtosecond Bessel beams,” *Optics Express* **16**, 15733 (2008)
- [52] P. Saari, Spatially and temporally nondiffracting ultrashort pulses, in *Ultrafast Processes in Spectroscopy*, O. Svelto, S. De Silvestri, and G. Denardo, eds. (Plenum Press, New York, 1996), pp. 151–156.
- [53] P. Saari and H. Sönaialg, “Pulsed Bessel Beams” *Laser Phys.* **7**, 32 (1997).
- [54] M. Bock, S. K. Das, and R. Grunwald, “Programmable ultrashort-pulsed flying images,” *Opt. Express* **17**, 7465–7478 (2009).
- [55] K. Saastamoinen, J. Turunen, P. Vahimaa, and A. T. Friberg, “Spectrally partially coherent propagation-invariant fields” *Phys. Rev. A* **80**, 053804 (2009).
- [56] J. Turunen, A. Vasara, and A. T. Friberg, “Propagation invariance and self-imaging in variable coherence optics,” *J. Opt. Soc. Am. A* **8**, 282–289 (1991).
- [57] K. Reivelt and P. Saari, “Angular spectrum analysis and synthesis of propagation invariant femtosecond-domain localized wave fields” in *Ultrafast Processes in Spectroscopy, Proceedings of the X International Symposium*, R. Kaarli, A. Freiberg, and P. Saari, eds. (Institute of Physics, Tartu, Estonia, 1998) pp. 168–175; physics/0309079.
- [58] H. Bateman and A. Erdelyi, *Tables of Integral Transforms I* (McGraw-Hill, New York, 1954).
- [59] J. Lu and J. F. Greenleaf “Nondiffracting X waves – exact solutions to free-space scalar wave equation and their finite aperture realizations”, *IEEE Trans. Ultrason. Ferroelectr. Freq. Control* **39**, 19 (1992)
- [60] L. Mackinnon, “A nondispersive de Broglie wave packet” *Found. Phys.* **8**, 157 (1978).
- [61] C. J. Zapata-Rodriguez and M. A. Porras, “X-wave bullets with negative group velocity in vacuum,” *Opt. Lett.* **31**, 3532–3534 (2006).
- [62] M. Clerici, D. Faccio, A. Lotti, E. Rubino, O. Jedrkiewicz, J. Biegert, and P. Di Trapani, “Finite-energy, accelerating Bessel pulses,” *Opt. Express* **16**, 19807–19811 (2008).

- [63] R. Grunwald, U. Griebner, F. Tschirschwitz, E. T. J. Nibbering, T. Elsaesser, V. Kebbel, H.-J. Hartmann, and W. Jüptner, "Generation of femtosecond Bessel beams with microaxicon arrays" *Opt. Lett.* **25**, 981 (2000).
- [64] D. J. Kane and R. Trebino, "Characterization of arbitrary femtosecond pulses using frequency-resolved optical gating," *J. Quantum Electron.* **29**, 571–579 (1993).
- [65] R. Trebino and D. Kane, "Using phase retrieval to measure the intensity and phase of ultrashort pulses: frequency-resolved optical gating," *JOSAA* **10**, 1101–1111 (1993).
- [66] R. Trebino, *Frequency-Resolved Optical Gating: The Measurement of Ultrashort Laser Pulses* (Kluwer Academic Publishers, Boston, 2002).
- [67] C. Iaconis and I. A. Walmsley, "Spectral phase interferometry for direct electric-field reconstruction of ultrashort optical pulses," *Opt. Lett.* **23**, 792–794 (1998).
- [68] C. Iaconis and I. A. Walmsley, "Self-referencing spectral interferometry for measuring ultrashort optical pulses," *IEEE J. Quantum Electron.* **35**, 501–509 (1999).
- [69] I. A. Walmsley, C. Dorrer "Characterization of ultrashort electromagnetic pulses" *Advances in Optics and Photonics* **1**, 308–437 (2009).
- [70] V. V. Lozovoy, I. Pastirk, and M. Dantus, "Multiphoton intrapulse interference. IV. Ultrashort laser pulse spectral phase characterization and compensation," *Opt. Lett.* **29**, 775–777 (2004).
- [71] C. Dorrer, E. M. Kosik, I. A. Walmsley "Spatio-temporal characterization of the electric field of ultrashort optical pulses using two-dimensional shearing interferometry," *Appl. Phys. B* **74**, S209-S217 (2002).
- [72] R. Grunwald, U. Neumann, U. Griebner, K. Reimann, and G. Steinmeyer, V. Kebbel "Ultrashort-pulse wave-front autocorrelation," *Opt. Lett.* **28**, 2399–2401, (2003).
- [73] F. Bragheri, D. Faccio, F. Bonaretti, A. Lotti, M. Clerici, O. Jedrkiewicz, C. Liberale, S. Henin, L. Tartara, V. Degiorgio, P. Di Trapani, "Complete retrieval of the field of ultrashort optical pulses using the angle-frequency spectrum," *Opt. Lett.* **33**, 2952–2955 (2008).
- [74] E. Rubino, D. Faccio, L. Tartara, P. K. Bates, O. Chalus, M. Clerici, F. Bonaretti, J. Biegert, P. Di Trapani "Spatiotemporal amplitude and phase retrieval of space-time coupled ultrashort pulses using the Shackled-FROG technique" *Opt. Lett.* **34**, 3854 (2009).
- [75] F. Träger (Ed.) *Springer Handbook of Lasers and Optics*, (Springer Science+Business Media, LLC New York, 2007).
- [76] E. Wolf, *Introduction to the Theory of Coherence and Polarization of Light* (Cambridge Univ. Press, 2007).
- [77] L. Mandel and E. Wolf, *Optical Coherence and Quantum Optics* (Cambridge Univ. Press, 1995).
- [78] R. Trebino, "Ultrafast Optics" lecture slides.
<http://www.physics.gatech.edu/frog/lectures/UltrafastOptics/lectures/UFO12UltrafastInterferometry.ppt>
- [79] C. Froehly, A. Lacourt, and J. C. Vienot, "Time impulse response and time frequency response of optical pupils. Experimental confirmations and applications," *J. Opt.*, **4**, 183, (1973).
- [80] L. Lepetit, M. Joffe, "Two-dimensional nonlinear optics using Fourier-transform spectral interferometry," *Opt. Lett.* **21**, 564–566 (1996).

- [81] D. N. Fittinghoff, J. L. Bowie, J. N. Sweetser, R. T. Jennings, M. A. Krumbügel, K. W. DeLong, R. Trebino, and I. A. Walmsley “Measurement of the intensity and phase of ultraweak, ultrashort laser pulses”, *Opt. Lett.* **21**, 884–886 (1996).
- [82] A. M. Weiner, D. E. Leaird, D. H. Reitze, and E. G. Paek “Femtosecond Spectral Holography”, *IEEE Journal of Quantum Electronics* **28**, 2251–2261 (1992).
- [83] A. C. Kovaecs, K. Osvay, and Zs. Bor, “Group-delay measurement on laser mirrors by spectrally resolved whitelight interferometry,” *Opt. Lett.* **20**, 788–791 (1995).
- [84] A. P. Kovaecs, K. Osvay, G. Kurdi, M. Gorbe, J. Klenbiczki, and Z. Bor, “Dispersion control of a pulse stretcher-compressor system with two-dimensional spectral interferometry,” *Appl. Phys. B* **80**, 165–170 (2005).
- [85] D. Meshulach, D. Yelin, and Y. Silberberg, “Real-time spatial-spectral interference measurements of ultrashort optical pulses,” *J. Opt. Soc. Am. B* **14**, 2095–2098 (1997).
- [86] E. M. Kosik, A. S. Radunsky, I. Walmsley, and C. Dorrer, “Interferometric technique for measuring broadband ultrashort pulses at the sampling limit,” *Opt. Lett.* **30**, 326–328 (2005).
- [87] P. Bowlan, P. Gabolde, A. Schreenath, K. McGresham, R. Trebino, and Selcuk Akturk “Crossed-beam spectral interferometry: a simple, high-spectral-resolution method for completely characterizing complex ultrashort pulses in real time,” *Opt. Express* **14**, 11892–11900 (2006).
- [88] P. Bowlan, P. Gabolde, M. A. Coughlan, R. Trebino, and R. J. Levis, “Measuring the spatiotemporal electric field of ultrashort pulses with high spatial and spectral resolution” *JOSAB* **25**, A81–A92 (2008).
- [89] P. Bowlan, P. Gabolde, and R. Trebino, “Directly measuring the spatio-temporal electric field of focusing ultrashort pulses,” *Opt. Express* **15**, 10219–10230 (2007).
- [90] P. Bowlan, “Measuring the spatiotemporal electric field of ultrashort pulses with high spatial and spectral resolution”, PhD thesis, (Georgia Institute of Technology, Atlanta, 2009).
- [91] R. Grunwald, U. Griebner, E. T. J. Nibbering, A. Kummrow, M. Rini, T. Elsaesser, V. Kebbel, H.-J. Hartmann, and W. Jüptner, “Spatially resolved small-angle noncollinear interferometric autocorrelation of ultrashort pulses with microaxicon arrays,” *J. Opt. Soc. Am. A* **18**, 2923–2931 (2001).
- [92] R. Grunwald, U. Neumann, U. Griebner, K. Reimann, G. Steinmeyer, and V. Kebbel, “Ultrashort-pulse wave-front autocorrelation,” *Opt. Lett.* **28**, 2399–2401 (2003).
- [93] Kaido Reivelt and Peeter Saari, “Optical generation of focus wave modes,” *J. Opt. Soc. Am. A* **17**, 1785–1790 (2000).
- [94] K. Reivelt, P. Saari. “Optically realizable localized wave solutions of the homogeneous scalar wave equation” *Physical Review E*, **65** 046622 (2002).
- [95] Maggi, G. A. “Sulla propagazione libera e perturbata delle onde luminose in un mezzo isotropo” *Ann. di Mat.* **IIa 16**, 21 (1888).
- [96] Rubinowicz, A. “Thomas Young and the theory of diffraction” *Nature* **180**, 160–162 (1957).
- [97] Born, M. & Wolf, E. *Principles of Optics* (6th ed. Pergamon Press, Oxford, 1987).
- [98] D. Chauvat, O. Emile, M. Brunel and A. Le Floch, “Direct measurement of the central fringe velocity in Young-type experiments,” *Phys. Lett. A* **295**, 78–80 (2002).

- [99] M. Vasnetsov, V. Pas'ko, A. Khoroshun, V. Slyusar and M. Soskin, "Observation of superluminal wave-front propagation at the shadow area behind an opaque disk," *Opt. Lett.* **32**, 1830–1832 (2007).

PUBLICATIONS

P. Saari, M. Menert and H. Valtna,
“Photon localization barrier can be overcome”,
Opt. Commun. **246**, 445–450 (2005).



Photon localization barrier can be overcome

P. Saari ^{a,b,*}, M. Menert ^a, H. Valtna ^a

^a Department of Physics, University of Tartu, Estonia

^b Institute of Physics, University of Tartu, Riia 142, Tartu 51014, Estonia

Received 29 August 2004; received in revised form 2 November 2004; accepted 4 November 2004

Abstract

In contradistinction to a widespread belief that the spatial localization of photons is restricted by a power-law falloff of the photon energy density, Bialynicki-Birula [Phys. Rev. Lett. 80 (1998) 5247] has proved that any stronger – up to an almost exponential – falloff is allowed. We are showing that for certain specifically designed cylindrical one-photon states the localization is even better in lateral directions. If the photon state is built from the so-called focus wave mode, the falloff in the waist cross-section plane turns out to be quadratically exponential (Gaussian) and such strong localization persists in the course of propagation.

© 2004 Elsevier B.V. All rights reserved.

PACS: 03.70.+k; 03.50.De; 03.65.Pm; 11.30.Cp

Keywords: Quantum optics; Polychromatic photons; Non-locality; Focus wave mode; Focused X wave; Paley–Wiener theorem

Whilst quantum electrodynamics (QED) underwent an impressive development and reached its maturity in the middle of the last century, one of its basic concepts – the photon wave function in free space – was deprived of such fortune. Although the photon wave function in coordinate representation was introduced already in 1930 by Landau and Peierls [1] the concept was found to suffer from inherent difficulties that were not overcome during the century (see review [2]). The common explanation

presented in textbooks (e.g., [3,4]) may be summed up as follows: (i) no position operator exists for the photon, (ii) while the position wave function may be localized near a space-time point, the measurable quantities like the electromagnetic field vectors, energy, and the photodetection probability remain spread out due to their non-local relation with the position wave function. However, just before the turn of the century both of these widely espoused notions were disproved [5,6] and in the new century a fresh interest in the photon localization problem seems to have been awakened (see, e.g., [7–9]), meeting the needs of developments in near-field optics, cavity QED, and quantum computing.

* Corresponding author. Tel.: +3725109018; fax: +3727383033.

E-mail address: Peeter.Saari@ut.ee (P. Saari).

Bialynicki-Birula [6] writes that the statement “even when the position wave function is strongly concentrated near the origin, the energy wave function is spread out over space asymptotically like $r^{-7/2}$ ” (citation from [4], p. 638) is incorrect and that both wave functions may be strongly concentrated near the origin. He demonstrates, on one hand, that photons can be essentially better localized in space – with an exponential falloff of the photon energy density and the photodetection rates. On the other hand, he establishes – and it is even somewhat startling that nobody has done it earlier – that certain localization restrictions arise out of a mathematical property of the positive frequency solutions which therefore are of a universal character and apply not only to photon states but hold for all particles. More specifically, it has been proven in the Letter [6] for the case of spherically imploding-exploding one-photon wavepacket that the Paley–Wiener theorem allows even at instants of maximal localization only such asymptotic decrease of the modulus of the wave function with the radial distance r that is *slower* than the linear exponential one, i.e., anything slower than $\sim \exp(-Ar)$, where A is a constant. The latter is what the Paley–Wiener theorem says about a function whose Fourier spectrum contains no negative frequencies.

The purpose of the present short communication is to indicate that one-photon wave functions of a specific type can break the localization restriction and exhibit the linear exponential and even faster falloff with the distance. Yet, there is no contradiction either with the result of [6] or with the Paley–Wiener theorem, since the wave functions are cylindrical and exhibit an exceptionally strong localization in two dimensions out of three. The paper is interdisciplinary and involves a “technology transfer” in the sense that in order to tackle the problem belonging to QED, we make use of certain very recent results obtained in the study of the so-called localized acoustical and (classical) electromagnetic waves.

As an introduction, we consider briefly the simplest case of a one-dimensional Landau–Peierls wave function in order to indicate how the Paley–Wiener theorem restricts the spatial localization of a photon. Then we study the radial falloff

for three different cylindrical wave functions, using exactly the same formalism that has been presented in [6]. Finally, the discussion of our results allows us to refine the analysis given in [6].

Let us consider a one-photon (1 ph) state that corresponds to a plane-wave pulse propagating unidirectionally, say, along the axis z , being polarized along a lateral axis (say, the x -axis)

$$|1 \text{ ph}\rangle = \int_0^\infty dk_z f(k_z) a^+(k_z) |\text{vac}\rangle, \quad (1)$$

where $a^+(k_z)$ is the creation operator of a photon and $f(k_z)$ is a properly normalized photon wave function in the momentum representation. Then the inverse Fourier transform (but including positive frequencies only!)

$$\Phi(z, t) = \frac{1}{2\pi} \int_0^\infty dk_z f(k_z) e^{i(k_z z - \omega t)} \quad (2)$$

$$= \frac{1}{2\pi} \int_0^\infty dk f(k) e^{ik(z-ct)} \quad (3)$$

represents the corresponding position space wave function of the photon in state $|1 \text{ ph}\rangle$ (see, e.g., [4], p. 636). The modulus squared $|\Phi(z, t)|^2$ gives the photon probability density, i.e., the degree of localization along the axis z (in the given case in the directions x and y any localization is absent). If $f(k)$ differs from zero within a wide frequency band, the probability $|\Phi(z, t)|^2$ may be strongly localized around a point z_0 moving along the axis z with the speed of light c . However, since $\Phi(z, t)$, due to the absence of negative frequencies in the integral of Eq. (2), is nothing but a complex analytic signal, according to the Paley–Wiener theorem (or criterion) the asymptotic decrease of $|\Phi(z, t)|^2$ with the distance $r = |z - z_0|$ has to be weaker than $\sim \exp(-Ar)$, where A is a constant. All the more excluded are any finite-support functions in the role of $\Phi(z, t)$. To conclude the introduction, let us notice that if the counterpropagating (with $k_z < 0$) Fourier components are involved in Eq. (2), the Paley–Wiener theorem does not apply at the instant $t = 0$.

Following [6], we shall study the photon localization by examining the asymptotic behavior of the positive frequency part of the Riemann–Silberstein vector $\mathbf{F}(\mathbf{r}, t)$ (called the energy wave function) which directly determines the energy density of a

one-photon state and is conveniently expressed through a “superpotential” $\mathbf{Z}(\mathbf{r}, \tau)$

$$\mathbf{F}(\mathbf{r}, t) = \nabla \times \left[\mathbf{i} \frac{\partial}{\partial \tau} \mathbf{Z}(\mathbf{r}, \tau) + \nabla \times \mathbf{Z}(\mathbf{r}, \tau) \right], \quad (4)$$

where $\tau \equiv ct$. The vector field $\mathbf{Z}(\mathbf{r}, \tau)$ is nothing but an analytic signal version of the Hertz potential, i.e., $\mathbf{Z}(\mathbf{r}, \tau) = \mathbf{m}\Psi(\mathbf{r}, \tau)$, where \mathbf{m} is a constant vector that includes the proper normalization factor and $\Psi(\mathbf{r}, \tau)$ is any solution of the scalar wave equation, which is taken in the form of the analytic signal. It should be stressed that $\mathbf{Z}(\mathbf{r}, \tau)$ is a complexified Hertz potential and it comprises the positive frequencies only, i. e., the complexification corresponds to the very nature of the number states of quantized EM field and is not involved merely for the sake of convenience as in the classical electrodynamics [2].

As the first example leading to a stronger localization that one might expect from the Paley–Wiener theorem, let us consider the photon field where \mathbf{m} is directed along the axis z (any other orientation gives similar results) and $\Psi(\mathbf{r}, \tau)$ is a superposition of cylindrically symmetric Bessel functions J_0 as a wavepacket with the exponential spectrum and a specific dispersion law for the axial wavenumber $k_z(\omega) = \text{constant} = k_0$

$$\Psi(\rho, z, \tau) = \int_{|k_0|}^{\infty} dk J_0(k_\rho \rho) e^{-k_A} e^{-i(k\tau - k_0 z)}, \quad (5)$$

where the radial coordinate ρ has been introduced and $k_\rho = (k^2 - k_0^2)^{1/2}$ is the lateral component of the wave vector of the monochromatic plane-wave constituents represented with the weight function e^{-k_A} whose width is Δ^{-1} . The integral can be taken with the help of a Laplace transform table and we obtain

$$\mathbf{Z}(\rho, z, \tau) = \mathbf{m} \frac{\exp\left(-|k_0| \sqrt{\rho^2 + (\Delta + i\tau)^2}\right)}{\sqrt{\rho^2 + (\Delta + i\tau)^2}} e^{ik_0 z}. \quad (6)$$

Eq. (6) describes a simple cylindrical pulse modulated harmonically in the axial direction and radially converging (when $\tau < 0$) to the axis and thereafter (when $\tau > 0$) expanding from it, the intensity distribution resembling an infinitely long

tube coaxial with the z -axis and with a time-dependent diameter (see Fig. 6. in [10]). It follows from Eqs. (6) and (4) that

$$|\mathbf{Z}(\rho \rightarrow \infty, z, \tau = 0)| \sim \rho^{-1} \exp(-\rho/l), \quad (7)$$

$$|\mathbf{F}(\rho \rightarrow \infty, z, \tau = 0)|^2 \sim [\rho^{-2} + O(\rho^{-3})] \times \exp(-2\rho/l), \quad (8)$$

where $l \equiv |k_0|^{-1}$ is the characteristic length (or length unit). Thus, while the photon is delocalized in the axial direction, its energy density falloff in the lateral directions is exactly the linear exponential one at all times the conditions $\tau \ll \rho \gg \Delta$ are fulfilled, see Fig. 1. The time derivative as well as the spatial derivatives contain the same exponential factor, ensuring the exponential falloff of the Riemann–Silberstein vector in Eq. (8). Hence, a one-photon field given by Eq. (6) serves as the first and simplest example where the localization in two transversal dimensions is governed by different rules than localization in three dimensions according to [6].

The next example is readily available via the Lorentz transformation of the wave function given by Eq. (5) along the axis z , which gives another possible solution of the scalar wave equation.

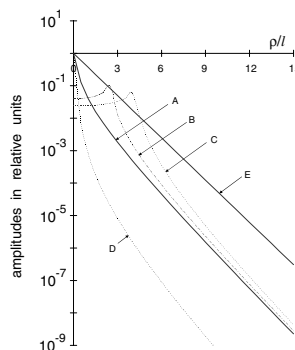


Fig. 1. Curves of the radial dependence in a decimal logarithmic scale. Curve A is for $|\mathbf{Z}(\rho, 0, \tau = 0)|$; B, $|\mathbf{Z}(\rho, 0, \tau = 2.5l)|$; C is the same as B but with Ψ taken from Eq. (9); D, $|\partial/\partial \tau \mathbf{Z}(\rho, 0, \tau = 0)|$; E is a reference curve $\exp(-\rho/l)$. The curves A–C have been normalized so that $|\mathbf{Z}(0, 0, 0)| = 1$. The values of the remaining free parameters are $\Delta = 0.1l$ and $\beta = 0.8$.

The result is a new independent solution but it can also be considered as the wave given by Eqs. (5) and (6), which is observed in another inertial reference frame [10]

$$\Psi(\rho, z, \tau) = \frac{\exp\left(-|k_0|\sqrt{\rho^2 + (\Delta - i\gamma(\beta z - \tau))^2}\right)}{\sqrt{\rho^2 + (\Delta - i\gamma(\beta z - \tau))^2}} \times \exp(i\gamma k_0(z - \beta\tau)), \tag{9}$$

where the relativistic factors $\gamma \equiv (1 - \beta^2)^{-1/2}$ and $\beta \equiv v/c < 1$ have been introduced, v being a free parameter – the relative speed between the frames.

In the waist region (see Fig. 2) this wave function has the same radial falloff as was given by Eq. (7), see curve ‘‘C’’ in Fig. 1, while the axial localization follows a power law. The strongly localized waist and the whole amplitude distribution move rigidly and without any spread along the axis z with a superluminal speed c/β . Such wave with intriguing properties, named the focused X wave (FXW) [11], belongs to the so-called propagation-invariant localized solutions to the wave equation – a research field emerged in the

1980s (see reviews [11–15]) and recently reached its first experimental results [16–21]. It should be noted here that there is nothing unphysical in the superluminality of the localized waves – which is, moreover, an experimentally verified fact – since a superluminal group velocity does not mean [13–16] as if energy or information could be transmitted faster than c (for a thorough discussion of this point see [22–24] and review [25]). Hence, in its waist (cross-sectional) plane a one-photon field given by the FXW possesses the same strong localization at any time as the previously considered cylindrical field does in any transversal plane at the instant $t = 0$.

By making use of the historically first representative of localized waves – the so-called focus wave mode (FWM) [26–28] (see also [10] and reviews [11,15] and references therein) one readily obtains an example of the field that exhibits even much stronger than exponential localization. FWM is given by the scalar function

$$\Psi(\rho, z, t) = \frac{\exp\left[-\frac{\rho^2}{2l(a-i(z-\tau))}\right]}{a-i(z-\tau)} \exp\left[-\frac{i(z+\tau)}{2l}\right], \tag{10}$$

where again l is a wavelength-type characteristic length and the constant a controls the axial localization length. Since the FXW in the limit $\beta \rightarrow 1$ becomes a FWM [10], Fig. 2 gives also an idea how a FWM looks like. Multiplying Eq. (10) by \mathbf{m} to build the vector $\mathbf{Z}(\rho, z, \tau)$ and inserting the latter into Eq. (4) we obtain that in this example the photon localization in the waist plane is quadratically exponential (Gaussian falloff):

$$|\mathbf{Z}(\rho \rightarrow \infty, z = \tau)| \sim \exp(-\rho^2/2la), \tag{11}$$

$$|\mathbf{F}(\rho \rightarrow \infty, z = \tau)|^2 \sim \rho^6 \exp(-\rho^2/la). \tag{12}$$

In Eq. (12) only the highest-power term with respect to ρ is shown.

To start discussing our results let us ask first whether the wave functions considered are something extraordinary. The answer is: yes, they are indeed, since the browsing of various integral transform tables reveals rather few examples where both the real and imaginary part of a wave function

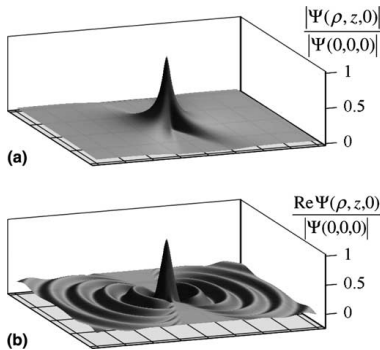


Fig. 2. The superluminal FXW given by Eq. (9). Shown are the dependences (a) of the modulus and (b) of the real part of the wavefunction on the longitudinal (z , increasing to the right) and a transverse (say, x) coordinates. The distance between the grid lines on the basal plane (x, z) is 22λ , where $\lambda = 2\pi|k_0|^{-1}$, k_0 being negative. The values of the remaining free parameters are $\Delta = 30\lambda$ and $\beta = 0.995$ or $\gamma = 10$.

and of its time derivative have simultaneously an exponential or stronger localization in conjunction with other requisite properties. Still, the list of proper wave functions with an extraordinary strong localization is not poor – in addition to an optically feasible version [29] of the FWM various new interesting solutions can be derived [30]. Yet, it could be argued that the well-known Gaussian beam pulse has the same quadratically exponential radial profile in the waist region. However, resorting to the family of the Gaussian beams (the Gauss–Laguerre and Gauss–Hermite beams, etc.) is irrelevant here. The reason is that all these beams are solutions of the wave equation only in the paraxial approximation not valid in the case of any significant localization of wide-band (pulsed) superpositions of the beams, whereas in fact, e.g., an exact solution corresponding to a lowest-order (axisymmetric) Gaussian beam has a weak power-law radial falloff in the waist region [31,32].

The next possible objection to the physical significance of the results obtained might arise from the infinite total energy [11] of the waves given by Eqs. (6), (9), and (10). However, at any spatial location the wave function is square integrable with respect to time, thus the condition of the Paley–Wiener theorem has been satisfied. Moreover, physically feasible finite-energy versions of localized waves generally exhibit even better localization properties, although not persistently. A finite-energy version of the FXW, called the modified focused X wave (MFXW [11]), has the same exponential factor as in Eq. (9), which is multiplied by a fraction that allows to force the axial localization to follow an arbitrarily strong power-law. The latter circumstance indicates that the strong lateral localization of the fields considered does not appear somehow at the expense of their axial localization. As a matter of fact, energy-normalization of a wave function depends on how many photons it describes. It is easy to see that our derivation and results hold for any number state with $N \geq 1$ and also for incoherent mixtures of such states (which is important for experimental studies). Here it is not of interest to consider coherent states since generally for states of electromagnetic field that have classical counterparts one can escape – already in the case of uniform spherical localization

– the constraints imposed by the Paley–Wiener theorem [6].

The final crucial question is, are our results not in contradiction with those of [6]? The answer is no, since in the case of the cylindrical waves the radial distance and temporal frequency are not directly Fourier-conjugated variables. In order to clarify this point, let us first take a closer look at the proof of the Paley–Wiener limit for three-dimensional isotropic localization. In [6] Eq. (24) for $\mathbf{Z}(\mathbf{r},\tau)$ contains a superposition of spherically symmetric standing waves

$$\int_0^\infty dk h(lk) \frac{\sin kr}{r} e^{-ik\tau} \propto ir^{-1} \left[g\left(\frac{\tau+r}{l}\right) - g\left(\frac{\tau-r}{l}\right) \right], \quad (13)$$

where $h(lk)$ is the spectrum and $g(\cdot)$ is its Fourier image. The sine in Eq. (13) results from the imploding and exploding spherical wave constituents of the standing wave, like an odd one-dimensional standing wave arises from counter-propagating waves. While the asymptotic behavior of the function $g(\cdot)$ and hence of the function $\mathbf{Z}(\mathbf{r},\tau)$ for large values of the radial distance r are generally restricted by the Paley–Wiener theorem, strictly at the instant $\tau = 0$ of maximal localization the integral is nothing but the sine transform for which the theorem does not apply. Indeed, the sine transform tables give examples of the resultant functions with arbitrarily abrupt falloff. However, it does not mean as if the localization restriction was lifted at the instant $\tau = 0$. The explanation is that according to Eq. (4) the energy wave function involves also the time derivative of $\mathbf{Z}(\mathbf{r},\tau)$, but the sine transforms of two functions $h(lk)$ and $h(lk)k$ cannot simultaneously possess arbitrarily abrupt falloffs. In contrast, the time derivative of the wave function given by Eq. (6) or Eq. (5) has the same strong exponential falloff as the function itself, which persists for some (not too long) time, see Fig. 1. By comparing Eqs. (5) and (13) we notice that while in Eq. (13) – as well as in its one-dimensional equivalent – the argument of the sine function is the product of the distance with the Fourier variable, in Eq. (5) the argument of the Bessel function is the product of the radial distance ρ with the radial wave-

number k_ρ , the latter depending on the Fourier variable through the square-root expression with the constant parameter k_0 – the lower limit of the integration. As it follows also from Eqs. (7) and (8) the condition $k_0 \neq 0$ is crucial for obtaining the exponential falloff. Hence, in the case of the cylindrical waves considered by us, the apparent violation of the rules set by the Paley–Wiener theorem results from the specific complicated relation between the radial distance and the Fourier variable.

In conclusion, we have shown that for certain cylindrical N -photon states ($N = 1, 2, \dots$) the localization in lateral directions breaks the limit established in [6] for the case of uniform spherical wave functions. These results hold not only for photons but for number states of any particles.

Acknowledgements

Saari is thankful to Iwo Bialynicki-Birula for stimulating hints, discussions, and remarks. The research was supported by the Estonian Science Foundation.

References

- [1] L.D. Landau, R. Peierls, *Z. Phys.* 62 (1930) 188.
- [2] I. Bialynicki-Birula, Photon Wave Function, in: E. Wolf (Ed.), *Progress in Optics*, vol. 36, North-Holland, Amsterdam, 1996.
- [3] A.L. Akhiezer, V.B. Berestetskii, *Quantum Electrodynamics*, Interscience, New York, 1965.
- [4] L. Mandel, E. Wolf, *Optical Coherence and Quantum Optics*, Cambridge University Press, Cambridge, 1995.
- [5] M. Hawton, *Phys. Rev. A* 59 (1999) 3223.
- [6] I. Bialynicki-Birula, *Phys. Rev. Lett.* 80 (1998) 5247.
- [7] O. Keller, *Phys. Rev. A* 62 (2000) 022111.
- [8] O. Keller, *JOSA B* 18 (2001) 206.
- [9] K.W. Chan, C.K. Law, J.H. Eberly, *Phys. Rev. Lett.* 88 (2002) 402.
- [10] P. Saari, K. Reivelt, *Phys. Rev. E* 69 (2004) 036612.
- [11] I. Besieris, M. Abdel-Rahman, A. Shaarawi, A. Chatzipetros, *Prog. Electrom. Res.* 19 (1998) 1.
- [12] J. Salo, J. Fagerholm, A.T. Friberg, M.M. Salomaa, *Phys. Rev. E* 62 (2000) 4261.
- [13] P. Saari, in: *Time's Arrows, Quantum Measurement and Superluminal Behavior*, D. Mugnai et al. (Eds.), CNR, Rome, 2001, also in: arXiv, physics/0103054.
- [14] E. Recami, M. Zamboni-Rached, K.Z. Nóbrega, C.A. Dartora, H.E. Hernández, *IIEEE J. Select. Top. Quantum Electron.* 9 (2003) 59.
- [15] K. Reivelt, P. Saari, in: arXiv, physics/0309079.
- [16] P. Saari, K. Reivelt, *Phys. Rev. Lett.* 79 (1997) 4135.
- [17] H. Sönajalg, M. Rätsep, P. Saari, *Opt. Lett.* 22 (1997) 310.
- [18] D. Mugnai, A. Ranfagni, R. Ruggeri, *Phys. Rev. Lett.* 84 (2000) 4830.
- [19] I. Alexeev, K.Y. Kim, H.M. Milchberg, *Phys. Rev. Lett.* 88 (2002) 073901.
- [20] K. Reivelt, P. Saari, *Phys. Rev. E* 66 (2002) 056611.
- [21] R. Grunwald, V. Kebbel, U. Griebner, U. Neumann, A. Kummrow, M. Rini, E.T.J. Nibbering, M. Piché, G. Rousseau, M. Fortin, *Phys. Rev. A* 67 (2003) 063820.
- [22] H. Ringermacher, L.R. Mead, *Phys. Rev. Lett.* 87 (2001) 059402.
- [23] A.M. Shaarawi, I.M. Besieris, *J. Phys. A: Math. Gen.* 33 (2000) 7255.
- [24] W.A. Rodrigues Jr., D.S. Thober, A.L. Xavier Jr., *Phys. Lett. A* 284 (2001) 217.
- [25] P.W. Milonni, *J. Phys. B: At. Mol. Opt. Phys.* 35 (2002) R31.
- [26] J.N. Brittingham, *J. Appl. Phys.* 54 (1983) 1179.
- [27] A. Sezginer, *J. Appl. Phys.* 57 (1984) 678.
- [28] R.W. Ziolkowski, *J. Math. Phys.* 26 (1985) 861.
- [29] K. Reivelt, P. Saari, *Opt. Lett.* 29 (2004) 1176.
- [30] A.P. Kiselev, *J. Phys. A: Math. Gen.* 36 (2003) L345.
- [31] C.J.R. Sheppard, S. Saghafi, *JOSA A* 16 (1999) 1381.
- [32] P. Saari, *Opt. Express* 8 (2001) 590.

H. Valtna, K. Reivelt and P. Saari,
“Modifications of the focused X wave as suitable models
of strongly localized waves for realization in the optical domain”,
J. Opt. A: Pure Appl. Opt. **8**, 118–121, (2006).

Modifications of the focused X wave as suitable models of strongly localized waves for realization in the optical domain

Heli Valtna¹, Kaido Reivelt² and Peeter Saari^{1,2,3}

¹ Department of Physics, University of Tartu, Tähe 4, 51010 Tartu, Estonia

² Institute of Physics, University of Tartu, Riia 142, 51014 Tartu, Estonia

E-mail: psaaari@fi.tartu.ee

Received 13 June 2005, accepted for publication 22 November 2005

Published 6 January 2006

Online at stacks.iop.org/JOptA/8/118

Abstract

Simple practical model approximations to the so-called focused X wave—a pulsed wave propagating superluminally in vacuum or in a linear medium, which attracts attention due to its spread-free strong spatial localization—are derived. The experimental feasibility of the model waves in the optical domain is discussed and their radial decay is analysed.

Keywords: ultrashort electromagnetic pulses, localized waves, X wave, focus wave mode, Bessel beam

1. Introduction

As is well known today, the scalar free-space wave equation has a class of solutions that seemingly defy the laws of diffraction and can preserve very sharp spatial and temporal localization in the course of propagation over distances that many times exceed the Rayleigh range. During the past two decades the physical nature, mathematical apparatus and experimental generation of such localized wave (LW) solutions have been investigated in numerous papers (see [1, 2] for a general overview of the topic). In particular, it has been shown that the general sub-class of LW solutions of the scalar free-space wave equation can be deduced by applying certain physical conditions to the corresponding general solution. In one approach the general expression for the LWs is derived by means of applying the condition of wavelength-independent group velocity along the optical axis over the entire spectrum of wavefield [3–5]. The bidirectional plane wave decomposition, introduced by Besieris *et al* [6], is based on a representation of the solutions of the scalar wave equations into the products of forward and backward travelling plane wave solutions. In another approach the general classification scheme of the LW solutions into luminal, super- and subluminal ones can be derived in terms of the special theory of relativity [1, 7]. Also, during the past few years the experimental generation

of LWs has been put in solid terms, so that the experimental realizability of every LW can be estimated by means of physically transparent conditions [2, 8, 9].

Though the general integral representations can be used to express the wavefunctions, it is advantageous to have explicit closed-form expressions in hand—not only for analytical studies of the spatio-temporal amplitude and phase distributions, but also since such expressions drastically reduce computing time for simulations of temporal evolution and propagation of the LWs, especially if long-range behaviour of the wavefields is under consideration. Moreover, in many practical cases when a detailed simulation of finite-energy approximations of the LWs is required, numerical calculations engender a very serious problem with the power of modern personal computers. However, no such closed-form expression is useful *per se*; it should also model some kind of practical situation, for example, the propagation of an experimentally feasible LW.

This paper deals with practical models of the so-called focused X waves (FXW) [1, 10, 11]—superluminally propagating LWs that due to their strong spatial localization not only are promising for various applications but also appear to be rather intriguing for mathematical and quantum optics [12].

We start by deriving a closed-form expression for the ideal FXW, which like an ideal plane wave has an infinite energy. We next derive and study two finite-energy modifications of the FXW and then discuss their properties.

³ Author to whom any correspondence should be addressed.

2. The model

2.1. Propagation-invariant focused X wave

The comprehension of the physical nature of the FXW is enhanced if its wavefunction is derived from a spectral picture. It is convenient to start with a general expression of an axisymmetric wavefield as a superposition of the zeroth order Bessel beams propagating along the z axis (see, e.g., [7]):

$$\Psi(\rho, z, t) = \int_{-\infty}^{\infty} dk_z \int_{|k_z|}^{\infty} dk \Phi(k_z, k) \times J_0\left(\rho\sqrt{k^2 - k_z^2}\right) \exp(ik_z z - ikct), \quad (1)$$

where ρ is the radial coordinate, $k = \omega/c$, the spectral distribution has been denoted by $\Phi(k_z, k)$ and k_z is the longitudinal wavenumber. One obtains the FXW by taking a specific singular spectrum [1, 7],

$$\Phi_{\text{FXW}}(k_z, k) = \text{constant} \times \delta[\gamma(k_z - \beta k) - k_{z0}] e^{-\gamma(k - \beta k_z)\Delta}, \quad (2)$$

which depends, apart from the strength constant, on three parameters: $\Delta > 0$ determines the spectrum (Δ^{-1} is the $1/e$ -width of the spectrum) and, consequently, spatial extension of the peak of the wavefield, k_{z0} expresses a certain cut-off value for longitudinal wavenumbers of the plane waves that constitute the FXW and $\gamma = (1 - \beta^2)^{-1/2}$ and $\beta = v/c$, $\beta < 1$ are the well known relativistic factors formed from a velocity-type parameter v . Integration over k and k_z in equation (1) with the help of Laplace transform tables (e.g. [13]) yields the following closed-form wavefunction of the FXW:

$$\Psi_{\text{FXW}}(\rho, z, t) = \text{const} \times \exp[i\gamma k_{z0}(z - \beta ct)] \times \frac{\exp(-|k_{z0}|\sqrt{\rho^2 + [\Delta - i\gamma(\beta z - ct)]^2})}{\sqrt{\rho^2 + [\Delta - i\gamma(\beta z - ct)]^2}}. \quad (3)$$

As the FXW moves with a superluminal velocity v_{sl} (which is also a constant group velocity in the wavepacket [2, 3, 7]), it is convenient to substitute the parameter v with this velocity $v_{\text{sl}} = c^2/v$ and, correspondingly, to use the superluminal counterpart of the relativistic factor $\gamma_{\text{sl}} = (\beta^{-2} - 1)^{-1/2}$ [1, 7]. In these designations it becomes obvious that the intensity profile of the wave moves along the z axis without any change, since the variables z and t enter the amplitude factor only through the combination $z - v_{\text{sl}}t$:

$$\Psi_{\text{FXW}}(\rho, z, t) = \frac{\exp(-|k_{z0}|\sqrt{\rho^2 + [\Delta - i\gamma_{\text{sl}}(z - v_{\text{sl}}t)]^2})}{\sqrt{\rho^2 + [\Delta - i\gamma_{\text{sl}}(z - v_{\text{sl}}t)]^2}} \times \exp\left[ik_{z0}\gamma_{\text{sl}}\left(\frac{v_{\text{sl}}}{c}z - ct\right)\right], \quad (4)$$

where the factor determining the amplitude has been written at the beginning and henceforth the arbitrary amplitude multiplier constant is omitted in the expressions.

A qualitative analysis of the FXW can be performed by studying its wavefunction and spectral distribution. The latter can be written as a product of two components: $\Phi_{\text{FXW}}(k_z, k) = \phi(k_z, k)\varphi(k_z, k)$. The first one $\phi(k_z, k) = \delta(\gamma(k_z - \beta k) - k_{z0})$ contains a singular function in the case of an ideal localized wave and a highly localized function in the case of a modified (finite-energy) wavefield. Here the singularity is brought in as a δ -function; it defines the vanishing

width of the support line and its argument defines the slope of the support line on the (k, k_z) -plane. By the slope one can tell the group velocity of the wavefield and the spatial distribution of the plane waves composing the wavefield. So, in our case, the slope $\beta^{-1} > 1$, thus the modulus of the wavefield moves at a superluminal speed and the projection of the support line into the (k_z, k_ρ) -plane is a hyperbola. The second component $\varphi(k_z, k)$ is the one that specifies the frequency spectrum of the wavefield, which for the FXW and its modifications is exponentially decaying, $\varphi(k_z, k) = e^{-\gamma(k - \beta k_z)\Delta}$.

2.2. Finite-energy modifications

The FXW itself is not physically feasible due to its infinite energy resulting from the singularity of the spectrum. Thus, in order to obtain a realistic model, the spectrum has to be modified so that (i) it is non-singular, yet (ii) it yields a closed-form expression for the wavefunction and (iii) the latter still approximates the spatio-temporal behaviour of the FXW sufficiently well. Of course, the propagation invariance will be inevitably lost and replaced by a finite depth of spread-free flight of the pulse, but its lateral strong localization need not be sacrificed [2].

Such a modified FXW was first derived by Besieris *et al* [1]—we call it ‘modification 1’ (M1). They have chosen an expression for the spectral distribution which in our notation reads

$$\Phi_{\text{M1}}(k_z, k) = (K - k_{z0})^{q-1} \exp[-a_2(K - k_{z0})] \times \Theta(K - k_{z0}) \exp[-\gamma(k - \beta k_z)\Delta]/\Gamma(q), \quad (5)$$

where Θ is the Heaviside unit step, Γ denotes the Gamma function and the Lorentz-transformed axial wavenumber $K = \gamma(k_z - \beta k)$ has been used for brevity and comparison with equation (4.5) of Besieris *et al* [4]. The new parameters a_2 and q ($a_2, q > 0$) adjust the finite width of the distribution across the support boundary line given by equation $K - k_{z0} = 0$. While this line is straight in the plane (k, k_z) , in the plane (k_ρ, k_z) of the lateral and axial components of the wave vector it transforms to a hyperbola [2, 7].

The insertion of (5) into (1) and corresponding integration indeed yields a closed-form expression, which in our notation reads

$$\Psi_{\text{M1}}(\rho, z, t) = \Psi_{\text{FXW}}(\rho, z, t) [F(\rho, z, t)]^{-q}. \quad (6)$$

This modified wavefunction differs from that of the original FXW by a negative power of the factor

$$F(\rho, z, t) = \sqrt{\rho^2 + [\Delta - i\gamma_{\text{sl}}(z - v_{\text{sl}}t)]^2} + a_2 - i\gamma_{\text{sl}}\left(\frac{v_{\text{sl}}}{c}z - ct\right), \quad (7)$$

which we call ‘the modifier’.

The modifier propagates with velocity c on the z -axis. Thus, to maintain the shape of the central peak of the wavefield during propagation, the group velocity v_{sl} has to be chosen almost equal to c and/or the effects caused by the modifier—e.g., decay of the pulse peak at $z = v_{\text{sl}}t$ at large times and distances—have to be suppressed by appropriate choice of the

⁴ There is obviously a typo in equation (4.5) of [1]: a factor κ is absent, which is equal to our K and—having in mind their slightly different general definition of the spectral distribution—should be present there.

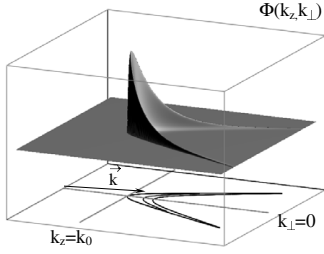


Figure 1. The spectrum Φ of the second modification of the FXW according to equation (8). In this figure the dependence on the wavevector component k_z and a lateral one $k_\perp = \pm k_\rho$ is depicted. Numerical values of the parameters have been chosen suitably for an optical realization: the pulse velocity $v = 1.001c$; the minimal wavenumber $k_0 = 2\pi(0.8 \mu\text{m})^{-1}$, i.e., the reddest plane-wave constituent of the pulse has wavelength $0.8 \mu\text{m}$; the width parameters $\Delta = 5 \mu\text{m}$, $a_2 = 100 \mu\text{m}$ and $q = 2$. The lateral scale is stretched in comparison to the axial scale: the plotting range for k_z is $25 \mu\text{m}^{-1}$ while for k_\perp it is only $2.5 \mu\text{m}^{-1}$. The curves of the contour plot at the bottom correspond to level $1/10$ and to level $1/100$ (the rightmost curve) of the maximum value of Φ . Shown also at the bottom is the wavevector of a plane-wave constituent of the pulse.

values of the parameters q and a_2 . Note, however, that the lateral localization is even improved for the modified FXW as the multiplier $[F(\rho, z, t)]^{-q}$ makes the radial decay stronger by a factor of ρ^{-q} .

Consulting the Laplace transform table [13] we found a possibility to derive another modified FXW which has a closed-form wavefunction. This ‘modification 2’ (M2) is generated by the following spectral function:

$$\Phi_{M2}(k_z, k) = \frac{1}{\gamma(k_z - \beta k)} \Phi_{M1}(k_z, k). \quad (8)$$

This spectrum is depicted in figure 1, which for the parameters chosen also represents well the spectrum $\Phi_{M1}(k_z, k)$.

Substituting (8) into (1) and integrating with the help of equation (4.3.8) [13] yields the following wavefunction:

$$\Psi_{M2}(\rho, z, t) = \frac{(k_{z0})^{q-1} \exp(k_{z0} a_2) \Gamma[1 - q, k_{z0} F(\rho, z, t)]}{\sqrt{\rho^2 + [\Delta - i\gamma_{sl}(z - v_{sl}t)]^2}}, \quad (9)$$

where $F(\rho, z, t)$ is defined by equation (7) and $\Gamma(\dots)$ denotes the incomplete Gamma function. The wavefunction $\Psi_{M2}(\rho, z, t)$ is plotted in figure 2 at the instant $t = 0$. In a good approximation the plots also depict the wavefunctions $\Psi_{M1}(\rho, z, t)$ and $\Psi_{FXW}(\rho, z, t)$ considered earlier, since we have chosen a set of parameter values which is suitable for optical-domain realizations of the waves as discussed in the following section.

Along the axis z the central peak of M1 decays as

$$\Psi_{M1}(0, z, t = z/v_{sl}) = \left| \frac{a_2 + \Delta}{a_2 + \Delta + i\gamma_{sl} \sqrt{v_{sl}^2 - c^2}} \right|^q, \quad (10)$$

while the decay of the modulus of M2 in the range of parameters we are interested in can also be approximated rather

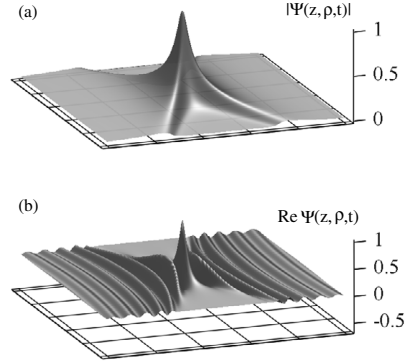


Figure 2. The modulus (a) and the real part (b) of the second modification of the FXW according to equation (9). Dependence on z (increasing from the left to right) and a lateral coordinate $x = \pm \rho$ while $ct = 0$ is depicted. Plots are normalized and numerical values of the parameters have been chosen suitably for an optical realization; see the previous figure caption. The axial scale is stretched in comparison to the lateral scale: the plotting range for the lateral coordinate ρ is $100 \mu\text{m}$ while for the axial coordinate z it is only $10 \mu\text{m}$. The grey shading in both plots is a result of ‘lighting’ used to better reveal the relief of the surface.

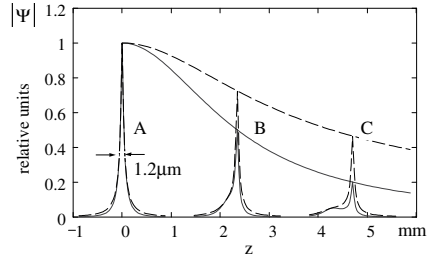


Figure 3. The evolution of the modulus of the central peak of the first modification (solid line) and second modification (dashed line) of the FXW over distance on the z -axis. A, B and C are axial profiles of the modulus of the waves at the instances $t = 0$, $t = \Delta z/v_{sl}$ and $t = 2\Delta z/v_{sl}$, respectively, where Δz is defined by (11), $q = 1$. Decaying curves show the behaviour of the modulus of the central peaks during propagation as a function of z , $t = z/v_{sl}$. Plots are normalized and numerical values of the parameters have been chosen suitably for an optical realization (see figure 1). In order to make axial profiles more distinguishable, they have been stretched 100-fold with respect to the scale on the z -axis.

well by equation (10) taken with $q = 1$. Both curves are plotted in figure 3. One can see from the curves that the waves propagate without any significant decay over distances exceeding their longitudinal dimensions by at least three orders of magnitude. Also, we see that only after a substantial propagation distance does the longitudinal profile change—curve C reveals the breakaway of the peaks attributable to the two factors in equation (6).

By our estimation, the spatial profile of the M1 modulus moves without remarkable change or spread until

$$\Delta z = v_{sl} \frac{a_2 + \Delta}{\sqrt{v_{sl}^2 + c^2}} \sqrt{\sqrt{2} - 1}. \quad (11)$$

The estimation has been derived from equation (10): the central maximum on the z -axis decreases $\sqrt{2}$ -fold while travelling the distance Δz . For non-spreading distance of the wave M2, again, $q = 1$ in (11) gives an adequate estimation.

Due to the spread-out caused by the modifier, both M1 and M2 lose their symmetry with respect to the co-propagating axis $z = v_{sl}t$ (see figure 3). However, the radial decay and symmetry of the wavefunction are unaffected and remain unchanged until $t \ll \frac{v_{sl}}{c}(a_2 + \sqrt{\rho^2 + \Delta^2})$.

3. Discussion

Apart from the requirement of finiteness of the total energy which in the case of the modified FXWs is satisfied by definition, there are three additional conditions for a model of LW to be useful for implementations in optics [14]. First, although its spectrum has to be a wideband one, it cannot extend down to zero frequency. Second, the LW has to contain neither backward-propagating nor radially propagating plane-wave constituents. Although the latter two conditions are not mandatory ones and need not be fulfilled, say, in the case of cavity-confined fields, they correspond to possibilities of optical elements designed for handling light beams. Note that in the case of the focus wave mode (FWM)—a luminal LW which is most thoroughly investigated in theory of LWs—these conditions are not met⁵. The reason is that for the FWM with its wide spectrum of specific exponential shape the support of the spectrum is a parabola which—as a conic section—surrounds the origin in the plane (k_{\perp}, k_z) [7], while the support of the FXW as a hyperbola has two options of its placement depending on the sign of k_{z0} and in the case of positive k_{z0} does not surround the origin (see figure 1). Choosing the positive value of k_{z0} sufficiently large so that the actual lowest wavenumber

$$k_0 = k_{z0} \sqrt{\frac{1 + \beta}{1 - \beta}}$$

falls into the red spectral region and adjusting values of the other parameters so that the spectrum essentially remains in the optical region, one can make both modifications M1 and M2 of the FXW realizable, in principle, from femtosecond-duration light pulses by making use of linear-optical devices (in particular, by conical mirrors and diffraction gratings). However, with the exception of certain approximations to the X waves (given by equation (3) or (4) if $k_{z0} = 0$), generation of LWs remains a complicated task, although a general approach [2] to optical synthesis of them is known.

The third, primarily technical, condition in optics is paraxiality, which means that the spectrum must contain only such plane-wave components that travel at reasonably small

⁵ This does not mean that luminal LWs are impossible in optics—a suitably band-limited spectrum gives so-called FWM in a wide sense, which is shown to be feasible in optics [8].

angles relative to the optical axis. The maximum of the angle for the FXW and its modifications is less than $\pi/2$ in the case of a positive value of k_{z0} but depends on the group velocity—the closer v_{sl} is to c , the smaller the angle θ : $\theta(k) = \arccos((ck + k_{z0}(v_{sl} - c))/kv_{sl})$. Asymptotically, $\theta(\infty) = \arccos(\beta)$, which is the maximum of the angle and is equal to half of the angle between the asymptotes of the hyperbola of the support boundary in figure 1 (called the Axicon angle in the literature on diffraction-free and localized waves).

As a matter of fact, an optical superluminal localized wave possessing a comparatively narrow-band spectrum which is much different from the one depicted in figure 1, but still has a hyperbolic support, had been experimentally generated from femtosecond laser pulses in the previous decade [15]. Thus, if we use the term FXW in a wide sense, i.e., regarding any superluminal LW whose spectrum—irrespective of its particular shape—possesses a hyperbolic support and the Axicon angle has a corresponding dispersion, then we could say that a certain approximation to the FXW has already been realized in practice.

Finally, having in mind the strong lateral localization of the FXW, let us consider the radial asymptotic behaviour of its two finite-energy modifications. Comparing the three model wavefunctions at $t = 0$, $z = 0$, and large values $\rho \rightarrow \infty$

$$|\Psi_{\text{FXW}}(\rho, 0, 0)| \sim \exp(-\rho k_{z0})/\rho$$

$$|\Psi_{\text{M1}}(\rho, 0, 0)| \sim \exp(-\rho k_{z0})/\rho^{q+1}$$

$$|\Psi_{\text{M2}}(\rho, 0, 0)| \sim \Gamma(1 - q, \rho k_{z0})/\rho$$

we see that—as far as a numerical approximation with chosen set of parameters and q at $q = 1, 2, 3$ reveals,

$$\Psi_{\text{M2}}(\rho \rightarrow \infty, 0, 0) \approx \exp(-\rho k_{z0})/\rho^2$$

—both modifications have even stronger lateral decay than that of the FXW. Apparently this difference in the lateral behaviour can be explained as a result of the additional radial decay which is introduced through the factor $F(\rho, z, t)$ given by (7).

4. Conclusion

We have found a new finite-energy modification with a closed-form wavefunction for the focused X wave—a specific superluminally propagating localized wave. This wave can be generated as a pulsed beam in the visible region and—due to its strong lateral localization preserved over an extended depth of propagation—is rather promising in various fields of optics.

Acknowledgment

The research was supported by the Estonian Science Foundation.

References

- [1] Besieris I, Abdel-Rahman M, Shaarawi A and Chatzipetros A 1998 *Prog. Electromagn. Res.* **19** 1

- [2] Reivelt K and Saari P 2003 *Preprint physics/0309079*
(<http://arxiv.org/abs/physics/0309079>)
- [3] Donnelly R and Ziolkowski R 1993 *Proc. R. Soc. A* **440** 541
- [4] Reivelt K and Saari P 2000 *J. Opt. Soc. Am. A* **17** 1785
- [5] Salo J and Salomaa M M 2001 *Pure Appl. Opt.* **3** 366
- [6] Besieris I M, Shaarawi A M and Ziolkowski R W 1989
J. Math. Phys. **30** 1254
- [7] Saari P and Reivelt K 2004 *Phys. Rev. E* **69** 036612
- [8] Reivelt K and Saari P 2002 *Phys. Rev. E* **66** 056611
- [9] Shaarawi A M 1997 *J. Opt. Soc. Am. A* **14** 1804
- [10] Borisov V V and Kiselev A P 2000 *Appl. Math. Lett.* **13** 83
- [11] Zamboni-Rached M, Recami E and
Hernández-Figueroa H E 2002 *Eur. Phys. J. D* **21** 217
- [12] Saari P, Menert M and Valtna H 2004 *Opt. Commun.* **246** 445
- [13] Bateman G and Erdelyi A 1954 *Tables of Integral Transforms*
vol 1 (New York: McGraw-Hill)
- [14] Reivelt K and Saari P 2004 *Opt. Lett.* **29** 1176
- [15] Sönajalg H, Rätsep M and Saari P 1997 *Opt. Lett.* **22** 310

P. Saari, K. Reivelt, H. Valtua,
“Ultralocalized superluminal light pulses”,
Laser Physics **17**, 297–301, (2007).

Ultralocalized Superluminal Light Pulses

P. Saari, K. Reivelt, and H. Valtna

Institute of Physics, University of Tartu, Riia 142, 51014 Tartu, Estonia

e-mail: Peeter.Saari@ut.ee

Received November 12, 2006

Abstract—We consider a sophisticated localized light wave—the so-called focused X wave which possesses a strong exponential localization in its waist region and propagates faster than the speed of light in a vacuum or in a linear medium. We show how this wave—until now considered in the literature as a mathematical object only—could be generated in reality by making use of cylindrical diffraction gratings.

PACS numbers:

DOI: 10.1134/S1054660X0704@@@

1. INTRODUCTION

In recent years, a lot of effort has been put into the study of certain few- and subcycle nonspreading light pulses—so-called localized waves (hereafter LWs, see reviews [1–6])—which are represented by somewhat exotic bullet-like Bessel wavepackets propagating in a vacuum or linear media. Obviously, such spatial and temporal localization makes the implementation of LW solutions very attractive for applications where the lateral and/or transversal diffractive spreading of optical wave fields is the major limitation to system performance (e.g., optical communication, metrology, monitoring, imaging, optical manipulation, and acceleration of particles and femtosecond spectroscopy). In recent years, it also has become obvious that the concept can be used in constructing pulse-like wave fields in dispersive media [7, 8] and in nonlinear optics [9, 10]. However, for more than a decade after the pioneering theoretical paper of J.N. Brittingham [11], the feasibility of electromagnetic LWs remained questionable due to their large spectral bandwidth and the spatiotemporal nonseparability inherent to LWs. The ideas that have been proposed for the generation of complicated LW solutions in the papers of that period of the field (see [1] for references) are hardly realizable in the optical domain.

Experiments in the optical domain started by launching Bessel-X pulses [7, 8, 12–15], where the conventional Bessel beam generators under wideband illumination were used. In [16], we proposed a physically transparent one-step derivation of fundamental LW solutions (focus wave modes (FWM)) and proved that good approximations to FWMs can be generated through a combination of an axicon and a circular diffraction grating [16–18]. The proposed principle has also been verified in experiment [19].

In this paper, we introduce a surprisingly elegant, one-step method for the optical generation of LWs. We show that superluminal LWs with hyperbolic support of angular spectrum of their plane wave constituents can

be generated by means of illuminating cylindrical diffraction gratings by conical wavepackets—Bessel-X pulses. We give the mathematical description of the method and discuss the pros and cons of the new type of setup.

2. DEFINITIONS AND GENEALOGY OF LWS

LWs can be introduced in several ways. Here, we start with the general axisymmetric expansion over the zero-order Bessel beams in the form

$$\Psi(\rho, z, t) = \int_{-\infty}^{\infty} dk_z \int_{|k_z|}^{\infty} dk A(k_z, k) J_0(\sqrt{k^2 - k_z^2} \rho) \times \exp(ik_z z - ickt), \quad (1)$$

where $A(k_z, k)$ is the angular spectrum of plane waves of the wave field. Here, we notice that for $|\Psi(\rho, z, t)|^2$ to be propagation-invariant, i.e., to depend on z and t only through the propagation variable $z - v_g ct$, where v_g is a constant group velocity along the z axis in units of c , the variables k and k_z must be bound linearly (see, e.g., [6])

$$k = v_g k_z + b, \quad (2)$$

where b is a constant (see Fig. 1a). Consequently, the spectrum has to be singular and may be factorized in the following form

$$A_{LW}(k_z, k) = A(k) \delta(k - v_g k_z - b) \Theta(k^2 - k_z^2), \quad (3)$$

where $A(k)$ is any complex valued function of one real positive variable and the Heaviside unit step $\Theta(x)$ has been introduced as a factor in order to allow for the k -integration in Eq. (1) to start from $k = 0$ instead of $k = |k_z|$.

We simply note that the physical meaning of condition (2) is obvious—it states, that the on-axis group velocity of the wave field $v_g c = d\omega/dk_z$ should be constant over the whole spectral range [16].

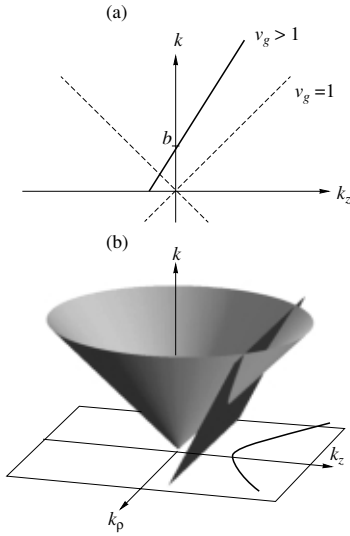


Fig. 1. (a) Graphical illustration of the defining property of an angular spectrum of the LWs in k -space, and (b) Formation of the hyperbolic spectral support as the intersection of a conic surface in k, k_z, k_p space.

An elegant graphical depiction of the general class of LW solutions of scalar homogeneous wave equations can also be given. Despite a general solution $\Psi(\mathbf{r}, t)$ of the free-space scalar wave equation which depends on four coordinates (x, y, z , and ct), its transform domain (k -space or spectral) representation $\tilde{\Psi}(\mathbf{k}, \omega/c)$ has only three independent arguments due to the dispersion-restriction $k_x^2 + k_y^2 + k_z^2 - (\omega/c)^2 = 0$ imposed by the wave equation. In other words, the four-vector $(\mathbf{k}, k \equiv \omega/c)$ of a light wave is always isotropic, whereas (\mathbf{r}, ct) needn't be and generally isn't. Thus, in the four-dimensional transform domain, the spectral function $\tilde{\Psi}(\mathbf{k}, k)$ is not equal to zero only on the surface of a three-dimensional cone given by equation $k^2 = k_x^2 + k_y^2 + k_z^2$. In other words, the support of the function $\tilde{\Psi}(\mathbf{k}, k)$ has to lie on that conical surface. In the case of azimuthal symmetry, one can introduce the cylindrical coordinates by replacing $k_x^2 + k_y^2 \rightarrow k_p^2$, thus reducing the dimensionality of the support to two and gaining the possibility of depicting the support as a conical surface in the k -space with three axes: k_z, k_p , and k (or ω/c), see Fig. 1b. In those terms, the spectral support of LW must be a line of intersection of the cone surface by a

plane perpendicular to the plane (k_z, k) , and the projection of the spectral support onto the plane (k_z, k) is a straight line with the slope v_g (see Fig. 1). Note that the two-dimensional integration in Eq. (1) covers the area of projection of the support on the cone onto the plane (k_z, k) [6].

If the slope of the spectral support on the (k_z, k) plane $v_g < 1$, Eq. (1) gives the family of subluminal LWs, and if $v_g = 1$, the corresponding LWs are luminal. In the case of $v_g > 1$, we get superluminal LWs. The special cases of $v_g > 1$ and $b = 0$ correspond to Bessel-X pulses [13].

3. OPTICAL GENERATION OF SUPERLUMINAL LWs

In the Fourier representation in Eq. (1) together with Eq. (3) have a straightforward interpretation as being the superposition of monochromatic Bessel beams of which the cone angle and wave number are related as

$$\cos\theta(k) = \frac{k-b}{v_g k}, \quad (4)$$

where $\theta(k)$ is the angle between the optical axis z and wave vector of the Fourier component (plane wave) of the wave field and $k_z(k) = k \cos\theta(k)$. It has been shown both theoretically and experimentally that in order to generate a LW, the necessary and sufficient condition is to control the spectral support of the generated wave field. In particular, if the generated spectral support obeys (4), then the corresponding wave field is always LW. The physical limitations of a setup like finite aperture or finite spectral bandwidth only have an effect on the propagation length of the generated LWs [1, 16]. Also, the need for a spectral chirp in the source pulse to generate LW with a transform-limited pulse length can be satisfied by standard pulse-compression techniques.

In [16, 19], we demonstrated both theoretically and experimentally that very good approximations to the optical LWs can be generated by means of combining a circular grating and axicon so that the angular dispersion required for a particular LW is obtained in the resulting wave field. However, it tends to be a complicated task to find the combination of angularly dispersive optical elements to generate the required spectral support of plane waves.

Consider a simple diffraction grating that is illuminated with a plane wave pulse as depicted in Fig. 2. Using the grating equation, we can write

$$\sin\phi_f - \sin\phi_i = \frac{m\lambda}{\Lambda}, \quad (5)$$

where m is the order of the diffracted field and Λ is the period of the grating (see Fig. 2). Now, if we assume that the grating is oriented parallel to the z axis (optical

axis) and note that in this case $\theta_0 = \pi/2 - \phi_i$, $\sin\phi_i = \cos\theta_0$ and $\sin\phi_j = \cos\theta(k)$, we get

$$\cos\theta(k) = \cos\theta_0 - \frac{2\pi m}{ka} = \frac{k - \frac{2\pi q}{\Lambda \cos\theta_{0i}}}{\frac{1}{\cos\theta_0}k}, \quad (6)$$

which is exactly the spectral support defined by the condition (4) if we choose $v_g = 1/\cos\theta_0$ and $b = 2\pi q/\Lambda \cos\theta_0$. Thus, unlike the setups considered so far in this case, the spectral support of plane waves of LWs can be generated *exactly* by means of a single diffraction grating that is illuminated by a plane wave pulse.

In cylindrically symmetric cases, we replace the plane diffraction grating with a cylindrical diffraction grating and illuminate it by a Bessel-X pulse [13] as shown in Fig. 3a. The initially conical spectral support of the Bessel-X pulse is transformed into a hyperboloidal by the angular dispersion of the grating, with the effect of the physical dimensions of the setup being the finite propagation length of the generated LW (see striped region in Fig. 3 and [1, 16] for a related discussion).

One can also calculate the spatiotemporal distribution of the wave field generated in such a setup. If we insert the spectral support (6) into the general expression (1) and assume the Gaussian frequency spectrum, we get

$$\Psi(\rho, z, t) \sim \int_0^\infty dk \exp\left[-\frac{k - k_z}{\Delta k}\right]^2 J_0(k\rho \sin\theta(k)) \times \exp(ikz \cos\theta(k) - ikct). \quad (7)$$

Clearly, this formula is a model, and not a simulation of a realistic experimental situation. In particular, it essentially assumes an infinite aperture of the system. However, in our previous publications, we have shown that as far as the aperture A of the generated LW (see Fig. 3) satisfies the condition $A \gg \lambda/\sin\theta_0$, where θ_0 stands for the mean cone angle of the Bessel beam components of LW, the integrals of the form of Eq. (7) can be used to calculate the spatial distribution of the wave field in the near-axis region inside the propagation length of the LW with a very good approximation [18]. In Fig. 3, this volume is depicted by the shaded region—this is where all the Bessel beam components of different color that diffract from the cylindrical grating overlap so that the constructive interference can take place. How to construct the setup so that the propagation length of the generated wave field is sufficiently large is dependent upon the choice of parameters.

In this setup, we have seven parameters: v_g and b define the spectral support, the frequency spectrum of the light source $A(k)$, the initial conical angle of the Bessel-X pulse θ_0 , the grating period Λ , the diameter D , and the length of the grating L_g . In order to under-

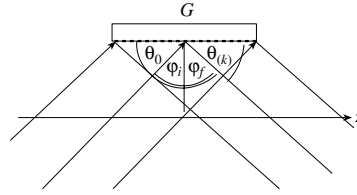


Fig. 2. On the principle of the proposed optical setup. The plane wave pulse propagating at angle θ_0 relative to the optical axis z (ϕ_i relative to the normal diffraction grating) diffracts off the diffraction grating so that a tilted pulse with angular dispersion (tilt) introduced by the grating is formed behind the grating. It appears that the tilt $\theta(k)$ introduced to a plane wave pulse in such a setup is exactly that of the LW.

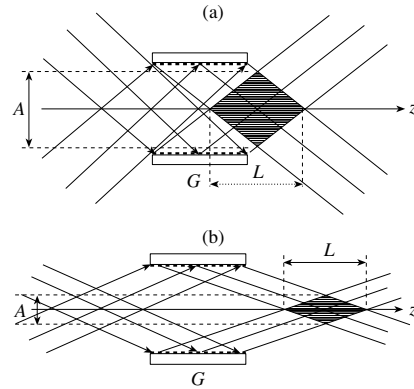


Fig. 3. (a) The proposed optical setup. The Bessel-X pulse diffracts off the cylindrical diffraction grating G so that a superposition of tilted pulses with angular dispersion (tilt) introduced by the grating is formed in the shaded region. A stands for the aperture of the generated LW and L for the propagation length of the LW; (b) If the Bessel-X pulse propagate at smaller angles relative to the propagation axis, the aperture A of the resulting LW is also smaller.

stand the interplay between the parameters, we should note that given the light source $A(k)$ the parameters of the spectral support v_g and b together can be used to optimize for the average propagation direction of the Bessel beam components $\theta(k_0)$ and the diameter of the central peak d —the two quantities are inversely proportional as $d \sim 1/\sin\theta(k_0)$. The simple geometrical arguments show that the parameters of the cylinder and cone angle θ_0 can be used to optimize for the propagation length and the position of the propagation volume (see Fig. 3). Comparing Figs. 3a and 3b, one can also

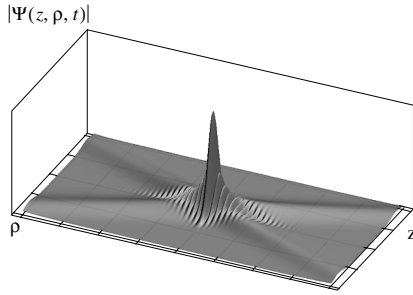


Fig. 4. The modulus of the superluminal LW that can be generated by the proposed setup. The wave field has a Gaussian frequency spectrum extending from 550 nm to 600 nm. The plotting range for the lateral coordinate ρ is 180 μm , and for the axial coordinate z it is 90 μm .

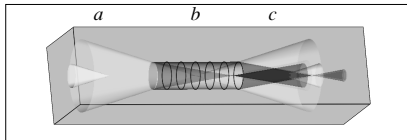


Fig. 5. 3D scheme of the superluminal localized wave generator. Ultra wideband conic light pulse (in region a) enters a cylindrical diffraction grating (b). The localized wave field is formed within the dark rhombic region (c). Brighter cones coming out from the generator depict propagation of the zero diffraction order and—in accordance with the range of the source spectrum $A(k)$ —the “red” and “blue” boundary surfaces of the first diffraction order.

see the general drawback of the optical schemes with elements oriented along the propagation axis—the aperture A of the generated LWs inevitably reduces as we move towards the paraxial angles $\theta(k)$, so that the optimization of the parameters must be treated carefully. One can also see that the propagation length L of the generated LWL is less than or equal to the length of the grating.

Working through the various choices of parameters in the setup, we were able to find several practical sets of parameters for the experiments. For example, if we choose $\theta_0 = 8$ deg, $\Lambda = 20$ μm , $D = 15$ mm, $L_g = 50$ mm, and use a Gaussian light source in the range of 55 nm—600 nm, we get an LW that propagates ≈ 30 mm at group velocity $v_g = 1.035$. The simulated field distribution with these parameters is depicted in Fig. 4. Experiments with this setup will be carried out in the near future.

4. DISCUSSION

A three-dimensional formation of an LW in a cylindrical grating is depicted in Fig. 5.

The main advantage of the proposed setup is its robustness. In the case of all the setups considered in the literature, the material dispersion of conical dispersive elements have been used to optimize for the required spectral support of LWs. In the present case, the exact spectral support of finite-energy superluminal LWs (see also [23]) is generated by means of a single optical element. From the very nature of LWs it is also implicit that, in principle, the setup is robust for the spectral shape of the input pulse and for its cone angle. Indeed, as it is constructed to generate certain support of the spectrum, the frequency spectrum does not really matter in the first approximation. As for the initial cone angle, this appears as a parameter in Eq. (6), so that the generated spectral support is this parameter of an LW in every possible occasion. One still needs to give the initial Bessel- X pulse the phase distortion (chirp) in order to generate the transform-limited pulse shape on the optical axis of the system. However, this can be easily achieved by applying standard pulse compression/expansion techniques. In fact, the only practical difficulty in the described setup is the fabrication of the cylindrical diffraction gratings.

5. CONCLUSIONS

We have proposed an easily realizable setup for the generation of optical superluminal LWs that is robust for the parameters of the source pulse (a Bessel- X pulse in this case). We discussed the working principle of the setup and presented numerical simulation for a practical set of parameters.

ACKNOWLEDGMENTS

This research was supported by the Estonian Science Foundation.

REFERENCES

1. K. Reivelt and P. Saari, physics/0309079 (2003); <http://arxiv.org/abs/physics/0309079>.
2. I. Besieris, M. Abdel-Rahman, A. Shaarawi, and A. Chatzipetros, Prog. Electromagn. Res. **19**, 1 (1998).
3. J. Salo, J. Fagerholm, A. T. Friberg, and M. M. Salomaa, Phys. Rev. E **62**, 4261 (2002).
4. A. P. Kiselev, J. Phys. A: Math. Gen. **36**, L345 (2003).
5. E. Recami, M. Zamboni-Rached, K. Z. Nóbrega, et al., IEEE J. Sel. Top. Quantum Electron. **9**, 59 (2003).
6. P. Saari and K. Reivelt, Phys. Rev. E **69**, 036612 (2004).
7. H. Sõnajalg and P. Saari, Opt. Lett. **21**, 1162 (1996).
8. H. Sõnajalg, M. Rätsep and P. Saari, Opt. Lett. **22**, 310 (1997).
9. P. Di Trapani, G. Valiulis, A. Piskarskas, et al., Phys. Rev. Lett. **91**, 093904 (2003).

10. R. Butkus, S. Orlov, A. Piskarskas, et al., *Opt. Comm.* **244**, 411 (2005).
11. J. N. Brittingham, *J. Appl. Phys.* **54**, 1179 (1983).
12. P. Saari and H. Sönajalg, *Laser Phys.* **7**, 32 (1997).
13. P. Saari and K. Reivelt, *Phys. Rev. Lett.* **79**, 4135 (1997).
14. I. Alexeev, K. Y. Kim, and H. M. Milchberg, *Phys. Rev. Lett.* **88**, 073901 (2002).
15. R. Grunwald, V. Kebbel, U. Griebner, et al., *Phys. Rev. A* **67**, 063820 (2003).
16. K. Reivelt and P. Saari, *J. Opt. Soc. Am. A* **17**, 1785 (2000).
17. K. Reivelt and P. Saari, *Phys. Rev. E* **65**, 046622 (2002).
18. K. Reivelt and P. Saari, *Opt. Lett.* **29**, 1176 (2004).
19. K. Reivelt and P. Saari, *Phys. Rev. E* **66**, 056611 (2002).
20. J. Salo and M. M. Salomaa, *J. of Opt. A: Pure. Appl. Opt.* **3**, 366 (2001).
21. P. Saari, M. Menert, and H. Valtna, *Opt. Commun.* **246**, 445 (2005).
22. P. Saari, in *Ultrafast Photonics* (Inst. of Phys. Publ., Bristol, 2004).
23. H. Valtna, K. Reivelt, and P. Saari, *J. Opt. A: Pure Appl. Opt.* **8**, 118 (2006).

SPELL: OK

H. Valtna, K. Reivelt, P. Saari,
“Methods for generating wideband localized waves of superluminal group velocity”,
Opt. Comm. **278**, 1–7 (2007).



Methods for generating wideband localized waves of superluminal group velocity

H. Valtna ^{*}, K. Reivelt, P. Saari

Institute of Physics, University of Tartu, Riia 142, Tartu, 51014, Estonia

Received 19 December 2006; received in revised form 16 April 2007; accepted 18 May 2007

Abstract

Formation of superluminal localized waves (SpLW) – ultrawideband light pulses propagating faster than c without any spread or distortion in free space – is studied. A general approach how to produce exactly the angular spectrum required for generating SpLW in optical domain is introduced and analyzed. An experimentally realizable scheme, most suitable for generating SpLW of infinite group velocity (shortly – infinitely superluminal localized wave – iSpLW) is derived from the general approach. Experimental set-up for launching the iSpLW has been designed and resulting wave field calculated.

© 2007 Elsevier B.V. All rights reserved.

PACS: 42.25.Bs; 42.15.Eq; 42.65.Re; 42.25.Kb

Keywords: Ultrashort light pulses; Localized waves; X wave; Focus wave mode

1. Introduction

Localized waves (also known as nondiffracting or undistorted progressive waves) are ultrawideband wave packets with both spatially and temporally highly localized instantaneous intensity distribution propagating without any spread or distortion in free space or in linear media. Physical nature of the localized waves (LW) has been put to solid terms [1–7] and number of different localized wave solutions to the scalar wave equation has been derived during the last quarter of century (see [8,9] and overviews [5–7]).

Optical LW-s are prospective in many areas of application – particle manipulation, trapping and acceleration, imaging, ultrafast spectroscopy, quantum optics and, especially, in nonlinear optics (see, e.g. [10–13] and references therein). However, a real breakthrough here requires development of practical methods of generation of LW-s.

Due to the sophisticated non-separable temporal and spatial dependencies in the wavefunctions of LW-s, in order to generate them in reality the first task is to form a specific quasi-singular spatial distribution of the plane wave constituents of the wave field. There are four families of LW-s distinguished by the shape of the support of the distribution of the plane waves in the momentum space and, correspondingly, by their superluminal, luminal or subluminal group velocity along the propagation axis [7]. Despite a number of experiments have been carried out on LW-s in acoustics, optics and microwave domain in free space and in dispersive media [14–17], the task has been satisfactorily solved only for simplest superluminal pulses – the so-called X- or Bessel-X waves which can be generated from an ultrashort pulse by conical optics or annular slit and convergent lens. More complex LW called focus wave mode which belongs to family of luminal LW-s has been obtained by approximating the resulting angular dispersion curve of optical elements to that required for the LW [18].

The motivation of this paper is to elaborate methods for obtaining exact spatial distribution of plane wave

^{*} Corresponding author. Tel.: +372 7374623.

E-mail addresses: heli.valtna@ut.ee (H. Valtna), psaari@fi.tartu.ee (P. Saari).

constituents of superluminally propagating localized waves (SpLW). The simplest generator of a SpLW is cylindrical diffraction grating [19]. In this paper we present a generalized optical scheme and analyze the formation of SpLW-s by means of an enhanced practical scheme.

In Section 2 the basic idea of generating the suitable spatial distribution of the plane wave constituents by means of diffraction grating is introduced. Generalized optical scheme is introduced in Section 3 and studied in detail in Section 4 which presents also a numerical example.

2. Formation of the support of the spectrum

It is instructive here to start with treatment of ultrawide-band localized waves as superpositions of monochromatic plane waves with various frequencies and propagation directions. To generate a nonspreading wave packet one must be able to form certain specific spatial distribution of the plane wave constituents. In the following we deduce the requirement for the distribution in the momentum space.

A general solution to the free space scalar wave equation depends on 4 coordinates $\Psi = \Psi(x, y, z, t)$. Transform of Ψ to the momentum space $\psi(k_x, k_y, k_z, \omega)$ depends on three independent spectral variables due to the dispersion relation $k^2 = \omega^2/c^2 = k_x^2 + k_y^2 + k_z^2$ resulting from the wave equation. In other words – the spectral function in the 4-dimensional momentum space (k_x, k_y, k_z, k) is nonzero only on the cone determined by the relation $k^2 = k_x^2 + k_y^2 + k_z^2$. Assuming cylindrical symmetry – as it is common in the study of LW-s – and introducing radial component of the wave vector by relation $k_\rho^2 = k_x^2 + k_y^2$, one can depict the domain of wave numbers as a cone in 3D space (k_ρ, k_z, k) , k_z being the propagation axis of the wave packet (see Fig. 1).

Intensity profile of a wave packet propagates without any spread or distortion in free space or linear medium in case the group velocity (along the propagation axis) is constant over the whole temporal spectrum of the pulse [6]. The condition for the group velocity v_g in k -space, in nondispersive media,

$$c \frac{dk}{dk_z} = v_g = \text{const} \quad (1)$$

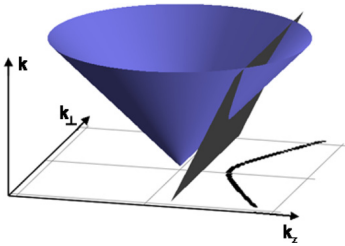


Fig. 1. Formation of the hyperbolic support of the spectrum. In order to depict the whole cone, a lateral component of the wave vector $k_\perp = \pm k_\rho$ has been taken as one of the axes instead of positively defined k_ρ .

shows that the variables k and k_z must be bound linearly

$$k = \frac{v_g}{c} k_z + \text{const}' \quad (2)$$

In the space (k_ρ, k_z, k) the condition defines a plane. The intersection of a plane (2) with the cone ($k^2 = k_\rho^2 + k_z^2$) is a line. The power spectrum of a wave packet traveling at constant group velocity must be determined only along the line – the support of the spectrum of the localized wave. The points of the support where the power spectrum of the wave packet is not zero define the spatial distribution of plane waves in k -space. Hence, for propagation invariance of the intensity profile of the wave packet the support of its spectrum in the momentum space has to be a line coinciding with a conical section.

All LW-s can be grouped into four families [7] according to the value of the slope v_g/c of the plane and, equivalently, according to the shape of the projection of the support line onto the plane (k_z, k_ρ) . The projection – as well as the support line itself – may be (i) hyperbola or (ii) its limiting case – a straight line crossing the origin, in both cases $v_g/c > 1$ and the pulse is superluminal, i.e. it propagates faster than c along the axis z (see Fig. 1), (iii) parabola, $v_g/c = 1$ and the pulse is luminal, (iv) ellipse, $v_g/c < 1$ and the pulse is subluminal. Like the cone sections differ qualitatively from each other, the formation methods of LW-s belonging to different families are dissimilar.

In this paper we restrict ourselves to superluminally propagating localized waves solely and thus are interested in formation of hyperbolic support of the spectrum. Henceforth we call the projection of the support onto the (k_z, k_ρ) -plane ‘the support line’ for brevity. Let us compare diffraction grating equation, on the one hand,

$$\sin(\theta) = \sin(\theta_i) + \lambda \frac{m}{d}, \quad (3)$$

where θ denotes the angle between the direction of diffracted beam with respect to the normal of grating, θ_i – the incidence angle, m – diffraction order, $\lambda = 2\pi/k$ – wavelength, d – groove period; and equation of the hyperbolic support line, on the other hand:

$$\sin(\theta) = \beta + \lambda \frac{k_0(1 - \beta)}{2\pi}, \quad (4)$$

where $\beta = (v_g/c)^{-1} < 1$ may be treated as the well-known parameter of Lorentz boost [7], k_0 – wavenumber of intersection of the support line and the axis k_z . Eqs. (3) and (4) both carry the same dependence on wavelength λ . Equivalence between these two equations and the condition Eq. (2) becomes even more obvious if we multiply Eqs. (3) and (4) by $k = 2\pi/\lambda$, introduce the grating vector $k_d = 2\pi/d$ and denote $k \sin(\theta) = k_\parallel$, $k \sin(\theta_i) = k_\parallel^i$ which are nothing but the components of the wave vector along the grating surface. The rewritten equations read

$$k_\parallel = k_\parallel^i + mk_d \quad (5)$$

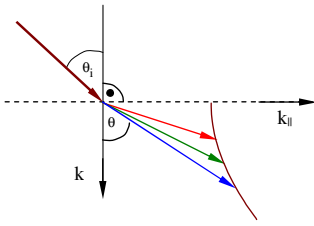


Fig. 2. Formation of the support of the spectrum while illuminating a diffraction grating (dotted vertical line) with plane wave impulse (upper left arrow). Incident light pulse travels at angle θ_i towards grating surface normal, the diffracted light at angle $\theta(k)$. As shown by Eqs. (3)–(6) the diffraction grating transforms straight line spectrum to a hyperbolic one.

and

$$k_{||} = k\beta + k_0(1 - \beta). \tag{6}$$

Having in mind orientation of the grating surface along the propagation axis z , Eq. (5) coincides with Eq. (6) (see Fig. 2).

Coincidence of wavelength or wavenumber dependencies in Eqs. (3)–(6) verifies that the support of the spectrum of a wideband pulse diffracted from a grating is always a hyperbola. Consequently, the correspondence between the constants in Eqs. (3) and (4) is as follows:

$$\begin{aligned} \sin(\theta_i) &= \beta, \\ \frac{m}{d} &= \frac{k_0(1 - \beta)}{2\pi}. \end{aligned}$$

The latter equality shows that without diffraction, i.e. if $m/d = 0$ the constant $k_0 = 0$ and k_z becomes simply proportional to k . In this case the hyperbola degenerates into straight line and we get the simple limiting case of the SpLW – the (Bessel) X wave propagating rigidly with superluminal velocity c/β , which has been generated experimentally already [11,15,16]. The equality $\sin(\theta_i) = \beta$

indicates that if the incident pulse falls along the normal of the grating surface, the group velocity of the wave packet generated will be infinitely large.

The following aspects have to be taken into account while constructing an optical scheme for forming SpLW experimentally:

- to generate cylindrically symmetric wave field one should use a cylindrical reflective diffraction grating, where ring-shaped grooves have been cut onto the inner surface of the cylinder;
- the impulse must be directed into the diffraction grating from one end, almost parallel to grating surface, i.e. the cylinder axis is also the propagation axis z of the output pulse;
- the maximum length of the invariant propagation of the SpLW is determined by the length of the diffraction grating and the wider the spectral bandwidth the shorter the length of the invariant propagation.

The possibilities and restrictions of the scheme based on cylindrical reflective diffraction grating are discussed more thoroughly in [19].

3. Generalized optical scheme

The scheme for generating pulsed wave field with the hyperbolic spectral support by means of cylindrical grating can be generalized to a better one consisting of a conical diffraction grating and a conical mirror as depicted in Fig. 3. A pulse passing through the grating obtains hyperbolic spectral support with respect to the direction of the grating surface. To form hyperbolic support with respect to the optical axis, the pulse needs to be rotated towards optical axis by the angle between grating surface and the optical axis. This is done by conical mirror with proper cone angle.

Let us verify that the hyperbolic support of the spectrum is formed in the scheme introduced. As the support line in

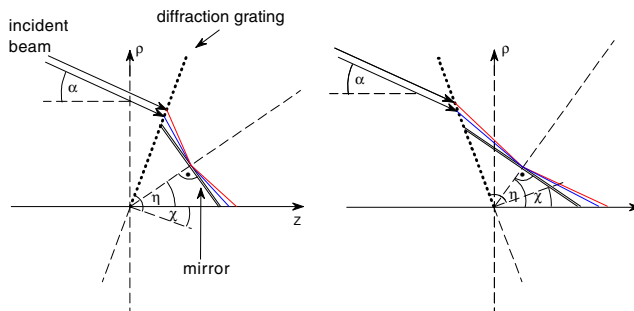


Fig. 3. Schemes for obtaining the SpLW by means of a conical diffraction grating and a conical mirror. Two versions of the scheme emphasize that the cone generatrix may have acute, right or obtuse angle with respect to the optical axis.

the plane (k_z, k_ρ) defines the propagation directions of monochromatic plane wave constituents of the wave packet we have to take a closer look at the angular dispersion introduced by the scheme. Describing the propagation direction of a plane wave as a vector

$$\mathbf{B} = \begin{pmatrix} k_\rho \\ k_z \end{pmatrix},$$

allows us to operate with well-known rotation and reflection matrixes.

The direction of the incident plane waves, traveling at the angle α towards the optical axis, is denoted as

$$\mathbf{B}_i = \begin{pmatrix} k_\rho^i \\ k_z^i \end{pmatrix} = \begin{pmatrix} k \sin \alpha \\ k \cos \alpha \end{pmatrix}.$$

The angle between the normal of the diffraction grating and the optical axis is denoted by χ . To introduce the dispersion of the diffraction grating, we describe the propagation of the plane waves relative to grating normal:

$$\mathbf{R}(-\chi) = \begin{pmatrix} \cos(-\chi) & \sin(-\chi) \\ -\sin(-\chi) & \cos(-\chi) \end{pmatrix}.$$

(The matrix performs rotation of the coordinate system clockwise by angle χ). Grating dispersion is described by matrix obtained from Eq. (3)

$$\mathbf{G} = \begin{pmatrix} \frac{\sin(\alpha-\chi)+2\pi m/kd}{\sin(\alpha-\chi)} & 0 \\ 0 & \frac{\sqrt{1-(\sin(\alpha-\chi)+2\pi m/kd)^2}}{\cos(\alpha-\chi)} \end{pmatrix}$$

and the application of the backward-rotation matrix $\mathbf{R}(\chi)$ gives the propagation directions towards optical axis. To introduce reflection we describe the plane waves with respect to mirror normal by rotating the system by the angle η , apply the reflection matrix $\mathbf{M} = \begin{pmatrix} 1 & 0 \\ 0 & -1 \end{pmatrix}$ and rotate backwards by $-\eta$. The angle between the normal of the mirror and optical axis η is half the angle between grating surface and optical axis $\eta = \pi/4 - \chi/2$. Propagation direction of emergent plane waves is described by

$$\mathbf{B}_r = \mathbf{R}(-\eta)\mathbf{M}\mathbf{R}(\eta)\mathbf{R}(\chi)\mathbf{G}\mathbf{R}(-\chi)\mathbf{B}_i \\ = \begin{pmatrix} k\sqrt{1-(\sin(\alpha-\chi)+2\pi m/kd)^2} \\ k\sin(\alpha-\chi)+2\pi m/d \end{pmatrix}.$$

For the hyperbolic support line the vector \mathbf{B} should read:

$$\mathbf{B} = \begin{pmatrix} k\sqrt{1-(\beta+k_0(1-\beta)/k)^2} \\ k\beta+k_0(1-\beta) \end{pmatrix}.$$

Since according to the previous section $\beta = \sin(\alpha - \chi)$ and $d = 2\pi m/k_0(1 - \beta)$, we have shown that the conical pulse passing through the system of the conical grating and mirror obtains the hyperbolic support of the spectrum.

4. Analysis of the scheme

With the described setup it is (theoretically) possible to generate the whole variety of SpLW-s – from cylindrical waves of infinite group velocity [6] to those propagating almost luminally. Following features of the scheme need to be emphasized:

- Parameters describing the wave field and the diffracting grating are related as follows:

$$v_g = \frac{c}{\sin(\alpha - \chi)}, \\ k_0 = \frac{2\pi m}{(1 - \sin(\alpha - \chi))d}.$$

- The scheme places some restrictions on the spectral width of the wave field. The reddest plane wave component transmitted by the scheme is the one that diffracts slightly less than by $\pi/2$ towards grating normal and its wavenumber is given as

$$k_r = \frac{2\pi m}{d(1 - \sin(\alpha - \chi))}. \quad (7)$$

The bluest plane wave (or Bessel wave) constituent reflects from mirror in case it is diffracted more than angle η and its wavenumber is given as

$$k_b = \frac{2\pi m}{d(\sin(\eta) - \sin(\alpha - \chi))}. \quad (8)$$

Therefore, if the width of the spectrum has been prescribed we can find allowable range for groove period values:

$$\frac{2\pi m}{k_b(\sin(\eta) - \sin(\alpha - \chi))} \leq d \leq \frac{2\pi m}{k_r(1 - \sin(\alpha - \chi))} \quad (9)$$

- One can see that by adjusting the incidence angle α of illuminating pulse a SpLW with the desired group velocity $v_g = c/\sin(\alpha - \chi)$ can be formed with the help of different diffraction gratings. In principle, one specific grating can be used to form the whole variety of SpLW-s.
- Fig. 3 emphasizes the freedom in the choice of the angles of the generatrix with respect to the optical axis. Let us compare two schemes with different grating angles χ . It follows from Eq. (9): the larger the angle, the larger the optimal groove period. Or, in case the gratings have the same period the grating with larger angle χ transmits narrower spectrum.
- As the cone angle can be used to define the group velocity of resulting wave packet, one can use a plane wave impulse ($\alpha = 0^\circ$) for illuminating the grating, hence the input pulse needn't to be pre-shaped into a conical one.

In real conditions such conical gratings with sufficiently small thickness – required in order to neglect the dispersion of the cone material – cannot be manufactured easily and the schemes described so far are rather of theoretical interest.

Still, some practically obtainable schemes can be derived from the approach based on conical grating and conical mirror. In what follows we analyze few cases with special values of the grating normal angle $\chi \in [-\pi/2; \pi/2]$.

In case $\chi = \pi/2$ the conical grating degenerates to a cylindrical grating, the mirror becomes unnecessary. Basically, this is the scheme described in [19].

In case $\chi = 0$ one gets planar diffraction grating with concentric, circular and radially equidistant grooves – a sort of zone plate. The mirror is conical with cone angle $\pi/2$, $\eta = \pi/4$. As stated earlier, with a conical grating and accompanying mirror it is possible to generate whole variety of SpLW-s. However, to form a SpLW traveling almost luminally with $v_g \gtrsim c$ by means of the plane grating the incidence angle α must be almost a right one and the illuminating pulse must be almost flat cylindrically symmetrical pulse converging to the optical axis – which is extremely difficult to accomplish. In contrast, the scheme proposed can be rather easily used for generation of the SpLW with infinite group velocity, since in this case the scheme is to be illuminated with plane wave pulse traveling along the optical axis.

Let us analyze possible setup for generating infinitely superluminally propagating localized wave (henceforth iSpLW) in further details. Altogether there are seven independent parameters to characterize the system: α – incidence angle of illuminating pulse; k_r , k_b – reddest and bluest plane wave components transmitted; d – grating period; m – diffraction order; l – cone height (cone angle is determined by $\chi = 0$) and as we see, it is useful to have a central hole in the conical mirror with radius D . Most important output parameters of the system are the propagation range of the wave field ΔZ , wave field aperture a (the largest diameter of the volume where the output wave field comprises the propagation-invariant SpLW) and the grating aperture A .

In the scheme for generating cylindrically symmetrical iSpLW, we have $\alpha = 0^\circ$. The grating period determines the widest possible spectrum width (k_r , k_b from Eq. (9)).

The grating period, mirror height and spectrum together determine the aperture of the illuminating pulse. From geometry of the scheme we can derive a formula for the aperture for which a monochromatic plane wave illuminates whole mirror. The aperture varies with the wavelength:

$$A(k) = 2D + 2l \frac{2\pi m}{\sqrt{(kd)^2 - (2\pi m)^2}}.$$

While illuminating the scheme with light pulse which aperture does not depend on the wavelength, one must take into account that not all plane wave constituents, especially with smaller wavelength, are reflected from the mirror and thus their spectral support is not hyperbolic towards the optical axis and they do not contribute to formation of the SpLW, instead coinciding with the wave field they shorten the range in which the SpLW can be registered

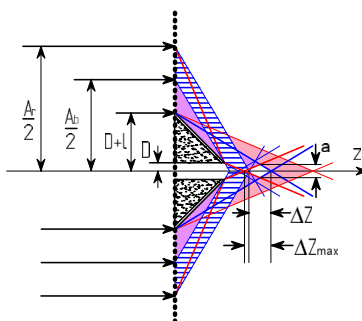


Fig. 4. Formation of cylindrical wave by means of plane grating (dotted line) and conical mirror (two “sandy” triangles). Arrows left from the grating depict illuminating pulse. Regions in which diffracted and reflected plane waves travel behind the grating are shown in solid fill. $A_b/2$ denotes radius of the illuminating aperture for the bluest wavelength and $A_r/2$ that for the reddest wavelength. From disk $A_r/2 - A_b/2$ originates a cone (hatched region) in which travel short wavelength plane waves which do not reflect on mirror and thus do not contribute to formation of SpLW. As seen from the figure those plane wave components shorten the range in which the invariant propagation of SpLW can be registered ($\Delta Z < \Delta Z_{\max}$). (For interpretation of the references to color in this figure legend, the reader is referred to the web version of this article.)

(see Fig. 4). The effect can be forced back by enlarging the central hole radius D^1 , by narrowing the spectrum or by shifting the spectrum to shorter wavelengths.

Cone height l is parameter characterizing the dimensions of the conical mirror. The larger l , the larger invariant propagation range ΔZ and the larger aperture has to be illuminated.

While designing an experimental set-up for specific grating one must bear in mind that the aperture of resulting wave field depends on the mean wavelength of the illuminating pulse as well. To widen the wave field aperture, its spectrum should be shifted towards smaller wavelengths.

From geometry of the scheme one can derive the formula describing maximum invariant propagation range ΔZ_{\max} dependence of the scheme parameters l, D, α and χ :

$$\Delta Z_{\max} = (D + l) \frac{\sin(\alpha - \chi) + \frac{2\pi m}{k_b d}}{\sqrt{1 - (\sin(\alpha - \chi) + \frac{2\pi m}{k_b d})^2}} - l - D \frac{\sin(\alpha - \chi) + \frac{2\pi m}{k_r d}}{\sqrt{1 - (\sin(\alpha - \chi) + \frac{2\pi m}{k_r d})^2}}.$$

One can see the equation describing the dependence is rather complicated. Intuitive comprehension of the scheme can be more easily achieved through understanding and analyzing the geometrical interplays (Fig. 4) instead of studying multi-dimensional space of parameters.

¹ The central hole in conical mirror can be used also for measuring the wavefield in interferometric experiment.

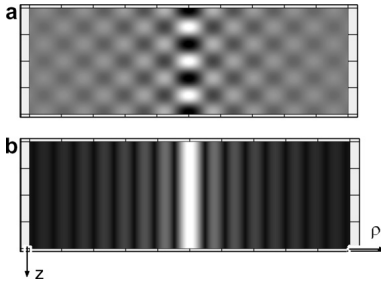


Fig. 5. Grey-scale plots of the real part (a) and the modulus (b) of iSpLW with a Gaussian spectrum of temporal frequencies shown at instant $t = 0$, generated by the optical scheme (see parameters in the text). The plotting range for the lateral coordinate ρ is $6 \mu\text{m}$ while for the axial coordinate z it is $1 \mu\text{m}$.

To conclude the analysis we present a numerical example verifying the realizability of the set-up.

The optimization calculations have been made for an optical scheme consisting of a planar grating diameter $A = 55.2 \text{ mm}$ and concentric grooves with density 1560 1/mm , a conical mirror with height $l = 10 \text{ mm}$ and radius $D = 1 \text{ mm}$ of the central hole. As input a 60 fs pulse with Gaussian spectrum was assumed, which can be generated by Ti:sapphire laser for example, with $\lambda_r = 600 \text{ nm}$ and $\lambda_b = 580 \text{ nm}$. If using the first diffraction order the invariant propagation range $\Delta Z \approx 10 \text{ mm}$ was shown to be achievable. The real part and modulus of the resulting wave field [20] is depicted in Fig. 5.

5. Discussion

A comparatively simple and already accomplished task (see optical launching of Bessel-X impulse: [11,15,16]) is to generate localized waves possessing equal superluminal group and phase velocities and therefore propagating rigidly with not only invariable intensity distribution but also with propagation-invariant wavefunction. Their spectral support has been degenerated from a hyperbola into a straight line and therefore simple methods of obtaining conical waves – annular slit imaging, conical mirrors or lens² (axicons) do the job well. In contrast, there is no one step technique to form parabolic support of a luminal LW – the focus wave mode. In the only experiment carried out so far [18,21,22] glass wedges and diffraction grating were used in order to fit the resulting angular dispersion curve to the required parabolic support line. One encounters similar difficulties in the case of any curved support line, including the hyperbolic one required for SpLWs.

The approach introduced in this paper for generation of any general-type SpLW is important in the sense that it

solves the task of obtaining the required shape of the spectral support *exactly* over a wide range of spectrum and without resorting to approximations.

The schemes proposed offer also the possibility to generate wave packets belonging to a family of superluminally propagating localized waves in the whole velocity range – $c \lesssim v_g \lesssim \infty$. The analysis of scheme reveals sophisticated interplay between the parameters and finding the most effective setup requires optimizing the parameter values.

Infinitely large group velocity, while being a rigorously defined quantity, means simply that the intensity (modulus squared) of the wave does not depend on the axial coordinate z in the given case and its movement – implosion and explosion – occurs in the radial direction only. Similarly is the speed of movement of crossing point of scissor blades infinitely large when the blades become parallel. That is why there is nothing unphysical with such superluminal movement – it cannot carry any causal signal between two points along the axis and do not correspond to energy flow (see [15] and a more thorough discussion in [23]).

It should be stressed that in order to generate a maximally localized (“transform-limited”) pulse on the optical axis inside the invariant propagation volume, one needs to give suitable chirp to the input pulse. The required linear chirp can be easily achieved with the help of standard pulse stretching techniques.

Finally, it is interesting to note the following. In a common arrangement with a planar circular grating only, whose normal has been directed along the optical axis, the output wave packet is not propagation-invariant and spreads out longitudinally with the distance. The pulse can be made localized only at a given distant point behind the grating by appropriately pre-chirping the input pulse. In this arrangement, however, Eq. (5) reduces to $k_\rho = mk_{\rho_0}$, i.e. to a straight line equation $k_\rho = \text{const}$. In turn, this means that all monochromatic Bessel-beam constituents of the wave packet have the same radial wavenumber and the wave field does not change *radially* in the course of propagation. The latter property of the wave field enables carrying out a signalling *along* the optical axis and therefore the pulse cannot be and really is not superluminal.

6. Conclusion

We have generalized the scheme of forming superluminally propagating localized waves and, in particular, proposed a new approach to generation of cylindrical waves traveling with infinitely large group velocity. The properties of different versions of the generalized scheme have been analyzed in detail. A realistic optical set-up has been designed and a numerical example of resulting wave field presented.

Acknowledgement

The research was supported by the Estonian Science Foundation.

² ... in case of small axicon angle and thus $v_g \gg c$ material dispersion can be neglected.

References

- [1] R.W. Ziolkowski, *J. Math. Phys.* 26 (1985) 861.
 [2] M.R. Palmer, R. Donnelly, *J. Math. Phys.* 34 (1993) 4007.
 [3] J. Salo, J. Fagerholm, A.T. Friberg, M.M. Salomaa, *Phys. Rev. Lett.* 83 (1999) 1171.
 [4] E. Recami, M. Zamboni-Rached, C.A. Dartora, *Phys. Rev. E* 69 (2004) 027602.
 [5] I. Besieris, M. Abdel-Rahman, A. Shaarawi, A. Chatzipetros, *Prog. Electromagn. Res.* 19 (1998) 1.
 [6] K. Reivelt, P. Saari, arXiv.org e-Print archive, physics/0309079 <http://arxiv.org/abs/physics/0309079> (2003).
 [7] P. Saari, K. Reivelt, *Phys. Rev. E* 69 (2004) 036612.
 [8] J.N. Brittingham, *J. Appl. Phys.* 54 (1983) 1179.
 [9] V.V. Borisov, A.P. Kiselev, *Appl. Math. Lett.* 13 (2000) 83.
 [10] P. Saari, M. Rätsep, H. Sõnajalg, *Opt. Lett.* 22 (1997) 310.
 [11] R. Grunwald, V. Kebbel, U. Griebner, U. Neumann, A. Kummrow, M. Rini, E.T.J. Nibbering, M. Piche, G. Rousseau, M. Fortin, *Phys. Rev. A* 67 (2003) 063820.
 [12] P. Saari, M. Menert, H. Valtna, *Opt. Commun.* 246 (2004) 445.
 [13] P. Di Trapani, G. Valiulis, A. Piskarskas, O. Jedrkiewicz, J. Trull, C. Conti, S. Trillo, *Phys. Rev. Lett.* 91 (2003) 093904.
 [14] J. Lu, J.F. Greenleaf, *IEEE Trans. Ultrason. Ferroelectr. Freq. Control* 39 (1992) 19.
 [15] P. Saari, K. Reivelt, *Phys. Rev. Lett.* 79 (1997) 4135.
 [16] I. Alexeev, K.Y. Kim, H.M. Milchberg, *Phys. Rev. Lett.* 88 (2002) 073901.
 [17] D. Mugnai, A. Ranfagni, R. Ruggeri, *Phys. Rev. Lett.* 84 (2000) 4830.
 [18] K. Reivelt, P. Saari, *Phys. Rev. E* 66 (2002) 056611.
 [19] P. Saari, K. Reivelt, H. Valtna, *Laser Phys.* 17 (2007) 297.
 [20] Wavefunction of cylindrically symmetrical iSpLW with Gaussian spectrum reads:

$$\psi(\rho, z, t) = \int_0^\infty dk \exp\left[-\left(\frac{k-k_m}{\Delta k}\right)^2\right] J_0\left(\rho\sqrt{k^2-k_0^2}\right) \exp(ik_z z - ikt).$$

 The integral does not have closed-form expression.
 [21] K. Reivelt, P. Saari, *J. Opt. Soc. Am. A* 17 (2000) 1785.
 [22] K. Reivelt, P. Saari, *Phys. Rev. E* 65 (2002) 046622.
 [23] P. Saari, *Ultrafast Photonics*, Institute of Physics Publishing, Bristol and Philadelphia, 2004, pp. 317.

A. Averchi, D. Faccio, E. Rubino, H. Valtna Lukner, A. Panagiotopoulos,
P. A. Loukakos, S. Tzortzakis, A. Couairon, and P. Di Trapani,
“Linear X-wave generation by means of Cross Phase Modulation in Kerr media”
Opt. Lett., **33**, 3028–3030 (2008).

Linear X-wave generation by means of cross-phase modulation in Kerr media

A. Averchi,^{1,6,*} D. Faccio,^{1,6} E. Rubino,^{1,6} H. Valtna Lukner,^{2,3} P. Panagiotopoulos,⁴ P. A. Loukakos,⁴ S. Tzortzakis,⁴ A. Couairon,^{5,6} and P. Di Trapani^{1,3,6}

¹Department of Physics and Mathematics, CNISM University of Insubria, Via Valleggio 11, IT-22100 Como, Italy

²Institute of Physics, University of Tartu, Riia 142, 51014 Tartu, Estonia

³Department of Quantum Electronics, Vilnius University, Sauletekio Avenue 9, Building 3, LT-10222 Vilnius, Lithuania

⁴Institute of Electronic Structure and Laser, Foundation for Research and Technology-Hellas (IESL-FORTH), P.O. Box 1527, 71110 Heraklion, Greece

⁵Centre de Physique Théorique, CNRS, École Polytechnique, F-91128 Palaiseau, France

⁶Virtual Institute for Nonlinear Optics, Centro di Cultura Scientifica Alessandro Volta, Villa Olmo, Via Simone Cantoni 1, 22100 Como, Italy

*Corresponding author: alessandro.averchi@uninsubria.it

Received July 25, 2008; accepted October 3, 2008;

posted November 17, 2008 (Doc. ID 99407); published December 12, 2008

We exploit cross-phase modulation by a strong driving pulse onto a weaker probe pulse at a different wavelength to induce the formation of an X wave possessing the typical nondispersive and nondiffractive propagation properties. © 2008 Optical Society of America
OCIS codes: 190.7110, 320.2250.

X waves belong to the wider class of so-called “conical waves,” i.e., wave packets in which the energy flow is not axial but is directed along a cone centered around the propagation axis. All conical waves share the property of being nondiffractive (experimentally, over a finite distance), but only X waves are able to achieve also nondispersive propagation in dispersive media [1], thanks to their angular dispersion that also determines the X-wave group velocity, which is in general different from that of a Gaussian pulse centered at the same wavelength. Among other systems, spontaneous X-wave formation has been predicted and extensively studied in the process of optical pulse filamentation in Kerr media [2–4], which is a spatiotemporal dynamic reshaping of the pulse driven by nonlinear effects in the medium manifested as the formation of a high intensity core propagating over long distances without spreading [5]. Recently, in the context of “two-color filamentation” studies—where the filamenting pulse copropagates with a pulse at a different wavelength—X-wave formation induced by filaments has been reported in [6,7]. In the presence of stimulated Raman scattering (SRS) the reshaping of a Gaussian seed into an X wave and its subsequent amplification by SRS were investigated. In this interaction, cross-phase modulation (XPM) was found to be responsible for seed reshaping. Its effect can be described as a scattering potential that drives the probe to travel at the same group velocity of the filament by transforming it into an X wave.

In this Letter for the first time (to our knowledge) we experimentally study in detail the effect of XPM in the absence of energy transfer between a filament (1055 nm) and a weak probe pulse (527 nm) in conditions similar to those simulated in [8]. We observe that XPM induces on the probe a reshaping into a linear X wave that travels at the same group velocity as

the filament. As the X wave is well spectrally isolated, we filter out the filament at the end of the sample and characterize the propagation of the X wave alone in air, which shows remarkable nondiffracting properties. Moreover we show that, as long as the XPM-inducing pulse maintains a high intensity over a long propagation distance, a filament is not strictly necessary to induce the X-wave reshaping; to this purpose we repeat the experiment using a Bessel pulse as the driving pulse.

Experiments in the filamentation regime were carried out using 1.2 ps duration (FWHM) 1055 nm laser pulses delivered by a 10 Hz amplified Nd:glass laser. The beam was split into two by means of a 50/50 beam splitter. On one arm the 527 nm pulse was generated by frequency doubling the fundamental pulse with a potassium diphosphate crystal beyond which a variable delay line was mounted. The green and IR pulses were then recombined with an IR high reflectivity dielectric mirror and focused with an $f=50$ cm lens (as in [6,7]) to a diameter of 100 μm onto the input facet of a 2-cm-long long fused silica sample. The energies of the two pulses ($E_{\text{pump}}, E_{\text{probe}}$) were controllable independently by first-order half-wave plates and polarizers. The absence of energy transfer from the filament to the green pulse was experimentally verified by measuring the energy of the green pulse before and after the sample with a power meter (OPHIR, Nova).

In Fig. 1 we show the angularly resolved (θ, λ) spectrum of the 527 nm pulse measured with an imaging spectrometer (Lot-Oriel, MS260i) after the sample and recorded with a digital Nikon D70 camera. In Fig. 1(a) the IR pulse was blocked, and the weak green pulse was let to propagate alone inside the sample; as expected the intensity profile in the spectrum is Gaussianlike. In Fig. 1(b) the filamenting IR pulse ($E_{\text{pump}}=20 \mu\text{J}$) was spatially and tempo-

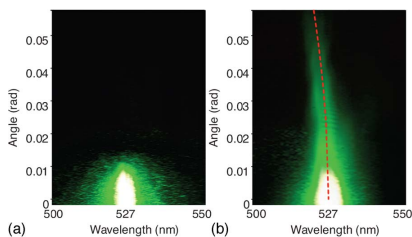


Fig. 1. (Color online) (θ, λ) Spectrum of the 527 nm probe pulse after the sample (a) when the IR pulse is blocked and (b) when the IR filamenting pulse is copropagating with the probe in the sample. XPM induces the formation of conical structures on the probe spectrum. The dashed curve is the plot of Eq. (1), describing the X-wave shape with the experimental group velocity of the X wave (v_x) deduced from the spectrum of the filament as described in [7].

rally superimposed to the central portion of the green pulse ($E_{\text{probe}} = 0.5 \mu\text{J}$). Although in the absence of any energy transfer from the filament, the green seed pulse clearly reshapes and develops conical tails, which in the angularly resolved spectrum are the well-known signature of X-wave formation [9].

To prove the genuine X-wave nature of this object, however, it is necessary to show its nondispersive and nondiffracting propagation. To demonstrate the first, in Fig. 1(b) we fit the spectrum using the X-wave relation that, for a given material and central wavelength, describes in the (θ, λ) spectrum the loci, where the angular dispersion is able to compensate the material dispersion. In (k_{\perp}, ω) coordinates—equivalent to (θ, λ) —this relation takes the simple form [7]

$$k_z(\omega) = k(\omega_0) + \frac{\omega - \omega_0}{v_x}, \quad (1)$$

where ω_0 is a reference central frequency and $k_{\perp}(\omega) = \sqrt{k(\omega)^2 - k_z(\omega)^2}$ and v_x is the group velocity of the X wave. As can be seen in Fig. 1(b), the curve matches very closely the experimental shape. We underline that this simple spectral intensity characterization is sufficient to prove that the pulse propagates without dispersing within the glass sample as, indeed, for a given medium; pulse spreading along the propagation direction is completely determined by the pulse dispersion relation $k_z = k_z(\omega)$. We note also that in our fit the group velocity of the X wave is not a free parameter; indeed, it is the group velocity of the driving pulse measured experimentally using the method described in detail in [7] and yielding $v_x = 2.22 \pm 0.03 \times 10^8$ m/s. This allows us to confirm experimentally the prediction made in [7,8] that the X wave induced by XPM travels at the same group velocity as the driving pulse.

We then verified the nondiffracting propagation of the X-reshaped green pulse. To demonstrate this we simply let the two pulses propagate out of the sample in air, where the nonlinear refractive index is about

1000 times smaller than in silica, thus quenching the filament and all nonlinear effects. We then removed the IR light with a low-pass filter and scanned the green beam profile along its propagation in air, starting from the output facet of the sample. Our imaging system was composed by a lens and a 12-bit CCD camera (DTA iCam 400 E).

In Fig. 2(a) the normalized intensity profile of the probe at the output facet of the sample is shown. The effect of XPM from the filament is evident, with the formation of a narrow (7.8 μm) FWHM central peak surrounded by slowly decaying tails. We could fit its radial intensity profile with a rational function having the form $a/(br^2+cr)$, which agrees well with the $1/r^2$ decay for large radii expected for a linear X wave [10]. In Fig. 2(d) the measured FWHM of the beam profile along the z axis is shown. As can be seen, the central peak propagates nondiffractively, keeping its FWHM constant within the experimental error for a distance of about 5 mm, and then diffracts abruptly. This behavior at the end of the nondiffracting zone is typical of all the experimental realizations of conical waves and is due to the finite energy contained in the conical wave packet. Notably, on the same distance of 5 mm a collimated Gaussian beam with the same initial diameter would have reached a FWHM of about 120 μm .

We performed a complementary experiment using a pulsed Bessel beam (PBB) instead of the filament as the driving pulse. Here our driving pulse was a 1 mJ, 35 fs pulse positively chirped to 1 ps (to optimize pump and seed temporal overlap) at 800 nm from an amplified Ti:sapphire laser system. The

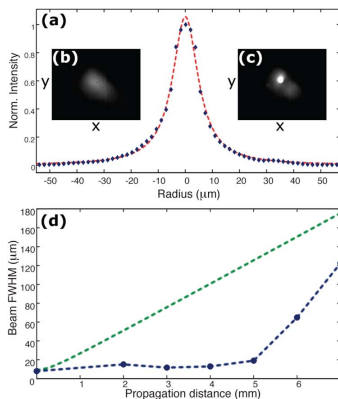


Fig. 2. (Color online) (a) Normalized intensity profile of the probe at the output of the sample in the presence of XPM. The dashed curve is the fit of the profile with a rational quadratic function. In the insets the near field of the green pulse is acquired with the CCD system (b) without XPM and (c) with XPM. Note that the probe energy was unchanged between the two measurements. (d) Probe beam FWHM along propagation after the sample (dashed curve with solid circles), nondiffracting over 5 mm. The theoretically predicted broadening for a Gaussian beam with the same FWHM is shown for comparison (dashed curve).

probe pulse was generated by frequency doubling with a β -barium borate crystal. The setup scheme was conceptually the same as the first experiment, with the addition of a 175 apex angle axicon mounted onto the IR beam line to reshape the driving pulse into a Bessel beam.

As we show in Fig. 3(a), the probe pulse—as expected—developed X wave tails in the (θ, λ) spectrum due to XPM. We also performed a series of numerical simulations to confirm the validity of this last experimental result, using a code described in detail in [5]. In Fig. 3 the numerically predicted (θ, λ) spectra of the probe pulse with and without XPM reshaping are reported. As may be seen, the numerics confirm our experimental findings. We note that the driving Bessel pulse suffered no significant changes owing to self-induced nonlinear effects as verified both numerically and experimentally (data not shown); i.e., no spectral broadening was observed. These last results confirm that the XPM reshaping of the probe pulse into an X wave is not necessarily related to filamentation of the pump pulse. Indeed Eq. (1) is derived under the sole assumption that the scattering polarization is localized in space (allowing the probe spectrum to spread in angle) and in time (allowing the probe to spread its temporal spectrum) [3].

In conclusion, in this Letter we have studied in detail the spatiotemporal reshaping induced by XPM from an intense driving pulse on a weaker probe at a different wavelength in a bulk Kerr medium. We

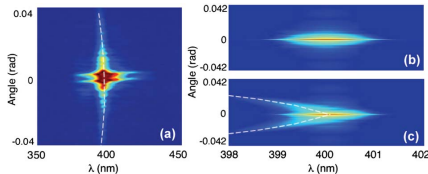


Fig. 3. (Color online) (a) Experimentally measured (θ, λ) spectrum for the probe pulse at 400 nm reshaped by XPM driven from a PBB at 800 nm. The white curve is the X -wave relation curve calculated with Eq. (1), where $v_x = 2.043 \times 10^8$ m/s is the theoretically predicted group velocity for the PBB. Numerically simulated (θ, λ) spectrum for the probe pulse (b) before interaction with the driving pulse and (c) with XPM induced by the PBB.

have shown that XPM can be exploited to generate spectrally isolated linear X waves that propagate over a finite distance with no dispersion and no diffraction. Moreover we have shown the generality of this mechanism, which holds as long as the driving pulse propagates for a distance long enough with a sufficient intensity. We think that these results will be useful both as a tool to better understand current studies on two-color systems in the field of ultrashort nonlinear optics and to provide a feasible method to generate X waves in the optical domain.

The authors acknowledge support from CNSIM, project INNESCO, from the Lithuanian Science and Technology Foundation project ConTeX, from Marie Curie Chair project STELLA, contract MEXC-CT-2005-025710, and Marie Curie Excellence grant MULTI-RAD MEXT-CT-2006-042683. H. V. Lukner acknowledges support from the Sixth European Union (EU) Framework Program (ATLAS), contract MEST-CF-2004-008048. The results have been partly obtained during the STELLA school 2008 (www.vino-stella.eu).

References

1. H. Sonajalg and P. Saari, *Opt. Lett.* **15**, 1163 (1996).
2. C. Conti, S. Trillo, P. Di Trapani, G. Valiulis, A. Piskarskas, O. Jedrkiewicz, and J. Trull, *Phys. Rev. Lett.* **90**, 170406 (2003).
3. D. Faccio, M. A. Porras, A. Dubietis, F. Bragheri, A. Couairon, and P. Di Trapani, *Phys. Rev. Lett.* **96**, 193901 (2006).
4. M. Kolesik, E. M. Wright, and J. V. Moloney, *Phys. Rev. Lett.* **92**, 253901 (2004).
5. A. Couairon and A. Mysyrowicz, *Phys. Rep.* **441**, 47 (2007).
6. D. Faccio, A. Averchi, A. Dubietis, P. Polesana, A. Piskarskas, P. Di Trapani, and A. Couairon, *Opt. Lett.* **32**, 184 (2007).
7. D. Faccio, A. Averchi, A. Couairon, M. Kolesik, J. V. Moloney, A. Dubietis, G. Tamosauskas, P. Polesana, A. Piskarskas, and P. Di Trapani, *Opt. Express* **15**, 13077 (2007).
8. M. Kolesik and J. V. Moloney, *Opt. Express* **16**, 2971 (2008).
9. D. Faccio, P. Di Trapani, S. Minardi, A. Bramati, F. Bragheri, C. Liberale, V. Degiorgio, A. Dubietis, and A. Matijosius, *J. Opt. Soc. Am. B* **22**, 862 (2005).
10. J. Lu and J. F. Greenleaf, *IEEE Trans. Ultrason. Ferroelectr. Freq. Control* **39**, 19 (1992).

P. Bowlan, H. Valtna-Lukner,
M. Lõhmus, P. Piksarv, P. Saari, and R. Trebino,
“Measurement of the spatio-temporal field of ultrashort Bessel-X pulses”,
Opt. Lett. **34**, 2276–2278 (2009).

Measuring the spatiotemporal field of ultrashort Bessel-X pulses

Pamela Bowlan,^{1,*} Heli Valtma-Lukner,² Madis Lõhmus,²
Peeter Piksarv,² Peeter Saari,² and Rick Trebino¹

¹Georgia Institute of Technology, School of Physics, 837 State Street, Atlanta, Georgia 30332, USA

²University of Tartu, Institute of Physics, 142 Riia Street, Tartu, 51014 Estonia

*Corresponding author: pambowlan@gatech.edu

Received May 13, 2009; revised June 22, 2009; accepted June 23, 2009;
posted June 25, 2009 (Doc. ID 111378); published July 21, 2009

We present direct measurements of the spatiotemporal electric field of an ultrashort Bessel-X pulse generated using a conical lens (axicon). These measurements were made using the linear-optical interferometric technique SEA TADPOLE, which has micrometer spatial resolution and femtosecond temporal resolution. From our measurements, both the superluminal velocity of the Bessel pulse and the propagation invariance of the central spot are apparent. We verified our measurements with simulations. © 2009 Optical Society of America

OCIS codes: 320.7100, 320.5550.

Bessel-X pulses are of great interest because they propagate in vacuum or linear media over large distances like an optical bullet—without exhibiting any diffraction or temporal spread. Bessel pulses have many applications, such as plasma generation [1], light filamentation (see reviews [2,3]), imaging [4], particle micromanipulation [5], and cell transfection [6]. Bessel-X pulses are one type of axially symmetrical localized wave (see [7–10] and references therein) that corresponds to a broadband wave packet of co-axial zeroth-order Bessel beams. Their longitudinal and transverse wavenumbers (which determine the spacing of the Bessel rings) are proportional to the temporal frequency of the individual Bessel beam constituents, and it is this characteristic that distinguishes them from other possible superpositions of Bessel beams [7]. Their three-dimensional intensity profile $I(x, y, z)$ or $I(x, y, t)$ consists of a bright central spot surrounded by weaker interference rings all inside of two cones that start at the origin, and one extends forwards and the other backwards in time (or z). Therefore, an $x-t$ or $x-z$ slice of the field resembles the letter X. In principle Bessel-X pulses can propagate over an infinite distance without any spread. But in practice, owing to finite aperture sizes and aberrations in the Bessel beam generators, the propagation invariant zone is restricted, though this is still usually several orders of magnitude larger than the Rayleigh range of a Gaussian beam with the same focal spot size. Interestingly, the field of a Bessel-X pulse propagates along the z axis with equal phase and group velocities that are greater than c in vacuum. It is important to measure these pulses, not only to observe their interesting and useful properties but also to aid in their generation and application. But Bessel-X pulses have a complex spatiotemporal shape, so a *spatiotemporal* measurement technique with simultaneous femtosecond temporal resolution and micrometer spatial resolution is needed.

Several previous publications have reported experimental studies of Bessel-X pulses. The propaga-

tion invariance of the small central spot of a Bessel-X pulse in a dispersive medium was first shown in [9], where a holographic element generated the field. Evidence of X-like spatial profiles and the superluminal propagation of Bessel-X waves were demonstrated using an annular slit and a pinhole to generate cross correlations of the fields with a white-light source [10]. Later, direct autocorrelation measurements were made of the X profile of the pulses generated from sub-10 fs laser pulses [11]. The superluminal speed of Bessel-X pulses has also been measured by observing the ionization front in argon gas owing to the central spot of an intense Bessel-X pulse generated using an axicon and 70 fs pulses [1]. Recently a Hartman–Shack sensor and frequency-resolved optical gating were used to separately characterize both the spatial and the temporal fields of a Bessel-X pulse [12]. But, to our knowledge, a direct measurement of the field [i.e., $E(x, z, t)$] of a Bessel-X pulse in the course of its propagation has never been made.

In this Letter we do so, reporting “snapshots in flight,” or measurements of the spatiotemporal X-like profile of a femtosecond Bessel-X pulse, including the phase versus time. Our results show propagation invariance over 8 cm, as well as the superluminal velocity of the Bessel-X pulse. To generate the Bessel-X pulse, we propagated ~ 37 nm bandwidth, ~ 30 fs pulses from a KM Labs Ti:Sa oscillator through a fused-silica axicon with an apex angle of 176° . The spot size of the beam at the axicon’s front surface was 4 mm. For the measurements we used the linear-optical spectral interferometric technique, SEA TADPOLE [13,14], and we compared our measurements with numerical simulations.

A detailed description of SEA TADPOLE can be found in [13,14]. Briefly, this device involves sampling a small spatial region of the Bessel pulse with a single-mode optical fiber (having a mode diameter of $5.4 \mu\text{m}$) and then interfering this with a reference pulse in a spectrometer to reconstruct the pulse intensity and phase $E(\lambda)$ [and hence also $E(t)$] at a point in space. We scan the fiber transversely (versus

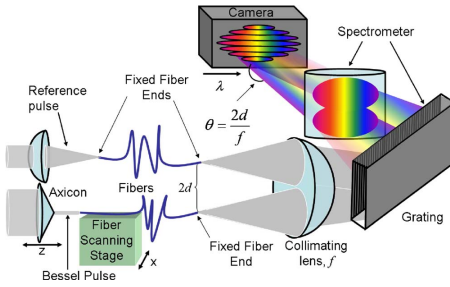


Fig. 1. (Color online) Experimental setup. A single-mode optical fiber samples a small region of a Bessel pulse, generated using an axicon. The reference pulse is coupled into an identical fiber. At the other end of the fibers, one lens is used to collimate both beams, and this also causes them to cross. A CCD camera is placed at their crossing point to record the resulting interference. Wavelength is mapped to the camera's horizontal dimension, so that a two-dimensional spectral interferogram is recorded, and $E(\lambda)$ is retrieved from this image [14]. To measure the spatiotemporal field, we scan the Bessel pulse's sampling fiber in x and the axicon in z , so that an interferogram at each fiber position is measured, and from this, the field $E(\lambda, x, z)$ is measured.

x) and the axicon longitudinally (versus z) to yield the spatiotemporal field, $E(x, z, t)$. Our Bessel-X pulses had cylindrical symmetry about the z axis, so we did not scan versus y , but we could if necessary. Our temporal resolution was 17 fs, enough to measure a pulse with 37 nm of bandwidth, and zero filling decreased the point spacing to 4.6 fs. Our spatial resolution is at most equal to the fiber's mode size, $\sim 5 \mu\text{m}$, but, because we resolve the complex field, rather than the intensity, we often measure features several micrometers smaller than this [14]. SEA TADPOLE measures the spectral phase difference between the unknown and the reference pulse. So, for these measurements we placed a flat glass window with a thickness equal to the center thickness of the axicon in the reference arm to cancel the group-delay dispersion (GDD) introduced at the center of the axicon. In principle there will still be a little radially varying

GDD left in the beam, but because the axicon angle is so large, considering our bandwidth, this will be negligible. Therefore, our measurements reflect the spatiotemporal intensity and phase introduced by the axicon geometry, and not the group-velocity dispersion (GVD) of its material, or the input pulse. Our experimental setup is shown in Fig. 1.

Three of our measurements are shown in Fig. 2. While our device measures the spatiotemporal intensity and phase, most of the interesting features are in the intensity, and the measured pulse is chirp-free owing to dispersion compensation, so here we only show the measured pulse amplitude (the square root of the intensity).

We also performed numerical simulations, shown on the right in Fig. 2 that are in good agreement with the measurements, except that the wings in the $z=5.5$ cm image are shorter in the measurement, and at $z=13.5$ cm the fringe patterns are slightly different. Both of these features are influenced by aberrations in the axicon that occur because they are difficult to machine perfectly and, for example, the tip of the cone is usually slightly round [15]. Although we have accounted for the shape of the tip in our simulations, these aberrations are difficult to model precisely, and so some discrepancies are present.

There are several interesting features in our measurements. The central maximum of the measured beam has a FWHM spot size of $17.2 \mu\text{m}$ at $z=5.5$ cm, $17.3 \mu\text{m}$ at $z=9.5$ cm, and $18.6 \mu\text{m}$ at $z=13.5$ cm, and the beam shape remains essentially unchanged over a propagation distance of 8 cm. At $z=13.5$ cm, the interference pattern is just beginning to change owing to the aberrations in the axicon. Note that, for a Gaussian beam of this size, the waist would have expanded by 26 times after propagating 8 cm. Also, the fringe periodicity is $27.8 \mu\text{m}$ in the first two images and $27 \mu\text{m}$ in the last image, which is in good agreement with the theoretical prediction of $27.8 \mu\text{m}$. Again, in our measurements this quantity changes with z by a small amount owing to the aberrations.

We also see the Bessel-X pulse's superluminal group velocity along the propagation axis, which does not violate Einstein's causality if distinguished from

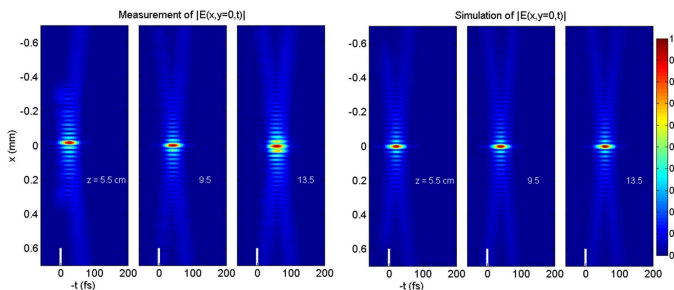


Fig. 2. (Color online) Left, the measured field amplitude at three different distances (z) after the axicon; right, the corresponding simulations. Intensity is indicated by the scale. We normalized each field to have a maximum of 1. The white bar is to emphasize the location of $t=0$.

the signal velocity [16]. SEA TADPOLE measures the Bessel-X pulse's arrival time with respect to the reference pulse, the latter of which is approximately Gaussian in both space and time and travels at the speed of light c . So, if the Bessel-X pulse were traveling at the speed of light, then for each value of z , its spatiotemporal intensity would be centered at the same time (here $t=0$ and emphasized with the white bar), but it is easy to see that this is not the case. Our simulations predict that for our axicon's angle the Bessel-X pulse's speed along the z axis should be $1.00013c$. Therefore, over a distance of 8 cm the Bessel-X pulse would lead our moving reference frame (the reference pulse) by 35 fs. In our results the center of the pulse is shifted in time by 32 fs between $z=5.5$ cm and $z=13.5$ cm, which is in good agreement with our theoretical prediction. To verify this result, we repeated the experiment five times and consistently measured time shifts close to our predictions for this axicon. We also realigned the experiment in between these trials to assure that this delay was not due to (or significantly affected by) misalignment of the axicon's scanning stage.

While both the phase and group velocity along the propagation axis of the Bessel-X pulse are superluminal, these velocities should not be confused with the propagation speed of the information or the signal velocity [10]. Because these pulses are solutions to the wave equation, they do not transmit information superluminally and do not violate Einstein's causality. Any attempt to make a signal "mark" in a Bessel-X pulse would result in reshaping of the spatial profile, and the mark would spread out luminally and not propagate superluminally. On the other hand, a different type of Bessel wavepacket, where the lateral wavenumbers of the constituent Bessel beams are all the same and are independent of their temporal frequencies, would not possess the X-like profile and can carry a signal without undergoing the reshaping. But such pulses propagate subluminally and spread out in time owing to their inherent free-space GVD.

In conclusion, using SEA TADPOLE, we made direct spatiotemporal recordings of the electric field of Bessel-X pulses, and we verified these results with simulations. We demonstrated both the propagation

invariance of the Bessel-X pulse and its superluminal group velocity along the z axis, which we found to be $1.00012c$ —within 0.001% error of the expected value.

R. Trebino and P. Bowlan acknowledge some support from National Science Foundation (NSF) Small Business Innovative Research grant 053-9595. P. Bowlan was also supported by NSF fellowship IGERT-0221600. The other authors were supported by the Estonian Science Foundation, grant 7870.

References

1. I. Alexeev, K. Y. Kim, and H. M. Milchberg, *Phys. Rev. Lett.* **88**, 073901 (2002).
2. C. Conti, P. Di Trapani, and S. Trillo, in *Self-Focusing: Past and Present* (Springer, 2009), pp. 439–456.
3. E. Gaizauskas, A. Dubietis, V. Kudriasov, V. Sirutkaitis, A. Couairon, D. Faccio, and P. Di Trapani, in *Self-Focusing: Past and Present* (Springer, 2009), pp. 457–479.
4. M. Bock, S. K. Das, and R. Grunwald, *Opt. Express* **17**, 7465 (2009).
5. D. McGloin and K. Dholakia, *Contemp. Phys.* **46**, 15 (2005).
6. C. T. A. Brown, D. J. Stevenson, X. Tsampoula, C. McDougall, A. A. Lagatsky, W. Sibbett, F. J. Gunn-Moore, and K. Dholakia, *J. Biophoton.* **1**, 183 (2008).
7. P. Saari and K. Reivelt, *Phys. Rev. E* **69**, 036612 (2004).
8. H. E. Hernández-Figueroa, M. Zamboni-Rached, and E. Recami, eds., *Localized Waves* (Wiley-Interscience, 2008).
9. H. Sönajalg, M. Rätsep, and P. Saari, *Opt. Lett.* **22**, 310 (1997).
10. P. Saari and K. Reivelt, *Phys. Rev. Lett.* **79**, 4135 (1997).
11. R. Grunwald, V. Kebbel, U. Griebner, U. Neumann, A. Kummrow, M. Rini, E. T. J. Nibbering, M. Piché, G. Rousseau, and M. Fortin, *Phys. Rev. A* **67**, 063820 (2003).
12. F. Bonaretti, D. Faccio, M. Clerici, J. Biegert, and P. Di Trapani, *Opt. Express* **17**, 9804 (2009).
13. P. Bowlan, P. Gabolde, and R. Trebino, *Opt. Express* **15**, 10219 (2007).
14. P. Bowlan, P. Gabolde, M. A. Coughlan, R. Trebino, and R. J. Levis, *J. Opt. Soc. Am. B* **25**, A81 (2008).
15. S. Akturk, B. Zhou, B. Pasquiou, M. Franco, and A. Mysyrowicz, *Opt. Commun.* **281**, 4240 (2008).
16. D. Mugnai and I. Mochi, in *Localized Waves*, H. E. Hernández-Figueroa, M. Zamboni-Rached, and E. Recami, eds. (Wiley Interscience, 2008), pp. 159–181.

H. Valtna-Lukner, P. Bowlan, M. Lõhmus, P. Piksarv, R. Trebino, and P. Saari
“Direct spatiotemporal measurements of accelerating ultrashort Bessel-type light bullets”
Opt. Express **17**, 14948–14955 (2009).

Direct spatiotemporal measurements of accelerating ultrashort Bessel-type light bullets

Heli Valtna-Lukner,^{1,*} Pamela Bowlan,² Madis Lõhmus,¹
Peeter Piksarv,¹ Rick Trebino,² and Peeter Saari^{1,*}

¹*Institute of Physics, University of Tartu, Riia 142, Tartu, 51014 Estonia*

²*Georgia Institute of Technology, School of Physics 837 State St NW, Atlanta, GA 30332 USA*

* *heli.lukner@ut.ee*

Abstract: We measure the spatiotemporal field of ultrashort pulses with complex spatiotemporal profiles using the linear-optical, interferometric pulse-measurement technique SEA TADPOLE. Accelerating and decelerating ultrashort, localized, nonspreading Bessel-X wavepackets were generated from a ~ 27 fs duration Ti:Sapphire oscillator pulse using a combination of an axicon and a convex or concave lens. The wavefields are measured with ~ 5 μm spatial and ~ 15 fs temporal resolutions. Our experimental results are in good agreement with theoretical calculations and numerical simulations.

©2009 Optical Society of America

OCIS codes: (320.0320) Ultrafast optics; (320.5540) Pulse shaping;

References and links

1. H. E. Hernández-Figueroa, M. Zamboni-Rached, and E. Recami, eds., *Localized Waves: Theory and Applications* (New Jersey: John Wiley & Sons Ltd, 2008).
2. P. Saari, and K. Reivelt, "Evidence of X-Shaped propagation-invariant localized light waves," *Phys. Rev. Lett.* **79**(21), 4135–4138 (1997).
3. H. Sõnajalg, M. Rätsep, and P. Saari, "Demonstration of the Bessel-X pulse propagating with strong lateral and longitudinal localization in a dispersive medium," *Opt. Lett.* **22**(5), 310–312 (1997).
4. K. Reivelt, and P. Saari, "Experimental demonstration of realizability of optical focus wave modes," *Phys. Rev. E Stat. Nonlin. Soft Matter Phys.* **66**(5), 056611 (2002).
5. I. Alexeev, K. Y. Kim, and H. M. Milchberg, "Measurement of the superluminal group velocity of an ultrashort Bessel beam pulse," *Phys. Rev. Lett.* **88**(7), 073901–073904 (2002).
6. R. Grunwald, V. Kebbel, U. Griebner, U. Neumann, A. Kummrow, M. Rini, E. T. J. Nibbering, M. Piché, G. Rousseau, and M. Fortin, "Generation and characterization of spatially and temporally localized few-cycle optical wave packets," *Phys. Rev. A* **67**(6), 063820–063825 (2003).
7. F. Bonaretti, D. Faccio, M. Clerici, J. Biegert, and P. Di Trapani, "Spatiotemporal amplitude and phase retrieval of Bessel-X pulses using a Hartmann-Shack sensor," *Opt. Express* **17**(12), 9804–9809 (2009).
8. P. Bowlan, H. Valtna-Lukner, M. Lõhmus, P. Piksarv, P. Saari, and R. Trebino, "Measuring the spatiotemporal field of ultrashort Bessel-X pulses," *Opt. Lett.* **34**(15), 2276–2278 (2009).
9. G. A. Siviloglou, J. Broky, A. Dogariu, and D. N. Christodoulides, "Observation of accelerating Airy beams," *Phys. Rev. Lett.* **99**(21), 213901–213904 (2007).
10. P. Saari, "Laterally accelerating airy pulses," *Opt. Express* **16**(14), 10303–10308 (2008).
11. P. Polynkin, M. Kolesik, J. V. Moloney, G. A. Siviloglou, and D. N. Christodoulides, "Curved plasma channel generation using ultraintense Airy beams," *Science* **324**(5924), 229–232 (2009).
12. Z. L. Horváth, and Z. Bor, "Diffraction of short pulses with boundary diffraction wave theory," *Phys. Rev. E Stat. Nonlin. Soft Matter Phys.* **63**(2), 026601–026611 (2001).
13. P. Bowlan, U. Fuchs, R. Trebino, and U. D. Zeitner, "Measuring the spatiotemporal electric field of tightly focused ultrashort pulses with sub-micron spatial resolution," *Opt. Express* **16**(18), 13663–13675 (2008).
14. P. Bowlan, M. Lohmus, P. Piksarv, H. Valtna-Lukner, P. Saari, and R. Trebino, "Measuring the spatio-temporal field of diffracting ultrashort pulses," *arXiv:0905.4381* (2009).
15. M. Clerici, D. Faccio, A. Lotti, E. Rubino, O. Jedrkiewicz, J. Biegert, and P. Di Trapani, "Finite-energy, accelerating Bessel pulses," *Opt. Express* **16**(24), 19807–19811 (2008).
16. P. Bowlan, P. Gabolde, A. Shreenath, K. McGresham, R. Trebino, and S. Akturk, "Crossed-beam spectral interferometry: a simple, high-spectral-resolution method for completely characterizing complex ultrashort pulses in real time," *Opt. Express* **14**(24), 11892–11900 (2006).
17. P. Bowlan, P. Gabolde, and R. Trebino, "Directly measuring the spatio-temporal electric field of focusing ultrashort pulses," *Opt. Express* **15**(16), 10219–10230 (2007).
18. S. Akturk, B. Zhou, B. Pasquiou, M. Franco, and A. Mysyrowicz, "Intensity distribution around the focal regions of real axicons," *Opt. Commun.* **281**(17), 4240–4244 (2008).

19. D. Abdollahpour, P. Panagiotopoulos, M. Turconi, O. Jedrkiewicz, D. Faccio, P. Di Trapani, A. Couairon, D. Papazoglou, and S. Tzortzakis, "Long spatio-temporally stationary filaments in air using short pulse UV laser Bessel beams," *Opt. Express* **17**(7), 5052–5057 (2009).
 20. J.-M. Manceau, A. Averchi, F. Bonaretti, D. Faccio, P. Di Trapani, A. Couairon, and S. Tzortzakis, "Terahertz pulse emission optimization from tailored femtosecond laser pulse filamentation in air," *Opt. Lett.* **34**(14), 2165–2167 (2009).
-

1. Introduction

Ultrashort, few-cycle optical pulses with special spatiotemporal properties have promising applications in many fields, including physical, quantum, and nonlinear optics; imaging; and particle and cell manipulation; to name a few. These applications often require pulses with a spatial and temporal profile that is much more sophisticated than a simple Gaussian beam in space or pulse in time.

One class of pulses with uncommon, but useful properties are the so-called localized waves [1]. These are ultrabroadband wave packets that are well localized both spatially and temporally and propagate over long distances in linear media without spreading in space or time. Localized waves are difficult to generate experimentally because a specific coupling between the frequency and wavenumber of their Bessel beam constituents is required, and over a broad spectrum. But still several successful experiments have been reported and evidence of the complex spatiotemporal profiles of some types of localized waves has been demonstrated [2–8]. Their distortion-free and superluminal propagation along the cylindrical-symmetry axis has also been observed.

More recently, a type of laterally accelerating localized wave called an Airy beam (or pulse, if generated using ultrashort pulses), has attracted attention [9–11]. Pulses can also accelerate due to diffraction, spherical aberration in lenses, and appropriately shaped nonlinear profiles of axicons [12–15].

In this paper, we report spatiotemporal measurements of accelerating and decelerating Bessel pulses. The term was proposed in [15] where generation and properties of such pulses have been theoretically investigated. These pulses are similar to the localized waves known as Bessel-X pulses [2,3,6–8], with the main difference being that they are generated by crossing and interfering focusing pulses that have curved pulse fronts and form part of a spindle torus surface, rather than the double conical surface that is present in Bessel-X pulses. As a result, their bullet-like, central, intense apex and accompanying Bessel rings become smaller or larger as the pulse propagates, depending on whether the torus shrinks towards a ring or expands towards a sphere. But the central spot of these pulses is still localized and intense over a propagation distance considerably longer than that of a Gaussian beam with a comparable waist size.

To make these measurements we used scanning SEA TADPOLE (Spatially Encoded Arrangement for Temporal Analysis by Dispersing a Pair of Light E-fields) [13,16], which is a linear-optical interferometric method for measuring the spatiotemporal field $E(x,y,z,t)$ of complicated ultrashort pulses. Briefly, this method involves sampling a small spatial region of the Bessel pulse with a single-mode optical fiber and then interfering this pulse with a reference pulse in a spectrometer to reconstruct $E(\lambda)$ for that spatial point. Then to measure the spatial dependence of the field, we scan the fiber axially (in x) throughout the cross section of the Bessel pulse, so that $E(\lambda)$ is measured at each x , yielding $E(\lambda,x)$. This field can be Fourier transformed to the time domain to yield $E(t,x)$. In order to measure the z (propagation direction) dependence of the spatiotemporal field, the axicon and lens are translated along the propagation direction to bring them nearer or further from the sampling point (the fiber). As demonstrated previously [8,13,14,16,17], SEA TADPOLE can measure optical pulses with complex spatiotemporal intensities and phases with sub-micron spatial and femtosecond temporal resolutions.

2. Theoretical description of accelerating Bessel pulses

The formation of accelerating Bessel pulses can be intuitively described using the Huygens-Fresnel principle. This involves treating each point on the wave-front as a source of

spherically expanding waves whose temporal profile is governed by that of the primary wave. Consider an ultrashort pulse impinging on a thin annular slit ($\sim 1 \mu\text{m}$ wide) at an instant $t = 0$. Thinking in terms of the Huygens-Fresnel principle, this will yield an expanding, semi-toroidal wave-field immediately behind the slit. As the pulse propagates further, the tube radius of the half torus becomes larger than the annular-slit radius R , and at times $t > R/c$ the wave-field evolves like a spindle torus, i.e., different parts of the torus start to overlap. Of course, the wave-field is treatable as a mathematical surface only for infinitesimally short delta-like pulses in time. Real ultrashort pulses are at least several cycles long, and so yield an interference pattern in the overlap region (see insets of Fig. 1). The radial dependence of the field in the interference region is approximately a zeroth-order Bessel function of the first kind.

As the wave-field evolves in time, the intersection region propagates along the z -axis and the angle between the normal of the torus surface and the z -axis (θ) decreases. For ultrashort pulses, this intersection region is small, and the angle θ is approximately the same for all points within it at a given instant. Therefore the field in the intersection region is approximately equivalent to the center of a Bessel beam or the apex of a Bessel-X pulse (see also [12]). The smaller the angle θ —also called the *axicon angle*—the larger the spacing between the Bessel rings and the smaller the superluminal velocity of the pulse. Hence, an annular ring transforms an ultrashort pulse into a decelerating Bessel wave-packet propagating along the z -axis. Of course, outside of the intersection region, where there is no interference to generate phase fronts that are perpendicular to the z -axis or a Bessel profile, the phase and pulse fronts expand with a constant velocity c and propagate in their normal directions.

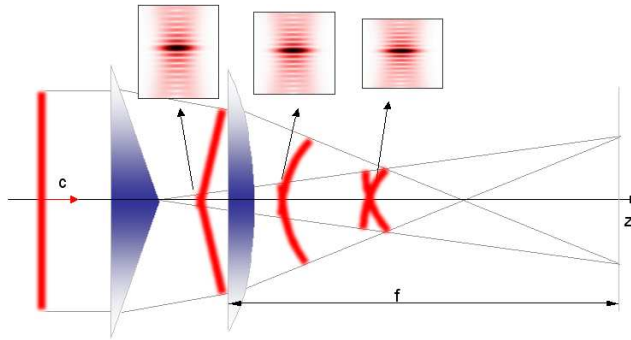


Fig. 1. Schematic of the formation of accelerating pulses from a plane-wave pulse moving to the right with velocity c . The red strips depict the pulses' intensity profiles in space at four different times. The conical surface of the axicon transforms the plane-wave pulse into a Bessel-X pulse, and the convex lens then yields the accelerating pulse. (In the actual experiments, the positions of the axicon and lens were interchanged, but this does not influence the results.) The inset plots show the expected intensity vs. x and t for three different positions z .

Since very little energy passes through an annular slit, it is more efficient to use an axicon in combination with a lens to generate such fields. If the lens is concave, the field behind it evolves similarly to what was described above, and a decelerating pulse is generated. On the other hand, a convex lens (see Fig. 1) results in an increasing angle θ as the pulse propagates and hence an accelerating pulse.

There are two approaches for calculations elaborating the above qualitative treatment. The first approach involves considering only the intersection region close to the optical axis. Here the field is approximately conical, or it is a cylindrically symmetrical superposition of plane waves propagating at a fixed angle θ to the z axis. In this case, the field can be described using the known expression for the field of a Bessel-X pulse, which is a broadband wave-packet of monochromatic Bessel beams [1–3,5–7,15]

$$\Psi(\rho, z, t) = \int_0^{\infty} d\omega G(\omega - \omega_0) J_0 \left[\frac{\omega}{c} \rho \sin \theta(z) \right] \exp \left\{ i \frac{\omega}{c} [z \cos \theta(z) - ct] \right\}, \quad (1)$$

where ρ , z , and t are the spatial (cylindrical) and temporal coordinates, and $G(\omega - \omega_0)$ is the (Gaussian-like) spectrum of the pulse having a central frequency ω_0 . However, unlike the case of the Bessel-X pulse, here the axicon angle depends on the propagation distance z from the lens with the focal length f as $\theta(z) = \arctan[|f - z|^{-1} \tan \theta_a]$, where θ_a is the axicon angle without the lens. Because the group velocity of the wave-packet along the z direction is given by $v_g = c/\cos(\theta)$ [1–3,5–7,15], the group velocity of the Bessel pulses will be superluminal and accelerate if f is positive and decelerate if f is negative. The approximations made in this approach are valid as long as the pulse duration τ is much shorter than its characteristic time of flight given by f/c . Considering our experimental parameters, which are given below, the phase fronts at the intersection (apex) region deviate from those of conical waves by less than 10^{-5} of the wavelength, which is negligible.

The second more general approach involves recognizing that a lens is a Fourier transformer and that the Fourier transform of the field just after the axicon is a good approximation to a thin ring. Therefore the temporally reversed field of the accelerating Bessel pulse can be calculated by integrating over monochromatic spherical wave pulses as if they were emerging from a thin annular slit:

$$\Psi_{sph}(\rho, z, t) \propto \int_0^{\infty} d\omega \int_0^{2\pi} d\varphi r_a \omega G(\omega - \omega_0) \frac{\exp \left\{ i \frac{\omega}{c} \left[\sqrt{\rho^2 + r_a^2 - 2r_a \rho \cos \varphi + z^2} - ct \right] \right\}}{\sqrt{\rho^2 + r_a^2 - 2r_a \rho \cos \varphi + z^2}}. \quad (2)$$

Here $r_a = |f| \tan(\theta_a)$ is the radius of the ring along which the integration is carried out by the polar coordinate φ of the source points and the origin of the z axis is in the plane of the ring. One advantage to this approach is that we can take into account aberrations in the lens and axicon. For example, chromatic aberrations can be modeled using a frequency-dependent ring radius $r_a(\omega)$. Also, this expression can be used for numerical calculations of the field under the conditions in which the previous approach is not valid, i.e., also outside of the apex region.

3. Experimental results

In our experiments, ultrashort, accelerating Bessel pulses were generated using a KM Labs Ti:Sa oscillator with 33 nm of bandwidth (FWHM) and an approximately Gaussian spectrum with a central wavelength $\lambda_0 = 805$ nm. The spot size of the laser beam was 4 mm (FWHM). A fused-silica axicon with an apex angle of 176° was used, which transforms plane wave pulses at $\lambda_0 = 805$ nm into conical wave pulses (Bessel-X pulses) with $\theta_a = 0.92^\circ$. We used lenses with focal lengths of +153 mm and -152 mm. For convenience in the actual set-up, the axicon was mounted behind the lens in a lens tube, i.e., in reverse order of Fig. 1. So the two components effectively constituted a single thin phase element, whose transmission function does not depend on the ordering of components. However, the small distance between them (a few mm) was taken into account in our simulations.

The spatiotemporal field after the compound optic was measured using SEA TADPOLE, using a reference pulse directly from our oscillator. At each position of the sampling fiber in SEA TADPOLE, we measured the spectral phase difference between the reference pulse and the Bessel pulse and its spectrum, so that our measurements reflect the phase added to the beam by the lens and axicon. Such differential measurements also allowed us to add glass to the reference arm of SEA TADPOLE, so that chirp introduced by the axicon and lens would essentially cancel out in the measurement.

Our device had a spatial resolution of about 5 μm , determined by the mode size of the fiber that we use to sample the Bessel pulse. Our temporal resolution was ~ 17 fs and with zero-filling we reduced the point spacing on the time axis to 4.5 fs. Because the temporal resolution of SEA TADPOLE is given by the inverse of the spectral range of the unknown

pulse, and the smallest possible temporal feature in the pulse is given by the inverse of its bandwidth (which is several times less than the spectral range), our device should always have sufficient temporal resolution to measure the unknown pulse, regardless of its duration (even for single cycle pulses). Because the Bessel pulses were approximately cylindrically symmetrical, we only measured the field along one transverse coordinate, x . For more details about the SEA TADPOLE device that we used, see reference [13].

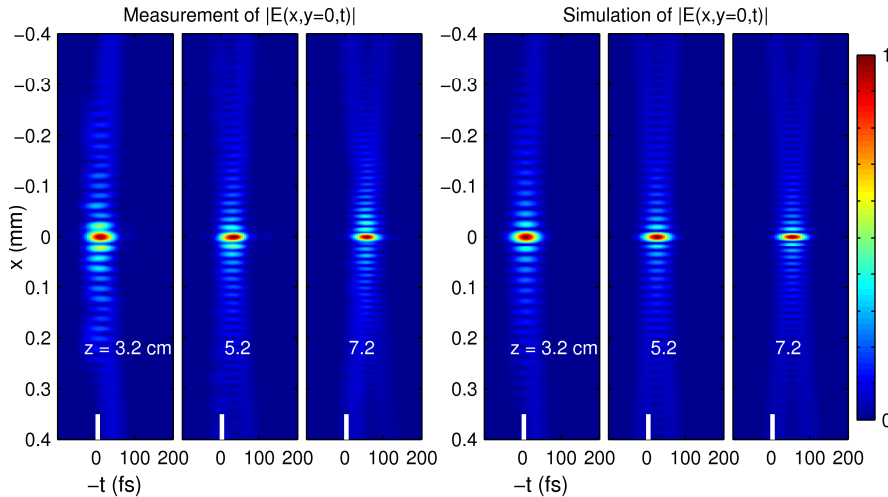


Fig. 2. Comparison of the measured and calculated spatiotemporal profiles of the electric field amplitude of an *accelerating* Bessel pulse at three positions along the propagation axis (z). The color bar indicates the amplitude scale normalized separately for each plot. The white bar emphasizes $t = 0$, which is where the pulse would be located if it were propagating at c .

The spatiotemporal profiles of the accelerating Bessel pulses were measured at five different z positions and for the decelerating Bessel pulse at nine positions. In all cases, we measured the complete spatiotemporal intensity and phase, but we show only the spatiotemporal intensities here, as this information is more interesting. Three of these measurements for each are shown in Fig. 2 and Fig. 4. For comparison, numerical simulations were performed using Eq. (1) with the experimental parameters, and as seen in the figures, the two are in very good agreement.

SEA TADPOLE also measures the Bessel-X pulse's arrival time with respect to the reference pulse, the latter of which, after passing through the compensating piece of glass, travels at the speed of light c . The origin of our time axis can be considered as the location of the reference pulse if it propagated along the axis z with the Bessel pulses. So, if the Bessel pulse were traveling at the speed of light, then, for each value of z , its spatiotemporal intensity would be centered at the same time origin $t = 0$ which is emphasized with the white bar in the figures. But it is easy to see in Figs. 2 and 3 that this is not the case. The superluminal group velocity and the pulse's acceleration or deceleration are both apparent from the z -dependent shifts of the pulses relative the origin $t = 0$. The time shifts were compared to theoretically calculated shift function and we found a good agreement, see Fig. 4.

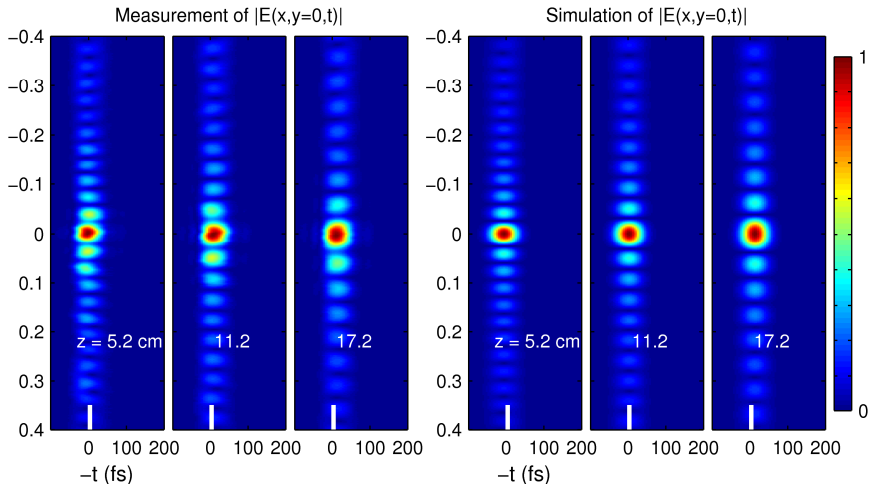


Fig. 3. Comparison of measured and calculated spatiotemporal profiles of the electric field amplitude of *decelerating* Bessel pulse at three positions along the propagation axis z .

The group velocity of Bessel pulses can also—indirectly but in the given case more precisely—be determined from the measured fringes in their spatial profile. This is because these fringes correspond to rings of intensity maxima, radii of which grow sequentially as governed by placement of maxima and minima of the Bessel function J_0 . Thanks to the many measurable fringes we could accurately determine the mean radial wavelength $\Lambda_B = \lambda_0 / \sin\theta$ of the Bessel profile.

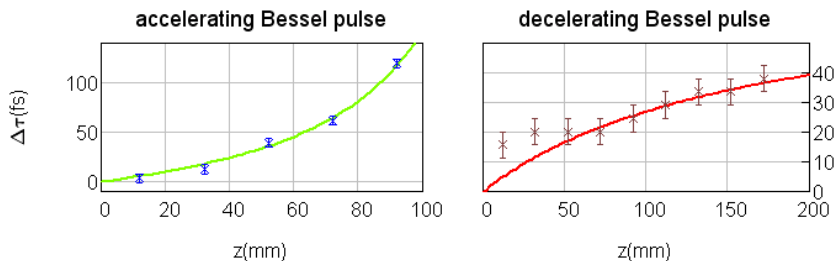


Fig. 4. Experimentally determined (points) and theoretically predicted (solid curves) temporal shifts (in femtoseconds) of the accelerating/decelerating Bessel pulses in respect of the reference pulse. z is the propagation distance.

Hence, having in mind the approximations that apply to Eq. (1) and the relation $v_g = c/\cos\theta$, the distance-dependent group velocity can be found using the following equation:

$$v_g(z) = c / \sqrt{1 - [\lambda_0 / \Lambda_B(z)]^2}. \quad (3)$$

Equation (3) was used to estimate the group velocity of the measured pulses at various propagation distances, and these results are shown in Fig. 5 along with the theoretical values. The experimental values are in good agreement with our theoretical predictions, except for two points at $z = 32$ mm and 52 mm for the decelerating pulses. This discrepancy is likely due to the imperfect surface of the axicon as discussed below.

Without a lens, the propagation depth over which the Bessel-X pulses last, starts, in principle, at the tip of axicon and ends at $z \approx w/\tan\theta_a$, where w is the radius of the input beam or aperture. Imperfections in our axicon reduce the distance over which the Bessel-X pulse maintains its perfect ring profile (let us call it the Bessel zone). At values of z less than 50

mm, the profile distortions were caused by the slightly spherical tip of the axicon (see, e. g., [18]). This axicon aberration also makes the pulse accelerate even without a lens, though this effect is small and did not significantly influence our measurements. Slight deviations of the surface of the axicon from an ideal cone are responsible for a reduction of the upper limit of the zone, which for our axicon stopped at $z \approx 130$ mm [8]. Therefore the Bessel zone only lasted half as long as it would be expected to in the absence of aberrations ($z_{\max} \approx w/\tan\theta_a$). At values of $z > 130$ mm, these deviations distort the phase-fronts of the interfering plane wave constituents of the conical wave to an extent that affects the shape of the central spot of the Bessel profile, but it does not noticeably affect the pulse's group velocity as established in [8] from direct temporal data.

Placing lenses before the axicon compresses or stretches the Bessel zone (see, e. g., [19,20]). Without the lens the Bessel zone for the axicon that we used lasts for 80 mm (= 130 mm – 50 mm). When the positive lens is added, this decreases to about 50 mm, going from $z \approx 30$ mm to 80 mm. With the negative lens (decelerating Bessel pulses) the Bessel zone is greatly lengthened, and in principle to tens of kilometers starting at $z \approx 70$ mm. Therefore the two points at $z = 32$ mm and 52 mm in Fig. 5 deviate (as clearly seen in the right plot with expanded ordinate scale) from the theoretical curve because they are outside of the Bessel zone. Although we could not measure the decelerating pulse kilometers from the axicon, the Bessel ring pattern was observable by eye on the lab wall ~ 10 m after the axicon, and, at this point, the radial wavelength Λ_B had increased to about 1 mm.

The full width of the central maximum of the accelerating Bessel pulse at $1/e$ of the maximum decreased by a factor of 1.6, from 23.0 μm to 14.8 μm , after 40 mm of propagation from $z = 32$ mm to 72 mm inside the Bessel zone. For the decelerating pulse, the spot size instead increased by a factor of 1.4, from 39.1 μm to 56.0 μm after 10 cm of propagation from $z = 72$ mm to 172 mm. This represents a much larger Rayleigh range than that of a Gaussian beam, which would only be 0.2 mm if the waist diameter were 14.8 μm or 1.5 mm if it were 39.1 μm .

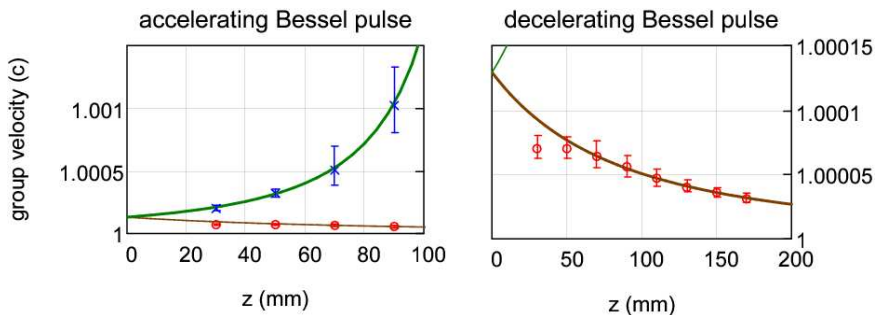


Fig. 5. Comparison of experimentally and theoretically calculated group velocities for accelerating and decelerating Bessel pulses. The measured group velocities for the accelerating Bessel pulses are marked with blue crosses, and, for decelerating pulses, with red circles. The error bars show the standard deviations from the mean value. The solid lines show the theoretically predicted dependences. At the position $z = 0$, the theoretical curves for both pulses coincide because the same axicon was used to generate them.

It should be stressed that the indirect evaluation of the group velocities from the interference patterns is slightly more precise than using the time shift data thanks to relatively high quality of our axicon (except the tip) and relatively narrow spectrum of the input pulse. In the case of shorter pulses—in certain sense “genuine” Bessel-X pulses contain only a few cycles—the number of fringes (Bessel rings) is correspondingly small and their spacing should be measurable with lower accuracy than the time shifts in the plots with femtosecond-range temporal resolution. Similarly, if there are substantial phase distortions present in the optical elements the fringe patterns acquire irregularities; hence again the direct approach based on the time shifts is preferable not only principally but also practically.

5. Conclusions

We directly measured the spatiotemporal field $E(x,t,z)$ of ultrashort accelerating and decelerating Bessel pulses with micron spatial resolution and femtosecond temporal resolution using SEA TADPOLE. The field after a lens and axicon was described and modeled theoretically, and we used this model to analyze our experimental results. The features in the measured spatiotemporal profiles, including the ring spacings and the central spot sizes, were found to be in good agreement with our theoretical calculations and numerical simulations. We also measured the group velocities of the pulses along the propagation direction and observed their acceleration and deceleration. The accelerating Bessel pulse's speed went from $1.0002 c$ after 3.2 cm of propagation to $1.0009 c$ at 7.2 cm and the decelerating Bessel pulse had a speed of $1.00007 c$ after 5.2 cm and $1.00003 c$ after 17.2 cm of propagation. The measured group velocities were also in good agreement with our theoretical calculations.

Acknowledgements

R. Trebino acknowledges support of the Georgia Research Alliance, and P. Bowlan was supported by an NSF fellowship IGERT-0221600 and NSF SBIR grant #053-9595. The Estonian authors were supported by the Estonian Science Foundation, grant #7870.

P. Saari, P. Bowlan, H. Valtna-Lukner, M. Lõhmus, P. Piksarv, R. Trebino
“Directly recording diffraction phenomena in time domain”
Laser Physics, **20**, 948–953 (2010).

Directly Recording Diffraction Phenomena in Time Domain¹

P. Saari^a, P. Bowlan^b, H. Valtna-Lukner^a, M. Lõhmus^a, P. Piksarv^a, and R. Trebino^b

^a University of Tartu, Institute of Physics, 142 Riia St, Tartu, 51014 Estonia

^b Georgia Institute of Technology, School of Physics, 837 State St NW, Atlanta, GA 30332 USA

*e-mail: peeter.saari@ut.ee

Received October 9, 2009; in final form, November 1, 2009; published online April 2, 2010

Abstract—By making use of a new technique for measuring the complete spatiotemporal electric field of light with micrometer spatial and femtosecond temporal resolution, we directly demonstrate the formation of the so-called boundary diffraction wave and Arago’s spot, as well as the superluminal propagation of a “diffraction-free” pulse. We believe that such spatiotemporally resolved measurements and the time-domain treatment of diffracting waves not only turn out to be useful for modern physical optics, especially in micro- and meso-optics, but also significantly aid in the understanding of diffraction phenomena in general.

DOI: 10.1134/S1054660X10090021

1. INTRODUCTION

The bending of light waves in the shadow region behind an opaque disk and the appearance of a bright “Spot of Arago” in the shadow’s centre are manifestations of diffraction and have been known for centuries. While the theory of diffraction, especially for monochromatic waves, is rather well developed, the subject has recently encountered some intriguing issues and new directions. The discovery of superluminally propagating “diffraction-free” wave-packets; the renaissance of an almost forgotten alternative interpretation of diffraction by the notion of the “boundary wave;” and the recent possibility of ultrashort-pulsed illumination all require some revisiting of the classical subject of optics.

Since the first observation of the diffraction of light in the middle of the 17th century by R.M. Grimaldi, tremendous progress was made in the mathematical treatment of the phenomenon, resulting in the well developed theory with Fresnel–Kirchhoff and Rayleigh–Sommerfeld versions (see, e.g., monographs [1, 2] and references therein). However, the approximations made in these theories, especially the neglect of the perturbations of light waves near the boundaries of openings and the treatment of obstacles as infinitely thin and made from totally absorbing or infinitely conducting idealized materials, remain under discussion. In particular, such approximations fail in near-field and subwavelength-geometry conditions, where material surface excitations play a decisive role (see, e.g., review [3]).

In the beginning of the 18th century, Thomas Young proposed, somewhat intuitively, that the diffraction pattern arises from the interference between the incident light propagating rectilinearly in accordance with the laws of geometrical optics and an omni-directionally propagating secondary wave origi-

nated from the edge of the diffracting body. On the other hand, Fresnel’s theory—relying on Huygens’ quite counter-intuitive assumption that each point of the incident wave front is a fictitious source of the secondary wave—proved more successful and consigned to oblivion Young’s idea. It was rediscovered in 1888 by Maggi [4] and only in the middle of the last century was Young’s idea developed into the theory of the boundary diffraction wave (BDW) by Rubinowicz [5], Miyamoto and Wolf (references given in [2]). This theory helped to resolve several issues of the standard Fresnel–Kirchhoff theory, to which it is mathematically equivalent, at least in the case of plane or spherical incident waves. In addition, calculation of diffracted fields according to the BDW theory is much less cumbersome than in the standard theory because only a simple contour integration along the opening boundary need be performed instead of a two-dimensional integration over the whole area of the opening, where Huygens’ fictitious sources are located. Results of Sommerfeld’s seminal rigorous calculation of diffraction of the electromagnetic field by a straight-edge—one of the few exactly solved diffraction problems—can easily be interpreted in terms of BDW. Yet, the BDW theory has remained outside the mainstream treatment of diffraction.

Nevertheless, diffraction from openings in opaque screens is well described and understood by the notion of the BDW theory. Especially intuitive should be the formation of a diffracted field in the case of illumination by ultrashort laser pulses, available in recent decades (see Fig. 1). Contrary to the traditional treatment using monochromatic fields, in which the transmitted waves fill large depths of space behind the screen and overlap with each other there, ultrashort pulses—typically femtoseconds long—are spatially only few micrometers “thick” and therefore behave almost like a solitary wave-front surface. Hence, the time-domain study of diffraction in terms of pulsed

¹ The article is published in the original.

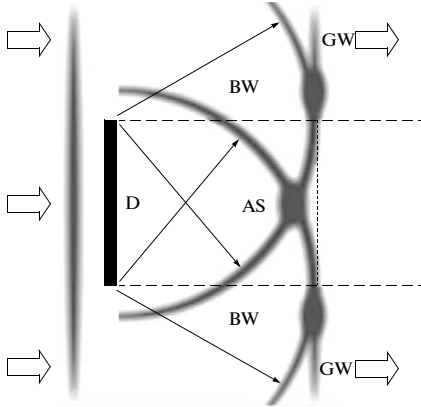


Fig. 1. Schematic of the formation of the Arago spot in the case of illumination with ultrashort pulses. A pancake-shaped pulsed wave hits a disk-shaped obstacle (D) from the left. On passage of the wave, the obstacle cuts off its central part according to the shadow boundaries (horizontal dashed lines) forming the geometrical wave (GW) component of the output field. Each point on the edge of the obstacle emits a secondary spherical pulsed wave as indicated by arrows, together forming the boundary diffraction wave (BW), which expands from a ring torus shape through a spindle-torus-like stage (cross-section depicted in the figure) into a spherical wave at infinity. On the axis, overlapping and interfering boundary waves form the Arago spot. Around the shadow boundary in the overlap regions (also indicated by red ovals) of the BW and GW the common interference rings appear. The Arago spot (AS) propagates behind the front (indicated by vertical dashed line) of the transmitted GW but catches up with the latter at infinity because its velocity is superluminal.

BDWs is not only didactically preferable but also opens new interesting directions and applications, such as in the study of focusing and other transformations of ultrashort pulses (see, e.g., paper [6] and references therein). The formation of an ultrashort boundary wave pulse on a circular aperture has been theoretically studied [7] and evidence for its existence experimentally identified by measuring modulations in the spectrum of the on-axis field and in CCD-recordings of the time-integrated radial intensity distribution of the field [8]. Our aim has been to directly record, with simultaneous spatial and temporal resolution, the evolution and interference of the boundary waves behind various screens.

In 1987 “diffraction-free” light beams [9] were introduced and now constitute a mature field with numerous applications (see review [10]). These beams—also known as Bessel beams—possess a controversial quality: they preserve their tightly focused central bright spot over large distances of propagation as if the beam does not obey the laws of diffraction.

At the same time, quite independently, the topic of undistorted or localized waves emerged in mathematical physics and deals with ultrabroadband pulses that are not only “diffraction-free” in space but also propagate without any spread in time [11–13]: “light bullets” and “electromagnetic missiles.” To date, various localized waves propagating in vacuum superluminally, luminally (i.e., with velocity $c = 299792.458$ km/s), or subluminally have been studied in detail, and promising applications have been proposed (see, e.g., reviews [14–17] and the first monograph [18] on the field). The feasibility of such light bullets moving faster than c has been experimentally demonstrated more than once [19–24], but, from time to time, papers still appear in which the superluminal group velocity of such wave-packets in vacuum is questioned. Therefore, our second aim has been to accomplish, for the first time, with appropriately high resolution and accuracy, a direct spatiotemporal measurement of the electric field and propagation velocity of the simplest superluminal localized wave—the so-called Bessel-X pulse [19], which comprises an energy lump of micrometer diameter at the joint apex of a sparse double-conical wave.

2. SPATIOTEMPORAL MEASUREMENT OF LIGHT FIELDS

Our measurements not only required high spatiotemporal resolution, but also high sensitivity. First of all, we routinely measure the relatively high-intensity spatially uniform reference pulse, which is the pulse directly out of our laser, using a technique called FROG (Frequency Resolved Optical Gating [25])—which utilizes nonlinear optics and a sophisticated inverse algorithm to retrieve the pulse’s field in time. To obtain ultrahigh temporal resolution in conjunction with the required sensitivity, we used a technique called SEA TADPOLE (Spatially Encoded Arrangement for Temporal Analysis by Dispersing a Pair of Light E-fields [26]), which is based on spectral interferometry. It involves measurement of the spectrum of the sum of the known reference pulse and the unknown pulse to yield the unknown pulse’s temporal field, much like monochromatic-beam spatial interferometry or holography, where measurement of the spatial intensity of the sum of a known spatial field and an unknown monochromatic wave yields the unknown wave field in space. A detailed description of SEA TADPOLE can be found in [27–29]. Finally, we achieved high spatial resolution by simply scanning the micrometer-sized tip of the SEA TADPOLE input fibre point-by-point through the space where the unknown light field propagated.

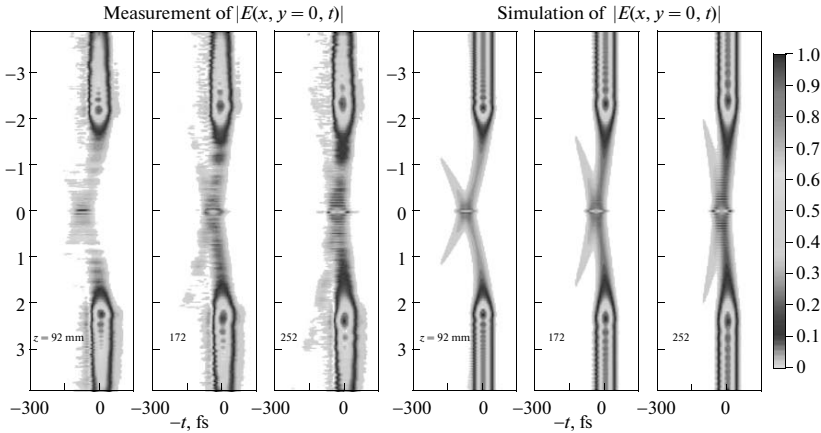


Fig. 2. Formation and evolution of the Arago spot behind an opaque disk of 4 mm in diameter. The magnitude of the electric field E is shown at three different propagation distances z in pseudo-color code according to the color bar (white has been taken for the zero of the scale in order to better reveal areas of weak field). In the measured plots the amplitude of the GW decreases with the transversal coordinate as the input pulses had a Gaussian radial profile, and in the simulations flat plane wave pulses were assumed according to our aim—to demonstrate how the simplest formula of the BDW theory describes properly the diffracted wave.

3. SPATIOTEMPORALLY RECORDED DIFFRACTION

Here we show two of our results on diffraction of pulses through screens. The plots in Figs. 2, 3, 5 can be viewed as still images or “snapshots in flight,” since they are spatiotemporal slices of the magnitude of the electric field $|E(x, y, z, t)|$ behind the screen. While we measured the complete pulse electric fields (amplitude and phase), we show only plots of the pulse amplitude because the phase of these pulses is less interesting. We show pulses measured at different propagation distances z . For comparison, theoretical simulations are presented on the right-hand side, which are carried out using the one-dimensional integral formula [7] of the boundary diffraction wave theory (the two-dimensional formula of the common diffraction theory gave the same results as expected).

First, according to the schematic in Fig. 1, we propagated ultrashort pulses past an opaque disk of 4 mm diameter, making a hole in the beam, and we measured the resulting spatiotemporal field at different distances from the aperture to observe its evolution. These measurements reveal the spatiotemporal structure of the weak boundary waves and the brighter spot at the centre of the beam due to their constructive interference, i.e., the spot of Arago, as it is known in conventional diffraction theory. Interestingly, the plots in Fig. 2 reveal that this spot is surrounded by coaxial interference rings and, in the axial region the field, generally resembles the Bessel-X pulse (considered in the next Section). Moreover, as shown in Fig. 2, the

spot is indeed delayed in time with respect to the main pulse front, and this delay decreases with z , indicating a superluminal propagation speed along the z axis (the main pulse front propagates at c), which has been observed indirectly in a previous study [8] (where a spherical initial wave was used). This occurs, because, as z (or the distance from the disk) increases, the extra distance that the boundary waves must propagate (compared to the main pulse front) to reach the z axis ($x = 0$) decreases, so the relative delay of the boundary waves and the bright spot due to their interference decreases. In fact, the group velocity of the Arago spot—geometrically located at one pole of a luminally expanding spindle torus—varies from infinity at $z = 0$ to c for very large values of z . Thus it is an example of a decelerating light pulse.

Next, using the same initial field parameters, we propagated the beam through a 4.4 mm diameter steel circular aperture and measured the resulting diffraction. Again our measurements (Fig. 3) are in good agreement with the simulations, but with a minor discrepancy in the brightness of the main pulse front, which is likely due to the thickness (3.1 mm) and imperfect surface quality of our aperture. These measurements show a boundary-wave pulse behind the main pulse-front in time that eventually catches up with it. The boundary-wave pulse in these measurements looks very similar to that shown in Fig. 2. (The boundary waves in these two measurements look a little different because all of the images are normalized to have maximum of 1, and the main pulse front is much brighter in Fig. 3.) In fact, according to the

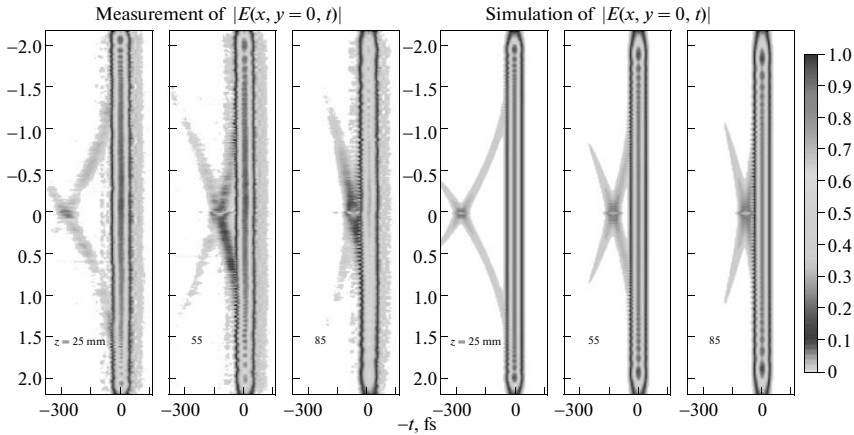


Fig. 3. Formation and evolution of the diffracted field behind a circular hole 4 mm in diameter. The boundary waves interfere with each other and with the directly transmitted pulse, but the interference maximum on the axis (actually a temporally resolved spot of Arago) lags behind the direct pulse, and eventually catches up with it.

boundary wave theory of diffraction, because the aperture and disk have similar diameters, their boundary waves are almost the same (but of opposite sign of the wave-function in accordance with the Babinet principle). So, interestingly, the Arago spot occurs due to any circular boundary and not just a circular disk. Moreover, due to the temporal localization of the pulsed illumination and the temporal resolution of our measurements, we can directly visualize the small delayed spot, which with longer pulses or continuous

radiation would have overlapped with the intense, undiffracted beam.

4. RESULTS ON “DIFFRACTION-FREE” BESSEL-X PULSE

The most effective Bessel beam generator—a conical lens (axicon)—refracts plane waves towards the axis and thus shapes a femtosecond pulse into the Bessel-X pulse with its characteristic double-conical profile, as shown in Fig. 4. If the aperture radius R of the axicon were infinitely large, the pulse would propagate rigidly and without any spread of its micrometer-size central bright spot at the joint apex of the cones over an infinitely large distance. In the case of a limited aperture, it follows from the geometry in Fig. 4 that the depth of the invariant propagation of the pulse (let us call it the Bessel zone) is restricted to $z_B = R/\tan\theta$, where θ (the so-called Axicon angle) is the angle of inclination of rays toward the axis z .

Some such measured “snapshots” are shown in Fig. 5, together with theoretical simulations (this time calculated as axisymmetric superposition of plane waves with Gaussian aperture). The two are in good agreement except that the wings in the $z = 5.5$ cm image are shorter in the measurement. This is because axicons are difficult to machine perfectly; in particular, the tip of the cones is always distorted and generally the Bessel zone is shorter than what would be achieved in the ideal case.

There are several interesting features in these plots. The central maximum of the pulse has a width of ~ 20 μm , which—as well as the coaxial intensity rings

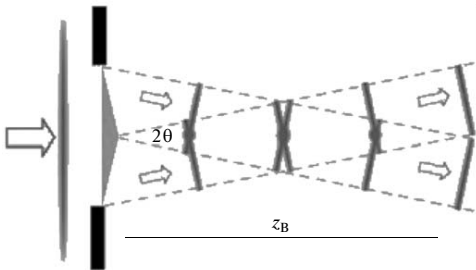


Fig. 4. Schematic of the formation of the Bessel-X pulse as a conical wave in the case of illumination of a conical lens (axicon) with ultrashort pulses. z_B indicates the range along the propagation axis, where the pulse can be considered as “diffraction-free.” Ovals indicate the apex regions where interference and formation of the Bessel ring pattern take place.

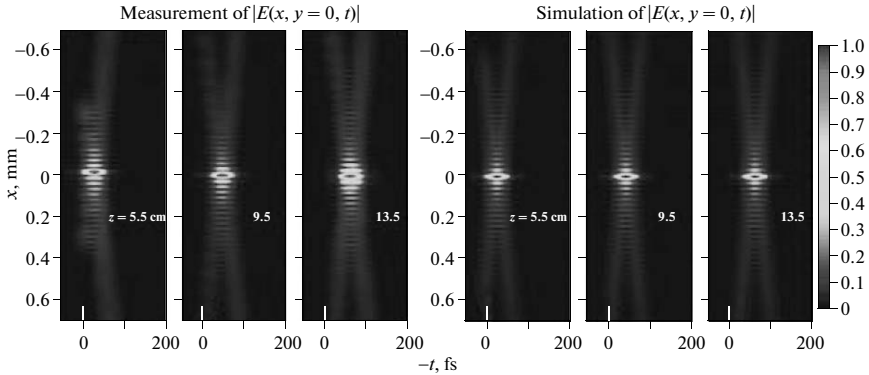


Fig. 5. Propagation of the Bessel-X pulse at three different distances after the axicon. The field magnitude in each plot has been normalized to have a maximum of 1. The white bar is to emphasize the location of a $t = 0$ of the luminally co-propagating reference.

surrounding it—remains essentially unchanged in shape from $z = 5$ cm through $z = 13.5$ cm. Thus the apex flies rigidly as a light bullet together with its sparse wings at constant speed. This is because the Bessel-X pulse is a propagation-invariant conical wave in distinction to the expanding toroidal wave forming the Arago spot, which possesses approximately the Bessel profile (with expanding rings) near the axis only.

Also, the Bessel X-pulse’s superluminal speed is apparent in these plots. SEA TADPOLE measures the pulse’s arrival time with respect to the reference pulse, which travels at the speed of light (c). Therefore, if the Bessel X-pulse were traveling at the speed of light, then at each z its spatiotemporal intensity would be centered at the same time (here $t = 0$ and emphasized with the white line), but it is easy to see that this is not the case. From our axicon’s angle θ (and from the simulations), we find that the Bessel-X pulse’s speed (axial group velocity) should be $1.00013c$. From our experimental plots we determined [29] it to be around $1.00012c$ —within 0.001% error of the expected value.

5. DISCUSSION

The superluminality of the Bessel-X pulse and that of the Arago spot pulse are intriguing. Indeed, while phase velocities greater than c are well known in various fields of physics, a superluminal group velocity more often than not is considered as a taboo, because, at first glance, it seems to be at variance with relativistic causality. However, thanks to the numerous studies throughout the previous century—starting from Sommerfeld’s works on propagation of plane wave pulses in dispersive media—it is well known (see, e.g., a thorough review [30]) that the group velocity need not be a physically profound quantity and by no means should be confused with the signal propagation velocity. But

in the case of Bessel-X-type pulsed waves no dispersive medium need to be involved and still, not only is the group velocity superluminal, but the pulse as a whole rigidly propagates faster than a plane wave.

Naturally, one feels some unease in accepting this startling circumstance. But here we experimentally observe it in the most direct way. When forced to concede the theoretically and experimentally verified superluminality, one might feel the need to make recourse to statements insisting that the pulse is not a “real” one, but instead simply an interference pattern rebuilt at every point of its propagation axis from truly real plane wave constituents travelling at a slight tilt with respect to the axis. Such argumentation is not wrong but, alas, it leads nowhere. Of course, there is a similarity between the superluminality of the X-wave and a simple geometrical faster-than-light movement of the cutting point in scissors (we refer here to Gedanken experiments described in textbooks on relativity). But in the central highest-energy part of the Bessel-X wave, there is nothing moving at the tilt angle. The phase planes are perpendicular to the axis and move rigidly with the whole pulse along the axis. The Poynting vector, indicating the direction of energy flow, lies also along the axis. However, the energy flux is not superluminal. Hence, to consider the Bessel-X waves as something inferior to “real” waves is not sound. If we thought so, by similar logic we would arrive at the conclusion that femtosecond pulses emitted by a mode-locked laser are not real but “simply an interference” between the continuous-wave laser modes. In other words, one should not ignore the essence of the superposition principle of linear fields, which implies a reversible relation between “resultant” and “constituent” fields and does not make any of the possible orthogonal bases—plane waves and

cylindrical (Bessel) waves, for the given example— inferior to others.

Another misunderstanding (the author of the review [30] seems to agree) stems from oversight of the fact that there are infinitely many ways to form a pulsed wave-packet from single-frequency Bessel beams. They depend on how the radial density of intensity rings in the beam cross section is related—or whether or not it is related at all—to the beam’s temporal frequency. In the case of the Bessel-X pulse, this is a proportionality relation, and therefore the group velocity is perfectly defined with a single superluminal value within the whole bandwidth of the wave-packet. If, on the contrary, the radial density is frequency-independent, we obtain a completely different wave-packet, which does not belong to localized waves since it has no definite group velocity over its whole spectrum and therefore spreads in the course of propagation. But such a wave-packet—named the “pulsed Bessel beam” in the literature—propagates with velocity less than c and can be used for sending signals along the propagation axis. On the other hand, if one tried to cut a signal “notch” into the core of the Bessel-X pulse, the notch would behave like the “pulsed Bessel beam”—spreading out while advancing subluminally. This is natural, since Maxwell’s equations or the wave equation for EM fields does not allow superluminal signalling.

6. CONCLUSIONS

By direct spatiotemporally resolved measurements of pulsed light fields behind the simplest diffracting screens we have shown for the first time experimentally how the transmitted wave-field is gradually formed as a superposition of the directly transmitted pulse and an expanding boundary wave according to the almost forgotten boundary diffraction wave theory. In particular, we observed the formation and superluminal, but decelerating, movement of a small peculiarity caused by interfering boundary waves, which is responsible for the appearance of the Arago spot in a common steady-state diffraction pattern. With appropriate and higher-than-in-previous-studies resolutions and accuracy we recorded directly the bullet-like propagation of a “diffraction-free” Bessel-X pulse and measured its superluminal speed. In summary, we believe that time-resolved measurements and time-domain treatment of diffracting waves not only turn out to be fruitful in modern physical optics, especially in micro- and meso-optics, but also promote the understanding of diffraction phenomena.

ACKNOWLEDGMENTS

R.T. was supported by NSF SBIR grant no. 053-9595, and P.B. by NSF fellowship IGERT-0221600. The other authors were supported by the Estonian Science Foundation, grant no. 7870.

REFERENCES

1. J. W. Goodman, *Introduction to Fourier Optics*, 3rd ed. (Roberts & Co, Englewood, 2005).
2. M. Born and E. Wolf, *Principles of Optics*, 6th ed (Pergamon, Oxford, 1987).
3. C. Genet and T. W. Ebbesen, *Nature* **445**, 39 (2007).
4. G. A. Maggi, *Ann. di Mat. Ila* **16**, 21 (1888).
5. A. Rubinowicz, *Nature* **180**, 160 (1957).
6. P. Bowlan, U. Fuchs, R. Trebino, and U. D. Zeitner, *Opt. Express* **16**, 13663 (2008).
7. Z. L. Horváth and Z. Bor, *Phys. Rev. E* **63**, 026601 (2001).
8. Z. L. Horváth, J. Klebniczki, G. Kurdi, and A. Kovács, *Opt. Commun.* **239**, 243 (2004).
9. J. Durnin, J. J. Miceli, Jr., and J. H. Eberly, *Phys. Rev. Lett.* **58**, 1499 (1987).
10. D. McGloin and K. Dholakia, *Contemp. Phys.* **46**, 15 (2005).
11. J. N. Brittingham, *J. Appl. Phys.* **54**, 1179 (1983).
12. R. W. Ziolkowski, *Phys. Rev. A* **39**, 2005 (1988).
13. J.-Y. Lu and J. F. Greenleaf, *IEEE Trans. Ultrason. Ferroelectr. Freq. Control* **39**, 19 (1992).
14. I. Besieris, M. Abdel-Rahman, A. Shaarawi, and A. Chatzipetros, *Prog. Electromagn. Res.* **19**, 1 (1998).
15. J. Salo, J. Fagerholm, A. T. Friberg, and M. M. Salomaa, *Phys. Rev. E* **62**, 4261 (2000).
16. P. Saari and K. Reivelt, *Phys. Rev. E* **69**, 036612 (2004).
17. E. Recami and M. Zamboni-Rached, *Adv. Imaging Electron Phys.* **156**, 235 (2009).
18. *Localized Waves: Theory and Applications*, Ed. by H. E. Hernandez-Figueroa, M. Zamboni-Rached, and E. Recami (Wiley, New York, 2008).
19. H. Sönajalg, M. Rätsep, and P. Saari, *Opt. Lett.* **22**, 310 (1997).
20. P. Saari and K. Reivelt, *Phys. Rev. Lett.* **79**, 4135 (1997).
21. K. Reivelt and P. Saari, *Phys. Rev. E* **66**, 056611 (2002).
22. I. Alexeev, K. Y. Kim, and H. M. Milchberg, *Phys. Rev. Lett.* **88**, 073901 (2002).
23. R. Grunwald, V. Kebbel, U. Griebner, U. Neumann, A. Kummrow, M. Rini, E. T. J. Nibbering, M. Piché, G. Rousseau, and M. Fortin, *Phys. Rev. A* **67**, 063820 (2003).
24. F. Bonaretti, D. Faccio, M. Clerici, J. Biegert, and P. Di Trapani, *Opt. Express* **17**, 2276 (2009).
25. P. Bowlan, P. Gabolde, A. Schreenath, K. McGresham, and R. Trebino, *Opt. Express* **14**, 11892 (2006).
26. R. Trebino, *Frequency-Resolved Optical Gating: The Measurement of Ultrashort Laser Pulses* (Kluwer Acad., Boston, 2002).
27. P. Bowlan, P. Gabolde, and R. Trebino, *Opt. Express* **15**, 10219 (2007).
28. P. Bowlan, R. Trebino, H. Valtna-Lukner, M. Löhmus, P. Piskarv, and P. Saari, *Opt. Lett.* **34**, 2276 (2009).
29. P. Bowlan, M. Löhmus, P. Piskarv, H. Valtna-Lukner, P. Saari, and R. Trebino, “Measuring the Spatiotemporal Field of Diffracting Ultrashort Pulses,” Preprint, <http://arxiv.org/abs/0905.4381> (2009).
30. P. W. Milonni, *J. Phys. B* **35**, R31 (2002).

M. Lõhmus, P. Bowlan, R. Trebino, H. Valtna-Lukner, P. Piksarv, P. Saari
“Directly recording diffraction phenomena in the time domain”
Lithuanian Journal of Physics **50**, 69–74 (2010).

DIRECTLY RECORDING DIFFRACTION PHENOMENA IN THE TIME DOMAIN

M. Lõhmus^a, P. Bowlan^b, R. Trebino^b, H. Valtna-Lukner^a, P. Piksarv^a, and P. Saari^a

^a *Institute of Physics, University of Tartu, 142 Riia St, Tartu, 51014 Estonia*
E-mail: madisl@ut.ee

^b *School of Physics, Georgia Institute of Technology, 837 State St NW, Atlanta, GA 30332, USA*

Received 15 October 2009; accepted 19 March 2010

The wave-field produced by a ~ 30 fs duration Ti:sapphire oscillator pulse behind a circular aperture and circular opaque disk is measured using the ultrashort-laser-pulse measurement technique, scanning SEA TADPOLE. The high spatial and temporal resolution of the measuring technique enables us to fully image the diffracted field behind the apertures and record the interference pattern produced by the so-called boundary diffraction wave pulses.

Keywords: diffraction, interference

PACS: 42.25.Fx, 42.25.Gy, 42.25.Hz

1. Introduction

Throughout the history of describing and viewing the effects of diffraction, it has usually been done by using monochromatic light in order to make the diffraction pattern visible. However, using ultrashort laser pulses and advanced techniques for measurement, it is now possible to study diffraction in the time domain. The diffraction of femtosecond pulses was theoretically studied in [1] in the context of boundary diffraction wave theory, where it was shown that, for the special case of a circular aperture, with incident fields having axial symmetry around the optical axis, the so-called geometrical wave (*geometric (direct) pulse*) U_G and the boundary wave (*boundary wave pulse*) U_B could have comparable amplitudes on the optical axis. Three cases for the incident femtosecond pulse front – plane, divergent, and convergent pulse fronts – were studied and it was shown that, when the pulses are short enough, one could have two pulses with the same temporal profile and comparable intensities propagating along the optical axis after the diffractive element. One pulse is caused by the incident field that goes through the aperture undisturbed and the other is caused by the so-called boundary diffraction wave pulse. The diffracted field is said to arise from the superposition of the direct and the boundary diffraction wave pulse. A later study [2] reported the experimental demonstration of the existence of the boundary wave pulse by measuring

the modulated spectrum on the optical axis (caused by the two separate pulses) and the integrated radial intensity distribution of the diffracted field behind a circular aperture.

In this paper we present the results of the direct measurement of the diffracted field behind a circular aperture and circular opaque disk using high spectral (temporal) and spatial resolution provided by the ultrashort pulse measurement method called scanning SEA TADPOLE [3]. The short nature of the pulses used in the experiment, combined with the high spatiotemporal resolution and sensitivity of the method used for measurement, enables us to fully image the boundary wave pulse and the direct pulse separated in time behind the circular aperture and opaque circular disk. Taking measurements at different distances from the apertures enables us to study the temporal evolution of the diffraction of the propagating ultrashort laser pulses, and show the superluminal speed of the boundary wave pulse on the optical axis.

2. Numerical simulations

We performed numerical simulations for the diffracted field behind the apertures on the basis of the equation (12) in [1] derived from the work of Miyamoto and Wolf [4]. According to the boundary diffraction wave theory, the field of the boundary

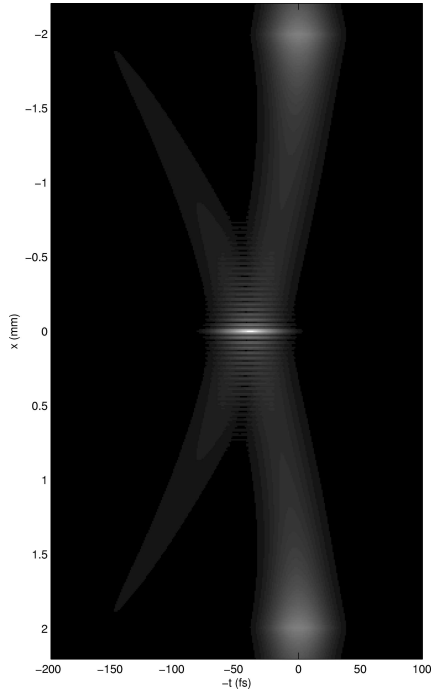


Fig. 1. The numerical simulation of a boundary diffraction wave pulse at 17 cm behind a 4 mm circular aperture under pulsed illumination. The interference fringes in the middle are caused by the interference of the elementary boundary diffraction waves originating from the edges of the aperture.

diffraction wave pulse behind a circular aperture with incident fields having axial symmetry around the optical axis can be expressed as

$$u_B(r, z, t) = \frac{u_0 e^{i\omega_0 t}}{2\pi} \times \int_0^\pi v\left(t - \frac{s(\psi)}{c}\right) e^{-ik_0 s(\psi)} \left(1 + \frac{z}{s(\psi)}\right) g(K, \psi) d\psi, \quad (1)$$

where $v(t)$ is the temporal envelope of the incident pulse, ω_0 is the central angular frequency, and k_0 is the wave number at ω_0 . The expression $s(\psi) = \sqrt{z^2 + a^2 + r^2 - 2ar \cos(\psi)}$, $K = r/a$ is a dimensionless variable, and $g(K, \psi) = [K \cos(\psi) - 1]/[1 + K^2 - 2K \cos \psi]^{-1}$. The structure of the boundary-wave pulse in the case of a plane wave illumination of a circular aperture can be seen on Fig. 1. The cylindrical

symmetry of the aperture leads to constructive interference of the elementary boundary diffraction waves originating from the edge of the aperture on the axis of symmetry of the circular aperture. This causes the boundary diffraction wave to have significant intensity on the optical axis that is comparable to the intensity of the direct pulse. The diffracted field is then calculated as the sum of the fields of the boundary wave pulse and direct pulse:

$$u(P, t) = u_G(P, t) + u_B(P, t), \quad (2)$$

where $P \equiv (x, y, z)$ is the point of measurement behind the aperture and u_G is calculated as

$$u_G = \begin{cases} u_i(P, t), & \text{if } P \text{ is in the direct beam,} \\ 0, & \text{if } P \text{ is in the shadow,} \end{cases} \quad (3)$$

where $u_i(P, t) = u_0 h(t - z/c)$ is the incident pulse. It is evident that the direct pulse in this theory has a discontinuity on the edge of the aperture. This is compensated by the discontinuity of the boundary wave pulse across the aperture (in the centre of the brighter areas of the boundary diffraction wave near the edge of the aperture on Fig. 1) so the resulting diffracted field is a continuous function of the position.

This equation for nonmonochromatic fields for circular apertures assumes that the incident field is a plane wave (pulse) with a normal incidence. In the case of laser-produced Gaussian beams, this assumption does not exactly hold, but for truncated Gaussian beams the boundary diffraction still appears as shown in [5]. A comparison of measurements and simulations shows that the error produced when the pulse fronts differ slightly from a plane wave is negligible.

3. Scanning SEA TADPOLE

In order to record the complex structure of the diffraction pattern behind the apertures, high spatial and temporal (spectral) resolutions are needed. An experimentally simple version of spectral interferometry called SEA TADPOLE was the first technique shown to be able to directly measure the spatiotemporal electric field of focusing ultrashort pulses [6]. The small mode size of the optical fibres used in this method naturally enables electric fields of ultrashort pulses to be measured with high spatial resolution. In a SEA TADPOLE set-up, the previously characterized reference pulse and the unknown pulse are coupled into two identical fibres as seen in Fig. 2. The entrance of the unknown

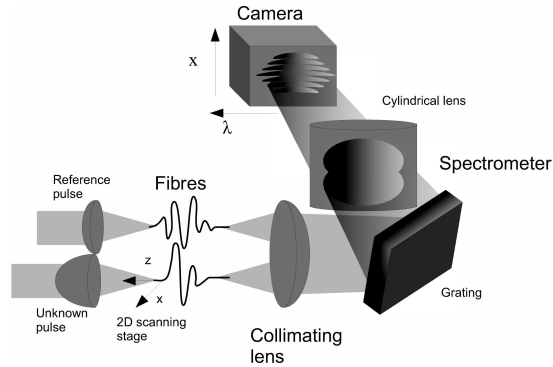


Fig. 2. Scanning SEA TADPOLE set-up. A reference pulse and an unknown pulse are coupled into two single-mode optical fibres. The diverging beams from the fibres are collimated with a spherical lens. The collimated beams cross and the interference pattern is recorded with a camera. In horizontal plane a grating and a cylindrical lens are used to make a spectrometer and to map the wavelength onto the camera's horizontal axis.

pulse's fibre is placed on a scanning stage. The reference pulse's fibre entrance and both of the fibres ends are fixed. The diverging beams from the fibres are collimated vertically by a spherical lens, and the collimated beams cross and interfere. The interference pattern is recorded with a camera. In the horizontal plane, a grating and a cylindrical lens are used to make a spectrometer and to map wavelength on the camera's horizontal axis. This interferogram, recorded for every position of the scanning stage, allows one to reconstruct the full spatiotemporal field $E(x, y, z, t)$.

4. Measurements

The experiments were carried out using KM Labs Ti:sapphire oscillator with ~ 37 nm FWHM bandwidth spectrum with a central wavelength of 805 nm and pulse duration of about 30 fs. The temporal resolution of our SEA TADPOLE set-up was 4.6 fs. The circular aperture and opaque disk were placed in the unknown pulse arm of the SEA TADPOLE set-up, where the optical fibre was placed on the 2D scanning stage. The unmodified pulse (pulse directly from the laser) was sent to the second fibre and was used as a reference. For each aperture, the tip of the scanning fibre was first moved into the bright central spot on the optical axis caused by the interference of the elementary boundary wave pulses. The fibre was then moved horizontally back over the edge of the aperture, and a full scan on the axis perpendicular to the pulse propagation was made to produce the images. Due to the cylindrical symmetry of the apertures and the resulting diffracted field,

only one scan in the plane of the aperture diameter (that is, for various longitudinal distances after the aperture and various transverse distances parallel to the plane of the aperture) was necessary to obtain the full information of the field. Measurements were taken at different distances from the aperture and disk to study the time evolution of the diffraction of the ultrashort pulses.

The spatial resolution of a SEA TADPOLE set-up is determined by the mode size of the scanning fibre [6]. In our set-up we used a fibre that had a core diameter of $5.4 \mu\text{m}$, which is also the achieved spatial resolution of our measurements. Our step size of each consecutive measurement in one scan was smaller than the actual spatial resolution to obtain smoother images of the interference pattern of the diffracted field.

5. Discussion

For the circular opaque disk, measurements at distances of 92, 172, and 252 mm are shown in Fig. 3 along with the simulations. The circular aperture measurements form distances of 25, 55, and 85 mm are shown in Fig. 4. The intensities in every image are in arbitrary units with maximum of 1. The scanning range of the fibre for the circular opaque disk was 8 mm and for the circular aperture 4.4 mm. Each image displays the amplitude of the electric field (square root of the intensity) versus $-t$ so that the parts of the diffracted field that arrive earlier in time appear on the right-hand side of the plots.

In the pictures it is easy to see two diffraction patterns. One has a lower spatial modulation on the edges

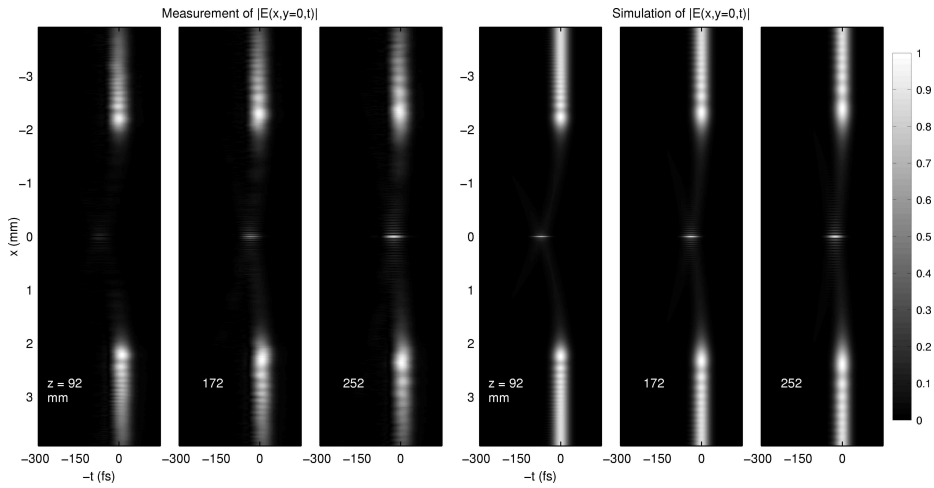


Fig. 3. The measured (left) and calculated (right) fields behind a 4 mm circular disk at different distances.

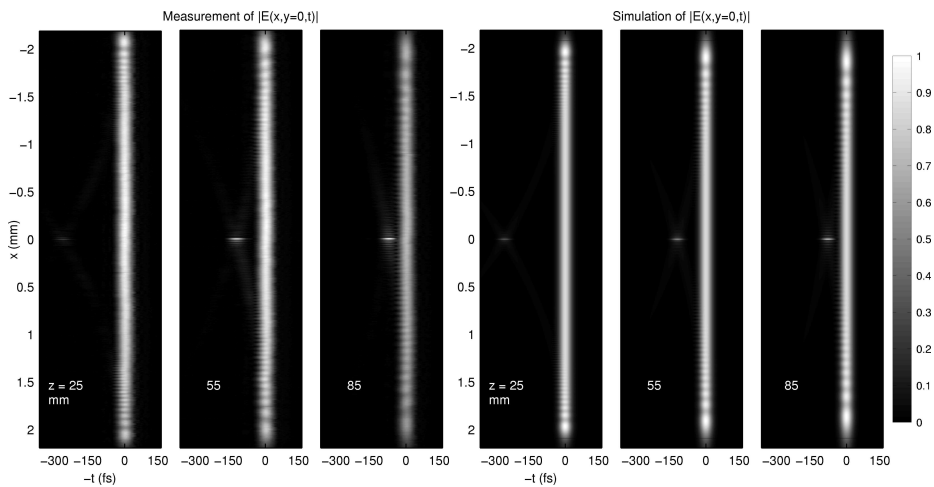


Fig. 4. The measured (left) and calculated (right) fields behind a 4 mm circular aperture at different distances.

of the direct pulse that is caused by the interference between boundary wave pulse and the direct pulse. Interference fringes can also be seen around the bright central spot analogous to the Bessel-X pulses [7, 8], which are caused by the interference between the elementary boundary diffraction waves originating from the edge of the aperture. Also similar to the Bessel-X

pulse the boundary wave pulse has a letter X-like axial cross-section and propagates on the optical axis superluminally. But while the group velocity of the former has a constant value exceeding c , the central spot of the boundary wave pulse is decelerating (see also [1, 9–11]). The elementary boundary diffraction waves emanating from the edges of the aperture must travel a longer

distance to reach the optical axis compared to the centre of the direct pulse and thus lag behind. The difference in distance they need to travel compared to the distance travelled by the direct pulse decreases as the pulse propagates. The superluminal speed can be easily seen as the constructive interference of the boundary wave pulse on the optical axis catching up with the direct pulse that has the propagation speed of c .

While the theoretical study shows that, when the laser pulses are short enough to separate the boundary wave pulse from the direct pulse, the two pulses propagating on the optical axis should have comparable intensities, this is not the case in our experiments. This is due to the fact that the transverse intensity profile of the pulses was Gaussian, with FWHM about 4 mm. So the pulse intensity on the aperture was approximately one half of that at the centre of the pulse. As a result, in our measurements, the intensity of the boundary wave pulse or the constructive interference of the elementary boundary-wave pulse on the optical axis is smaller than the intensity of the direct pulse on the optical axis. Also the accurate measurement of the intensity of the boundary wave pulse is difficult to accomplish since, at the maximum distance from the aperture (about 25 cm) where the interference pattern has the lowest spatial modulation, the size of the central bright spot of the interference pattern is still only about $50 \mu\text{m}$. So any deviation from exact alignment of the scanning fibre tip from the plane of the diameter of the aperture will inevitably cause the maximum intensity of the spot to be inaccurately measured. This becomes even more critical when one considers measurements that are done closer to the aperture where the fringe spacing of the diffraction pattern becomes denser and fringes themselves smaller.

6. Conclusion

The complete diffracted field, $E(x, y, z, t)$, of ultrashort laser pulses behind circular opaque disk and circular aperture is measured with high spectral and temporal resolution using a method called scanning SEA TADPOLE. The pulsed illumination of the apertures allows us to image the so-called boundary diffraction

wave separately from the direct pulse. The high spatial resolution reveals the fine diffraction fringes caused by the interference of the elementary boundary wave pulses near the optical axis. We also carried out numerical simulations based on the boundary diffraction wave theory. The simulations and the experimental data are found to be in good agreement.

References

- [1] Z.L. Horváth and Zs. Bor, Diffraction of short pulses with boundary diffraction wave theory, *Phys. Rev. E* **63**(2), 026601-1–11 (2001).
- [2] Z.L. Horváth, J. Klebniczki, G. Kurdi, and A.P. Kovács, Experimental investigation of the boundary wave pulse, *Opt. Commun.* **239**(4–6), 243–250 (2004).
- [3] P. Bowlan, P. Gabolde, M.A. Coughlan, R. Trebino, and R.J. Levis, Measuring the spatiotemporal electric field of ultrashort pulses with high spatial and spectral resolution, *J. Opt. Soc. Am. B* **25**(6), A81–A91 (2008).
- [4] K. Miyamoto and E. Wolf, Generalization of the Maggi–Rubinowicz theory of the boundary diffraction wave – Part II, *J. Opt. Soc. Am.* **52**(6), 626–637 (1962).
- [5] Z.L. Horváth and Zs. Bor, Reshaping of femtosecond pulses by the Gouy phase shift, *Phys. Rev. E* **60**(2), 2337–2346 (1999).
- [6] P. Powlan, P. Gabolde, and R. Trebino, Directly measuring the spatio-temporal electric field of focusing ultrashort pulses, *Opt. Express* **15**(16), 10219–10230 (2007).
- [7] P. Saari and K. Reivelt, Evidence of X-shaped propagation-invariant localized light waves, *Phys. Rev. Lett.* **79**(21), 4135–4138 (1997).
- [8] P. Powlan, H. Valtna-Lukner, M. Löhmus, P. Piksarv, P. Saari, and R. Trebino, Measuring the spatiotemporal field of ultrashort Bessel-X pulses, *Opt. Lett.* **34**(15), 2276–2278 (2009).
- [9] P. Saari and K. Reivelt, Generation and classification of localized waves by Lorentz transformations in Fourier space, *Phys. Rev. E* **69**(3), 036612-1–12 (2004).
- [10] M. Clerici, D. Faccio, A. Lotti, E. Rubino, O. Jedrkiewicz, J. Biegert, and P. Di Trapani, Finite-energy, accelerating Bessel pulses, *Opt. Express* **16**(24), 19807–19811 (2008).
- [11] H. Valtna-Lukner, P. Bowlan, M. Löhmus, P. Piksarv, R. Trebino, and P. Saari, Direct spatiotemporal measurements of accelerating ultrashort Bessel-type light bullets, *Opt. Express* **17**(17), 14948–14955 (2009).

TIESIOGINIS DIFRAKCIJOS REIŠKINIŲ REGISTRAVIMAS LAIKINĖJE SRITYJE

M. Lõhmus^a, P. Bowlan^b, R. Trebino^b, H. Valtna-Lukner^a, P. Piksarv^a, P. Saari^a

^a *Tartu universiteto fizikos institūtas, Tartu, Estija*

^b *Džordžijos technologijos universiteto Fizikos mokykla, Atlanta, JAV*

Santrauka

Bangų laukas, sukurtas ~30 fs trukmės Ti:safyro osciliatoriaus impulsais už apskritos apertūros ir apskrito neperšviečiamo disko, matuojamas ultratrumpųjų lazerio impulsų metodu, kuris angliškai

vadinamas skenuojančiuoju SEA TADPOLE. Taikyto metodo didelė erdvinė ir laikinė skyra leidžia atvaizduoti visą už apertūrų difragavusį lauką ir užfiksuoti interferencinį vaizdą, susidarantį dėl vadinamųjų kraštinių difragavusių bangų impulsų.

P. Saari, P. Bowlan, H. Lukner, M. Lõhmus, P. Piksarv, R. Trebino
“Time-and-space-domain study of diffracting and “non-diffracting” light pulses”
Lithuanian Journal of Physics **50**, 121–127 (2010).

TIME-AND-SPACE-DOMAIN STUDY OF DIFFRACTING AND NON-DIFFRACTING LIGHT PULSES

P. Saari^a, P. Bowlan^b, H. Valtna-Lukner^a, M. Lõhmus^a, P. Piksarv^a, and R. Trebino^b

^a *Institute of Physics, University of Tartu, 142 Riia St, Tartu, 51014 Estonia*

E-mail: peeter.saari@ut.ee

^b *School of Physics, Georgia Institute of Technology, 837 State St NW, Atlanta, GA 30332, USA*

Received 27 October 2009; revised 17 February 2009; accepted 19 March 2010

We present an overview of our very recent results on the evolution of ultrashort pulses after propagating through various optical elements. Direct spatiotemporal measurements of the electric field were made using the technique SEA TADPOLE. Our SEA TADPOLE device can resolve spatial features as small as $\sim 5 \mu\text{m}$ and temporal features as small as $\sim 5 \text{ fs}$. The experimental results are verified by theoretical calculations. The superluminality of pulses with Bessel-function-like radial profiles is discussed.

Keywords: Bessel beam, boundary diffraction wave, Bessel-X pulse, superluminal propagation, Arago spot

PACS: 42.25.Fx, 42.25.Gy, 42.65.Re, 42.79.Bh

1. Introduction

In 1987 Bessel light beams [1] were introduced and now constitute a mature field with numerous applications (see review [2]). These beams are important because they possess a controversial quality: they are “diffraction-free” and so preserve their tightly focused central bright spot over large distances of propagation as if the beam were not obeying the laws of diffraction. At the same time, quite independently, in mathematical physics, the topic of undistorted or localized waves emerged, dealing with ultrabroadband pulses that are not only “diffraction-free” in space but also propagate without any spread in time [3–5]: “light bullets” or “electromagnetic missiles.” To date, various localized waves propagating in vacuum superluminally (faster than the speed of light in vacuum), luminally, or sub-luminally have been studied in detail, and promising applications have been proposed (see, e.g., reviews [6–10] and the first monograph [11] on the field). The feasibility of such light bullets moving faster than c has been experimentally demonstrated more than once [12–17], but, from time to time, papers still appear in which the superluminal group velocity in vacuum of such wave packets is questioned. Therefore, recently [18] we accomplished, for the first time, with appropriately high resolution and accuracy, a direct spatiotemporal measurement of the electric field and propagation

velocity of the simplest superluminal localized wave – the so-called Bessel-X pulse [13], which comprises an energy lump of a micrometre in diameter at the joint apex of a sparse double-conical wave. In this paper, we first present an overview of this result.

Secondly, we touch briefly on our spatiotemporal measurements of accelerating and decelerating Bessel pulses [19]. The term was proposed in [20] where the generation and properties of such pulses were theoretically investigated. These pulses are similar to the Bessel-X pulses, with the main difference being that they are generated by crossing and interfering focusing (or defocusing) pulses, which have curved pulse fronts and form part of a spindle torus surface, rather than the double conical surface of Bessel-X pulses. As a result, their bullet-like, central, intense apex and accompanying Bessel rings become smaller or larger as the pulse propagates, depending on whether the torus shrinks towards a ring or expands towards a sphere. But the central spot of these pulses is still localized and intense over a propagation distance considerably longer than that of a Gaussian beam with a comparable waist size.

The third topic that we will discuss involves viewing simple, well-known cases of diffraction, but in the time domain. The bending of light waves in the shadow region behind an opaque disk and the appearance of a bright “Spot of Arago” in the shadow centre are well-known manifestations of diffraction. Tremendous

progress was made in the mathematical treatment of diffraction, resulting in the well developed theory with Fresnel–Kirchhoff and Rayleigh–Sommerfeld versions (see, e. g., monographs [21, 22] and references therein). An alternative theory, inspired by the early ideas of Thomas Young, has been developed by Maggi [23], Rubinowicz [24], Miyamoto, and Wolf (references given in [22]). The boundary diffraction wave (BDW) theory, as it was called, describes diffraction from openings in opaque screens in a mathematically simple manner. The BDW theory is especially intuitive when describing the formation of the diffracted field for the case of illumination with ultrashort laser pulses.

Contrary to the traditional treatment using monochromatic fields, in which the transmitted waves fill large depths of space behind the screen and overlap with each other there, ultrashort pulses – typically only few micrometres “thick” – behave almost like a solitary wave-front surface. Hence, the time-domain study of diffraction in terms of pulsed BDWs is not only didactically preferable but also opens new interesting directions and applications, such as in the study of focusing and other transformations of ultrashort pulses (see, e. g., paper [25] and references therein). The formation of an ultrashort boundary wave pulse just after a circular aperture has been theoretically studied [26], and experimental evidence for its existence was obtained by measuring modulations in the spectrum of the on-axis field as well as with CCD-recordings of the time-integrated radial intensity distribution of the field [27]. Our aim has been to directly record, with simultaneous spatial and temporal resolution, the evolution and interference of the boundary waves behind various screens. The results obtained are presented in the paper by Löhmus et al. which can be found in this issue, and here we consider only the spot of Arago.

2. Spatiotemporal measurement of light fields

In our experiments we used a KM Labs Ti:Sa oscillator with 33 nm of bandwidth (FWHM) and an approximately Gaussian spectrum with a central wavelength $\lambda_0 = 805$ nm. The spot size of the laser beam was 4 mm (FWHM). Our measurements not only required high spatiotemporal resolution, but also high sensitivity. First of all, we routinely measure the relatively intense, spatially uniform pulse directly out of our laser, which is the input pulse in these experiments, and which also acts as a reference pulse in the measurements, using the FROG technique [28]. To obtain

ultra-high spatiotemporal resolution in both the intensity and phase, in conjunction with the required sensitivity, we used a technique called SEA TADPOLE (Spatially Encoded Arrangement for Temporal Analysis by Dispersing a Pair of Light E-fields [29]), which is based on spectral interferometry. It involves measuring the spectrum of the sum of the known reference pulse and the unknown pulse to yield the unknown pulse’s temporal field. This approach is much like monochromatic-beam spatial interferometry or holography, where measurement of the spatial intensity of the sum of a known spatial field and an unknown monochromatic wave yields the unknown wave field in space. Finally, we achieve the high spatial resolution of the unknown field by simply scanning the micrometre-sized tip of the SEA TADPOLE input fibre point-by-point through the space where the unknown light field propagates. SEA TADPOLE has demonstrated a spatial resolution as small as 0.5 micrometres by using near-field scanning optical microscopy fibre tips, but 5 micrometres is sufficient for these measurements, allowing the use of standard off-the-shelf fibres. A description of the SEA TADPOLE set-up used can be found in Refs. [18, 25] and in the paper by Löhmus et al. in the given issue. The plots from our SEA TADPOLE measurements, which are shown below, can be viewed as still images or “snapshots in flight,” since they are spatiotemporal slices of the magnitude of the electric field $|E(x, y, z, t)|$ of the pulses.

3. Results on “diffraction-free” Bessel-X pulse

The most effective Bessel beam generator – a conical lens (axicon) – refracts plane waves towards its axis and thus shapes a femtosecond pulse into the Bessel-X pulse with its characteristic double-conical profile, as shown in Fig. 1. If the aperture radius R of the axicon were infinitely large, the pulse would propagate rigidly and without any spread of its micrometre-size central bright spot at the joint apex of the cones over an infinitely large distance. In the case of a limited aperture, it follows from the geometry that the depth of the invariant propagation of the pulse (let us call it the Bessel zone) is restricted to $z_B = R/\tan \theta$, where θ (the so-called axicon angle) is the angle of inclination of the wave vectors of the constituent plane waves toward the axis z .

Some measured “snapshots” of propagation of the Bessel-X pulse are shown in Fig. 1, together with theoretical simulations (this time calculated as an axisymmetric superposition of plane waves with a Gaussian

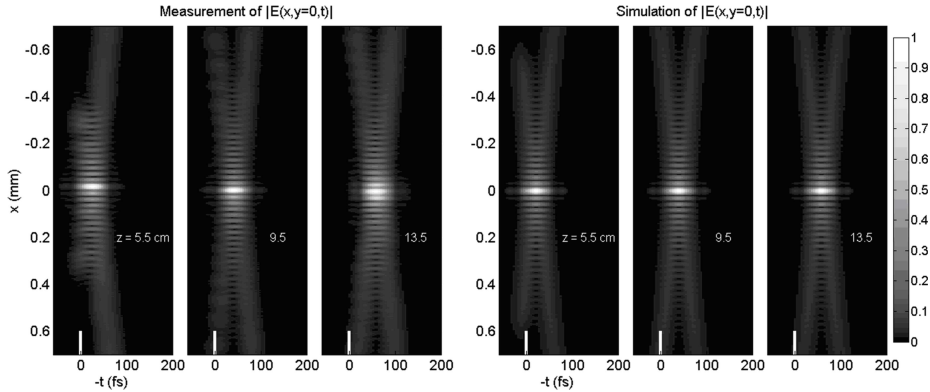


Fig. 1. Left: the measured field amplitude at three different distances (z) after the axicon. Right: the corresponding simulations. The greyscale bar indicates the amplitude, and we have normalized each field to have a maximum of 1. The white bar on the time axis emphasizes $t = 0$ relative to the reference pulse, which is where the pulse would be located if it were propagating at velocity c . The “thickness” of each of the X-branches indicates the duration of the input (and reference) pulse.

aperture). The two are in good agreement except that the wings in the $z = 5.5$ cm image are shorter in the measurement. This is because axicons are difficult to machine perfectly; in particular, the tip of the cone is always distorted, so the Bessel zone is shorter than what would be expected in the ideal case.

There are several interesting features in these plots. The central maximum of the pulse has a width of $\sim 20 \mu\text{m}$, which – as well as the coaxial intensity rings surrounding it – remains essentially unchanged in shape from $z = 5$ cm through $z = 13.5$ cm. Thus the apex flies rigidly as a light bullet together with its sparse wings at constant speed. This is because the Bessel-X pulse is a propagation-invariant conical wave. Also, the Bessel-X pulse’s superluminal speed is apparent in these plots. SEA TADPOLE measures the pulse’s arrival time with respect to the reference pulse, which travels at the speed of light (c). Therefore, if the Bessel-X pulse were travelling at the speed of light, then at each z its spatiotemporal intensity would have the same centre on the time axis (here $t = 0$ and emphasized with the white line), but it is easy to see that this is not the case. From the axicon angle value $\theta = 0.92^\circ$ (corresponds to our axicon’s apex angle 176°) as well as from the simulations, we find that the Bessel-X pulse’s speed (axial group velocity) should be $1.00013c$. From our experimental plots we determined [18] it to be $1.00012c$ – within 0.001% error of the expected value.

4. Results on accelerating and decelerating Bessel pulses

In order to generate accelerating (or decelerating) pulses we mounted a lens with focal length of $+153$ mm (or -152 mm) before the axicon. All these results were published in [19], and here we restrict ourselves to the decelerating pulse case only.

The spatiotemporal profiles of the decelerating Bessel pulse at nine positions were measured. In all cases, we measured the complete spatiotemporal intensity and phase, but we show only the spatiotemporal intensities here, as this information is more interesting. Three of these measurements for each case are shown in Fig. 2. For comparison, numerical simulations were carried out, and as seen in the figure, the two are in very good agreement. The X-branching corresponding to the double conical profile of the pulse is not seen because, due to the lens and deceleration, the axicon angle θ is less than in Fig. 1 and decreases with propagation distance. Due to the negative lens the fronts of the pulses (and phase fronts) obtain a curvature which decreases in the course of propagation and therefore the axicon angle θ on the axis also decreases – resulting in deceleration of the movement of the strong interference field on the axis, which is still in a good approximation nothing but a Bessel-X pulse.

SEA TADPOLE measures the pulse’s arrival time with respect to the reference pulse, the latter of which, after passing through the compensating piece of glass, travels at the speed of light c . The origin of our time

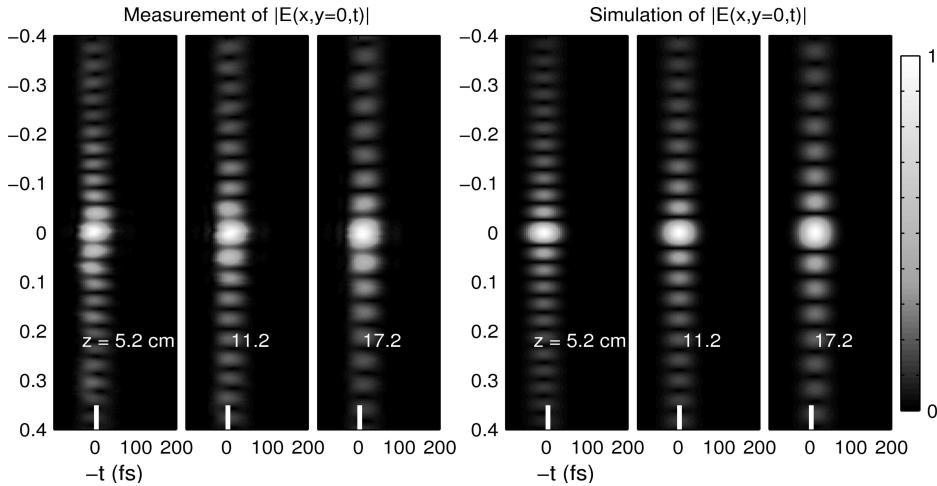


Fig. 2. Comparison of the measured and calculated spatiotemporal profiles of the electric field amplitude of a decelerating Bessel pulse at three positions along the propagation axis z .

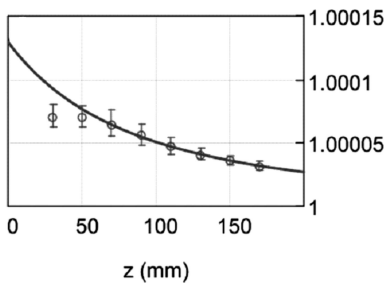


Fig. 3. Experimentally determined group velocity of the decelerating Bessel pulse as a function of the propagation distance. The solid curve shows the theoretical function for comparison.

axis can be considered as the location of the reference pulse if it propagated along the axis z with the Bessel pulses. So, if the Bessel pulse were travelling at the speed of light, then, for each value of z , its spatiotemporal intensity would be centred at the same time origin $t = 0$ which is emphasized by the white bar in the figure. Again in Fig. 2, note that the superluminal group velocity and the pulse's deceleration are both apparent from the z -dependent shifts of the pulses with respect to the origin $t = 0$. The time shifts were used for calculation of the pulse's velocity at different propagation distances (see Fig. 3). The decreasing superluminal velocity manifests itself also in the increase

of the fringe spacing (increasing radial period of the Bessel profile; see Fig. 2). Accelerating and decelerating Bessel pulses can be also observed when tightly focusing an ultrashort pulse by a lens with spherical aberration [25].

5. Spatiotemporally recorded diffraction

Here we consider formation of the Arago spot pulse (for more results on diffraction of pulses through various screens, see the paper by Löhmus et al., also in this issue).

We propagated ultrashort pulses past an opaque disk of 4 mm diameter, making a hole in the beam, and we measured the resulting spatiotemporal field at different distances after the aperture to observe its evolution. These measurements reveal the spatiotemporal structure of the weak boundary waves and the brighter spot at the centre of the beam due to their constructive interference, i. e., the spot of Arago, as it is known in conventional diffraction theory for stationary (monochromatic) fields. Interestingly, the plots (like the one in Fig. 4 for a particular propagation distance) reveal that this spot is surrounded by coaxial interference rings and, in the axial region the field, is identical to a decelerating Bessel pulse, which we have considered in the previous section. Moreover, the spot is delayed in time with respect to the main pulse front, and this delay decreases with z , indicating a superluminal propagation

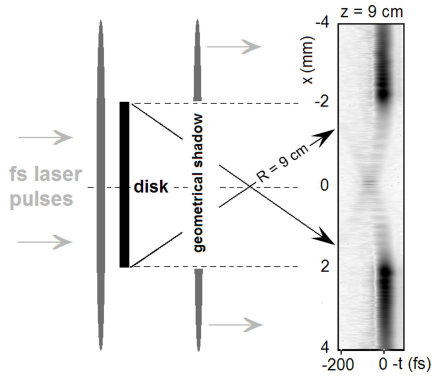


Fig. 4. Schematic of the experiment and the measured time-domain formation of the Arago spot behind an opaque disk with radius 2 mm. Inset: measured electric field amplitude (actually square root of it $-|E|^{1/2}$ – for better contrast) 9 cm behind the disk. This measurement reveals the weak boundary waves that originate from the points along the perimeter of the disk. The boundary waves interfere with the plane wave pulse or the part of the field coming from radii greater than that of the disk, which propagates according to the rules of geometrical optics. Constructive interference between the expanding boundary waves produces a brighter superluminally propagating spot on the axis. The strength of the field is shown “in a negative colormap”, in which black corresponds to the maximum strength.

speed along the z axis (the main pulse front propagates at c). This occurs, because, as z (or the distance from the disk) increases, the extra distance that the boundary waves must propagate (compared to the main pulse front) to reach the z axis ($x = 0$) decreases, so the relative delay of the boundary waves and the bright spot due to their interference decreases. As a result, the group velocity of the Arago spot – geometrically located at one pole of a luminally expanding spindle torus formed by the boundary diffraction wave pulse – varies from infinity at $z = 0$ to c for very large values of z . Therefore, the spot of Arago is in fact just a decelerating Bessel pulse.

6. Discussion

The superluminality of the Bessel-X-type pulses is intriguing. Indeed, while phase velocities greater than c are well known in various fields of physics, a superluminal *group velocity* is still somewhat taboo, because, at first glance, it seems to be in violation of relativistic causality. However, thanks to the numerous studies throughout the previous century – starting from Sommerfeld’s works on the propagation of plane

wave pulses in dispersive media – it is well known (see, e. g., a thorough review [30]) that the group velocity need not be a physically profound quantity and by no means should be confused with the signal propagation velocity (which must be less than or equal to c in vacuum). But in the case of Bessel-X-type pulsed waves, no dispersive medium is needed, and still not only is the group velocity superluminal, but the pulse as a whole is also, that is, it rigidly propagates faster than a plane wave.

Naturally, one may feel some unease in accepting this startling circumstance. But here we experimentally observe it in the most direct way. When forced to concede the theoretically and experimentally verified superluminality, one might feel the need to make recourse to statements insisting that the pulse is not a “real” one, but instead simply an interference pattern rebuilt at every point of its propagation axis from truly real plane-wave constituents travelling at a slight tilt with respect to the axis. Such argumentation is not wrong but, alas, leads nowhere. Of course, there is a similarity between the superluminality of the X-wave and a simple geometrical faster-than-light movement of the cutting point in scissors (we refer here to Gedanken experiments described in textbooks on relativity). But in the central highest-energy part of the Bessel-X wave, there is nothing moving at the tilt angle. The phase planes are perpendicular to the axis and move rigidly with the whole pulse along the axis. The Poynting vector, indicating the direction of energy flow, lies also along the axis. However, the energy flux is not superluminal. Hence, to consider the Bessel-X waves as something inferior to “real” waves is not sound. If we thought so, by similar logic we would arrive at the conclusion that femtosecond pulses emitted by a mode-locked laser are not real but “simply an interference” between the continuous-wave laser modes. In other words, one should not ignore the essence of the superposition principle of linear fields, which implies a reversible relation between “resultant” and “constituent” fields and in which no possible orthogonal bases – plane waves or cylindrical (Bessel) waves, for the given example – are inferior to any others.

Another misunderstanding (the author of the review [30] seems to agree) stems from oversight of the fact that there are infinitely many ways to form a pulsed axisymmetric wave packet from single-frequency Bessel beams. They depend on how the radial density of intensity rings in the beam cross-section is related – or whether or not it is related at all – to the beam’s temporal frequency. In the case of the Bessel-X pulse,

this is a proportionality relation, and therefore the axial group velocity is perfectly defined with a single superluminal value within the whole bandwidth of the wave packet. If, on the contrary, the radial density is frequency-independent, we obtain a completely different wave packet which is not a localized wave because it has no definite group velocity over its whole spectrum and therefore spreads as it propagates. But such a wave packet – named the ‘pulsed Bessel beam’ in the literature – propagates with velocity less than c and can be used for sending signals along the propagation axis. On the other hand, if one tried to cut a signal “notch” into the core of the Bessel-X pulse, the notch would behave like the ‘pulsed Bessel beam’ – spreading out while advancing subluminally. This is expected since Maxwell’s equations, or the wave equation for EM fields, do not allow superluminal signalling.

7. Conclusion

We have performed direct spatiotemporally resolved measurements of pulsed light fields behind various optical refracting and diffracting elements. We believe that time-resolved measurements and a time-domain treatment of diffracting waves not only turn out to be fruitful in modern physical optics, especially in micro- and meso-optics, but also promote the understanding of diffraction phenomena.

Acknowledgements

Some support was provided by NSF SBIR grant #053-9595, and P. B. was also supported by NSF fellowship IGERT-0221600. The other authors were supported by the Estonian Science Foundation, grant #7870.

References

- [1] J. Durin, J.J. Miceli Jr, and J.H. Eberly, *Phys. Rev. Lett.* **58**, 1499 (1987).
- [2] D. McGloin and K. Dholakia, *Contemp. Phys.* **46**, 15 (2005).
- [3] J.N. Brittingham, *J. Appl. Phys.* **54**, 1179 (1983).
- [4] R.W. Ziolkowski, *Phys. Rev. A* **39**, 2005 (1988).
- [5] J.-Y. Lu and J.F. Greenleaf, *IEEE Trans. Ultrason. Ferroelectrics Freq. Control* **39**, 19 (1992).
- [6] I. Besieris, M. Abdel-Rahman, A. Shaarawi, and A. Chatzipetros, *Prog. Electromagn. Res.* **19**, 1 (1998).
- [7] J. Salo, J. Fagerholm, A.T. Friberg, and M.M. Salomaa, *Phys. Rev. E* **62**, 4261 (2000).
- [8] P. Saari and K. Reivelt, *Phys. Rev. E* **69**, 036612 (2004).
- [9] E. Recami and M. Zamboni-Rached, *Adv. Imaging Electron Phys.* **156**, 235 (2009).
- [10] E. Gaižauskas, A. Dubietis, V. Kudriašov, V. Sirutkaitis, A. Couairon, D. Faccio, and P. Di Trapani, in: *Self-focusing: Past and Present* (Springer, 2009), p. 457–479.
- [11] *Localized Waves: Theory and Applications*, eds. H.E. Hernandez-Figueroa, M. Zamboni-Rached, and E. Recami (J. Wiley, New York, 2008).
- [12] H. Sönaialg, M. Rätsep, and P. Saari, *Opt. Lett.* **22**, 310 (1997).
- [13] P. Saari and K. Reivelt, *Phys. Rev. Lett.* **79**, 4135 (1997).
- [14] K. Reivelt and P. Saari, *Phys. Rev. E* **66**, 056611 (2002).
- [15] I. Alexeev, K.Y. Kim, and H.M. Milchberg, *Phys. Rev. Lett.* **88**, 073901 (2002).
- [16] R. Grunwald, V. Kebbel, U. Griebner, U. Neumann, A. Kummrow, M. Rini, E.T.J. Nibbering, M. Piché, G. Rousseau, and M. Fortin, *Phys. Rev. A* **67**, 063820 (2003).
- [17] F. Bonaretti, D. Faccio, M. Clerici, J. Biegert, and P. Di Trapani, *Opt. Express* **17**, 2276 (2009).
- [18] P. Bowlan, R. Trebino, H. Valtna-Lukner, M. Löhmus, P. Piksarv, and P. Saari, *Opt. Lett.* **34**, 2276 (2009).
- [19] H. Valtna-Lukner, P. Bowlan, M. Löhmus, P. Piksarv, R. Trebino, and P. Saari, *Opt. Express* **17**, 14948 (2009).
- [20] M. Clerici, D. Faccio, A. Lotti, E. Rubino, O. Jedrkiewicz, J. Biegert, and P. Di Trapani, *Opt. Express* **16**, 19807 (2008).
- [21] J.W. Goodman, *Introduction to Fourier Optics*, 3rd ed. (Roberts & Co, Englewood, 2005).
- [22] M. Born and E. Wolf, *Principles of Optics*, 6th ed. (Pergamon Press, Oxford, 1987).
- [23] G.A. Maggi, *Ann. di Matem. Pura ed Appl.*, Ila **16**, 21 (1888).
- [24] A. Rubinowicz, *Nature* **180**, 160 (1957).
- [25] P. Bowlan, U. Fuchs, R. Trebino, and U.D. Zeitner, *Opt. Express* **16**, 13663 (2008).
- [26] Z.L. Horváth and Z. Bor, *Phys. Rev. E* **63**, 026601 (2001).
- [27] Z.L. Horváth, J. Klebniczki, G. Kurdi, and A. Kovács, *Opt. Commun.* **239**, 243 (2004).
- [28] R. Trebino, *Frequency-Resolved Optical Gating: The Measurement of Ultrashort Laser Pulses* (Kluwer Academic Publishers, Boston, 2002).
- [29] P. Bowlan, P. Gabolde, and R. Trebino, *Opt. Express* **15**, 10219 (2007).
- [30] P.W. Milonni, *J. Phys. B* **35**, R31 (2002).

DIFRAGUOJANTYS IR NEDIFRAGUOJANTYS ŠVIESOS IMPULSAI ERDVĖJE IR LAIKE

P. Saari ^a, P. Bowlan ^b, H. Valtna-Lukner ^a, M. Löhmus ^a, P. Piksarv ^a, R. Trebino ^b

^a *Tartu universiteto fizikos institutas, Tartu, Estija*

^b *Džordžijos technologijos universiteto Fizikos mokykla, Atlanta, JAV*

Santrauka

Pateikiame savo naujausių rezultatų apžvalgą apie ultratrum-pųjų impulsų, perėjusių įvairius optinius elementus, evoliuciją. Elektrinis laukas tiesiogiai matuotas erdvėje ir laike metodu, angliškoje literatūroje vadinamu SEA TADPOLE. Mūsų SEA

TADPOLE prietaisas registruoja net $\sim 5 \mu\text{m}$ smulkumo ir vos ~ 5 fs trunkančius pokyčius. Eksperimentiniai rezultatai patvirtinti teoriniais skaičiavimais. Aptartas impulsų, turinčių Beselio funkcijos pavidalo radialųjį pjūvį, virššviesinis pobūdis.

P. Saari, P. Bowlan, H. Valtna-Lukner, M. Lõhmus, P. Piksarv, and R. Trebino
“Basic diffraction phenomena revisited in time domain”
Opt. Express **18**, 11083–11088 (2010).

Basic diffraction phenomena in time domain

Peeter Saari,¹ Pamela Bowlan,^{2,*} Heli Valtna-Lukner,¹ Madis Lõhmus,¹
Peeter Piksarv,¹ and Rick Trebino²

¹*Institute of Physics, University of Tartu, 142 Riia St, Tartu, 51014, Estonia*

²*School of Physics, Georgia Institute of Technology, 837 State St NW, Atlanta, GA 30332, USA*

**pambowlan@gatech.edu*

Abstract: Using a recently developed technique (SEA TADPOLE) for easily measuring the complete spatiotemporal electric field of light pulses with micrometer spatial and femtosecond temporal resolution, we directly demonstrate the formation of the so-called boundary diffraction wave and Arago's spot after an aperture, as well as the superluminal propagation of the spot. Our spatiotemporally resolved measurements beautifully confirm the time-domain treatment of diffraction. Also they prove very useful for modern physical optics, especially in micro- and meso-optics, and also significantly aid in the understanding of diffraction phenomena in general.

©2010 Optical Society of America

OCIS codes: (320.5550) Pulses; (320.7100) Ultrafast measurements; (050.1940) Diffraction.

References and links

1. G. A. Maggi, "Sulla propagazione libera e perturbata delle onde luminose in mezzo isotropo," *Ann. di Mat IIa*, **16**, 21–48 (1888).
2. A. Rubinowicz, "Thomas Young and the theory of diffraction," *Nature* **180**(4578), 160–162 (1957).
3. g. See, monograph M. Born and E. Wolf, *Principles of Optics* (Pergamon Press, Oxford, 1987, 6th ed) and references therein.
4. Z. L. Horváth, and Z. Bor, "Diffraction of short pulses with boundary diffraction wave theory," *Phys. Rev. E Stat. Nonlin. Soft Matter Phys.* **63**(2), 026601 (2001).
5. P. Bowlan, P. Gabolde, A. Shreenath, K. McGresham, R. Trebino, and S. Akturk, "Crossed-beam spectral interferometry: a simple, high-spectral-resolution method for completely characterizing complex ultrashort pulses in real time," *Opt. Express* **14**(24), 11892–11900 (2006) (and references therein).
6. Z. L. Horváth, J. Klebniczki, G. Kurdi, and A. Kovács, "Experimental investigation of the boundary wave pulse," *Opt. Commun.* **239**(4-6), 243–250 (2004).
7. D. Chauvat, O. Emile, M. Brunel, and A. Le Floch, "Direct measurement of the central fringe velocity in Young-type experiments," *Phys. Lett. A* **295**(2-3), 78–80 (2002).
8. M. Vasnetsov, V. Pas'ko, A. Khoroshun, V. Slyusar, and M. Soskin, "Observation of superluminal wave-front propagation at the shadow area behind an opaque disk," *Opt. Lett.* **32**(13), 1830–1832 (2007).
9. P. Saari, and K. Reivelt, "Evidence of X-shaped propagation-invariant localized light waves," *Phys. Rev. Lett.* **79**(21), 4135–4138 (1997).
10. P. Bowlan, H. Valtna-Lukner, M. Lõhmus, P. Piksarv, P. Saari, and R. Trebino, "Measuring the spatiotemporal field of ultrashort Bessel-X pulses," *Opt. Lett.* **34**(15), 2276–2278 (2009).
11. H. Valtna-Lukner, P. Bowlan, M. Lõhmus, P. Piksarv, R. Trebino, and P. Saari, "Direct spatiotemporal measurements of accelerating ultrashort Bessel-type light bullets," *Opt. Express* **17**(17), 14948–14955 (2009).
12. P. Piksarv, MSc thesis, University of Tartu (2009).
13. P. Bowlan, P. Gabolde, and R. Trebino, "Directly measuring the spatio-temporal electric field of focusing ultrashort pulses," *Opt. Express* **15**(16), 10219–10230 (2007).
14. P. Bowlan, U. Fuchs, R. Trebino, and U. D. Zeitner, "Measuring the spatiotemporal electric field of tightly focused ultrashort pulses with sub-micron spatial resolution," *Opt. Express* **16**(18), 13663–13675 (2008).
15. If viewing the plots without magnification in a computer screen the Moiré effect may obscure the actual small period of the intensity oscillations and increase of the period.

1. Introduction

The bending of light waves in the shadow region behind an opaque disk and the appearance of a bright "Spot of Arago" in the shadow centre are well-known manifestations of diffraction. Tremendous progress was made in the mathematical treatment of diffraction in the last two centuries, resulting in the well developed theory with Fresnel-Kirchhoff and Rayleigh-

Sommerfeld versions. An alternative theory, inspired by the early ideas of Thomas Young, has been developed by Maggi [1], Rubinowicz [2], Miyamoto and Wolf (references given in [3]). The boundary-diffraction wave (BDW) theory, as it was called, describes diffraction from openings in opaque screens in a mathematically simple manner. The BDW theory is especially intuitive when describing the formation of the diffracted field for the case of illumination with ultrashort laser pulses [4].

In the traditional diffraction treatment using monochromatic fields, the transmitted waves fill large depths of space behind the screen and overlap with each other there. In contrast, diffracted ultrashort pulses—typically only a few micrometers “thick”—behave almost like solitary spherical wave-front surfaces emitted from the boundaries of the screen. As a result, for ultrashort pulses, the study of diffraction in terms of pulsed BDW’s in the time domain is not only didactically preferable but also opens new interesting directions and applications, such as in the study of focusing and other transformations of ultrashort pulses [5]. The formation of an ultrashort boundary-wave pulse just after a circular aperture has been theoretically studied [4], and experimental evidence for its existence was obtained by measuring modulations in the spectrum of the on-axis field, with CCD-recordings of the time-integrated radial intensity distribution of the field, or using spatial interference [6–8].

In this publication, our aim has been to directly record, with simultaneous spatial and temporal resolution, the evolution and interference of the boundary waves behind an opaque disk and also behind a circular opening. We show that our high temporal resolution reveals similar spots of Arago for both types of screens. It also reveals that the spots are actually decelerating versions of the superluminal Bessel-X pulse (see [9–11] and references therein).

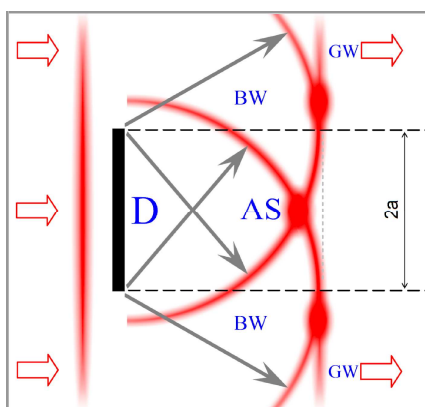


Fig. 1. Schematic of the formation of the Arago spot in the case of illumination with ultrashort pulses. A pancake-shaped pulsed wave from the left illuminates a disk-shaped obstacle (D) with radius a . The obstacle removes its central region according to the shadow boundaries (horizontal dashed lines), forming the geometrical-wave (GW) component of the output field. In addition, the edges of the obstacle excite the boundary diffraction wave (BW), which expands from a ring torus shape through a spindle-torus-like stage (cross-section depicted in the figure) into a spherical wave at infinity. On the axis, overlapping and interfering boundary waves form the Arago spot. Around the shadow boundary in the overlap regions (also indicated by ovals) of the BW and GW, the common interference rings appear. The Arago spot (AS) propagates along the axis behind the front (indicated by vertical dashed line) of the transmitted GW but catches up with the latter at infinity because its velocity is superluminal.

2. Theoretical description of the boundary wave pulse

According to the BDW theory [3] and its modification [4] for plane-wave incident pulses, the field after the diffracting screen consists of two components (see Fig. 1). The first—the so-called geometrical wave—propagates in accordance with geometrical optics, i. e., it is identical to the incident pulse, except in the region of the geometrical shadow, where it is zero. The second component—the BDW pulse—is simply a sum of spherical waves emitted

along the disk's edge having the temporal profile of the incident pulse. Therefore the BDW pulse for the case of a disk of radius a is given by the wave-function [12]

$$\Psi_{BW}(r, z, t) \propto e^{-i\omega_0 t} \int_0^\pi v \left(t - \frac{s}{c} \right) e^{ik_0 s} \frac{ra \cos \phi - a^2}{(z-s)s} d\phi, \quad (1)$$

where r and z are, respectively, the radial and axial coordinates of the field point; ω_0 and k_0 are, respectively, the carrier frequency and wave-number, $\omega_0 = c k_0$; v is the pulse envelope and $s = (r^2 + z^2 + a^2 - 2racos\phi)^{1/2}$. The integration over ϕ stems from contour integration along the disk's boundary and is one-dimensional—this is the known advantage of the BDW theory as compared to common diffraction theories based on 2D surface integrals. The BDW pulse in the case of a circular hole is given also by Eq. (1), but with the opposite sign [4,12]. This could be expected if we recall Babinet's principle. Equation (1) was used for the numerical simulations of diffracted fields, which will be considered below.

3. Experimental results in comparison with simulations

In our measurements, we used a KM Labs Ti:Sa oscillator with 33 nm of bandwidth (FWHM) and an approximately Gaussian spectrum with a central wavelength $\lambda_0 = 805$ nm. The spot size of the laser beam was 4 mm (FWHM). To perform the complete-spatiotemporal-intensity-and-phase pulse measurements with the required resolution in both space and time, in conjunction with the required sensitivity, we used a technique called scanning SEA TADPOLE (Spatially Encoded Arrangement for Temporal Analysis by Dispersing a Pair of Light E-fields [13,14]) which is a variation of spectral interferometry. To make a measurement, we sample a small spatial region of the unknown field with a micrometer sized fiber and then interfere this with a known reference pulse in a spectrometer to reconstruct $E(\lambda)$ for that spatial point. Then to measure the spatial dependence of the field, we simply scan the fiber point by point through the space where the unknown light field propagates, so that $E(\lambda)$ is measured at each position, yielding $E(\lambda, x, z)$. This field can be Fourier transformed to the time domain to yield $E(t, x, z)$. The plots from our SEA TADPOLE measurements, which are shown below, can be viewed as still images or "snapshots in flight," since they are spatiotemporal slices of the magnitude of the electric field $|E(x, z, t)|$ of the pulses. While we could also scan along the y -dimension of the beam, our set up had cylindrical symmetry, so we only scanned along the x -dimension with the fiber at $y = 0$.

First we propagated ultrashort pulses past an opaque disk with a 4mm, generating a hole in the beam. We measured the resulting spatiotemporal field at different distances after the aperture to observe its evolution (Fig. 2). These measurements reveal the spatiotemporal structure of the weak boundary waves and the brighter spot at the center of the beam due to their constructive interference, i. e., the spot of Arago, as it is known in conventional diffraction theory for stationary (monochromatic) fields. Aside from the noise in the experimental results they are in good agreement with the simulations. The only discrepancy is in the spatial intensity profile of the GW pulse. This is because our beam's spatial profile was Gaussian in the experiments, but to simplify the simulations we used a plane wave spatial profile (see Eq. (1)). In the measured spatiotemporal intensities shown in Fig. 2, two interference patterns are seen. The one with a broader spatial modulation consisting of rings at the edge of the direct (GW) pulse is due to the GW overlapping and interfering with the BW pulse. Another with a much higher spatial frequency—which decreases with the propagation distance [15]—can be seen around the bright central spot and is due to the interfering boundary waves. This part of the field is analogous to a Bessel-X pulse.

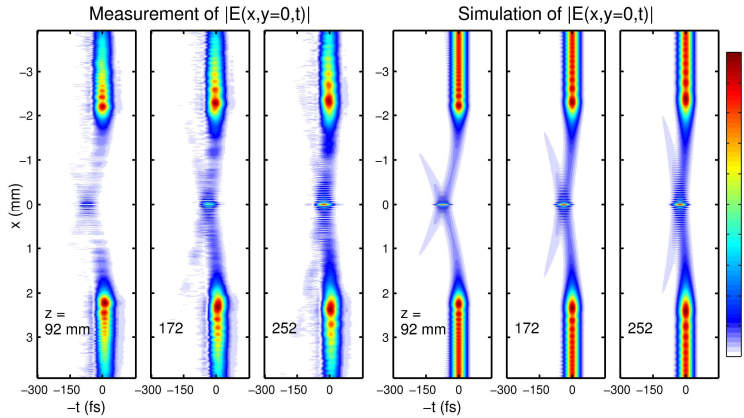


Fig. 2. Formation and evolution of the Arago spot behind an opaque disk 4mm in diameter. The magnitude of the electric field E is shown at three different propagation distances z in pseudo-color code according to the color bar (white has been taken for the zero of the scale in order to better reveal areas of weak field).

In the next measurement we propagated the beam through a circular hole with a diameter of 4.4mm (Fig. 3), which is almost the same as the disk's diameter. The temporal localization of the pulse and our high temporal resolution allows the BW pulse with its central spot to be separated from the direct pulse. If longer pulses or steady-state illumination were used, these two contributions to the diffracted field would overlap and be indistinguishable from one another. These measurements make it clear that the so-called spot of "Arago" is also present due to diffraction from an aperture. This is expected considering that both the aperture and disk have the same boundaries, and should therefore also have the same boundary waves.

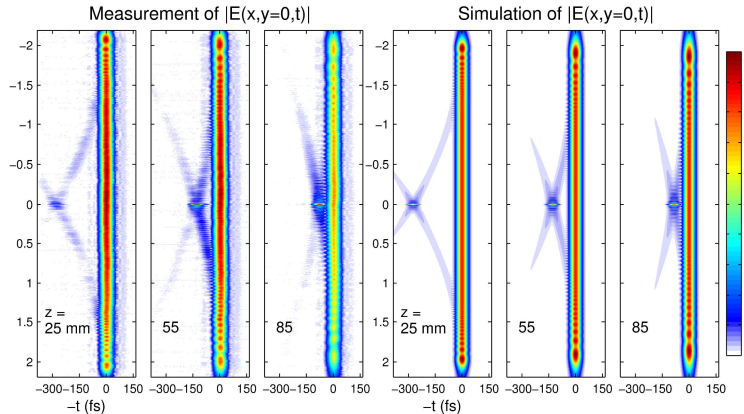


Fig. 3. Formation and evolution of the diffracted field behind a circular hole 4mm in diameter. The boundary waves interfere with each other and with the directly transmitted pulse, but the interference maximum on the axis (actually a temporally resolved spot of Arago) lags behind the direct pulse, and eventually catches up with it.

Interestingly, the plots for both screens reveal that the spot of Arago is surrounded by coaxial interference rings which, in the axial region the field, almost exactly follow the Bessel (J_0) radial profile. Moreover, the spot is delayed in time with respect to the main pulse front, and this delay decreases with z , indicating a superluminal propagation speed along the z axis (the GW pulse front propagates at c). This occurs, because, as z (the distance from the screen) increases, the extra distance that the boundary waves must propagate (compared to the GW

pulse front) to reach the z axis ($x = 0$) decreases, so the relative delay of the boundary waves on the axis decreases. As a result, the axial group velocity of the Arago spot—geometrically located at one pole of a luminally expanding spindle torus formed by the boundary diffraction wave pulse—varies from infinity at $z = 0$ to c for very large values of z . Therefore, the spot of Arago is in fact just a decelerating superluminal Bessel pulse like that recently generated using compound refractive optical elements and also studied with SEA TADPOLE [11].

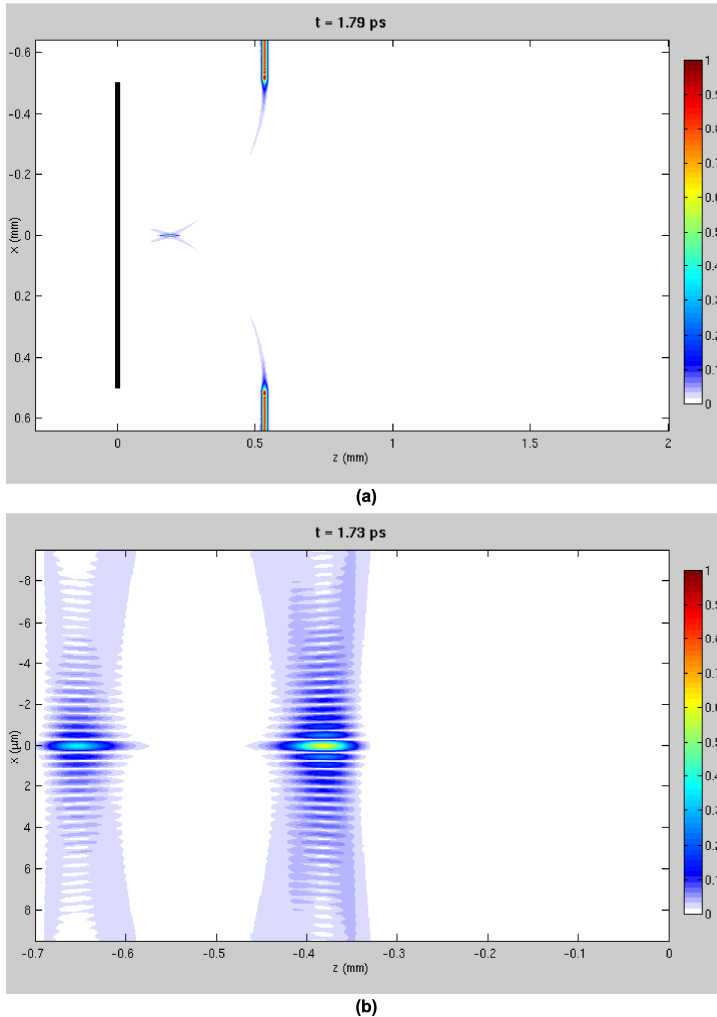


Fig. 4. Videos showing simulations of the diffraction of a plane wave pulse from a circular disc of $d = 1$ mm diameter. The pulse parameters are the same as in Figs. 2 and 3. Color represents the normalized amplitude of the electric field. (a) The reference frame is fixed with respect to the disc at $z = 0$ (Media 1). The diffracted field is calculated for $z > 0$ mm. (b) Close-up of the evolution of the boundary wave pulse in a reference frame moving at the luminal velocity c , or with the incident plane wave pulse (Media 2). Note that the x -scale in (b) is finer than in (a) by two orders of magnitude.

Naturally, there is nothing startling about the superluminal speed of the spot, because it cannot carry any information superluminally. This is because it is reformed at every point along its propagation axis (the z -axis) by the expanding spherical-wave constituents, which travel at an angle with respect to the z -axis. It is important to realize that the central

interference region of the BDW pulse is not moving at this tilt angle. Its phase (and pulse) fronts are perpendicular to the z -axis and move along this axis. Its Poynting vector, indicating the direction of energy flow, also lies along the z -axis. However, the energy flux is not superluminal. The superluminal pulse's velocity should not, of course, be confused with the signal velocity. As is well known, Maxwell's equations, or the wave equation for electromagnetic fields, does not allow superluminal signaling.

To further study the formation and evolution of the boundary-wave pulse, the propagation of an ultrashort pulse was computed in detail behind an opaque disk 1mm in diameter. In the simulations a smaller disk diameter was used in order to reveal the subtleties of the formation of the boundary wave pulse. Figure 4(a) (Media 1) shows the incident and diffracted pulse propagation in the laboratory reference frame where $z = 0$ mm is the location of the disc. The simulations show the creation of the Arago spot at the moment when the expanding ring torus of the boundary-wave pulse becomes an expanding spindle torus. In the close vicinity after the disc, speeds much greater than c can be seen, where the boundary wave pulse literally jumps out of it. Due to the discrete color scale of the animations, the expanding spindle torus shape of the BDW pulse seems discontinuous during the first few picoseconds of the spot evolution, albeit it is only low in intensity in these particular directions.

The Bessel-like radial pattern is depicted in greater detail in Fig. 4(b) (Media 2) where only the field near the axis' center is shown. This time we use a reference frame that is moving with the incident plane-wave pulse. The origin of the frame $z = 0$ mm is bound to the plane-wave pulse moving at velocity c to the right. The fringe pattern in the axial region of the boundary-wave pulse stretches during the propagation as the angle of intersection between the elementary wavelets decreases continuously. Correspondingly, the pulse velocity decreases as the fringe periodicity increases. Since the expansion rate of the spindle-torus is constant (equal to c), the spot on the axis propagates superluminally, decelerating toward the limiting value c . Interestingly, the first seconds of the video also reveal the back-diffracted pulse, which follows from the direct evaluation of Eq. (1). This backward propagating contribution is expected since the spherical waves generated at the boundary of the disk are emitted at all angles in the x - z plane. Of course, the intensity of the backward-moving pulse quickly decreases towards negative values of z and practically ceases to exist within the first millimeter of propagation.

4. Conclusions

In summary, we have performed direct spatiotemporally resolved measurements of pulsed light fields behind basic types of diffracting screens and have interpreted the results using the boundary diffraction wave theory. The latter provides a one-dimensional integral expression for the diffracted field, which enabled us in a computationally simple way to simulate the evolution of the diffracted field. We believe that time-resolved measurements and a time-domain treatment of diffracting waves not only turn out to be fruitful in modern physical optics, especially in micro- and meso-optics, but also promote the understanding of diffraction phenomena.

Acknowledgements

R. T. and P. B. were supported by Georgia Research Alliance and NSF SBIR grant #053-9595, the other authors were supported by the Estonian Science Foundation.

K. Reivelt, H. Valtna, and P. Saari
“Optical generation of superluminal localized wave solutions
of homogeneous wave equation”,
Northern Optics Conference Proceedings,
IEEE, 13–16 (2006).

This material is posted here with permission of the IEEE. Such permission of the IEEE does not in any way imply IEEE endorsement of any of the University of Tartu's products or services. Internal or personal use of this material is permitted. However, permission to reprint/republish this material for advertising or promotional purposes or for creating new collective works for resale or redistribution must be obtained from the IEEE by writing to pubs-permissions@ieee.org. By choosing to view this material, you agree to all provisions of the copyright laws protecting it.

Optical generation of superluminal localized wave solutions of homogeneous wave equation

Kaido Reivelt
and Heli Valtma
Institute of Physics, University of Tartu
Riia 142, 51014 Tartu, Estonia
Telephone: (372) 383-028
Fax: (888) 383-033
Email: Kaido.Reivelt@ut.ee

Peeter Saari
University of Tartu
Ülikooli 18, 50090 Tartu, Estonia
Institute of Physics of University of Tartu
Riia 142, 51014 Tartu, Estonia
Email: Peeter.Saari@ut.ee

Abstract—The feasibility of localized waves – the best approximation to non-diffracting, spatially and temporally localized "light bullets" in vacuum – has been discussed over the past two decades. Recently the first experimental evidence of their generation has been published. In this paper we propose an optical setup for launching optical superluminal localized waves that take advantage of the diffraction properties of a special optical element – cylindrical diffraction grating.

I. INTRODUCTION

During the last two decades it has been established, that the homogeneous wave equation has a number of so called localized wave (LW) solutions, instantaneous, Gaussian pulse-like intensity distribution of which propagates without any distortions in free space (see, Refs. [1], [2] and references therein). Obviously such spatial and temporal localization makes the implementation of LW solutions very attractive for applications, where the lateral and/or transversal diffractive spreading of optical wave fields is the major limitation of system performance (e.g., optical communication, metrology, monitoring, imaging, optical manipulation and acceleration of particles and femtosecond spectroscopy). In recent years it became also obvious, that the concept can be used in constructing pulse-like wave fields in dispersive media [3], [4] and in nonlinear optics [5], [6]. However, for more than a decade after the pioneering theoretical paper of J. N. Brittingham [7] the feasibility of electromagnetic LWs remained questionable due to their large spectral bandwidth and the spatio-temporal non-separability inherent to LWs. The ideas that had been proposed for generation of complicated LW solutions in the papers of that period of the field (see [1] for the references) are hardly realizable in optical domain.

The experiments in optical domain have been started by launching the Bessel-X pulses [3], [4], [8], [9], [10], [11], where the conventional Bessel beam generators under the wideband illumination have been used. In Ref. [12] we proposed a physically transparent, one step derivation of fundamental LW solutions – focus wave modes (FWM) and proved that good approximations to FWM's can be generated by means of a combination of an axicon and a circular diffraction grating [12]-[14]. The proposed principle has been

also verified in experiment [15].

In this paper we introduce a surprisingly elegant, one-step method for the optical generation of LWs. We show, that superluminal LWs with hyperbolic support of angular spectrum of their plane waves constituents can be generated by means of illuminating cylindrical diffraction gratings by conical wave packets – Bessel-X pulses. We give the mathematical description of the method and discuss the pros and cons of the new type of setup.

II. ON DEFINITIONS AND GENEALOGY OF LWs

The LWs can be introduced in several ways. Here we start with the general axisymmetric expansion over the zeroth-order Bessel beams in the form

$$\Psi(\rho, z, t) = \int_{-\infty}^{\infty} dk_z \int_{|k_z|}^{\infty} dk A(k_z, k) J_0\left(\sqrt{k^2 - k_z^2} \rho\right) \times \exp(ik_z z - ikct) . \quad (1)$$

where $A(k_z, k)$ is the angular spectrum of plane waves of the wave field. Here we notice that for $|\Psi(\rho, z, t)|^2$ to be propagation-invariant, i. e., to depend on z and t only through the propagation variable $z - v_g ct$, where v_g is a constant group velocity along z axis in units of c , the variables k and k_z must be bound linearly (see e.g. [16])

$$k = v_g k_z + b , \quad (2)$$

where b is a constant (see Fig. 1a). Hence, the spectrum has to be singular and may be factorized in the following form

$$A_{LW}(k_z, k) = A(k) \delta(k - v_g k_z - b) \Theta(k^2 - k_z^2) , \quad (3)$$

where $A(k)$ is any complex-valued function of one real positive variable and the Heaviside unit step $\Theta(x)$ has been introduced as a factor in order to allow the k -integration in Eq. (1) to start from $k = 0$ instead of $k = |k_z|$.

We just note, that the physical meaning of the condition 2 is obvious – it states, that the on-axis group velocity of the wave field $v_g c = d\omega/dk_z$ should be constant over the whole spectral range [12].

An elegant graphical depiction of the general class of LW solutions of scalar homogeneous wave equations can also be

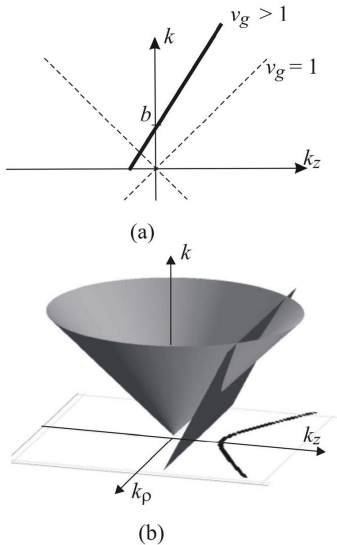


Fig. 1. (a) The graphical illustration of the defining property of angular spectrum of the LWs in k -space, (b) formation of the hyperbolic spectral support as the intersection of conic surface in k, k_z, k_ρ space.

given. Despite a general solution $\Psi(\mathbf{r}, t)$ of the free-space scalar wave equation depends on 4 coordinates x, y, z, ct , its transform domain (k -space or spectral) representation $\tilde{\Psi}(\mathbf{k}, \omega/c)$ has only 3 independent arguments due to the dispersion-relation restriction $k_x^2 + k_y^2 + k_z^2 - (\omega/c)^2 = 0$ imposed by the wave equation. In other words, the 4-vector $(\mathbf{k}, k \equiv \omega/c)$ of a light wave is always an isotropic one, whereas (\mathbf{r}, ct) needn't and generally isn't. Thus, in the 4-dimensional transform domain the spectral function $\tilde{\Psi}(\mathbf{k}, k)$ is not equal to zero only on the surface of a 3-dimensional cone given by equation $k^2 = k_x^2 + k_y^2 + k_z^2$. In other words, the support of the function $\tilde{\Psi}(\mathbf{k}, k)$ has to lie on that conical surface. In the case of azimuthal symmetry one can introduce the cylindrical coordinates by replacing $k_x^2 + k_y^2 \rightarrow k_\rho^2$ thus reducing the dimensionality of the support to 2 and gaining a possibility to depict the support as a conical surface in the k -space with 3 axes: k_z, k_ρ, k (or ω/c), see Fig. 1b. In those terms the spectral support of LW must be a line of intersection of the cone surface by a plane perpendicular to the plane (k_z, k) and the projection of the spectral support onto the plane (k_z, k) is a straight line with the slope v_g (see Fig. 1). Note, that the two-dimensional integration in 1 covers the area of projection of the support on the cone onto the plane (k_z, k) [16].

If the slope of the spectral support on the (k_z, k) plane $v_g < 1$ the Eq. (1) gives the family of subluminal LW's, if

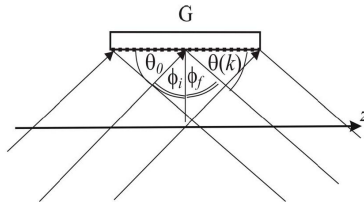


Fig. 2. On the principle of the optical setup proposed. The plane wave pulse propagating at angle θ relative to the optical axis z (ϕ_i relative to the normal of the diffraction grating) diffracts off the diffraction grating so that tilted pulses with angular dispersion (tilt) introduced by the grating is formed behind the grating. It appears, that the tilt introduced to a plane wave pulse in such setup is that of the LW $\theta(k)$.

$v_g = 1$ the corresponding LW's are luminal. In the case $v_g > 1$ we get superluminal LW's. The special case $v_g < 1$ and $b = 0$ corresponds to Bessel-X pulses.

III. OPTICAL GENERATION OF SUPERLUMINAL LW'S

In Fourier representation the Eq. (1) together with Eq. (3) has a straightforward interpretation as being the superposition of monochromatic Bessel beams the cone angle and wave number of which are connected as

$$\cos \theta(k) = \frac{k - b}{v_g k} \quad (4)$$

where $\theta(k)$ is the angle between the optical axis z and wave vector of the Fourier component (plane wave) of the wave field and $k_z(k) = k \cos \theta(k)$. It has been shown both theoretically and experimentally, that to generate a LW the necessary and sufficient condition is to control the spectral support of the generated wave field. In particular, if the generated spectral support obeys (4) the corresponding wave field is always LW. The effects of physical limitations of a setup like finite aperture or finite spectral bandwidth have effect only when estimating the propagation length of the generated LWs [1], [12]. Also, the need for a spectral chirp in the source pulse to generate LW with transform limited pulse length can be satisfied by standard pulse compression techniques.

In Ref. [12], [15] we demonstrated both theoretically and experimentally, that a very good approximations to the optical LW's can be generated by means of combining a circular grating and axicon so that the angular dispersion of the LW's is generated in the resulting wave field. However, it tends to be a complicated task to find the combination of angularly dispersive optical elements to generate the required spectral support of plane waves.

Consider a simple diffraction grating that is illuminated with a plane wave pulse as depicted on Fig 2. Using the grating equation we can write

$$\sin \phi_f - \sin \phi_i = \frac{m\lambda}{\Lambda} \quad (5)$$

where m is the order of the diffracted field and Λ is the period of the grating (see Fig. 2). Now, if we assume that the grating

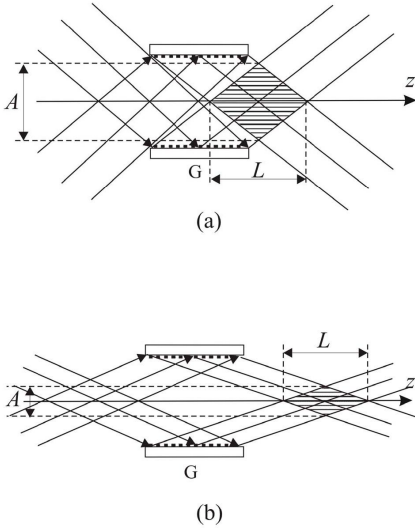


Fig. 3. (a) The optical setup proposed. The Bessel-X pulse diffracts off the cylindrical diffraction grating G so that a superposition of tilted pulses with angular dispersion (tilt) introduced by the grating is formed in the striped region. A stands for the aperture of the generated LW and L for the propagation length of the LW; (b) If the Bessel-X pulse propagate at smaller angles relative to propagation axis the aperture A of the resulting LW is also smaller.

is oriented parallel to the axis z (optical axis) and note that in this case $\theta_0 = \pi/2 - \phi_i$, $\sin \phi_i = \cos \theta_0$ and $\sin \phi_f = \cos \theta(k)$ we get

$$\cos \theta(k) = \cos \theta_0 - \frac{2\pi m}{ka} = \frac{k - \frac{2\pi q}{\Lambda \cos \theta_{0i}}}{\frac{1}{\cos \theta_0} k} \quad (6)$$

and this is exactly the spectral support defined by the condition (4) if we choose $v_g = 1/\cos \theta_0$ and $b = 2\pi q/\Lambda \cos \theta_0$. Thus, unlike in the setups considered so far in this case the spectral support of plane waves of LWs can be generated *exactly* by means of a single diffraction grating that is illuminated by a plane wave pulse.

In cylindrically symmetric case we replace the plane diffraction grating with a cylindrical diffraction grating and illuminate it by a Bessel-X pulse [9] as shown on Fig. 3a. As the effect of the cylindrical symmetry the initially conical spectral support of the Bessel-X pulses is transformed into the hyperboloidal one by the angular dispersion of the grating, the effect of the physical dimensions of the setup being the finite propagation length of the generated LW (see striped region in Fig. 3 and [1], [12] for a related discussion).

One can also calculate the field distribution of the wave field generated in such setup. If we insert the spectral support

(6) into the general expression (1) and assume the Gaussian frequency spectrum, we get

$$\Psi(\rho, z, t) \sim \int_0^\infty dk \exp \left[-\frac{k - k_z}{\Delta k} \right]^2 \times J_0(k\rho \sin \theta(k)) \exp(ikz \cos \theta(k) - ikt) \quad (7)$$

Clearly, this formula is a model, not a simulation of a realistic experimental situation, for example, it essentially assumes infinite aperture of the system. However, in our previous publications we have shown that as far as the aperture of the generated LW A (see Fig. 3) satisfies the condition $A \gg \lambda/\sin \theta_0$ where θ_0 stands for the mean cone angle of the Bessel beam components of LW, the integrals of the form 7 can be used to calculate the spatial distribution of the wave field in the near-axis region inside the propagation length of the LW in very good approximation [14]. In Fig. 3 this volume is depicted by the striped region – this is the region where all the Bessel beam components that diffract from the cylindrical grating are overlapped so that the constructive interference can take place. How to construct the setup so that the propagation length of the generated wave field is sufficiently large is up to the choice of parameters.

In this setup we have seven parameters: v_g and b to define the spectral support, the frequency spectrum of the light source $A(k)$, the initial conical angle of the Bessel-X pulse θ_0 , the grating period Λ , the diameter D and the length of the grating L_g . As to understand the interplay between the parameters we have to notice, that given the light source $A(k)$ the parameters of the spectral support v_g and b together can be used to optimize for the average propagation direction of the Bessel beam components $\theta(k_0)$ and the diameter of the central peak d – the two quantities are inversely proportional as $d \sim 1/\sin \theta(k_0)$. The simple geometrical arguments show, that the parameters of the cylinder and cone angle θ_0 can be used to optimize for the propagation length and the position of the propagation volume (see Fig. 3). Comparing Figs. 3a and 3b one can also see the general drawback of the optical schemes with elements oriented along the propagation axis – the aperture of the generated LWs A inevitably reduces as we move towards the paraxial angles $\theta(k)$ so that the optimization of the parameters have to be treated carefully. One can also see, that the propagation length of the generated LW L is less or equal to the length of the grating.

Working through the various choices of the parameters of the setup we were able to find several practical sets of parameters for the experiments. For example, if we choose $\theta_0 = 8$ deg, $\Lambda = 20\mu\text{m}$, $D = 15\text{mm}$, $L_g = 50\text{mm}$ and use Gaussian light source in the range 550nm–600nm we get the LW that propagates 30.2mm at the group velocity $v_g = 1.04$. The simulated field distribution is that depicted in Fig. 4. The experiments with such setup will be carried out in near future.

IV. DISCUSSION

The main advantage of the proposed setup is its robustness. In all the setups discussed so far the material dispersion of conical dispersive elements have been used to optimize for

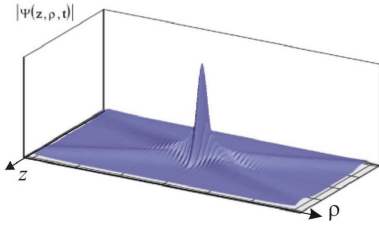


Fig. 4. The modulus of the superluminal LW that can be generated by the proposed setup. The wave field has Gaussian frequency spectrum that extends from 550nm to 600nm having bandwidth 50nm. The plotting range for the lateral coordinate ρ is 180 μ m and for the axial coordinate z it is 90 μ m.

the required spectral support of LWs. In present case the exact spectral support of superluminal LWs is generated by means of a single optical element. From the very nature of the LWs it is also implicit, that in principle the setup is robust for the spectral shape of the input pulse and for its cone angle. Indeed, as it is constructed to generate certain *support* of the spectrum the frequency spectrum does not really matter in first approximation. As for the initial cone angle - it appears as parameter in Eq. (6), so that the generated spectral support is this of a LW in every possible occasion. One still needs to give the initial Bessel-X pulse the phase distortion (chirp) as to generate the transform-limited pulse shape on the optical axis of the system, however, this can be easily achieved by applying standard pulse compression/expansion techniques. In fact, the only practical difficulty in the described setup is the fabrication of the cylindrical diffraction gratings.

V. CONCLUSION

We have proposed well-realizable setup for generation of optical superluminal LWs that is robust on the parameters of the source pulse (Bessel-X pulse in this case). We discussed the working principle of the setup and presented numerical simulation for a practical set of parameters.

ACKNOWLEDGMENT

This research was supported by the Estonian Science Foundation.

REFERENCES

- [1] Reivelt K and Saari P, 2003 *arXiv.org e-Print archive, physics/0309079* <http://arxiv.org/abs/physics/0309079>.
- [2] I. Besieris, M. Abdel-Rahman, A. Shaarawi, and A. Chatzipetros, *Progr. In Electromagn. Research* **19**, 1 (1998).
- [3] H. Sönajalg and P. Saari, *Opt. Lett.* **21**, 1162 (1996).
- [4] H. Sönajalg, M. Rätsep and P. Saari, *Opt. Lett.* **22**, 310 (1997).
- [5] P. Di Trapani, G. Valiulis, A. Piskarskas, O. Jedrkiewicz, J. Trull, C. Conti, S. Trillo, *Phys. Rev. Lett.* **91**, 093904 (2003).
- [6] R. Butkus, S. Orlov, A. Piskarskas, V. Smilgevičius, A. Stabinis, *Opt. Comm.* **244**, 411 (2005).
- [7] J. N. Brittingham, *J. Appl. Phys.* **54**, 1179 (1983).
- [8] P. Saari and H. Sönajalg, *Laser Physics* **7**, 32 (1997).
- [9] P. Saari and K. Reivelt, *Phys. Rev. Lett.* **79**, 4135 (1997).
- [10] I. Alexeev, K. Y. Kim, and H. M. Milchberg, *Phys. Rev. Lett.* **88**, 073901 (2002).

- [11] R. Grunwald, V. Kebbel, U. Griebner, U. Neumann, A. Kummrow, M. Rini, E. T. J. Nibbering, M. Piché, G. Rousseau, and M. Fortin, *Phys. Rev. A* **67**, 063820 (2003).
- [12] K. Reivelt and P. Saari, *J. Opt. Soc. Am. A* **17**, 1785 (2000).
- [13] K. Reivelt and P. Saari, *Phys. Rev. E* **65**, 046622 (2002).
- [14] K. Reivelt and P. Saari, *Opt. Lett.* **29**, 1176 (2004).
- [15] K. Reivelt and P. Saari, *Phys. Rev. E* **66**, 056611 (2002).
- [16] Saari P and Reivelt K *Phys. Rev. E* **69**, 036612 (2004).
- [17] J. Salo, and M. M. Salomaa, *J. of Opt. A: Pure. Appl. Opt.* **3**, 366 (2001).
- [18] P. Saari, M. Menerit, and H. Valtua, *Opt. Commun.* **246**, 445 (2005).
- [19] P. Saari, in: *Ultrafast Photonics*, Institute of Physics Publishing, Bristol and Philadelphia (2004), pp. 317-340.

P. Bowlan, H. Valtna-Lukner, M. Lõhmus, P. Piksarv, P. Saari, R. Trebino
“Measurement of the spatiotemporal electric field
of ultrashort superluminal Bessel-X pulses”
Optics and Photonics News, **20**, 42 (2009).

Measurement of the Spatiotemporal Electric Field of Ultrashort Superluminal Bessel-X Pulses

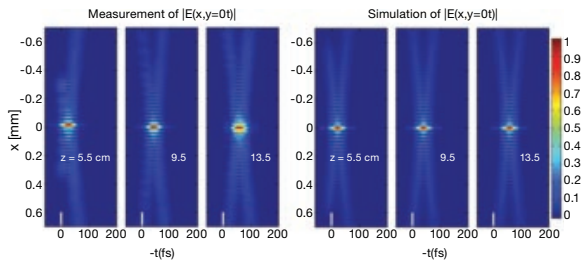
Pamela Bowlan, Heli Valtna-Lukner, Madis Lõhmus, Peeter Piksarv, Peeter Saari and Rick Trebino

Bessel-X pulses are of great interest because they propagate unchanged in vacuum or linear media over large distances.¹ In other words, they act like optical bullets—without exhibiting any diffraction or dispersion—and do not spread in space or time. Bessel pulses have many applications, such as plasma generation, light filamentation, imaging, particle micromanipulation and cell transfection. An x - z or x - t slice of a Bessel-X pulse's spatiotemporal intensity profile $I(x, y, z)$ or $I(x, y, t)$ resembles the letter "X." Interestingly, theory predicts that the electric field of a Bessel-X pulse propagates with equal phase and group velocities, both greater than c in a vacuum. This has been experimentally demonstrated several times since the original pioneering publication,¹ nevertheless, the pulses' superluminal group velocity is still occasionally questioned.

This makes it important to directly measure these pulses. The catch is that Bessel-X pulses have a complex spatiotemporal shape, requiring a measurement technique with simultaneous femtosecond temporal resolution and micrometer spatial resolution.

We recently accomplished this task.^{2,3} To measure the electric field of a Bessel-X pulse, we used the new ultrashort-laser-pulse measurement technique, SEA TADPOLE.⁴ It involves sampling a small spatial region of the pulse with a single-mode optical fiber and then interfering this with a known reference pulse from another identical fiber in a spectrometer, yielding the pulse intensity and phase $E(\lambda)$ —and hence also $E(t)$ —at each point in space.

To generate the Bessel-X pulse, we propagated roughly 30 fs pulses from a Ti:sapphire oscillator through a fused-silica axicon with an apex angle of 176°. While SEA TADPOLE measured the spatiotemporal intensity and phase, most



(Left) Measured field amplitude vs. transverse position (x) and time (t) at three different distances (z) after the axicon. (Right) Corresponding simulations. Color indicates the modulus of electric field, normalized to have a maximum of 1. The white bar emphasizes the location of $t = 0$.

of the interesting features were in the intensity, which is shown in the figure. Numerical simulations of the optical wave-packet are in good agreement.

Note that the central part (the apex of the double-conical shape) containing the bright spot remains essentially unchanged over a propagation distance of 8 cm. In contrast, a Gaussian beam of the same waist would have expanded by 26 times over this distance. We also measured the Bessel-X pulse's superluminal speed. SEA TADPOLE conveniently measured the Bessel-X pulse's arrival time relative to the reference pulse, which traveled at the speed of light c . So, if the Bessel-X pulse were traveling at the speed of light, then, for each value of z , its spatio-temporal intensity would be centered at $t = 0$. However, it is easy to see that this was not the case. We measured our pulse's speed along the z axis to be $1.00012c$ —within 0.001 percent of the predicted value. (A superluminal Bessel-X pulse's velocity should not, of course, be confused with the signal velocity.)

In a related study, we added a convex (or concave) lens in front of the axicon,³ which resulted in an accelerating (or decelerating) modification of the Bessel-X pulse, which had been theoretically studied in a recent paper.⁵ The Bessel pulse's group velocity accelerated from $1.0002c$ to $1.0009c$ during 4 cm of propagation, and the decelerating Bessel pulse slowed down from $1.00007c$ to $1.00003c$ over a 12-cm distance. Δ

Pamela Bowlan (pambowlan@gatech.edu) and Rick Trebino are with the Georgia Institute of Technology, School of Physics, Atlanta, Ga., U.S.A. Heli Valtna-Lukner, Madis Lõhmus, Peeter Piksarv and Peeter Saari are with the University of Tartu, Institute of Physics, Tartu, Estonia.

References

1. P. Saari and K. Reivelt. *Phys. Rev. Lett.* **79**, 4135-8 (1997).
2. P. Bowlan et al. *Opt. Lett.* **34**, 2276-8 (2009).
3. H. Valtna-Lukner et al. *Opt. Express* **17**, 14948-55 (2009).
4. P. Bowlan et al. *J. Opt. Soc. Am. B* **25**, A81-A92 (2008).
5. M. Clerici et al. *Opt. Express* **16**, 19807-11 (2008).

CURRICULUM VITAE

Name: Heli Valtna-Lukner
Date and place of birth: 1.11.1982, Tallinn, Estonia
Citizenship: Estonia
Marital status : married, 1 child
Occupation: University of Tartu, Institute of Physics, researcher;
(currently on parental leave, since 03.2009)
Phone: +372 5691 5519 (cell phone)
E-mail: heli.lukner@ut.ee

Education

1989–1997 Lasnamäe Üldgümnaasium (primary school)
1997–2000 Tallinn Secondary Science School
2000–2004 University of Tartu, BSc in physics
2004–2006 University of Tartu, MSc in physics, specializing to optics and spectroscopy
2006–2010 University of Tartu, PhD studies, physics, optics and spectroscopy

Professional Employment

03.2006–11.2008 University of Tartu, Institute of Physics, engineer.
12.2007–... University of Tartu, Institute of Physics, researcher.

Fellowships

07–08 2006 Summer student in European Nuclear Research Centre (CERN), Geneva, Switzerland.
03.2007–04.2008 Junior research fellow in Vilnius University Laser Research Centre, Lithuania; Marie Curie early stage training, ATLAS project.

Awards and Honours

- Estonian National Contest for Young Scientists at university level, I Prize (for master thesis) 2007.
- Estonian Academy of Sciences, II award from student research contest (for master thesis), 2006.
- Estonian National Contest for Young Scientists at university level, II Prize (for bachelor thesis) 2004.

ELULOOKIRJELDUS

Nimi: Heli Valtna-Lukner
Sünniaeg ja -koht: 1. november, 1982, Tallinn
Rahvus: eestlane
Kodakondsus: Eesti
Perekonnaseis: abielus, 1 laps
Praegune töökoht, amet: Tartu Ülikooli Füüsika Instituut, erakorraline teadur;
(lapsehoolduspuhukusel alates 03.2009)
Telefon: 5691 5519 (mobiil)
E-post: heli.lukner@ut.ee

Haridustee

1989–1997 Lasnamäe Üldgümnaasium
1997–2000 Tallinna Reaalkool
2000–2004 Tartu Ülikool, BSc füüsikas
2004–2006 Tartu Ülikool, MSc füüsikas, spetsialiseerumine:
optika ja spektroskoopia
2006–2010 Tartu Ülikool, doktorantuur, füüsika, optika ja spektroskoopia

Erialane teenistuskäik

03.2006–11.2007 Tartu Ülikool, Füüsika Instituut, insener
12.2007–... Tartu Ülikool, Füüsika Instituut, erakorraline teadur

Erialane enesetäiendus

07–08 2006 osavõtt Euroopa Tuumauuringute Keskuse (CERN)
suvetudengite programmist, Genf, Šveits.
03.2007–04.2008 stažeerimine Vilniuse Ülikooli Laseriuuringute Keskuses,
Leedus, nooremteadur Marie Curie mobiilsusprojekti ATLAS
raames.

Erialane tunnustus

- Teadus- ja haridusministeeriumi üliõpilaste teadustööde riikliku konkursi preemia (magistritöö eest) 2007 a.
- Eesti Teaduste Akadeemia tudengite teadustööde konkursi II preemia (magistritöö eest) 2006 a.
- Teadus- ja haridusministeeriumi üliõpilaste teadustööde riikliku konkursi II preemia (bakalaureuse töö eest) 2004 a.

DISSERTATIONES PHYSICAE UNIVERSITATIS TARTUENSIS

1. **Andrus Ausmees.** XUV-induced electron emission and electron-phonon interaction in alkali halides. Tartu, 1991.
2. **Heiki Sõnajalg.** Shaping and recalling of light pulses by optical elements based on spectral hole burning. Tartu, 1991.
3. **Sergei Savihhin.** Ultrafast dynamics of F-centers and bound excitons from picosecond spectroscopy data. Tartu, 1991.
4. **Ergo Nõmmiste.** Leelishalogeniidide röntgenelektronemissioon kiiritamisel footonitega energiaga 70–140 eV. Tartu, 1991.
5. **Margus Rätsep.** Spectral gratings and their relaxation in some low-temperature impurity-doped glasses and crystals. Tartu, 1991.
6. **Tõnu Pullerits.** Primary energy transfer in photosynthesis. Model calculations. Tartu, 1991.
7. **Olev Saks.** Attoampri diapsoonis voolude mõõtmise füüsikalised alused. Tartu, 1991.
8. **Andres Virro.** AlGaAsSb/GaSb heterostructure injection lasers. Tartu, 1991.
9. **Hans Korge.** Investigation of negative point discharge in pure nitrogen at atmospheric pressure. Tartu, 1992.
10. **Jüri Maksimov.** Nonlinear generation of laser VUV radiation for high-resolution spectroscopy. Tartu, 1992.
11. **Mark Aizengendler.** Photostimulated transformation of aggregate defects and spectral hole burning in a neutron-irradiated sapphire. Tartu, 1992.
12. **Hele Siimon.** Atomic layer molecular beam epitaxy of A^2B^6 compounds described on the basis of kinetic equations model. Tartu, 1992.
13. **Tõnu Reinot.** The kinetics of polariton luminescence, energy transfer and relaxation in anthracene. Tartu, 1992.
14. **Toomas Rõõm.** Paramagnetic H^{2-} and F^+ centers in CaO crystals: spectra, relaxation and recombination luminescence. Tallinn, 1993.
15. **Erko Jalviste.** Laser spectroscopy of some jet-cooled organic molecules. Tartu, 1993.
16. **Alvo Aabloo.** Studies of crystalline celluloses using potential energy calculations. Tartu, 1994.
17. **Peeter Paris.** Initiation of corona pulses. Tartu, 1994.
18. **Павел Рубин.** Локальные дефектные состояния в CuO_2 плоскостях высокотемпературных сверхпроводников. Tartu, 1994.
19. **Olavi Ollikainen.** Applications of persistent spectral hole burning in ultrafast optical neural networks, time-resolved spectroscopy and holographic interferometry. Tartu, 1996.
20. **Ülo Mets.** Methodological aspects of fluorescence correlation spectroscopy. Tartu, 1996.
21. **Mikhail Danilkin.** Interaction of intrinsic and impurity defects in CaS:Eu luminophors. Tartu, 1997.

22. **Ирина Кудрявцева.** Создание и стабилизация дефектов в кристаллах KBr, KCl, RbCl при облучении ВУФ-радиацией. Tartu, 1997.
23. **Andres Osvet.** Photochromic properties of radiation-induced defects in diamond. Tartu, 1998.
24. **Jüri Örd.** Classical and quantum aspects of geodesic multiplication. Tartu, 1998.
25. **Priit Sarv.** High resolution solid-state NMR studies of zeolites. Tartu, 1998.
26. **Сергей Долгов.** Электронные возбуждения и дефектообразование в некоторых оксидах металлов. Tartu, 1998.
27. **Кауро Kukli.** Atomic layer deposition of artificially structured dielectric materials. Tartu, 1999.
28. **Ivo Heinmaa.** Nuclear resonance studies of local structure in $\text{RBa}_2\text{Cu}_3\text{O}_{6+x}$ compounds. Tartu, 1999.
29. **Aleksander Shelkan.** Hole states in CuO_2 planes of high temperature superconducting materials. Tartu, 1999.
30. **Dmitri Nevedrov.** Nonlinear effects in quantum lattices. Tartu, 1999.
31. **Rein Ruus.** Collapse of 3d (4f) orbitals in 2p (3d) excited configurations and its effect on the x-ray and electron spectra. Tartu, 1999.
32. **Valter Zazubovich.** Local relaxation in incommensurate and glassy solids studied by Spectral Hole Burning. Tartu, 1999.
33. **Indrek Reimand.** Picosecond dynamics of optical excitations in GaAs and other excitonic systems. Tartu, 2000.
34. **Vladimir Babin.** Spectroscopy of exciton states in some halide macro- and nanocrystals. Tartu, 2001.
35. **Toomas Plank.** Positive corona at combined DC and AC voltage. Tartu, 2001.
36. **Kristjan Leiger.** Pressure-induced effects in inhomogeneous spectra of doped solids. Tartu, 2002.
37. **Helle Kaasik.** Nonperturbative theory of multiphonon vibrational relaxation and nonradiative transitions. Tartu, 2002.
38. **Tõnu Laas.** Propagation of waves in curved spacetimes. Tartu, 2002.
39. **Rünno Lõhmus.** Application of novel hybrid methods in SPM studies of nanostructural materials. Tartu, 2002.
40. **Kaido Reivelt.** Optical implementation of propagation-invariant pulsed free-space wave fields. Tartu, 2003.
41. **Heiki Kasemägi.** The effect of nanoparticle additives on lithium-ion mobility in a polymer electrolyte. Tartu, 2003.
42. **Villu Repän.** Low current mode of negative corona. Tartu, 2004.
43. **Алексей Котлов.** Оксианионные диэлектрические кристаллы: зонная структура и электронные возбуждения. Tartu, 2004.
44. **Jaak Talts.** Continuous non-invasive blood pressure measurement: comparative and methodological studies of the differential servo-oscillometric method. Tartu, 2004.
45. **Margus Saal.** Studies of pre-big bang and braneworld cosmology. Tartu, 2004.

46. **Eduard Gerškevičš.** Dose to bone marrow and leukaemia risk in external beam radiotherapy of prostate cancer. Tartu, 2005.
47. **Sergey Shchemelyov.** Sum-frequency generation and multiphoton ionization in xenon under excitation by conical laser beams. Tartu, 2006.
48. **Valter Kiisk.** Optical investigation of metal-oxide thin films. Tartu, 2006.
49. **Jaan Aarik.** Atomic layer deposition of titanium, zirconium and hafnium dioxides: growth mechanisms and properties of thin films. Tartu, 2007.
50. **Astrid Rekker.** Colored-noise-controlled anomalous transport and phase transitions in complex systems. Tartu, 2007.
51. **Andres Punning.** Electromechanical characterization of ionic polymer-metal composite sensing actuators. Tartu, 2007.
52. **Indrek Jõgi.** Conduction mechanisms in thin atomic layer deposited films containing TiO_2 . Tartu, 2007.
53. **Aleksei Krasnikov.** Luminescence and defects creation processes in lead tungstate crystals. Tartu, 2007.
54. **Küllike Rägo.** Superconducting properties of MgB_2 in a scenario with intra- and interband pairing channels. Tartu, 2008.
55. **Els Heinsalu.** Normal and anomalously slow diffusion under external fields. Tartu, 2008.
56. **Kuno Kooser.** Soft x-ray induced radiative and nonradiative core-hole decay processes in thin films and solids. Tartu, 2008.
57. **Vadim Boltrushko.** Theory of vibronic transitions with strong nonlinear vibronic interaction in solids. Tartu, 2008.
58. **Andi Hektor.** Neutrino Physics beyond the Standard Model. Tartu, 2008.
59. **Raavo Josepson.** Photoinduced field-assisted electron emission into gases. Tartu, 2008.
60. **Martti Pärs.** Study of spontaneous and photoinduced processes in molecular solids using high-resolution optical spectroscopy. Tartu, 2008.
61. **Kristjan Kannike.** Implications of neutrino masses. Tartu, 2008.
62. **Vigen Issahhanjan.** Hole and interstitial centres in radiation-resistant MgO single crystals. Tartu, 2008.
63. **Veera Krasnenko.** Computational modeling of fluorescent proteins. Tartu, 2008.
64. **Mait Müntel.** Detection of doubly charged higgs boson in the CMS detector. Tartu, 2008.
65. **Kalle Kepler.** Optimisation of patient doses and image quality in diagnostic radiology. Tartu, 2009.
66. **Jüri Raud.** Study of negative glow and positive column regions of capillary HF discharge. Tartu, 2009.
67. **Sven Lange.** Spectroscopic and phase-stabilisation properties of pure and rare-earth ions activated ZrO_2 and HfO_2 . Tartu, 2010.
68. **Aarne Kasikov.** Optical characterization of inhomogeneous thin films. Tartu, 2010.